



Investigating Sphingolipid Metabolism in Glioblastoma

Author:

Abuhusain, Hazem Jasim

Publication Date:

2013

DOI:

<https://doi.org/10.26190/unsworks/16952>

License:

<https://creativecommons.org/licenses/by-nc-nd/3.0/au/>

Link to license to see what you are allowed to do with this resource.

Downloaded from <http://hdl.handle.net/1959.4/53729> in <https://unsworks.unsw.edu.au> on 2024-05-01

Investigating Sphingolipid Metabolism in Glioblastoma

Hazem J. Abuhusain

A thesis submitted in fulfilment of the requirements for the degree of
Doctor of Philosophy (PhD)

Cure for Life Neuro-Oncology Group
Prince of Wales Clinical School
Faculty of Medicine
University of New South Wales

August 2013

Thesis/Dissertation Sheet

THE UNIVERSITY OF NEW SOUTH WALES
Thesis/Dissertation Sheet

Surname or Family name: **Abuhusain**

First name: **Hazem**

Other name/s: **Jasim**

Abbreviation for degree as given in the University calendar: **PhD**

School: **Prince of Wales Clinical School**

Faculty: **Faculty of Medicine**

Title: **Investigating sphingolipid metabolism in glioblastoma**

Abstract (350 words maximum)

Glioblastoma (GBM), a genetically heterogeneous disease, has a significant burden on our society. Currently, the standard treatment for newly diagnosed GBM patients consists of surgery followed by concomitant radiotherapy and temozolomide chemotherapy, resulting in a median survival of 12-15 months. Targeted therapies are being developed to inhibit oncogenes based upon GBM molecular profiling, though have not been as successful as expected. Our understanding of DNA and RNA alterations in GBM has grown considerably over the past few years. However, our understanding of the lipid biology, specifically sphingolipids, in GBM is lagging and may prove useful in the arsenal of targeted therapies. The sphingolipid pathway contains lipid signalling molecules, which modulate cellular survival through the balance of ceramide, a pro-apoptotic metabolite, and Sphingosine-1-Phosphate (S1P), a pro-survival metabolite.

Herein, I characterise for the first time the sphingolipid profile of normal grey matter (NGM), diffuse astrocytomas (AII), anaplastic astrocytomas (AIII), and GBM using liquid chromatography tandem mass spectrometry. The lipid profile is supported by an enzyme expression profile favouring ceramide catabolism and S1P formation, including upregulation of acid ceramidase (ASAH1) and sphingosine kinase 1 (SPHK1), and a down regulation of S1P phosphatase 2 (SGPP2). Significantly, C18 ceramide was reduced 5-fold in GBM compared to NGM, while S1P was increased in GBM by approximately 9-fold compared to NGM. Based on the sphingolipid profiles, ASAH1 and SPHK1 were assessed for functional relevance *in vitro*. Using gene silencing and pharmacological inhibition, I found SPHK1 to be critical for U87MG-induced angiogenesis through S1P paracrine signalling, which was independent of VEGF levels. *EGFR* mutations were associated with increased C16 and C22 ceramide levels. For the first time, I measured sphingolipid metabolites in plasma extracted from GBM patients and healthy controls. Elevated levels of S1P were found in GBM plasma and together with tumour S1P levels, were associated with a poor survival outcome. In contrast low S1P levels in tissue combined with MGMT methylation was associated with a good survival outcome.

Overall, the data presented in this thesis reaffirm the importance of sphingolipid metabolism in GBM biology, reflected by a shift in the ceramide-S1P balance, favouring the pro-angiogenic S1P. Additionally, sphingolipid interactions with altered genetic pathways and potential biomarker capacity are novel findings that require further validation, with the hope of informing and monitoring therapeutic responses for GBM patients.

Declaration relating to disposition of project thesis/dissertation

I hereby grant to the University of New South Wales or its agents the right to archive and to make available my thesis or dissertation in whole or in part in the University libraries in all forms of media, now or here after known, subject to the provisions of the Copyright Act 1968. I retain all property rights, such as patent rights. I also retain the right to use in future works (such as articles or books) all or part of this thesis or dissertation.

I also authorise University Microfilms to use the 350 word abstract of my thesis in Dissertation Abstracts International (this is applicable to doctoral theses only).

.....
Signature

.....
Witness

.....
Date

The University recognises that there may be exceptional circumstances requiring restrictions on copying or conditions on use. Requests for restriction for a period of up to 2 years must be made in writing. Requests for a longer period of restriction may be considered in exceptional circumstances and require the approval of the Dean of Graduate Research.

FOR OFFICE USE ONLY

Date of completion of requirements for Award:

THIS SHEET IS TO BE GLUED TO THE INSIDE FRONT COVER OF THE THESIS

Originality Statement

ORIGINALITY STATEMENT

'I hereby declare that this submission is my own work and to the best of my knowledge it contains no materials previously published or written by another person, or substantial proportions of material which have been accepted for the award of any other degree or diploma at UNSW or any other educational institution, except where due acknowledgement is made in the thesis. Any contribution made to the research by others, with whom I have worked at UNSW or elsewhere, is explicitly acknowledged in the thesis. I also declare that the intellectual content of this thesis is the product of my own work, except to the extent that assistance from others in the project's design and conception or in style, presentation and linguistic expression is acknowledged.'

Signed

Date

Copyright Statement

COPYRIGHT STATEMENT

I hereby grant the University of New South Wales or its agents the right to archive and to make available my thesis or dissertation in whole or part in the University libraries in all forms of media, now or here after known, subject to the provisions of the Copyright Act 1988. I retain all proprietary rights, such as patent rights. I also retain the right to use in future works (such as articles or books) all or part of this thesis or dissertation.

I also authorise University Microfilms to use the 350 word abstract of my thesis in Dissertation Abstract International (this is applicable to doctoral theses only).

I have either used no substantial portions of copyright material in my thesis or I have obtained permission to use copyright material where permission has not been granted. I have applied/will apply for a partial restriction of the digital copy of my thesis or dissertation.

Signed

Date

AUTHENTICITY STATEMENT

I certify that the Library deposit digital copy is a direct equivalent of the final officially approved version of my thesis. No emendation of content has occurred and if there are any minor variations in formatting, they are the result of the conversion to digital format.

Signed

Date

Abstract

Glioblastoma (GBM), a genetically heterogeneous disease, has a significant burden on our society. Currently, the standard treatment for newly diagnosed GBM patients consists of surgery followed by concomitant radiotherapy and temozolomide chemotherapy, resulting in a median survival of 12-15 months. Targeted therapies are being developed to inhibit oncogenes based upon GBM molecular profiling, though have not been as successful as expected. Our understanding of DNA and RNA alterations in GBM has grown considerably over the past few years. However, our understanding of the lipid biology, specifically sphingolipids, in GBM is lagging and may prove useful in the arsenal of targeted therapies. The sphingolipid pathway contains lipid signalling molecules, which modulate cellular survival through the balance of ceramide, a pro-apoptotic metabolite, and Sphingosine-1-Phosphate (S1P), a pro-survival metabolite.

Herein, I characterise for the first time the sphingolipid profile of normal grey matter (NGM), diffuse astrocytomas (AII), anaplastic astrocytomas (AIII), and GBM using liquid chromatography tandem mass spectrometry. The lipid profile is supported by an enzyme expression profile favouring ceramide catabolism and S1P formation, including upregulation of acid ceramidase (ASAH1) and sphingosine kinase 1 (SPHK1), and a down regulation of S1P phosphatase 2 (SGPP2). Significantly, C18 ceramide was reduced 5-fold in GBM compared to NGM, while S1P was increased in GBM by approximately 9-fold compared to NGM. Based on the sphingolipid profiles, ASAH1 and SPHK1 were assessed for functional relevance *in vitro*. Using gene silencing and pharmacological inhibition, I found SPHK1 to be critical for U87MG-induced angiogenesis through S1P paracrine signalling, which was independent of VEGF levels. *EGFR* mutations were associated with increased C16 and C22 ceramide levels. For the

first time, I measured sphingolipid metabolites in plasma extracted from GBM patients and healthy controls. Elevated levels of S1P were found in GBM plasma and together with tumour S1P levels, were associated with a poor survival outcome. In contrast low S1P levels in tissue combined with MGMT methylation was associated with a good survival outcome.

Overall, the data presented in this thesis reaffirm the importance of sphingolipid metabolism in GBM biology, reflected by a shift in the ceramide-S1P balance, favouring the pro-angiogenic S1P. Additionally, sphingolipid interactions with altered genetic pathways and potential biomarker capacity are novel findings that require further validation, with the hope of informing and monitoring therapeutic responses for GBM patients.

Publications

1. Wong JW, Abuhusain HJ, McDonald KL, Don AS. *MMSAT: automated quantification of metabolites in selected reaction monitoring experiments*. *Anal Chem*. 2012 Jan 3; 84(1):470-4.
2. Abuhusain HJ, Matin A, Qiao Q, Shen H, Kain N, Day BW, Stringer BW, Daniels B, Laaksonen MA, Teo C, McDonald KL, Don AS. *A metabolic shift favoring sphingosine 1-phosphate at the expense of ceramide controls glioblastoma angiogenesis*. *J Biol Chem*. 2013 Dec 27; 288(52):37355-64.

Conference Abstracts

1. H.J. Abuhusain, K.L. McDonald, A.S. Don. High Throughput Liquid Chromatography-Mass Spectrometry measurements of bioactive lipids integrated with gene expression data in Glioblastoma. November 2011, California, USA.

Poster presentation at SNO 16th Annual Scientific Meeting

2. H.J. Abuhusain, A. Don, S. Tiwari, K. Okada, C. Teo, K. McDonald. Sphingolipids – A Potential Target Pathway in Glioblastoma. April 2012, Miami, USA.

E-Poster presentation at AANS 80th Annual Scientific Meeting

3. H.J. Abuhusain, A. Matin, C. Lee, Q. Qiao, H. Shen, C. Teo, B. Daniels, M. Laaksonen, K. McDonald, A. Don. Sphingolipid Metabolism in Glioblastoma: Rationale for Therapeutic Targeting. September 2013, Seoul, South Korea.

Oral presentation at WFNS 15th World Congress of Neurosurgery

4. H.J. Abuhusain, A. Matin, Q. Qiao, H. Shen, C. Teo, B. Daniels, M. Laaksonen, A. Don, K. McDonald. S1P: an alternative anti-angiogenic target in GBM. November 2013, San Francisco, USA.

Poster presentation at WFNO 4th Quadrennial Meeting

Acknowledgements

I would like to thank a number of people who have been of great support for me throughout my PhD, which would not have been possible without them. Firstly, I would like to sincerely thank my supervisor, Dr. Kerrie L. McDonald, for giving me the opportunity to join her lab. She has been a great supervisor, mentor, and educator during my 3.5 years, and has pushed me to keep on improving and asking the right questions. I would also like to sincerely thank my co-supervisor, Dr. Anthony Don, who has taught me a great deal of biochemistry, have been supportive, and generous with his time and effort. I am fortunate to have you both to guide me in this process.

To the Neuro-Oncology Group (past and present): I have had a wonderful time with you all. We shared a lot of laughs through the long hours and experimental troubleshooting. You have all been supportive and made my PhD a phase filled with great memories (not organic solutions)! To the Adult Cancer Program: I have been privileged to be a part of this group. You are all great colleagues! I will miss you and our many conversations!

I would also like to thank the Prince of Wales Clinical School, Cure for Life Foundation, TCRN, and UNSW for the scholarships over the years that have been of great support. As well, I would like to thank Dr. Charlie Teo, who has imparted his neurosurgical knowledge, and has supported the research through providing tissue specimens. Importantly, I would like to thank the patients, who have dedicated their samples for us to examine and ask the scientific and clinical questions that form the basis of my thesis.

Finally, I would like to thank my mom and dad (to whom I dedicate this work), for their love and support, along with my family (Hameeda, Hussam, Ali, my wonderful Uncle Fatah, Aunt Shaima'a and their nuclear families). Endearingly, to my loving wife who has been there for me throughout this journey: I love you like bees love honey.

Abbreviations

5-ALA	5-aminolevulinic acid
ABBN	Australian Brain Bank Network
ABC	ATP-binding cassette
ACER2	Alkaline ceramidase 2
ACER3	Alkaline ceramidase 3
AGOG	Australian Genomics and Clinical Outcomes of Glioma
AII	Diffuse astrocytoma
AIII	Anaplastic astrocytoma
ANOVA	Analysis of variance
ASAH1	Acid ceramidase
ATF6	Activating transcription factor 6
Bcl-2	B cell lymphoma gene 2
bFGF	Basic fibroblast growth factor
Bim	Bcl-2 interacting mediator of cell death
CDKN2A	Cyclin-dependent kinase inhibitor 2A
Cer	Ceramide
CERS1-6	Ceramide synthase 1-6
CHI3L1/YKL40	Chitinase 3-like 1
DMSO	Dimethyl sulfoxide
EC	Extracellular domain
EDTA	Ethylenediaminetetraacetic acid
EGF	Epidermal growth factor
EGFR	Epidermal growth factor receptor
EGFRvIII	EGFR variant III
emPCR	Emulsion PCR
eNOS	Endothelial nitric oxide synthase
ER	Endoplasmic reticulum
ERK	Extracellular signal-regulated kinase
ESTDs	External standards
FBS	Fetal bovine serum
FD	Farber Disease
GABRA1	Gamma-aminobutyric acid A receptor, subunit alpha 1
GBM	Glioblastoma
GPCR	G protein-coupled receptor
Gy	Gray

HDAC 1	Histone deacetylase 1
HDAC 2	Histone deacetylase 2
HDL	High density lipoprotein
HexCer	Hexosylceramide
HIF-1	Hypoxia inducible factor-1
HMEC-1	Human Microvascular Endothelial Cell line
HNSCC	Head and neck squamous cell carcinomas
HUVEC	Human umbilical vein endothelial cells
IDH1	Isocitrate dehydrogenase 1
IgE	Immunoglobulin E
ISTDs	Internal standards
JNK/SAPK	c-Jun amino-terminal kinase/stress-activated protein kinase
KSR	Kinase suppressor of Ras
LacCer	Lactosylceramide
LC-MS/MS	Liquid chromatography tandem mass spectrometry
LOH	Loss of heterozygosity
LTS	Long term survivors
MERTK	C-mer proto-oncogene tyrosine kinase
MET	Met proto-oncogene
MMSAT	Metabolite Mass Spectrometry Analysis Tool
MRS	Magnetic resonance spectroscopy
MS	Multiple Sclerosis
mt	Mutant
NEFL	Neurofilament
NF1	Neurofibromin
NGM	Normal grey matter
NMR	Nuclear magnetic resonance
NOE	N-oleoylethanolamine
-OH	Hydroxylated
PBS	Phosphate buffered saline
PDG	Patient derived GBM
PDGFRA	Platelet-derived growth factor receptor alpha
PHB2	Prohibitin
PIK3CA	Phosphatidylinositol-4,5-bisphosphate 3-kinase A
PIK3R1	Phosphoinositide-3-kinase, regulatory unit 1
PKC	Protein kinase C

PP2A	Protein phosphatase 2A
PTEN	Phosphatase and tensin homology
QoL	Quality of life
qRT-PCR	Quantitative Real Time- Polymerase Chain Reaction
Rb	Retinoblastoma
S1P	Sphingosine-1-phosphate
S1P ₁₋₅	S1P receptors 1-5
SCD1	Stearoyl-CoA desaturase 1
SDS	Sodium dodecyl sulfate
SEALS	South Eastern Area Laboratory Services
SGPL1	S1P lyase
SGPP1	Sphingosine phosphate phosphatase 1
SGPP2	Sphingosine phosphate phosphatase 2
siRNA	Small interfering RNA
SKI-1a	SPHK1 inhibitor 1a
SKI-1b	SPHK1 inhibitor 1b
SLC12A5	Solute carrier family 12, member 5
SM	Sphingomyelin
SPHK1	Sphingosine kinase 1
SPHK2	Sphingosine kinase 2
SREBP-1	Sterol regulatory element-binding protein 1
STS	Short term survivors
SYT1	Synaptotagmin
TCGA	The Cancer Genome Atlas
TESS	Tris, EDTA, Sodium Chloride, SDS
TMZ	Temozolomide
TNF	Tumour necrosis factor
TRAF2	TNF receptor-associated factor 2
UGCG	UDP-glucose ceramide glucosyltransferase
VEGF	Vascular endothelial growth factor
VPF	Vascular permeability factor
WHO	World Health Organisation
wt	Wild-type
YLL	Years of life lost

Table of Contents

Thesis/Dissertation Sheet.....	I
Originality Statement.....	II
Copyright Statement.....	III
Abstract.....	IV
Publications.....	VI
Conference Abstracts.....	VII
Acknowledgements.....	VIII
Abbreviations.....	IX
Chapter 1: Literature Review.....	1
1.1 Introduction.....	1
1.2 Normal Brain Parenchyma.....	1
1.3 Glioma.....	2
1.4 GBM.....	3
1.4.1 Clinical Presentation.....	4
1.4.2 Neuropathology.....	4
1.4.3 Molecular Pathology.....	6
1.4.4 Treatment.....	9
1.4.5 Tumour Angiogenesis.....	11
1.5 Sphingolipids.....	12
1.5.1 Ceramide.....	16
1.5.2 Sphingosine-1-Phosphate.....	18
1.6 Aims of Thesis.....	27

Chapter 2: Methods	29
2.1 Introduction.....	29
2.2 Clinical Samples	29
2.3 Lipid Methods.....	30
2.3.1 Tissue Sample Preparation.....	30
2.3.2 Sphingolipid Extraction	30
2.3.2.1 Tissue Samples and Cell Lines	30
2.3.2.2 Plasma Samples.....	32
2.3.3 Liquid Chromatography Mass Spectrometry	32
2.4 RNA Methods	38
2.4.1 RNA Extraction.....	38
2.4.2 RNA Quantification	39
2.4.3 LiCl Precipitation of RNA.....	40
2.4.4 Synthesis of cDNA.....	40
2.4.5 Quantitative Real Time – Polymerase Chain Reaction (qRT-PCR)	41
2.5 Cell Culture Methods.....	43
2.5.1 Cell Culture Conditions	43
2.5.2 Small Interfering RNA (siRNA) Transfections	45
2.5.3 Drug Treatments	46
2.5.4 MTT Assay	47
2.5.5 Flow Cytometry	47
2.5.6 Clonogenic Assay	48
2.5.7 Angiogenesis Assay	48
2.6 DNA Methods.....	50
2.6.1 DNA Extraction from fresh frozen tissue	50
2.6.2 Bisulfite Treatment	52

2.6.3	MGMT Pyrosequencing.....	53
2.6.4	Ion Torrent Sequencing.....	54
2.6.4.1	Library Preparation	54
2.6.4.2	Emulsion PCR and Sequencing	56
2.6.4.3	Coverage and Data Analysis	56
2.7	Statistical Analysis.....	57
Chapter 3: A Sphingolipid Map for Normal Grey Matter & Gliomas.....		59
3.1	Introduction.....	59
3.1.1	Hypothesis and Aims	61
3.2	Results.....	62
3.2.1	Sphingolipid Levels in Normal and Glioma Tissues	62
3.2.1.1	Sphingomyelin Levels in Normal and Glioma Tissues.....	63
3.2.1.2	Hexosylceramide Levels in Normal and Glioma Tissues	64
3.2.1.3	Lactosylceramide Levels in Normal and Glioma Tissues.....	65
3.2.1.4	Sulfatide Levels in Normal and Glioma Tissues.....	67
3.2.1.5	Ceramide Levels in Normal and Glioma Tissues	69
3.2.1.6	Sphingosine Levels in Normal and Glioma Tissues	71
3.2.1.7	S1P Levels in Normal and Glioma Tissues.....	72
3.2.2	Sphingolipid Enzymes Expression in Normal and Glioma Tissues.....	73
3.2.2.1	Ceramide Synthases in Normal and Glioma Tissues	74
3.2.2.2	Ceramide Conversion in Normal and Glioma Tissues.....	77
3.2.2.3	S1P Formation and Catabolism in Normal and Glioma Tissues.....	79
3.3	Discussion.....	84

Chapter 4: Assessing the Functional Effects of ASAH1 and SPHK1 Reduction in GBM cells	94
4.1 Introduction.....	94
4.1.1 ASAH1.....	95
4.1.2 SPHK1	96
4.1.3 Hypothesis and Aims	96
4.2 Results.....	98
4.2.1 Ceramide, Sphingosine, and SIP Levels in GBM Cell Lines.....	98
4.2.2 ASAH1 and SPHK1 Relative Gene Expression in GBM Cell Lines.....	102
4.2.3 ASAH1 and SPHK1 Knockdown Validation	103
4.2.4 Functional Consequences of SPHK1 and ASAH1 Knockdown	108
4.2.5 Pharmacological Inhibition of SPHK1.....	113
4.2.6 Effect of SPHK1 Drug Inhibition on Proliferation	114
4.2.7 Anti-angiogenic Effect of SPHK1 Drug Inhibition	115
4.3 Discussion.....	119
4.3.1 Cell Line Screen and Knockdown Validation.....	119
4.3.2 Proliferation, Clonogenicity, and Angiogenesis in siRNA Experiments	123
4.3.3 SPHK1 Drug Inhibition and Functional Effects	125
Chapter 5: Examining Sphingolipids in GBM Tissue and Plasma	129
5.1 Introduction.....	129
5.1.1 Hypothesis and Aims	131
5.2 Results.....	133
5.2.1 Clinical Cohort Overview	133
5.2.2 Clinical Outcomes.....	134
5.2.3 Correlating Sphingolipids with Mutations in GBM.....	136

5.2.4	Sphingolipids in GBM Tissue and Survival.....	138
5.2.5	Sphingolipids in GBM Plasma and Normal Plasma	142
5.2.6	Sphingolipids in GBM Tissue and GBM Plasma	143
5.2.7	Sphingolipids in GBM Plasma and Survival	144
5.3	Discussion.....	147
Chapter 6: Summary & Future Directions		152
References		163

List of Figures

Figure 1.1 Primary and Secondary Glioblastoma Characteristics	6
Figure 1.2 Schematic Diagram of the Sphingolipid Pathway	14
Figure 1.3 Basic Sphingolipid Structures	15
Figure 1.4 S1P Extracellular and Intracellular Signalling Targets	23
Figure 2.1 Schematic Diagram for the Angiogenesis <i>In Vitro</i> Model	50
Figure 3.1 Schematic Diagram of the Sphingolipid Pathway	60
Figure 3.2 Sphingolipids in NGM, AII, AIII, and GBM	62
Figure 3.3 Sphingomyelin Levels in NGM, AII, AIII, and GBM	64
Figure 3.4 Hexosylceramide Levels in NGM, AII, AIII, and GBM	65
Figure 3.5 Lactosylceramide Levels in NGM, AII, AIII, and GBM	67
Figure 3.6 Sulfatide Levels in NGM, AII, AIII, and GBM	68
Figure 3.7 Ceramide Levels in NGM, AII, AIII, and GBM	70
Figure 3.8 Balance between C16 Ceramide and C18 Ceramide in NGM, AII, AIII and GBM.....	71
Figure 3.9 Sphingosine Levels in NGM, AII, AIII, and GBM	72
Figure 3.10 S1P Levels in NGM, AII, AIII, and GBM	73
Figure 3.11 Sphingolipid Enzymes Expression in NGM, AII, AIII, and GBM	74
Figure 3.12 Ceramide Synthases Expression in NGM, AII, AIII, and GBM	77
Figure 3.13 Ceramide Glycosylation and Ceramidase Enzymes Expression in NGM, AII, AIII, and GBM	78

Figure 3.14 S1P-Related Enzymes Expression in NGM, AII, AIII, and GBM.....	81
Figure 4.1 Ceramide-Sphingosine-S1P Levels in Immortalised GBM Cell Lines	100
Figure 4.2 C16 and C18 Ceramide Levels in Immortalised GBM Cell Lines.....	101
Figure 4.3 ASAH1 and SPHK1 Relative Gene Expression in GBM Cell Lines	103
Figure 4.4 Gene Expression Analysis Post ASAH1 and SPHK1 Knockdown in U87MG Cells	105
Figure 4.5 Sphingolipid Analysis Post ASAH1 and SPHK1 Knockdown in U87MG Cells	107
Figure 4.6 Gene Expression Analysis Post ASAH1 and SPHK1 Knockdown in RN1 Cells	108
Figure 4.7 Effect of SPHK1 and ASAH1 Knockdown on Proliferation in U87MG and RN1 Cells.....	109
Figure 4.8 Effect of SPHK1 and ASAH1 Knockdown on Clonogenicity in RN1 Cells	110
Figure 4.9 Effect of SPHK1 and ASAH1 Knockdown on Angiogenesis in Co-cultured U87MG and HMEC-1 Cells	112
Figure 4.10 S1P, Sphingosine, and Ceramide Levels Post SPHK1 Drug Inhibition in U87MG Cells	114
Figure 4.11 Effect of SPHK1 Drug Inhibition on Proliferation in U87MG, RN1, and HMEC-1 Cells.....	115
Figure 4.12 Effect of SPHK1 Drug Inhibition on Angiogenesis in Co-cultured U87MG and HMEC-1 Cells.....	116
Figure 4.13 Effect of SPHK1 Drug Inhibition on Angiogenesis in Co-cultured U87MG Treated CM and HMEC-1 Cells	117

Figure 4.14 Effect of SPHK1 Drug Inhibition on Angiogenesis in Co-cultured U87MG Untreated CM and HMEC-1 Cells	118
Figure 5.1 Design Overview Examining GBM Sphingolipids with Several Factors ...	131
Figure 5.2 Survival Outcomes of Cohort Clinical Characteristics.....	136
Figure 5.3 Ceramide Levels in <i>EGFR</i> Wild-Type (wt) and Mutant (mt) GBM Tissues	138
Figure 5.4 Survival Outcome of S1P in GBM Tissue.....	141
Figure 5.5 SM-Ceramide-Sphingosine-S1P Levels in GBM and Normal Plasma	142
Figure 5.6 Correlations between GBM Tissue and Plasma Sphingolipids	144
Figure 5.7 Survival Outcome of S1P in GBM Plasma.....	146

List of Tables

Table 2.1 Sphingolipids Parameter Settings on the LC-MS/MS	33
Table 2.2 Taqman® Probes for qRT-PCR.....	42
Table 2.3 SYBR® Green Primers for qRT-PCR	42
Table 2.4 Ion AmpliSeq™ Cancer HotSpot Panel v2.....	55
Table 3.1 List of Ceramide Synthases and Target Ceramide Chain Length.....	75
Table 3.2 Correlations between S1P-Related Measurements	82
Table 3.3 Mean (95% CI) Values of Sphingosine and S1P Measurements According to Median Levels of SPHK1, SPHK2, SGPP1, and SGPP2 (N=67)	83
Table 5.1 Clinical Cohort Characteristics	133
Table 5.2 Non-Synonymous Gene Mutations in GBM Cohort	137
Table 5.3 Summary of Sphingolipids in GBM Tissue.....	143

Chapter 1: Literature Review

1.1 Introduction

Significant improvements in survival, reduced morbidity, and improved quality of life have been seen for many cancer patients. Cancer nowadays does not hold the same connotation of being incurable, with the exception of a few types. Malignant brain tumours remain a difficult entity to treat and improve survival times and when diagnosed, the impact on a patients' life is devastating. Diffuse gliomas are the most common form of brain tumour in adults. Gliomas are typically classified into three grades (II-IV) according to the World Health Organisation (WHO) (increased grade in accordance with increased malignancy).

1.2 Normal Brain Parenchyma

Normal brain tissue is composed of a various number of cellular components, but the most important cells of the brain are subdivided into glial cells and neuronal cells, in addition to endothelial cells which form the vasculature. There are equal numbers of neuronal and glial cells, with approximately 85 billion of each, though ratios differ depending on the brain region [1, 2]. The interconnecting processes of both cell types form a mesh network known as the neuropil. Glial cells, Greek for glue, include astrocytes, oligodendrocytes, microglia, and ependymal cells [3, 4]. The brain is divided into the cerebral cortex (four lobes), basal ganglia, and limbic system in the supratentorial compartment, and the cerebellum and brain stem in the infratentorial

compartment. The cerebral cortex is composed of white and grey matter. White matter is characterised by densely myelinated axonal tracts supported by oligodendrocytes and fibrous astrocytes, while grey matter has a mixture of neurons and glial cells (protoplasmic astrocytes) [4], hence the variability in tissue colour.

1.3 Glioma

Glioma is a broad term to describe glial-derived neoplasms, therefore astrocytomas, oligodendrogliomas, and ependymomas fall under this grouping. However, in the following work to be presented, gliomas are in reference to astrocytomas. Adult astrocytomas are subdivided into diffuse astrocytoma (AII), anaplastic astrocytoma (AIII), and glioblastoma (GBM). The spectrum of disease begins in the early stage with AII tumours, characterised by infiltrating, well-differentiated, neoplastic astrocytes. Cellular density exceeds normal white matter by more than double. Histologically, they are defined by nuclear atypia and pleomorphism. AII tumours progress to AIII tumours in approximately a 3-year window (although time to progression is highly variable). AIII tumours are more aggressive, have higher mitotic activity, and similar cytological atypia, therefore differentiating AII and AIII tumours can be difficult if non-representative tumour sections were sampled. AIII tumours eventually progress to GBM in approximately a 2-year window, and accounts for approximately 5-10% of all GBMs diagnosed [5, 6]. Where there is progression of a lower grade lesion to GBM, these GBMs are termed secondary GBMs (detailed in section 1.4.2.).

1.4 GBM

Primary or *de novo* occurring GBM, a common glial-derived neoplasm accounting for 12-15% of all intracranial tumours and 70% of malignant glial-derived neoplasms [6], has a poor 5-year survival of 3-9.8% [7-10]. Despite a multimodal treatment approach, consisting of surgical resection followed up the Stupp protocol (concurrent chemotherapy and radiotherapy, plus adjuvant chemotherapy), the median survival is only 12-15 months [11]. Fortunately the incidence is only 3-5 per 100,000 population per year, hence it is relatively uncommon [6, 11, 12]. However, GBM has the highest burden on society compared to all other cancers for years of life lost (YLL), with an average YLL at approximately 20 years [13]. Men are affected slightly more than women, with ratios ranging between 1.26:1 to 1.5:1 [5, 6]. The age at clinical presentation is frequently between 61-64 years, but it is important to note that it can occur at any age. To put into perspective, approximately 80% of patients diagnosed with GBM are above 50 years, and less than 1% is below 20 years of age. Of note, the only proven risk factor linked to the development of GBM is ionizing radiation. Moreover, some genetic syndromes such as Li-Fraumeni syndrome, Turcot's syndrome, neurofibromatosis, and Maffucci's syndrome have been linked to a small number of familial cases accounting for GBMs [5, 11, 14]. Recently, in a large nested case-control study, stored serum samples were examined for IgE levels in glioma patients (n=594) and matched controls (n=1177). High allergen-specific and total IgE levels were inversely associated with glioma diagnosis, and this association was positive 20 years prior to diagnosis [15]. GBM is a challenging disease with complex clinical, neuropathological, and molecular factors, which has had some modest improvement in therapeutic management over the past decades.

1.4.1 Clinical Presentation

The cranial vault is a confined space, whereby the cerebrum can accommodate for small variations in the intracranial pressure. Depending on the location of the tumour, it may produce seizures if located in an epileptogenic area, or headaches reflecting a rise in intracranial pressure. These headaches may be accompanied by nausea, vomiting, and papilloedema. Some headaches may be non-specific tension headaches, and therefore would delay the diagnosis at times. Focal neurological deficits, confusion, and personality changes can also occur [5, 6, 11]. With vague symptoms, and a fast growing tumour, GBMs usually present at a late stage, and therefore pose a challenge in treatment. The tumour is frequently supratentorially, hence affecting any of the cerebral hemisphere lobes, and rarely occurs at the optic nerve, cerebellum, or spinal cord. Brain stem GBM is uncommon in the adult population [5, 6]. Tumour involvement in eloquent regions, such as the pre-central gyrus responsible for motor function, would result in an incomplete total resection. Moreover, if a dominant lobe is affected, surgical resection may result in long-term neurological deficits such as memory loss, speech or comprehension deficits, or even cognitive impairment, depending on the area infiltrated by the tumour.

1.4.2 Neuropathology

In addition to the difficulty in early diagnosis, GBM is a heterogeneous tumour, thus creating a challenge in developing a 'one-treatment fits all' approach. Histologically, GBM is classified as a WHO grade IV. The standard histological grading is based on microscopic features, which accounts for histologic heterogeneity but not molecular heterogeneity. Nuclear atypia, mitosis, microvascular proliferation, and necrosis are the

diagnostic criteria for GBM. These features do not correspond to differences in clinical outcome with the exception of a few debatable subtypes. Cellular pleomorphism in GBM ranging from poorly differentiated cells to well differentiated cells, can be small, gemistocytic, granular, large, or have an oligodendroglial component. Regarding the diagnostic criteria, atypical nuclei with a ‘glassy’ cytoplasm is commonly seen, with an increase in proliferation identified by mitosis and staining with Ki-67/MIB-1. Microvascular proliferation is represented by actively dividing endothelial cells alongside pericytes and smooth muscle cells. Necrosis usually occurs centrally in these tumours, as cells continually proliferate and expand outwards, and necrosis may be outlined by “palisading” neoplastic cells termed palisading necrosis. The microvascular proliferation and necrosis distinguish a GBM from an AIII tumour [5, 6, 14].

Although histologically GBM is classified as a WHO grade IV, further sub-classifications exist, reflecting the variation in outcome and progression. Two types have been described in 1940 by Scherer, known as primary and secondary GBMs, and are summarised below in Figure 1.1 [16]. Primary or *de novo* GBMs represent approximately 90% of the tumours diagnosed, maintaining a short clinical duration of less than 3-6 months, with no identifiable precursor lesion, and tend to affect the elderly population. In contrast, secondary or progressive GBMs form the remaining 10%, arising from lower grade astrocytic lesions such as diffuse or anaplastic astrocytomas, have an average clinical progression interval of 4-5 years, and occur in a younger population with a mean age of 45 years [5, 6, 17]. Of interest, secondary GBMs tend to have well-differentiated neoplastic cells, while primary GBMs are usually poorly differentiated [6]. Molecularly, secondary GBMs are characterised by frequent *TP53* mutations, an absence of epidermal growth factor receptor (*EGFR*) mutations, and 19q

loss [18, 19]. In contrast, primary GBMs are characterised by EGFR amplification, frequent phosphatase and tensin homology (*PTEN*) mutations, and loss of chromosome 10 [18, 20]. Recently, isocitrate dehydrogenase 1 (*IDH1*) mutations, associated with a hypermethylation phenotype [21], have been described as a cell lineage marker to differentiate secondary GBM and primary GBM, which are likely to arise from different neural precursors [22].

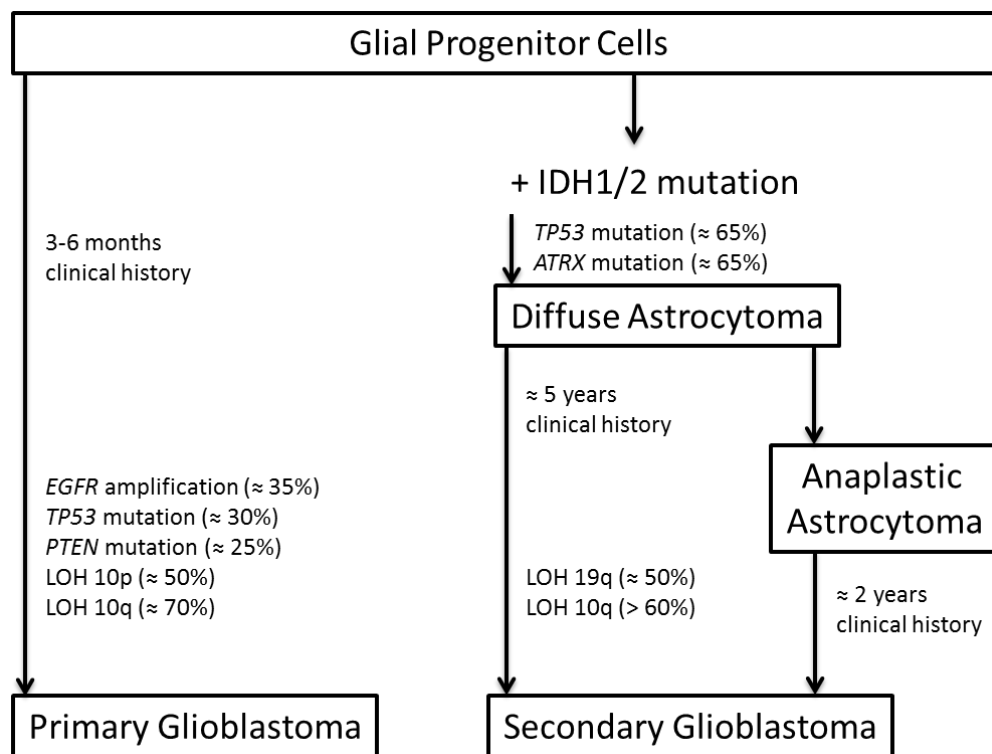


Figure 1.1 Primary and Secondary Glioblastoma Characteristics

A summary of genetic and clinical differences between primary and secondary GBMs is presented [22].

1.4.3 Molecular Pathology

The variability in molecular profiling and classification continues to evolve constantly; reaffirming the heterogeneity and complexity of this tumour. Primary and secondary

GBMs exhibit different genetic aberrations, but this classification has been further refined by defining new subclasses. In 2006, three subgroups of GBM were identified, using gene expression profiling, termed as proneural, mesenchymal, and proliferative [23]. Further emphasizing the molecular heterogeneity of GBMs, The Cancer Genome Atlas (TCGA) Research Network classified GBMs into four subgroups, termed classical, mesenchymal, proneural, and neural. The initial gene expression analysis of approximately 200 GBM samples and 2 normal brain samples was further validated with an independent sample size of 260 GBMs, collated from previous publications. The four subtypes identified describe the molecular heterogeneity of primary GBMs, while only the proneural group represents the molecular signature of secondary GBMs. Of note, immortalized cell lines did not reflect all four subgroups; instead they mirrored the mesenchymal subtype [24].

Classical GBMs are characterized by several genomic aberrations, including loss of heterozygosity (LOH) on chromosome 10 with amplification on chromosome 7, and *EGFR* amplification including a variant III (*EGFRvIII*) mutation in more than 50% of the subtype. *PTEN* mutations are present, but *TP53* gene is generally intact. Moreover, other frequent mutations include the homozygous deletion of 9p21.3, affecting cyclin-dependent kinase inhibitor 2A (*CDKN2A*), along with the retinoblastoma (Rb) pathway are evident. Overexpression of *NES*, a stem cell marker, and activation of Notch and Sonic hedgehog signalling are associated features of this subtype. Clinically, the classical subtype illustrates a benefit from the standard treatment regimen of concurrent radiotherapy and chemotherapy following surgical resection, possibly because the *TP53* gene is unaffected [24, 25].

Similar to the classical category, the mesenchymal subgroup also benefits from the standard treatment, but exhibits different genomic alterations. Loss of the neurofibromin (*NFI*) gene, through 17q11.2 deletions, or mutation is frequent. In addition, overexpression of mesenchymal markers such as met proto-oncogene (*MET*), chitinase 3-like 1 (*CHI3LI/YKL40*), and the astrocytic markers *CD44* and c-mer proto-oncogene tyrosine kinase (*MERTK*) are present. More necrosis is manifested in this subtype, which may be attributed to the activation of the tumour necrosis factor (TNF) family and NFκB pathways. Loss or mutations of *TP53* and *PTEN* genes are frequent in the mesenchymal subtype [24, 25]. In a recent study identifying a 9-gene set for predicting the outcome for GBMs, the mesenchymal subtype correlated with a poor survival outcome, while the proneural subtype correlated with a relatively better prognosis [26].

Interestingly, the proneural subgroup exhibit mutations in the *IDH1* gene and aberrations in platelet-derived growth factor receptor alpha (*PDGFRA*) with overexpression or mutations. Additionally, mutations in *TP53* and *PTEN* are present. LOH of chromosome 10 and amplification of chromosome 7 are present in the classical subtype, but the prevalence in the proneural group is almost at 50%. Where the *PDGFRA* gene was unaffected, phosphatidylinositol-4,5-bisphosphate 3-kinase A / phosphoinositide-3-kinase, regulatory unit 1 (*PIK3CA/PIK3R1*) mutations were prevalent. Moreover, overexpression of oligodendrocytic genes (e.g. *OLIG2*) and proneural development genes (e.g. *SOX*) are unique to this subtype. Notably, the proneural subtype is more prevalent in the younger age groups and represents both a subset of primary GBMs and the general profile of secondary GBMs [24, 25].

The neural subtype is the least defined. Neurofilament (*NEFL*), gamma-aminobutyric acid A receptor, subunit alpha 1 (*GABRA1*), synaptotagmin (*SYTI*), and solute carrier family 12, member 5 (*SLC12A5*) are overexpressed neuronal markers for this category. Axonal and synaptic transmissions, along with neuronal projection, were pathways associated with these tumours. Interestingly, the two normal control brains in the study were classified as neural, but histologically normal cells were rarely seen in the tumour sections [24].

Through the molecular profiling and identification of multiple GBM subtypes, refinement and specific therapeutic targeting is ongoing to yield a deeper understanding of tumour biology and translation into a survival benefit for patients. Moreover, new targets are being pursued, specifically *IDH1* mutation [27], which may benefit a subpopulation of GBM patients. Clearly, GBM is a disease spectrum that requires personalising treatment management to improve the outcome of current standard treatments.

1.4.4 Treatment

Identifying beneficial life-prolonging therapies must be taken in the context of the patient population. Currently, there are several known prognostic factors that contribute to a survival advantage, which confound results evaluating the efficacy of therapies, therefore controlling these factors in clinical studies is essential. These include age, histological features, Karnofsky score, and incomplete tumour resection [28].

Although GBM commonly affects patients in their 5th and 6th decades of life, younger patients may also be affected. Age is an independent prognostic factor, whereby older

patients tend to survive shorter periods compared to younger patients [29, 30]. Additionally, the clinical neurological status of patients when first presenting with symptoms, determined by the Karnofsky scale, independently affects patient outcome. Simply put, patients with poor neurological function at presentation (i.e. loss of speech or motor function) would have a worse outcome compared to an aged-matched patient that is neurologically intact [29, 30]. However, interactions between these factors have been documented. For example, GBM patients older than 50 years would have a favourable outcome if their Karnofsky score was greater than 90 (a score of 100 is normal) [28].

Surgical resection has been shown to improve survival by approximately 5 months [31]. Importantly, in a study of 416 patients, a greater safe extent of resection (>98%) independently correlated with improved patient survival [32]. Since extent of resection may be described differently, an objective approach was applied in assessing the extent of resection. Using a fluorescent guided marker intra-operatively, 5-aminolevulinic acid (5-ALA), extent of resection was determined and shown to be an independent prognostic marker when taking into account potential treatment bias [33]. In a landmark paper in 2005, Stupp *et al.* demonstrated that combined radiotherapy and chemotherapy (TMZ) had a significant survival advantage compared to radiotherapy alone. The median survival increased by 2.5 months, while the 2-year survival increased by 16.1%. As a result, the Stupp protocol has become a standard treatment regimen in GBM management, consisting of radiotherapy at 60 gray (Gy) in 30 fractions, with a TMZ dose at 75 mg/m², followed by adjuvant TMZ at 150-200 mg/m² for six months [34]. Interestingly, silencing of the *MGMT* gene through methylation was shown to be a positive prognostic factor for patients receiving TMZ [35].

In an attempt to improve quality of life and survival, targeted therapies are being investigated to augment current treatment modalities. Unfortunately, most therapies have not successfully translated to the clinical setting, and only recently a single anti-angiogenic therapy is FDA approved for recurrent GBMs.

1.4.5 Tumour Angiogenesis

The concept of tumour-induced angiogenesis as a therapeutic target was proposed by Folkman in 1971 [36]. He recognised that for tumours to grow and metastasise, they would require the ability to produce their own vasculature stemming from existing vessels. The induction of angiogenesis was thought to originate through the activities of a diffusible factor; therefore, intense work in the 1970s and 1980s followed to identify and isolate these factors [37]. In 1983, vascular endothelial growth factor (VEGF) was discovered from ascites and conditioned media derived from a hepatocarcinoma cell line injected into guinea pigs, which was termed Vascular Permeability Factor (VPF) at the time, resulting in an increase in microvascular permeability [38]. In 1989, VEGF was independently discovered from conditioned media of pituitary follicular cells, resulting in a pro-proliferative effect on endothelial cells [39]. In the same year, it was identified that VPF and VEGF contain the same sequence, and are indeed the same growth factor. In 1997, a humanised anti-VEGF monoclonal antibody (bevacizumab) was developed [40]. Clinically, following positive clinical trials [41, 42], bevacizumab was approved for first line therapy in metastatic colorectal cancer in 2004. Since GBMs are characterised as highly vascular tumours, and neoplastic growth is maintained by acquiring new blood supply, the selection of an inhibitor to angiogenesis followed shortly. In recurrent GBM clinical trials, bevacizumab has increased progression free

survival, and the quality of life (QoL) for patients by reducing steroids required to manage tumour oedema [43, 44]. In 2009, bevacizumab was approved as a treatment in recurrent GBMs. However, recent trials of bevacizumab in primary GBM did not improve overall survival [45].

Although VEGF has been the mainstream anti-angiogenic target for tumours, a recent study, screening multiple angiogenic factors on a biomimetic *in vitro* angiogenesis model, identified VEGF and S1P as two critical factors for angiogenesis [46]. Of interest, cross-talk between VEGF and S1P was observed previously, whereby S1P activation of endothelial nitric oxide synthase (eNOS) involves transactivation of VEGFR-2 [47]. Moreover, VEGF potentiates S1P activation of eNOS through upregulating S1P₁ receptor expression [48]. Of note, S1P₁ receptor in endothelial cells is essential for stabilising blood vessels [49]. The interlink between VEGF and S1P, a soluble sphingolipid with versatile signalling properties, is only one of many features that make S1P, and sphingolipids, an important lipid family in disease modulation.

1.5 Sphingolipids

In 1884, Thudichum first described sphingolipids, naming them “Sphingosin” due to their enigmatic nature [50]. The sphingolipid pathway accounts for 1 of 6 major lipid-based families in mammalian cells [51]. Moreover, it has known structural and metabolic functions, including cell membrane organisation, activation of kinases, binding to G protein-coupled receptors (GPCRs), and modulation of transcription factors [52, 53]. Functionally, these lipids regulate cellular proliferation and migration, modulate inflammation, and support neovascularisation [53-55]. There are several sphingolipid hubs, as shown in Figure 1.2 below, with more than 300 distinct

metabolites. All hubs are interconnected in a complex network that recycles most metabolites through a 'salvage' pathway, with ceramide, sphingosine, and sphingosine-1-phosphate (S1P) as a central axis in the pathway.

The most abundant sphingolipid is sphingomyelin (SM), which is ubiquitously found at the plasma membrane, and accounts for approximately 10% of brain lipids [56], contributing significantly to myelin in white matter [57]. Ceramide, a bioactive metabolite, is synthesised through three routes: SM hydrolysis by sphingomyelinase (SMase), reacylating sphingosine by ceramide synthases (salvage pathway), or through serine and palmitoyl CoA formation (*de novo* synthesis). Within each sphingolipid hub, except for sphingosine and S1P, different acyl chain lengths are categorised as short chain (<C6), medium chain (C6-C12), long chain (C13-C21), and very long chain (C22>), which may be either unsaturated, double bonds between carbons (i.e. C=C), or saturated, single bonds between carbons (i.e. C-C). Basic illustrations of sphingolipid biochemical structures are outlined in Figure 1.3. The abundant mammalian sphingolipids are long chain and very long chain sphingolipids. Individually, sphingolipids are referred to by the number of carbon atoms forming the acyl chain length, such as C18 ceramide or C24 ceramide, which are formed by ceramide synthase 1 (CERS1) and ceramide synthase 2 (CERS2), respectively. The difference in acyl chain length translates to specific biological functions. For example, the specific loss of C18 ceramide observed in mice with *CERS1* mutations resulted in cerebellar ataxia and lipo-fusion accumulation [58]. In contrast, *CERS2* knockout mice resulted in a reduction of C24 ceramide, and biologically a loss of myelin and the development of hepatocarcinomas at 7 months [59]. Conversion of ceramide to other complex glycolipids, such as glucosylceramide (GlcCer) and galactosylceramide (GalCer), which

in turn can be converted to lactosylceramide (LacCer) and sulfatide, respectively, maintain the same carbon chain length. *CERS2* knockout mice with neurological deficits due to myelin degeneration have been attributed to a reduction in long chain GalCer and not just a loss of C24 ceramide [60]. This supports the notion that alteration of a specific sphingolipid can have downstream changes to other sphingolipids that is characterised as a loss or a compensatory gain, reflecting the interconnectedness of the sphingolipid pathway [53]. Importantly, each sphingolipid class contributes specific physiological functions, such as supporting angiogenesis for LacCer [61], stabilising myelination for sulfatide [62], or promoting migration for S1P [63, 64]. Moreover, the structural heterogeneity within a class of sphingolipids can exhibit different biological functions, and this will be discussed further within the ceramide family.

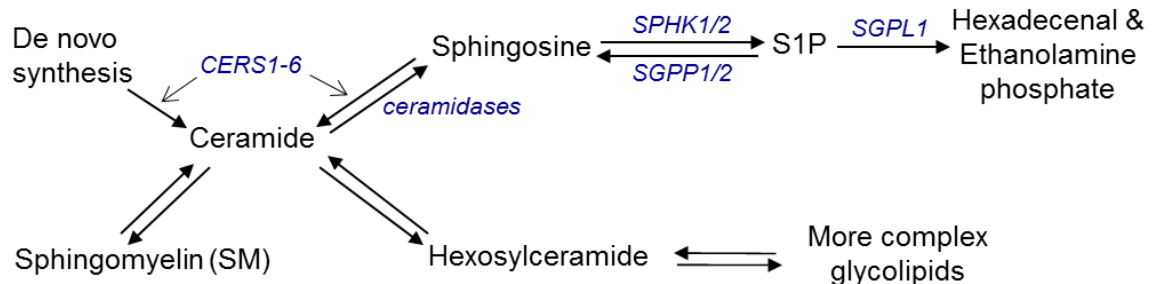


Figure 1.2 Schematic Diagram of the Sphingolipid Pathway

A basic outline of the relationship between the various sphingolipids, noting only a single entry point (*de novo* synthesis) and exit point (S1P catabolism by SGPL1) in the pathway. Metabolites are denoted in black, and enzymes forming the ceramide-S1P axis are in blue.

In addition to ceramide conversion back to SM, or glycosylation into GlcCer or GalCer, collectively referred to as hexosylceramide (HexCer), ceramide is converted to sphingosine through acidic, neutral, and alkaline ceramidases. Sphingosine, a monoacyl lipid, is the simplest functional sphingolipid structure [56]. As an intermediate

metabolite between ceramide and S1P, sphingosine has been shown to be a pro-apoptotic metabolite, although exogenous sphingosine *in vitro* does not produce an apoptotic response in all systems [65, 66]. Sphingosine is then recycled into ceramide through the activity of ceramide synthases 1-6 (CERS1-6), which are acyl chain length specific, or phosphorylated to S1P. Sphingosine kinase 1 (SPHK1) and 2 (SPHK2) are responsible for S1P formation, while sphingosine 1 phosphate phosphatases and lipid phosphate phosphatases dephosphorylate S1P to sphingosine. Alternatively, S1P is degraded irreversibly by S1P lyase (SGPL) into hexadecenal and ethanolamine phosphate, and is referred to as the only “exit” to the pathway.

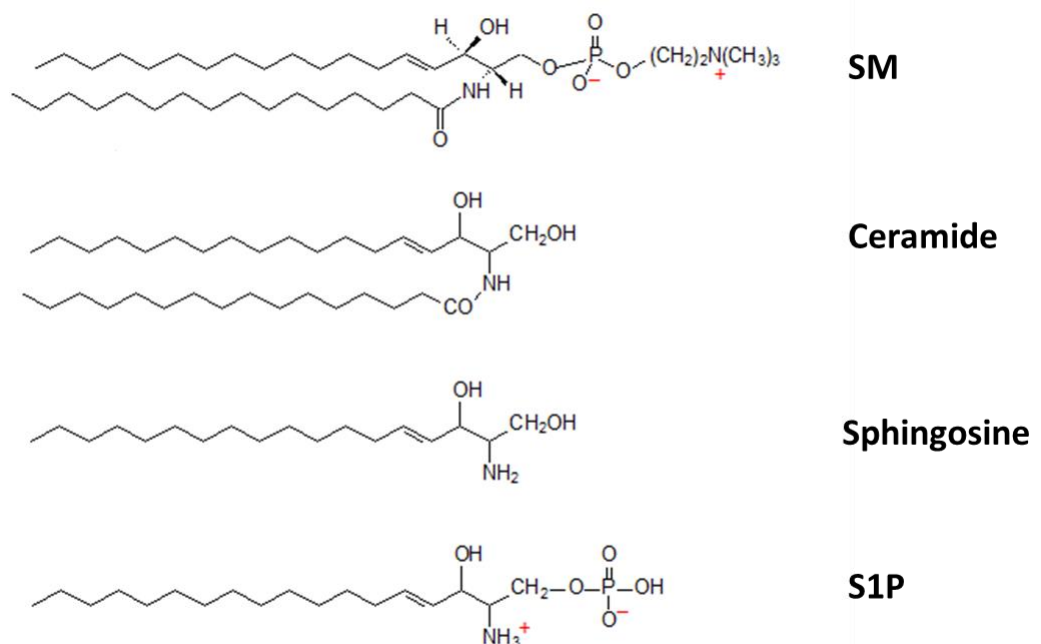


Figure 1.3 Basic Sphingolipid Structures

SM, ceramide, sphingosine, and S1P biochemical structures are depicted above (from the AOCs Lipid Library). Sphingosine is the simplest structure, forming the backbone for all sphingolipids. Both sphingosine and S1P are single molecular entities, while SM, ceramide, and other sphingolipids have varying fatty acid chain lengths, hence have multiple molecular entities [56].

1.5.1 Ceramide

Ceramide, an active sphingolipid mediator, plays a central role as a secondary messenger in cell growth arrest and apoptosis, in addition to cellular proliferation and differentiation. Moreover, ceramide has a unique characteristic in inducing plasma membrane structural changes as a result of its hydrophobicity, thereby altering signal transduction [67]. Since ceramide production impacts cellular fate, it is important to understand the formation and metabolism of this bioactive lipid. The synthesis of ceramides can occur in minutes by the catabolism of SM, whereby SMase is induced at the plasma membrane by a variety of stimuli. Alternatively, ceramide generation can occur over hours through a *de novo* process at the endoplasmic reticulum involving the condensation of serine and palmitoyl-CoA, leading to the generation of 3-ketosphinganine, then dihydrosphingosine, and finally dihydroceramide before conversion into ceramide [56, 68-72]. The pool of ceramide created from each pathway is distinct. Moreover, different stimuli activate each pathway. In general, the factors that produce cellular stress increase the production of ceramide. The *de novo* pathway, for example, upon activation by different chemotherapeutic agents, tumour necrosis factor- α (TNF α), hypoxia, or FAS/FAS ligand generates ceramide. The accumulated ceramide will lead to growth arrest at the G0/G1 phase, and apoptosis. Equally, the SM pathway is activated by chemotherapeutic agents, radiation (UV or γ), oxidative stress or inflammatory cytokines, resulting in rapid hydrolysis of SM at the plasma membrane to produce ceramide. The ceramide generated through the *de novo* pathway has a prolonged elevation compared to ceramide generated through the SM pathway [68, 71]. Furthermore, it has been illustrated in MCF-7 breast cancer cells that TNF α can activate both pathways independently [73]. Of note, although inflammatory cytokines, such as

TNF α , induce sphingomyelinase to increase ceramide levels, ceramidase activity is not increased; consequently downstream metabolites such as sphingosine and S1P are unchanged [74].

Ceramide, a neutral sphingolipid metabolite, has more than 50 distinct molecular species, including dihydroceramide, α -hydroxyceramide, and phytoceramide to name a few [53]. Additionally, different head groups may be added to give rise to more complex sphingolipids and glycosphingolipids. Ceramide itself plays an important role in the execution of cell death induced by radiotherapy, chemotherapeutics, lethal autophagy, or pro-apoptotic TNF family ligands [53, 75-77]. These pro-death functions of ceramide are mediated through direct binding to protein targets such as the tumour suppressor protein phosphatase 2A (PP2A) [78], Kinase Suppressor of Ras (KSR) [79], and autophagy protein LC3B-II [75]. Ceramides also play an essential role in neural stem cell differentiation, mediated via direct binding to the kinase PKC ζ [77].

Although ceramide has been shown to induce apoptosis [80], the premise that all ceramides produce a pro-apoptotic response is debatable. Ceramide chain lengths differ in physiological functions, as described above, but more importantly, specific chain lengths may produce opposing functions, such as C16 and C18 ceramide. C16 ceramide has been described to have both pro-apoptotic and anti-apoptotic properties. In prostate cancer cells, elevation of C16 ceramide correlated with a loss of mitochondrial mass and apoptosis following inhibition of acid ceramidase (ASAH1) with N-oleoylethanolamine (NOE) or serum deprivation [81]. However, C16 ceramide in squamous cell carcinomas protected against endoplasmic reticulum (ER) stress mediated apoptosis [82]. Furthermore, reducing C16 ceramide mediated an increase in activating

transcription factor 6 (ATF6) and Golgi fragmentation due to calcium release from the ER [83]. Clinically, elevated C16 ceramide levels correlated with positive lymph node for breast cancer, suggesting a role in metastasis [84]. In contrast, C18 ceramide mediated pro-apoptotic signalling in squamous cell carcinomas through activating caspase-3 and caspase-9, and reducing C18 ceramide prevented cellular apoptosis by 50% for cells treated with gemcitabine/doxorubicin [85]. Interestingly, head and neck squamous cell carcinomas (HNSCC) were screened for ceramide chain lengths using liquid chromatography tandem mass spectrometry (LC-MS/MS), and identified that C18 ceramide was specifically reduced in comparison to adjacent normal tissue [86].

Importantly, ceramide activity is opposed by downstream metabolites. In 1996, the first evidence for the rheostat balance between ceramide and S1P was shown in leukaemic cells [65]. As mentioned previously, ceramide accumulation can be triggered through Fas-ligand or TNF- α stimulation, which results in apoptosis via c-Jun amino-terminal kinase/stress-activated protein kinase (JNK/SAPK). In contrast, platelet-derived growth factor (PDGF), stimulating ceramidases and sphingosine kinases to yield S1P [74], or protein kinase C (PKC), stimulating sphingosine kinase to yield S1P [65], activates extracellular signal-regulated kinase (ERK) pathway. S1P induction of ERK successfully blocked JNK/SAPK activity, thereby preventing ceramide-induced apoptosis and producing a cytoprotective effect critical for cellular survival [65].

1.5.2 Sphingosine-1-Phosphate

S1P, an end metabolite of the sphingolipid cycle, has numerous physiological functions. As a pleiotropic secondary messenger, S1P has been shown to promote cell growth and survival, inhibit apoptosis, alongside modulating cellular migration and invasion. S1P

also plays a role in the angiogenic process through inducing endothelial cell migration, in addition to regulating the immune system via lymphocyte trafficking [55]. Crucially, S1P is an essential metabolite for vascular and neuronal development. S1P deficiency in mice, which require both SPHK1 and SPHK2 knockout, was embryonically lethal due to the development of intracranial haemorrhages, in addition to neural tube defects and disruption in neurogenesis [87]. These physiological roles, when applied to pathological conditions only further emphasize the importance of this small bioactive lipid molecule. Cancer, inflammation, and the metabolic syndrome are areas which S1P is currently being investigated, whereby the levels of this metabolite are elevated [72, 88].

The dual role, intracellular and extracellular, of S1P in signalling reflects its biological versatility. S1P is involved in intracellular signalling as a secondary messenger, and is also capable of extracellular signalling as it binds to GPCRs known as S1P₁₋₅. Sphingosine, located at the plasma membrane is converted to S1P through the activity of SPHK1 or SPHK2. S1P can then signal intracellularly and have a multitude of interactions. Equally, S1P can signal extracellularly through an ‘inside-out’ mechanism, whereby intracellular S1P is secreted via a transporter, thereby S1P can bind to its respective cell surface receptors or nearby cells and further propagate the signal in an autocrine or paracrine mode [55, 88]. The ATP-binding cassette (ABC) family has been implicated as the transporter involved in mediating release of intracellular S1P [89, 90]. Moreover, there are seven major subfamilies classed as ABCA to ABCG, each containing further subgroups, but only a few are related to the export of S1P, such as ABCA1 in astrocytes [91], along with ABCC1 and ABCG2 in breast cancer cells [92]. The ABC receptor is cell specific, and would have a varying

degree of efficiency, as has been illustrated between endothelial cells in comparison to fibroblasts and colon cancer cells [93, 94]. Of interest, circulating S1P found in plasma is more abundant than interstitial fluid, and a host of cells including platelets, red blood cells (RBCs), and the vascular endothelium all contribute to this phenomenon [93, 95, 96]. The differential gradient created has an impact on the trafficking of immune cells. Notably, S1P is degraded rapidly in plasma, with a 15 min half-life, and is inactive when bound to lipoproteins such as albumin or high density lipoprotein (HDL) [52, 88, 96], although mounting evidence suggests S1P bound to HDL is functionally active [97-99]. Of note, S1P bound to HDL increases its' half-life by four folds, hence protecting S1P from degradation and increases circulating S1P [88]. This interaction is currently being evaluated in the setting of atherosclerosis [88, 100, 101], but the impact on cancer regulation has not been defined.

Extracellular and intracellular S1P signalling is summarised in Figure 1.4 [102]. S1P is secreted through an efflux transporter, and binds with low nanomolar (nM) potency to S1P₁₋₅ receptors. The activation of specific receptors stimulates functional responses that potentiate cell characteristics or modulate neighbouring cells. For example, in the human GBM cell line U-373 MG, activation of S1P₁₋₃ receptors with 10nM of S1P resulted in an increase in cellular proliferation due to ERK2 stimulation [103]. Additionally, activation of S1P₁ and S1P₃ receptors in GBM cell lines with 10nM of S1P increased cellular motility via Rho and Rac signalling, while activation through S1P₂ reduced cellular motility through Rho activation, but increased cellular invasion through upregulating CCN1/Cyr61 [63, 104, 105]. The antagonistic effect of S1P₂ on motility and invasion was also confirmed in B16 melanoma cells [106, 107]. Moreover, inhibiting S1P₁ receptor with a small interfering RNA (siRNA) *in vivo* for Lewis lung

carcinoma cells significantly reduced tumour volume through reducing tumour-induced angiogenesis and vascular stabilisation [108]. Of note, S1P receptor distribution and expression is cell specific, therefore activation of a specific receptor does not induce the same physiological effect in all cells [64]. In contrast to the functional consequences of extracellular signalling, intracellular S1P signalling regulates various proteins to induce epigenetic changes, suppress apoptosis, control mitochondrial respiration, and influence inflammatory cascades [102]. For example, S1P regulates histone acetylation by binding to and inhibiting histone deacetylase 1 (HDAC1) and 2 (HDAC2) through SPHK2 activity, in turn, HDAC1/2 directly affects the transcription of cyclin-dependent kinase inhibitor p21 and c-fos [109]. The anti-apoptotic property of S1P is mediated through upregulating Bcl-2 and Mcl-1, and down regulating Bad and Bax [110-113]. Another intracellular target of S1P, Prohibitin 2 (PHB2), is localised at the mitochondria and regulates mitochondrial respiration. A reduction in S1P, through SPHK2 depletion, or the reduction in PHB2 affected mitochondrial respiration, which suggests an interaction between S1P and PHB2 is required for maintaining adequate mitochondrial functioning [114]. Recently, S1P has been shown to be a vital co-factor for activating NF- κ B by binding to TNF receptor-associated factor 2 (TRAF2) and resulting in RIP1 polyubiquitination, which is required to facilitate NF- κ B dimer release [115, 116]. NF- κ B downstream regulation influences the immune system and cellular fate [117], therefore S1P is implicated in contributing to inflammatory-based disease models. Finally, an important outcome for potentiating S1P signalling is to counteract the precursor metabolite [65, 118], ceramide, hence blocking apoptosis, autophagy, and senescence; all key pathways induced through ceramide accumulation, and thus creating a sustainable environment for cells to survive. Of note, not all S1P produced inhibits

ceramide accumulation. Intracellular ceramide in HEK 293 cells was reduced due to overexpression of SPHK1, which supports an anti-apoptotic effect. In contrast, intracellular ceramide was increased due to the overexpression of SPHK2, which supports a pro-apoptotic effect [119]. Of interest, exogenous S1P added to HEK 293 cells stimulated the incorporation of [3H] palmitate to form C16 ceramide specifically through the activity of SGPP1 and ceramide synthases, while the incorporation of L-3-[3H] serine formed longer chain ceramides through the de novo pathway [120], hence suggesting C16 ceramide formation is contributed to significantly through S1P recycling more so than the de novo process. However, S1P can act as an inhibitor to specific ceramide synthases (i.e. CERS2), albeit C16 ceramide is commonly produced through CERS5/6 and not CERS2 activity [121]. The tight regulation of ceramide and S1P is a complex process, and the outcome of cellular fate is likely to depend on a host of factors, including enzyme-mediated activation, specific chain length accumulation, and subcellular localisation.

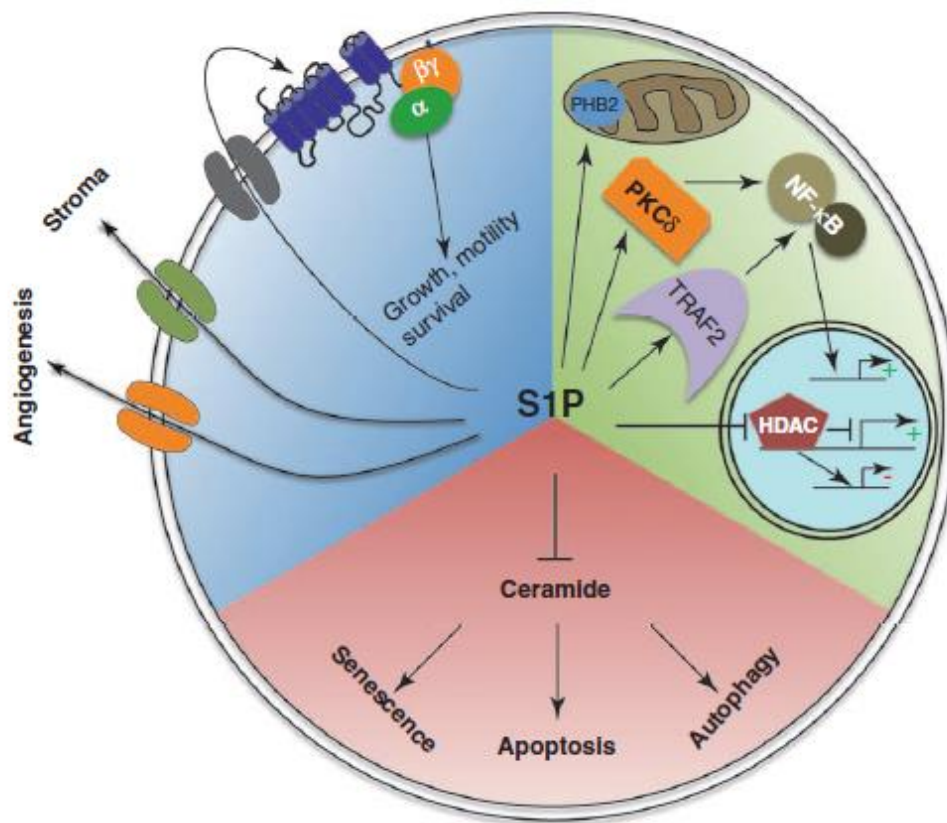


Figure 1.4 S1P Extracellular and Intracellular Signalling Targets

Schematic diagram illustrating S1P activity and targets (from Maceyka *et al.*). In blue, S1P extracellular signalling modulates the microenvironment in a paracrine mode, in addition to autocrine activity to promote cellular growth and migration. In green, S1P intracellular signalling affects mitochondrial metabolism, NF κ B pathway, and epigenetic regulation. In red, S1P intracellular signalling inhibits ceramide, therefore protects cells from senescence, apoptosis, and autophagy [102].

S1P signalling has pleiotropic effects as described earlier, though this is mediated through different enzymes associated with forming and degrading S1P, in addition to specific S1P receptor activation. The pathological effects of S1P will be addressed in the context of SPHK1, which has substantial sequence homology with SPHK2, but differs in subcellular localisation and tissue distribution [122, 123]. SPHK1, described previously, is located in the cytoplasm and when activated translocates to the plasma membrane to phosphorylate sphingosine to S1P [122].

Since the first study that illustrated SPHK1 overexpression results in normal fibroblasts acquiring an oncogenic phenotype and developed tumour *in vivo* [124], several studies followed linking an increase in SPHK1 expression with various malignancies. SPHK1 overexpression in cancer tissue was reported in breast [125, 126], lung [127, 128], colon [129, 130], head and neck [131, 132], and glioma [133, 134]. Clinically, SPHK1 overexpression correlated with a poor survival outcome in GBM [134], as well as in breast [126], lung [128], and gastric cancer [135]. More specifically, in relation to GBM, the increased expression correlated with an increase in glioma progression. The study examined more than 200 patient glioma tissue samples, and a direct correlation between SPHK1, at the mRNA and protein level, with tumour grade progression was identified. Moreover, the 3-year overall survival for patients with high SPHK1 expression amounted to 10.3%, in contrast with 57.7% survival for patients with low SPHK1 expression. The authors of the study further advocate that SPHK1 may potentially be a prognostic marker for all astrocytomas [133].

The impact of SPHK1 in oncogenesis has been further delineated in a knockout mouse model, in the setting of intestinal tumours, which revealed a significant reduction in colon cancer development and tumour size [129, 130]. Moreover, the actions of SPHK1 are not limited to promoting cell survival and growth, but seem to extend into evading apoptosis and regulating angiogenesis. The anti-apoptotic effect and therapeutic resistance via SPHK1 seems to occur through different mechanisms. In leukaemic cell lines, S1P and SPHK1 stimulation both inhibited cytochrome c and Smac/DIABLO translocation from the mitochondria, thereby inhibiting caspase-3 activation, and preventing apoptosis. Moreover, SPHK1 inhibition sensitised the cells to pro-apoptotic factors [136]. Additionally, in endothelial cell lines, overexpression of

SPHK1 resulted in activation of the PI3K/Akt pathway, accompanied with an increase in B cell lymphoma gene 2 (Bcl-2), an anti-apoptotic protein, and a decrease in Bcl-2 interacting mediator of cell death (Bim), a pro-apoptotic protein [137, 138]. In the setting of GBM, SPHK1 inhibitors were used to treat temozolomide (TMZ) resistant and sensitive cells, and although the study aimed to focus on the role of SPHK1 with TMZ resistance, it unexpectedly led to apoptosis in both groups via the activation of caspase-3 [139].

The angiogenic component of GBM cells is commonly present as microvascular proliferation, occurring frequently with central necrosis. In both the hypoxic conditions and pro-angiogenic state, SPHK1 is highly expressed. In hypoxia, which occurs in 50-60% of solid tumours, hypoxia inducible factor-1 (HIF-1) translocates to the nucleus and activates several targets promoting angiogenesis (e.g. VEGF) [140]. In glioma cell lines, SPHK1 was upregulated in hypoxic conditions as a function of HIF-2 α . In addition, HIF-2 α binds to SPHK1 promoter [141]. During angiogenesis, SPHK1 affects the endothelial cell migration and the subsequent stabilization, via junction assembly, of the newly formed vessels. Interestingly, conditioned media from hypoxic tumour cells induced angiogenesis in human umbilical vein endothelial cells (HUVEC) partly via S1P₁ receptor signalling [141]. The paracrine effect of SPHK1 mediating S1P formation, and not SPHK2, has been demonstrated in glioma and breast cancer cells, whereby a reduction in SPHK1 caused a reduction in secreted S1P and HUVEC tube formation [142]. Importantly, VEGF and VEGF-C silencing, did not attenuate the effect of tube formation driven by SPHK1 in glioma cells [142].

Therapies targeting SPHK1 or S1P have been developed and utilized pre-clinically, with significant *in vitro* and *in vivo* efficacy at inducing apoptosis, reducing proliferative and angiogenic potential. In glioma cell lines, a specific SPHK1 inhibitor (SK1-I) suppressed the growth, migration, and invasion of the cells. Moreover, SK1-I reduced the growth rate of GBM xenografts and enhanced survival [143]. A separate study examined apoptotic sensitivity for glioma cells following SPHK1 inhibition with a siRNA or inhibitor. The cells were sensitised *in vitro* and *in vivo*, partly through upregulating Bim, which was down regulated in SPHK1 overexpressing cells and tissue samples [144]. Under hypoxic conditions, upregulated SPHK1 in glioma cells induce proliferation through activating extracellular signal-regulated kinase (ERK), and SPHK1 inhibition resulted in reduced cell proliferation and attenuation of ERK [145]. In addition, a colorectal cancer model with resistance to cetuximab (an EGFR inhibitor), was partially sensitised to treatment following SPHK1 inhibition. High SPHK1 expression had also correlated with cetuximab resistance in tissue samples. Of clinical benefit, treatment with fingolimod, an oral drug approved for multiple sclerosis (MS), also sensitised the colorectal cells and improved survival outcome in tumour xenografts for cetuximab treatment [146]. Fingolimod, an S1P receptor antagonist, has also been shown to inhibit SPHK1 [147, 148]. In a GBM stem cell xenograft model, fingolimod has shown efficacy in reducing tumour growth, potentiating the effect of TMZ treatment, and increasing survival [149]. In lung cancer, fingolimod mediated tumour suppression *in vivo* partly through reactivating PP2A, a tumour suppressor enzyme, which was inactivated by inhibitor 2 of PP2A (I2PP2A/SET) [150].

SPHK1/S1P production systemically also plays an important role in promoting tumour progression and metastasis. In prostate cancer, *SPHK1*^{-/-} mice inhibited lung metastasis

through the activation of breast carcinoma metastasis suppressor 1 (Brms1). Furthermore, S1P inhibition with a monoclonal antibody (Sphingomab) inhibited lung metastasis, and knockdown of Brms1 blocked the effect of Sphingomab [151]. Sphingomab was also shown previously to inhibit VEGF-mediated angiogenesis and the release of pro-angiogenic cytokines in a panel of tumour cell lines [152]. Finally, in a murine model of breast cancer, SPHK1 inhibition with SK1-I reduced S1P levels, metastasis, and tumour burden. Of interest, S1P stimulated angiogenesis was inhibited both *in vitro* and *in vivo* with SK1-I treatment [153]. To conclude, SPHK1/S1P inhibition has positive therapeutic potential based on extensive preclinical testing.

1.6 Aims of Thesis

For more than 25 years several groups around the globe have been diligently delineating the importance of specific sphingolipids in cancer, yet an overview of sphingolipid changes has not been presented for any cancer. Therefore, the premise of my work begins with a basic yet fundamental question that remains unanswered until now: what are the levels of sphingolipids in normal brain tissue and glioma? What are the levels in plasma? Understanding the bigger picture and building a “roadmap” of changes in the sphingolipid pathway will assist in identifying therapeutic targets with functional relevance. By integrating sphingolipid levels in GBM with clinical and genetic factors, this thesis will provide a novel platform to assess the potential correlations between lipids and the expression of cancer driver mutations.

The specific aims of the thesis are:

1. To establish sphingolipid levels in normal grey matter (NGM), diffuse astrocytoma (AII), anaplastic astrocytoma (AIII), and glioblastoma (GBM) samples.
2. To identify potential sphingolipid targets, and examine the biological effect of their modulation in the context of proliferation, clonogenicity, and angiogenesis in GBM cells.
3. To correlate sphingolipid levels in GBM tissue to patient survival, genetic mutations, and MGMT methylation.
4. To compare sphingolipid levels in GBM plasma with normal plasma, GBM tissue with matched GBM plasma, and to correlate GBM plasma with patient survival.

Chapter 2: Methods

2.1 Introduction

This section will outline the methods applied throughout the thesis. Methods are presented in a similar order as they appear in Chapters 3, 4, and 5 where possible. Methods applied to later chapters are only described when they are first applied, including all variations of the method.

2.2 Clinical Samples

Fresh frozen tissue samples were obtained for diffuse astrocytoma (n=26), anaplastic astrocytoma (n=10), and GBM (n=20) samples from the Steve & Lynette Waugh Brain Tumour Bank. Normal grey matter (n=20) samples were obtained from the New South Wales Tissue Resource Centre, Australian Brain Bank Network (ABBN). The analysis and results for these samples are presented in Chapter 3.

Fresh frozen tissue samples were obtained for an independent primary GBM cohort (n=47) from the Australian Genomics and Clinical Outcomes of Glioma (AGOG), which included relevant clinical data. GBM plasma samples (n=47) were also obtained from AGOG, of which 43 were matched to tissue samples. Normal plasma samples (n=21) were obtained from the South Eastern Area Laboratory Services (SEALS), Haematology Department, Prince of Wales Hospital. The analysis and results for these samples are presented in Chapter 5.

All experiments conducted on clinical samples had the required ethics approval, **HREC reference number 10/174**, which was granted from the South Eastern Sydney Illawarra Area Health Service Human Research Ethics Committee.

2.3 Lipid Methods

2.3.1 Tissue Sample Preparation

All tissue samples (Chapter 3 and 5) used for sphingolipid or DNA extractions were prepared in the same manner. Appropriate protective equipment (lab coat, gloves, closed shoes, eye shield, and a face mask) were used during the tissue preparation, and performed in a biosafety cabinet. Samples were removed from the -80°C freezer and cut into small sections on dry ice, collecting approximately 20-30 mg per sample. Samples were placed in a pre-weighed and pre-labelled 1.5 ml Eppendorf tube, and crushed on dry ice using a micropestle (Eppendorf, Hamburg, Germany). Micropestles were decontaminated between samples in 1% sodium hypochlorite, washed in MilliQ water, and then 70% (v/v) ethanol. Samples were weighed again to record the accurate tissue weight prior to sphingolipid extraction. Sphingolipid levels measured were adjusted to the tissue weight, cell numbers, or plasma volume. Cell line preparation will be discussed in Cell Culture Methods (section 2.5). DNA extraction will be discussed in DNA Methods (section 2.6).

2.3.2 Sphingolipid Extraction

2.3.2.1 Tissue Samples and Cell Lines

Tissue samples or cell pellets stored at -80°C were slowly defrosted on ice. Extraction solution prepared, referred to herein as Solution 1, was composed of

isopropanol/water/ethyl acetate (30:10:60 v/v/v). Solution 1 was added to each sample at a total volume of 1.5 ml, and transferred to 16 x 125 mm borosilicate glass tubes with lids (Thermo Scientific, Waltham, MA, USA). Internal standards (ISTDs) were added at 50 μ l per sample, containing: C17 S1P, C17 ceramide, C17 sphingosine at concentrations of 1 μ M, in addition to C12 HexCer, C12 LacCer, C12 sulfatide at 5 μ M concentrations, and C17 SM at 25 μ M. Note, ISTDs are only added once during the first lipid extraction. Samples were vortexed and then sonicated (WUC-A10H, Thermoline Scientific, Australia) for 30 min at 38°C, which were repeated twice. Subsequently, samples were centrifuged (Megafuge 1.0R, Heraeus, Thermo Scientific, Waltham, MA, USA) at room temperature (4000 rpm, 10 min) and the supernatant was transferred using disposable glass pipettes into new 12 x 75 mm borosilicate glass tubes (Livingstone International Pty Ltd, Australia). The remaining residue was re-extracted again with 1 ml of Solution 1, followed by the same steps as above, but performed once only. The supernatants were combined for each sample and dried overnight using a speed vacuum (SC210 SpeedVac, Thermo Scientific, Waltham, MA, USA). The dry residues were reconstituted in a mobile phase (200 μ l) containing 1mM ammonium formate in methanol/milliQ water (80:20 v/v) with 0.2% formic acid. Samples were vortexed and centrifuged for 5 min at 3000 rpm, and the supernatant (150 μ l) was transferred to a liquid chromatography (LC) vial with a 300 μ l glass insert (03-FISV, Chromacol, Thermo Fisher, Waltham, MA, USA). Samples were stored at -20°C, or directly run for sphingolipid analysis. All organic solvents used were analytical grade (Merck KGaA, Darmstadt, Germany). Importantly, sphingolipid extraction was conducted in a fume hood with appropriate protective equipment as previously stated (no face mask required).

2.3.2.2 Plasma Samples

Plasma samples (250 µl) stored at -80°C were thawed on ice. RPMI 1640 media (Gibco®, Invitrogen, Life Technologies, CA, USA) was added to each sample to a total volume of 2 ml in a 16 x 125 mm borosilicate glass tube. Samples were then extracted with 2 ml of solution 2, which was composed of isopropanol/ethyl acetate (15:85 v/v). ISTDs (50 µl) were added per sample. Samples were vortexed well and centrifuged at 3000 rpm for 15 min to separate the phases. The upper organic phase was transferred into a new 12 x 75 mm borosilicate glass tube, and the remaining lower aqueous phase was acidified with 100 µl of formic acid (98%) and re-extracted with another 2 ml of solution 2. Samples were vortexed and centrifuged as described previously. The supernatants were combined with the first extract, dried overnight and reconstituted as per the sphingolipid tissue sample extraction (section 2.3.2.1).

2.3.3 Liquid Chromatography Mass Spectrometry

Liquid Chromatography tandem Mass Spectrometry (LC-MS/MS) was performed on a triple quadrupole mass spectrometer, TSQ Quantum Access (Thermo Scientific, Waltham, MA, USA), with an electrospray ionisation (ESI) source, run in positive ion mode at the Bioanalytical Mass Spectrometry Facility (BMSF, UNSW). Samples were separated using an Eclipse XDB-C8 column with a 5 µm particle size (Agilent Technologies Australia Pty Ltd, Australia). The liquid chromatography and sampling injection used the Accela™ UPLC system (Thermo Scientific, Waltham, MA, USA), at a flow rate of 500 ml/min with mobile phase A and B. Mobile phase A contained 2 mM ammonium formate in water with 0.2% formic acid, and mobile phase B contained 1

mM ammonium formate in methanol with 0.2% formic acid. The chromatography gradient was: 0 min 20:80 A/B, 7 min 13:87 A/B, 14 min 0:100 A/B; 28 min 0:100 A/B; and 30 min 20:80 A/B. Injections of 20 µl were used for all samples, blanks, and external standards (ESTDs). The ESTD curve covered the following concentrations in a serial dilution: 8000 nM, 4000 nM, 2000 nM, 500 nM, 125 nM, 32 nM, 8 nM, and 2 nM. All ISTDs and ESTDs were purchased from the distributor Auspep Pty. Ltd., Australia (Avanti Polar Lipids, Inc., Alabaster, AL, USA). Table 2.1 below contains the parameters for the sphingolipids analysed in the LC-MS/MS run. ISTDs are highlighted in blue, and were used for assessing the extraction efficiency for their respective sphingolipid class only. In bold are the commercial ESTDs, which were used for quantification. For sphingolipids with no commercial ESTD, the nearest chain length ESTD was used to quantify those sphingolipids. Visualisation and quantification of peaks was performed using the XCalibur software 2.0.7 (Thermo Scientific, Waltham, MA, USA) and Metabolite Mass Spectrometry Analysis Tool (MMSAT) as described previously [154, 155].

Table 2.1 Sphingolipids Parameter Settings on the LC-MS/MS

Sphingolipid	Parent Mass (m/z)	Fragment Mass (m/z)	Collision Energy (eV)	Retention Time (min)
C17_Sphingosine	286.1	268	17	2.603
Sphingosine	300.2	264.1	18	2.959
C17_S1P	366.1	250.1	23	3.728
S1P	380.1	264.1	23	4.465
C14_Cer	510.6	264.1	24	14.938

C16_Cer	538.6	264.1	30	15.864
C17_Cer	552.7	264.1	30	16.300
C18:1_Cer	564.6	264.1	30	16.175
C18_Cer	566.7	264.1	30	16.783
C20:1_Cer	592.7	264.1	30	17.105
C20_Cer	594.7	264.1	30	17.847
C22:1_Cer	620.7	264.1	30	18.159
C22_Cer	622.7	264.1	30	19.143
C23:1_Cer	634.7	264.1	30	18.807
C23_Cer	636.7	264.1	30	19.873
C24:1_Cer	648.8	264.1	30	19.448
C24_Cer	650.8	264.1	30	20.689
C25:1_Cer	662.8	264.1	30	20.194
C25_Cer	664.8	264.1	30	21.537
C26:1_Cer	676.8	264.1	30	21.021
C26_Cer	678.8	264.1	30	22.370
C12_Sulfatide	724.5	264.1	40	12.118
C14_Sulfatide	752.5	264.1	40	13.466
C16_Sulfatide	780.5	264.1	40	14.315
C18:1_Sulfatide	806.6	264.1	40	14.379
C18_Sulfatide	808.6	264.1	40	15.232
C20_Sulfatide	836.6	264.1	40	16.028
C22:1_Sulfatide	862.6	264.1	40	16.236
C22_Sulfatide	864.6	264.1	40	16.921

C23:1_Sulfatide	876.6	264.1	40	16.665
C23_Sulfatide	878.6	264.1	40	17.414
C24:1_Sulfatide	890.6	264.1	40	17.047
C24_Sulfatide	892.6	264.1	40	17.912
C25:1_Sulfatide	904.6	264.1	40	17.561
C25_Sulfatide	906.6	264.1	40	18.492
C26:1_Sulfatide	918.6	264.1	40	18.088
C26_Sulfatide	920.6	264.1	40	19.120
C18_Sulfatide_OH	824.6	264.1	40	14.880
C22:1_Sulfatide_OH	878.6	264.1	40	15.956
C22_Sulfatide_OH	880.6	264.1	40	16.657
C23_Sulfatide_OH	894.6	264.1	40	17.078
C24:1_Sulfatide_OH	906.6	264.1	40	16.811
C24_Sulfatide_OH	908.6	264.1	40	17.602
C25:1_Sulfatide_OH	920.6	264.1	40	17.248
C25_Sulfatide_OH	922.6	264.1	40	18.041
C26:1_Sulfatide_OH	934.6	264.1	40	17.769
C12_LacCer	806.6	264.1	40	12.391
C16_LacCer	862.6	264.1	40	14.529
C18_LacCer	890.6	264.1	40	15.496
C24:1_LacCer	972.6	264.1	40	17.370
C24_LacCer	974.6	264.1	40	18.255
C25:1_LacCer	986.6	264.1	40	17.911
C25_LacCer	988.6	264.1	40	18.856

C26:1_LacCer	1000.6	264.1	40	18.470
C12_HexCer	644.6	264.1	35	12.855
C14_HexCer	672.7	264.1	35	13.991
C16_HexCer	700.7	264.1	35	15.005
C18:1_HexCer	726.7	264.1	35	15.361
C18_HexCer	728.7	264.1	35	15.931
C20:1_HexCer	754.7	264.1	35	16.133
C20_HexCer	756.7	264.1	35	16.747
C22:1_HexCer	782.7	264.1	35	16.982
C22_HexCer	784.7	264.1	35	17.752
C23:1_HexCer	796.7	264.1	35	17.497
C23_HexCer	798.7	264.1	35	18.324
C24:2_HexCer	808.6	264.1	40	17.262
C24:1_HexCer	810.8	264.1	35	17.976
C24_HexCer	812.7	264.1	35	18.963
C25:1_HexCer	824.6	264.1	40	18.584
C25_HexCer	826.8	264.1	35	19.646
C26:2_HexCer	836.6	264.1	40	18.412
C26:1_HexCer	838.8	264.1	35	19.231
C26_HexCer	840.8	264.1	35	20.400
C18_HexCer_OH	744.7	264.1	35	15.571
C20_HexCer_OH	772.7	264.1	35	16.441
C22:1_HexCer_OH	798.7	264.1	35	16.690
C22_HexCer_OH	800.7	264.1	35	17.360

C23:1_HexCer_OH	812.7	264.1	35	17.390
C23_HexCer_OH	814.7	264.1	35	17.950
C24:1_HexCer_OH	826.8	264.1	35	17.869
C24_HexCer_OH	828.8	264.1	35	18.494
C25:1_HexCer_OH	840.8	264.1	35	18.456
C25_HexCer_OH	842.8	264.1	35	19.275
C26:1_HexCer_OH	854.8	264.1	35	18.865
C26_HexCer_OH	856.8	264.1	35	19.959
C12_SM	647.5	184.0	35	13.178
C14_SM	675.5	184.0	35	14.329
C16:1_SM	701.6	184.0	35	14.625
C16_SM	703.6	184.0	35	15.321
C18:1_SM	729.6	184.0	35	15.607
C18_SM	731.6	184.0	35	16.195
C20:1_SM	757.6	184.0	35	16.497
C20_SM	759.6	184.0	35	17.203
C22:1_SM	785.6	184.0	35	17.515
C22_SM	787.6	184.0	35	18.335
C23:1_SM	799.6	184.0	35	17.938
C23_SM	801.6	184.0	35	19.010
C24:1_SM	813.7	184.0	35	18.553
C24_SM	815.7	184.0	35	19.610
C25:1_SM	827.7	184.0	35	19.257
C25_SM	829.7	184.0	35	20.393

C26:1_SM	841.7	184.0	35	20.011
----------	-------	-------	----	--------

Abbreviations: S1P – sphingosine-1-phosphate, Cer – ceramide, OH – hydroxylated, HexCer – hexosylceramide, LacCer – lactosylceramide, SM – sphingomyelin.

2.4 RNA Methods

All equipment and workspace was cleaned with RNaseZap® (Invitrogen, Life Technologies, CA, USA) prior to any RNA work. RNA methods described below relate to Chapter 3 (tissue work) and Chapter 4 (cell line work).

2.4.1 RNA Extraction

RNA extraction was performed using a commercial kit (RNeasy® Mini Kit, Qiagen, Hilden, Germany). Steps described are as per the manufacturer's protocol. Tissue samples and cell pellets stored at -80°C were gently thawed on ice.

For tissue extractions, 20-30 mg of tissue was used, requiring 600 µl of Buffer RLT after homogenising each sample as described in section 2.3.1. Samples with Buffer RLT were transferred to a QIAshredder homogeniser and centrifuged at full speed for 2 min. The lysate was centrifuged for 3 min at full speed, and the supernatant was transferred to a new 1.5 ml Eppendorf tube for further RNA extraction. An equal volume of 70% (v/v) ethanol was added to each sample and mixed by pipetting several times. The mixed sample was added onto an RNeasy spin column with a 2 ml collection tube, then centrifuged at $\geq 10,000$ rpm for 15 sec. The flow-through in the collection tube was discarded and 700 µl of Buffer RW1 was added to the spin column. Samples were centrifuged at $\geq 10,000$ rpm for 15 sec to wash the column membrane. The flow-through was discarded. Subsequently, 500 µl of Buffer RPE was added to the

spin column and centrifuged as previously mentioned. The flow-through was discarded and the step was repeated, but the centrifuge component was set at $\geq 10,000$ rpm for 2 min. The collection tube used for each spin column was replaced with a new 2ml collection tube, and placed in the centrifuge for 1 min at full speed. The spin column was then placed in a new 1.5 ml collection tube, and 30 μ l of RNase-free water was added directly to the spin column membrane. Each sample was centrifuged at $\geq 10,000$ rpm for 1 min. The eluted RNA collected in the 1.5 ml collection tube was quantified using the NanoDrop® ND-1000 spectrophotometer (Thermo Fisher Scientific, Wilmington, DE, USA).

For cell lines, 350 μ l of Buffer RLT was used for the RNA extraction. If cells were more than 5×10^6 , then 600 μ l of Buffer RLT was added instead. A mixture of β -mercaptoethanol (β -ME, Sigma-Aldrich, St. Louis, MO, USA) and Buffer RLT was made using a ratio of 10 μ l of β -ME per 1 ml of Buffer RLT. An equal volume of the mixture was added to the Buffer RLT with the sample. Samples were homogenized by vortexing. An equivalent amount of 70% ethanol (350 μ l or 600 μ l) was added to each sample and mixed by pipetting several times. The extraction steps followed the same steps as the tissue extraction at this stage.

2.4.2 RNA Quantification

RNA was quantified and assessed for quality with the NanoDrop® spectrophotometer. First, 2 μ l of nuclease-free water (Ambion®, Life Technologies, CA, USA) was used as a blank. Samples, at 2 μ l volumes, were then measured at an absorbance of 260 and 280 nm. A ratio greater than 2.0 for the 260/280 ratio, indicating RNA purity, was used as a cut-off for further sample processing. Lower ratios indicated potential contamination

with protein, phenol or other substances. Therefore, samples were treated with Lithium Chloride (LiCl) (described in detail in 2.4.3) and measured again using the NanoDrop®. RNA samples were equalised to 250 ng/µl, then stored at -80°C. Nuclease-free water was used to dilute the concentrated RNA samples.

2.4.3 LiCl Precipitation of RNA

Total RNA extracted, as described in section 2.4.1, was mixed with LiCl (Ambion®, Life Technologies, CA, USA) to a final concentration of 2.5 mol/l. Samples were vortexed and incubated for 2 h at -20°C. Thereafter, samples were centrifuged at 4°C, 12,000 rpm, for 10 min. The supernatants were discarded, and 1 ml of 75% ethanol (v/v) was added to each pellet and vortexed. This was repeated (centrifuge, discard supernatant, and add ethanol). Samples were centrifuged and the ethanol was discarded, but the pellet was air dried for 1-2 min to insure ethanol evaporation. The pellet was dissolved in nuclease-free water and the RNA was quantified again with the NanoDrop® as described in section 2.4.2.

2.4.4 Synthesis of cDNA

Equalised RNA samples at 250 ng/µl were converted to cDNA using the SuperScript™ III First-Strand Synthesis System (Invitrogen, Life Technologies, CA, USA). Each component, in addition to the RNA samples, were thawed on ice, mixed, and centrifuged briefly. Each RNA sample (1 µl) was added to the following mixture: 50 ng/µl Random Hexamers (1 µl), 10 mM dNTP mix (1 µl), and nuclease-free water (7 µl). The new mixture was incubated in the thermal cycler (S1000™, Bio-Rad, CA, USA) at 65°C for 5 min, followed by 1 min on ice before adding the cDNA Synthesis

Mix (10 µl) to each sample. The cDNA Synthesis Mix contains: 10X RT buffer (2 µl), 25 mM MgCl₂ (4 µl), 0.1 M DTT (2 µl), 40 U/µl RNaseOUT™ (1 µl), and 200 U/µl SuperScript™ III RT (1 µl). The new RNA mixture of 20 µl was mixed and centrifuged briefly before incubation in the thermal cycler. An RT control, with 1 µl of nuclease-free water instead of SuperScript™ III was added for cDNA synthesis. The cycling conditions were 10 min at 25°C, then 50 min at 50°C, and finally 85°C for 5 min. Samples were chilled on ice and diluted (1:10) with nuclease-free water prior to storage at -80°C.

2.4.5 Quantitative Real Time – Polymerase Chain Reaction (qRT-PCR)

The total RNA converted to cDNA was 250 ng / 20 µl (12.5 ng/µl). Samples dilution (1:10) produced a concentration of 1.25 ng/µl. Input cDNA for both tissue and cell line qRT-PCR was 5 ng (4 µl per well) in a MicroAmp™ Optical 96-Well Reaction Plate (Applied Biosystems, Life Technologies, CA, USA).

Taqman® and SYBR® Green chemistries were used for the tissue sample analysis in Chapter 3. Setup for the 96-well plate was done using an automated pipetting system, epMotion 5075 (Eppendorf, Hamburg, Germany), which dispensed 5 ng cDNA template, followed by a 16 µl mixture of Taqman® or SYBR® Green chemistry into each well. The Taqman® chemistry mixture contained: 1 µl Taqman® probe (Applied Biosystems, Life Technologies, CA, USA), 10 µl Taqman® Gene Expression Master Mix (Applied Biosystems, Life Technologies, CA, USA), and 5 µl nuclease-free water. The SYBR® Green chemistry mixture contained: 0.3 µl forward primer, 0.3 µl reverse

primer, 10 µl SensiFAST SYBR Lo-ROX (Bioline Australia Pty. Ltd, Australia), and 5.4 µl nuclease-free water.

An optical sealant was applied to each 96-well plate. The plate was mixed for 30 sec on the MixMate (Eppendorf, Hamburg, Germany), and briefly centrifuged (Centrifuge 5804 R, Eppendorf, Hamburg, Germany) prior to starting a qRT-PCR run. Taqman® probes were run on the ABI 7900HT platform (Applied Biosystems, Life Technologies, CA, USA) using standard run parameters. SYBR® Green probes were run on the Stratagene Mx3005P platform (Agilent Technologies, Santa Clara, CA, USA) using the following cycling parameters: 95°C for 15 sec, 62°C for 30 sec, and 72°C for 45 sec; 40 cycles in total. SYBR® Green probes were assessed with a melt curve analysis at the end of the run. A cDNA standard curve was setup on all plates; hence absolute gene expression was quantified and adjusted to each house keeping gene (18S and GAPDH) separately. Each probe was repeated twice for all samples.

Table 2.2 Taqman® Probes for qRT-PCR

CERS1: Hs04195319_s1	CERS2: Hs00371958_g1	CERS4: Hs00226114_m1
UGCG: Hs00234293_m1	ACER2: Hs01892094_g1	ACER3: Hs00218034_m1
ASAH1: Hs00602774_m1	ASAH2: Hs01015655_m1	SGPL1: Hs00900722_m1
SGPP1: Hs00229266_m1	SGPP2: Hs00544786_m1	SPHK1: Hs00184211_m1
SPHK2: Hs00219999_m1	GAPDH: Hs03929097_g1	18S rRNA: 4319413E-0909046

Table 2.3 SYBR® Green Primers for qRT-PCR

CERS1 forward: GCT ACA GTG CCT ACC TGC TGT TT
CERS1 reverse: TAG GAG GAG ACG ATG AGG ATG AG
CERS2 forward: TTC TGG TGG GAA CGT CTG TG

CERS2 reverse: GCC ACG TAC AGC TCA AAG AAG
CERS5 forward: AGA TTT CTC TGG TCG TCA CCT TG
CERS5 reverse: AGG AGA AGG AGA TAA GCC CAA TG
CERS6 forward: TCA TGA TTC AGC TGA TGC TCT TC
CERS6 reverse: CTC CCA GCT TTC AAA TAA TGT GG
SPHK1 forward: AGG CTG AAA TCT CCT TCA CGC
SPHK1 reverse: GTC TCC AGA CAT GAC CAC CAG
SPHK2 forward: GCT GCT GCG CCT TTT CTT G
SPHK2 reverse: CCT GTA GCG GCC CAT ACT C
GAPDH forward: TGT TGC CAT CAA TGA CCC CTT
GAPDH reverse: CTC CAC GAC GTA CTC AGC G
18S rRNA forward: GTA ACC CGT TGA ACC CCA TT
18S rRNA reverse: CCA TCC AAT CGG TAG TAG CG

Cell line cDNA, which was assessed in Chapter 4.2.2-4.2.3, was run using Taqman® chemistry only. The parameter setup was similar to tissue sample qRT-PCR, except that cell line samples were pipetted manually, were run on the ViiA™ 7 platform (Applied Biosystems, Life Technologies, CA, USA), and relative quantification was performed using the ViiA™ 7 software.

2.5 Cell Culture Methods

2.5.1 Cell Culture Conditions

The human GBM cell line, U87-MG (American Type Culture Collection) was cultured in minimum essential medium (MEM), supplemented with 10% fetal bovine serum (FBS) and 2 mM L-glutamine, in a humidified atmosphere with 5% CO² at 37°C. Cells were passaged as they near confluence. Cells were washed with phosphate buffered saline (PBS), and then cells were detached with a mixture of trypsin (2.5 mg/ml) and

ethylenediaminetetraacetic acid (EDTA; 1 mg/ml). U87MG culture media was used to neutralise the trypsin-EDTA (Sigma-Aldrich, St. Louis, MO, USA). Cells were centrifuged at 1000 rpm for 5 min, and resuspended in fresh culture media for plating.

RN1, a patient derived glioma cell line kindly supplied by the Boyd Laboratory [156], QIMR was cultured in Neurobasal™ A Medium with Advanced DMEM/F12 (1:1), supplemented with 2 mM L-glutamine, B27 supplement, 20 ng/ml beta fibroblast growth factor (bFGF) and 20 ng/ml epidermal growth factor (EGF) [157]. Cell culture flasks and plates were pre-coated with matrigel (1:100 dilution in PBS). Cells were passaged as described for U87MG cells, but with accutase (Sigma-Aldrich, St. Louis, MO, USA) instead of Trypsin-EDTA. Accutase was neutralised with trypsin inhibitor (Sigma-Aldrich, St. Louis, MO, USA).

The Human Microvascular Endothelial Cell line (HMEC-1) was cultured in MCDB 131 medium (Gibco®, Life Technologies, CA, USA), supplemented with 10% FBS, 5 U/ml penicillin/streptomycin, 2 mM L-glutamine, 10 ng/ml EGF, and 1 µg/ml hydrocortisone (Sigma-Aldrich, St. Louis, MO, USA). Cells were passaged as per U87MG cells.

Cell counting for determining seeding density, or cell numbers for lipid extraction, was performed using 2 x 10⁶ µl cell suspensions for each sample. Each 10 µl suspension was mixed with 10 µl of trypan blue. From the mixture, 10 µl was placed on a disposable haemocytometer. Cells were counted using the Countess® Automated Cell Counter (Invitrogen, Life Technologies, CA, USA).

Cell culture reagents were purchased from Life Technologies Australia Pty. Ltd., Australia. Growth factors were purchased from Sigma-Aldrich, St. Louis, MO, USA.

Matrigel was purchased from BD Biosciences, Franklin Lakes, NJ, USA. Tissue culture flasks and plates were purchased from Nunc, Thermo Fisher Scientific Australia Pty. Ltd., Australia. Cell culture work was performed aseptically in a Class II Biosafety Cabinet. All cells were regularly tested for Mycoplasma, which was not present in our cell lines.

2.5.2 Small Interfering RNA (siRNA) Transfections

Transfections with ASAHI and SPHK1 siRNAs were carried out for U87MG and RN1 cell lines to assess gene silencing and effect on sphingolipid levels (Chapter 4.2.3), along with functional consequences (Chapter 4.2.4). The ASAHI siRNA, s498 (Ambion®, Life Technologies Australia Pty. Ltd., Australia), the SPHK1 siRNA, Hs_SPHK1_6 (Qiagen Australia Pty. Ltd., Australia), and a non-targeting negative control siRNA, *Silencer*® Select Negative Control No. 1 (Ambion®, Life Technologies Australia Pty. Ltd., Australia) were utilised for those experiments.

U87MG cells were plated 12-16 h prior to siRNA transfection with Lipofectamine 2000 (Invitrogen, Life Technologies Australia Pty. Ltd., Australia). Lipofectamine was diluted (1:100) in Opti-MEM® (Invitrogen, Life Technologies Australia Pty. Ltd., Australia) and combined with the siRNA. The mixture was briefly vortexed and incubated at room temperature for 30 min. U87MG standard media was washed and replaced with Opti-MEM®, and then the siRNA mixture was added to each well at a concentration of 50 nM. The siRNA transfection mixture was replaced after 6 h with MEM (10% FBS and 2mM L-glutamine). Transfection efficiency for U87MG cells was confirmed (seeding density: 7×10^4 cells/well on a 6-well plate) with qRT-PCR at 48 h, and following a time course as presented in Chapter 4.2.3. Moreover, cells were

seeded on 10 cm dishes at a density of 1×10^6 cells/dish for 72 h to identify the sphingolipid changes as presented in Chapter 4.2.3.

RN1 cells were transfected with Lipofectamine as well, but in suspension, as transfections on matrigel were not efficient. Additionally, the siRNA transfection mixture was halved; therefore the incubation of RN1 cells with the mixture was at a concentration of 25 nM. Following 30 min incubation, RN1 cells were seeded onto pre-coated matrigel wells. Transfection efficiency for RN1 cells was confirmed (seeding density: 5×10^4 cells/well on a 6-well plate) with qRT-PCR at 72 h.

2.5.3 Drug Treatments

Dimethyl sulfoxide (DMSO, Sigma-Aldrich, St. Louis, MO, USA), SKI-1a (potent SPHK1 inhibitor), and SKI-1b (stereoisomer control for SKI-1a) examined the effect of specific SPHK1 inhibition on sphingolipid levels, cell proliferation, and angiogenesis *in vitro*. The SPHK1 inhibitors (SphynKx Therapeutics LLC, University of Virginia, Charlottesville, VA, USA) were prepared in DMSO; therefore DMSO was the vehicle control in all experiments. U87MG cell density for sphingolipid level assessment was 1×10^6 cells / 10 cm dish for a 72 h time course. Cell counting (section 2.5.1), sphingolipid extraction (section 2.3.2.1), and analysis (2.3.3) were described previously. Seeding densities for the cell proliferation assay (section 2.5.4) and angiogenesis assay (section 2.5.7) are detailed below. Drug concentrations are presented in Chapter 4.2.5-4.2.7.

2.5.4 MTT Assay

The MTT assay was used to assess cellular proliferation for the SPHK1 drug inhibition experiments in U87MG, RN1, and HMEC-1 cell lines. Cells were seeded (500 cells/well) onto a 96-well plate in quadruplicate as per standard culture conditions, and allowed to settle for 24 h prior to the addition of vehicle control (DMSO) or drugs (SKI-1a and SKI-1b) at various concentrations as indicated in Chapter 4.2.6. Surrounding wells were loaded with 200 μ l of PBS to reduce medium evaporation from treatment wells. Media and drug treatments were replaced every 48 h. On day 7 from treatment, cells were incubated for 2 h with 10 μ l of 5 mg/mL MTT (Sigma-Aldrich Pty. Ltd., Australia) in PBS. Formation of MTT formazan crystals (blue) was observed under a light microscope (CKX41 Olympus, Olympus Australia Pty. Ltd., Olympus Corporation, Tokyo, Japan). Subsequently, 100 μ l of 100 mg/mL sodium dodecyl sulfate (SDS) / 10 mM HCl was added to each well. Wells were mixed on a plate shaker for 6 h to dissolve the crystals, and absorbance was measured at 570 nm using a spectraMAX 190 absorbance microplate reader (Molecular Devices, Sunnyvale, CA, USA). Blank wells with media only were used to subtract the cell culture media background.

2.5.5 Flow Cytometry

Flow cytometry was used to assess cellular proliferation for the siRNA experiments (Chapter 4.2.4). Cells (U87MG and RN1) were siRNA transfected and cultured in 24-well plates as previously described (section 2.5.1 and 2.5.2). U87MG cells were seeded at 1.25×10^4 cells/well and collected after 96 h. U87MG cells were detached with 150 μ l of trypsin-EDTA in PBS, and neutralised with 300 μ l of MEM (10% FBS and 2 mM

L-glutamine). RN1 cells were seeded at 1×10^4 cells/well and collected after 10 days. RN1 cells were detached with 150 μ l of accutase, and neutralised with 300 μ l of trypsin inhibitor. Cells were centrifuged at 1000 rpm for 5 min, and then washed in 500 μ l of PBS. Cells were resuspended in 300 μ l of 2 μ g/ml propidium iodide (PI, Invitrogen Australia Pty. Ltd., Australia) in PBS for 10 min on ice. A positive PI control (cells treated with 5 μ M staurosporine) was also used. Cell counting and PI staining were determined on a BD FACSCanto™ II flow cytometer (BD Biosciences, Franklin Lakes, NJ, USA). Cell counting was performed over a 30 sec collection period, and at a constant high flow rate. PI staining analysis (positive = dead cells, negative = alive cells) was performed on the FlowJo software (TreeStar Inc., USA).

2.5.6 Clonogenic Assay

Clonogenicity was measured by seeding RN1 cells (5000 cells/well) post siRNA transfection in 6-well plates, which were pre-coated with matrigel. Cell culture media was replaced every 96 h. Following 14 days, cells were fixed with 4% paraformaldehyde. Each well was washed gently with PBS, and stained with 0.5% crystal violet (Sigma-Aldrich, St. Louis, MO, USA) at 500 μ l/well, and placed for 30 min on a plate shaker. Crystal violet staining was washed twice with PBS. Colonies were counted using ImageJ 1.46 image analysis software (NIH, USA).

2.5.7 Angiogenesis Assay

The angiogenesis assay assessed the effect of siRNA (Chapter 4.2.4) and SPHK1 drug treatments (Chapter 4.2.7) on U87MG cells inducing HMEC-1 sprout formation as shown in Figure 2.1. The 3D fibrin gel co-culture model has been established

previously [158]. Briefly, near confluent HMEC-1 cells were incubated with Cytodex™ 3 microcarrier beads (GE Healthcare, Buckinghamshire, UK) for 72 h. Following the 72 h incubation, the fibrin gel was setup. Fibrinogen (Sigma-Aldrich, St Louis, MO, USA) was mixed with 2 ml of saline (10 mg/ml) for 30 min at 37°C. DMEM media (5 ml) with no phenol red (Invitrogen, Life Technologies, CA, USA) was mixed with the fibrinogen, the solution pH was adjusted to 7.6 (+/-0.05), and then filtered through a 0.2 µm filter (Millex®-GP, Millipore Ireland Ltd., Tullagreen, Co. Cork, Ireland). Microcarriers were detached by manually shaking the HMEC-1 culture flask, washed twice with PBS adjusted to pH 7.6 (+/-0.05), and resuspended in 10 ml of PBS. For each well, on a 24-well plate, 525 µl fibrinogen solution, 50 µl microcarriers, 18 µl aprotinin (Sigma-Aldrich, St Louis, MO, USA), and 7.5 µl thrombin (Sigma-Aldrich, St Louis, MO, USA) were mixed quickly. A final volume of 500 µl was added per well. The fibrin gel polymerises with the addition of thrombin within 1 min, allowed to settle at room temperature for 10 min, then placed in the cell culture incubator for 30 min prior to equilibrating with 500 µl of MEM (2% FBS and 2 mM L-glutamine). U87MG cells (1 x 10⁴ cells/well for siRNA transfections; 2.5 x 10⁴ cells/well for SPHK1 drug treatments) in 1 ml of media (with drug treatment if indicated) were seeded on top.

Media, drug treatments, and 30 µl aprotinin (reduces rate of gel degradation by proteasomes) were replaced every 48 h. Control wells with no U87MG cells seeded were included in all experiments, and minimal background sprouting was observed under these conditions. U87MG cell conditioned medium for use in this assay was prepared by taking supernatant from near confluent U87MG cells after 72 h of culture in

MEM (2% FBS and 2 mM L-glutamine). Quantification of angiogenic sprouts was performed after 96 h. Images of 6-10 beads per well were acquired with an Axio Vert.A1 inverted microscope (Zeiss, Jena, Germany). The number and length of angiogenic sprouts was quantified using AxioVision V4.8.2.0 software (Zeiss, Jena, Germany), and verified by a second (treatment blinded) assessor.

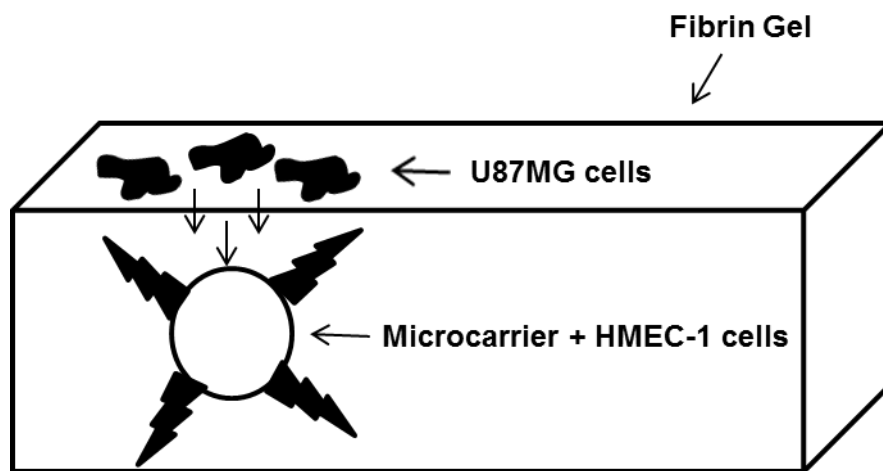


Figure 2.1 Schematic Diagram for the Angiogenesis *In Vitro* Model

2.6 DNA Methods

2.6.1 DNA Extraction from fresh frozen tissue

Fresh frozen tissue samples were prepared as described in section 2.3.1. Samples stored at -80°C were placed on ice. All work performed was in a fume hood, and adequate personal protective equipment was used. All waste was disposed of as per standard regulations.

Each sample was homogenised in 450 μl TESS lysing agent (10 mM Tris at pH 7.8, 1 mM EDTA, 100 mM NaCl, 1% SDS) with a micropestle. Proteinase K (Roche,

Indianapolis, IN, USA) was added at a final concentration of 0.5 mg/ml (11 μ l from 20 mg/ml proteinase K stock). Samples were vortexed for 2 sec and incubated on a heat block overnight at 55°C.

Phase Lock Gel™ (PLG, 5 Prime, Hamburg, Germany) tubes were centrifuged at 12,000 rpm for 5 min prior to usage. Tissue lysates incubated overnight were also centrifuged at 12,000 rpm for 5 min, then transferred (approximately 500 μ l) to the PLG tubes. Phenol/chloroform/isoamyl alcohol (25:24:1 v/v/v) was added (450 μ l) to the aqueous samples and mixed thoroughly, but not vortexed. The PLG tubes were centrifuged (12,000 rpm for 5 min) to separate the phases in the fume hood microfuge (Centrifuge 5415 D, Eppendorf, Hamburg, Germany). RNase If was added to each PLG tube at a final concentration of 250 U (i.e. 5 μ l of 50 U/ μ l of RNase If). Samples were mixed gently by inversion, and then incubated on a heat block for 45-90 min at 37°C. Another 450 μ l of phenol/chloroform/isoamyl alcohol was added to each PLG tube, mixed thoroughly (not vortexed), and centrifuged at 12,000 rpm for 5 min. Chloroform was added (450 μ l) to the aqueous samples, mixed thoroughly (not vortexed), and centrifuged at 12,000 rpm for 5 min. The upper aqueous phase was transferred to a new 1.5 ml Eppendorf tube. Ice-cold absolute ethanol (900 μ l) and 3 M sodium acetate (45 μ l) were added to the aqueous samples, and the tubes were gently inverted until DNA precipitates were visible. For samples with no visible DNA, glycogen at a concentration of 1 μ g/ μ l (i.e. 70 μ l from a 20 mg/ml stock) was added, and then samples were left at -20°C overnight to co-precipitate the DNA. Samples were centrifuged at 12,000 rpm for 30 min, and the supernatant was discarded. DNA pellets were washed with 1 ml of 70% ethanol (v/v), centrifuged at 12,000 rpm for 5 min, and the

supernatant was discarded. Samples were centrifuged again at 12,000 rpm for 2 min, and residual 70% ethanol was removed. DNA pellets were air dried for 30 min prior to resuspending in 100 μ l of 1x Tris-EDTA (TE) solution. DNA extracts were quantified with the NanoDrop® as previously described in section 2.4.2, and then stored at -80°C.

2.6.2 Bisulfite Treatment

Extracted tissue DNA was bisulfite treated using the EZ DNA Methylation-Gold™ Kit (Zymo Research, Irvine, CA, USA). The kit only converts unmethylated cytosine into uracil, while methylated cytosine remains unchanged. A negative control, unmethylated DNA Epiect human DNA (Qiagen, Hilden, Germany), and positive control, human HCT 116 DKO Methylated DNA Standard (Zymo Research Corp., CA, USA) were included in the experiment. Sample DNA input of 500 ng was used for bisulfite treatment, for a total volume of 20 μ l (i.e. 25 ng/ μ l). The CT Conversion Reagent was prepared by mixing water (900 μ l), M-Dilution Buffer (300 μ l), and M-Dissolving Buffer (50 μ l) regularly over 10 min. DNA samples (20 μ l) were combined with the CT Conversion Reagent (130 μ l) in PCR tubes, and placed on a thermal cycler with the following conditions: 98°C for 10 min, 64°C for 2.5 h, and held at 4°C. DNA samples were then added onto a Zymo-Spin™ IC Column containing the M-Binding Buffer (600 μ l), and placed in a collection tube. The column was inverted several times to mix the DNA and buffer, and centrifuged at full speed (>10,000 rpm) for 30 sec. Flow-through was discarded and M-Wash Buffer (100 μ l) was added to the column, followed by centrifuging at full speed for 30 sec, and discarding the flow-through again. M-Desulphonation Buffer (200 μ l) was added to the column, incubated for 15 min at room temperature, centrifuged at full speed for 30 sec, and the flow-through was discarded.

The column was washed twice with M-Wash Buffer (200 μ l). Each column was transferred to a 1.5 ml Eppendorf tube, and M-Elution Buffer (10 μ l) was added to the column matrix directly. The columns were centrifuged at full speed for 30 sec, and the eluted bisulfite treated DNA was stored at -20°C.

2.6.3 MGMT Pyrosequencing

MGMT promoter pyrosequencing for bisulfite treated DNA was performed using the PyroMark Q96 CpG MGMT kit (Qiagen, Hilden, Germany). PCR reaction mixture (50 μ l) was prepared using the following reagents: 1x PCR buffer (5 μ l), 1.5 mM MgCl₂ (1.5 μ l), 10 mM dNTP mix (1 μ l), 20 μ M forward primer (1 μ l), 20 μ M reverse primer (1 μ l), nuclease-free water (37.25 μ l), 1.25 U Taq DNA polymerase (0.25 μ l), and bisulfite treated DNA (3 μ l). Sample mixture was mixed on the MixMate® for 30 sec, followed by a short centrifuge (5 sec). Thermal cycling conditions were: 95°C for 15 min, followed by 45 cycles of 95°C for 20 sec, 53°C for 20 sec, and 72°C for 20 sec, and ending at 72°C for 5 min before holding at 4°C. PCR products (5 μ l) were run on a 1.5% agarose gel to confirm target amplification. The remaining 45 μ l was incubated with 3 μ l streptavidin sepharose beads (GE Healthcare, Buckinghamshire, UK) and 37 μ l pyrosequencing binding buffer for 20 min on the MixMate® (1600 rpm). While mixing the sample, 0.4 μ M primer sequence (40 μ l) in annealing buffer was prepared and added onto the pyrosequencing plate. The vacuum machine was prepared; PCR tubes were removed from the MixMate®, and placed on the vacuum to capture the beads. The vacuum was washed with 70% ethanol for 10 sec, denaturation solution (0.2 M NaOH) for 5 sec, and wash buffer for 10 sec. The vacuum prep tool was turned off and transferred to the pyrosequencing 96 well plate (pre-filled with 0.4 μ M primer

sequence). The prep tool was washed with MilliQ water for 15 sec. The pyrosequencing plate was then heated at 90°C for 2 min to denature the template. Instrument parameters were selected according to the manufacturer's instructions, and the cartridge was loaded with the substrate, enzyme and dNTPs as per the program calculations. The plate was placed into the PyroMark Q96 ID instrument, and analysed for the following sequence: `_T/CGTTTTGT/CGTTTT/CGAT/CGTTT/CGT/CAGG` (Qiagen, Hilden, Germany), entered into the PyroMark™ CpG software version 1.0.11 (Qiagen, Hilden, Germany). The software evaluated the sequence quality and methylation percentage over five CpG sites. Samples were considered methylated when MGMT methylation was $\geq 10\%$. The negative control (unmethylated sample) had less than 3% MGMT methylation, while the positive control (methylated sample) had greater than 80% MGMT methylation. The bisulfite treatment and pyrosequencing were done with Wendy Ha.

2.6.4 Ion Torrent Sequencing

Sequencing of 44 primary GBM tissue samples was performed at the University of Western Australia by Tania Tabone. The extracted DNA was quantified using the Qubit 2.0 Fluorometer and Qubit dsDNA HS Assay Kit (Life Technologies, CA, USA). Library preparation, sample sequencing, and data analysis are briefly summarised below.

2.6.4.1 Library Preparation

Preparation of amplicon libraries for each sample, amplifying 50 gene targets, was performed using the Ion AmpliSeq Ready-to-use Panel with an input of 10 ng genomic

DNA. A single multiplex PCR reaction used the Ion AmpliSeq™ Cancer HotSpot Panel v2 and AmpliSeq HiFi Master Mix (Ion AmpliSeq Library Kit 2.0, Life Technologies, CA, USA) to amplify the target regions. The output multiplexed amplicons, 207 primer pairs, were treated with FuPa Reagent (Life Technologies, CA, USA) to partly digest primer sequences and phosphorylate amplicon ends. Agencourt AMPure XP Reagent (Beckman Coulter, Brea, CA, USA) was used to ligate the sequence adapters with unique barcodes (Ion Xpress Barcode Adapters 1-96, Life Technologies, CA, USA) to the amplified products and purify them. The amplicon libraries were amplified again using the Agilent 2100 Bioanalyser and Agilent High Sensitivity DNA Kit (Agilent Technologies, Santa Clara, CA, USA) to quantify and visualise the library fragments. The library concentration used for sequencing was standardised to 100 pM in low TE buffer (Life Technologies, CA, USA).

Table 2.4 Ion AmpliSeq™ Cancer HotSpot Panel v2

<i>ABL1</i>	<i>EZH2</i>	<i>JAK3</i>	<i>PTEN</i>
<i>AKT1</i>	<i>FBXW7</i>	<i>IDH2</i>	<i>PTPN11</i>
<i>ALK</i>	<i>FGFR1</i>	<i>KDR</i>	<i>RB1</i>
<i>APC</i>	<i>FGFR2</i>	<i>KIT</i>	<i>RET</i>
<i>ATM</i>	<i>FGFR3</i>	<i>KRAS</i>	<i>SMAD4</i>
<i>BRAF</i>	<i>FLT3</i>	<i>MET</i>	<i>SMARCB1</i>
<i>CDH1</i>	<i>GNA11</i>	<i>MLH1</i>	<i>SMO</i>
<i>CDKN2A</i>	<i>GNAS</i>	<i>MPL</i>	<i>SRC</i>
<i>CSF1R</i>	<i>GNAQ</i>	<i>NOTCH1</i>	<i>STK11</i>
<i>CTNNB1</i>	<i>HNF1A</i>	<i>NPM1</i>	<i>TP53</i>
<i>EGFR</i>	<i>HRAS</i>	<i>NRAS</i>	<i>VHL</i>
<i>ERBB2</i>	<i>IDH1</i>	<i>PDGFRA</i>	
<i>ERBB4</i>	<i>JAK2</i>	<i>PIK3CA</i>	

2.6.4.2 Emulsion PCR and Sequencing

Barcoded libraries with eight samples, 100 pM per sample, were pooled and a final concentration was adjusted to 9 pM in nuclease-free water. Biotinylated primers were then used to clonally amplify the pooled barcoded libraries onto Ion Sphere Particles (ISPs; Ion Xpress Template Kit 2.0) by emulsion PCR (emPCR) using the OneTouch 2 System (Life Technologies, CA, USA). Streptavidin-coated beads (Ion OneTouch 2 Kit) bound to template positive ISPs following centrifugation and recovered the ISPs. Enriched ISPs were ligated with a sequencing primer prior to loading onto an Ion 316™ Chip for sequence analysis. Sequencing was performed on the Ion Personal Genome Machine (PGM™) Sequencer using the Ion PGM™ 200 Sequencing Kit (Life Technologies, CA, USA). All reagents in this section were produced by Life Technologies.

2.6.4.3 Coverage and Data Analysis

Torrent Suite v3.6.2 Software (Life Technologies, CA, USA) was used to extract barcoded reads, align reads to the reference genome (human genome build 19; hg19), and base call. Additionally, sequence run parameters, such as chip loading efficiency, total read counts, total coverage and quality were also extrapolated. Variant identification and amino acid alterations were analysed with the ANNOVAR (Biobase) software. Visualising read alignment, variants, and confirming variant calling (i.e. strand bias or sequencing errors) was performed using the Integrative Genomics Viewer (IGV).

2.7 Statistical Analysis

Chapter 3 statistics was performed using SPSS Statistics Software 21.0 (SPSS Inc., IBM® Company, Chicago, IL, USA) with Benjamin Daniels and Maarit A. Laaksonen. Sphingolipid levels and enzyme gene expression data were normalised for distribution through log transformation. One-Way ANOVA was applied to determine statistical significance. Variance was tested using Levene's test. If the variance between groups was equal, Tukey's post-hoc test was applied. If the variance between groups was unequal, Dunnett T3 post-hoc test was applied. Correlation analysis was performed using Spearman correlations due to non-normal distribution of data.

Chapter 4 statistics was performed using GraphPad Prism 6.0 (GraphPad Software, Inc., CA, USA). One-Way ANOVA was used to determine statistical significance with a Dunnett's post-hoc test. For the SPHK1 drug inhibition experiments using the stereoisomer control, a 2-Way ANOVA was used to determine statistical significance with a Bonferroni's post-hoc test to compare SKI-1a and SKI-1b.

Chapter 5 statistics was performed using R software with Chris Pardy, SAS (SAS Institute Inc., Cary, NC, USA) with Jake Olivier, and GraphPad Prism 6.0. Assessment of gene mutation correlation with metabolite levels was screened using Mutual Information [159], followed by unpaired Student's t-test to determine significance. Mutual Information examines the dependency between variables. Comparison between plasma groups was assessed with unpaired Student's t-test. Spearman correlations examined the relationship between tissue and plasma sphingolipids. Survival analysis was examined using Kaplan Meier curves, Log-Rank p-value to determine significance, and cox proportional hazard regression model to determine hazard ratio. For each

metabolite of interest, the cut-off value to separate “high” vs. “low” levels was determined using ROC curve analysis, and grouping was informed by specificity and sensitivity outcomes. Statistical significance for all data presented in this thesis was defined as a p-value < 0.05.

Chapter 3: A Sphingolipid Map for Normal Grey Matter & Gliomas

3.1 Introduction

Sphingolipids are a major lipid-based family in mammalian cells [51], with known structural and metabolic functions as discussed previously. There are several sphingolipid hubs, and all are interconnected in a complex network that recycles most metabolites, with ceramide, sphingosine, and S1P as a central axis in the pathway.

As shown in Figure 3.1, SM is catabolised into ceramide. Ceramide, an important sphingolipid hub, is broken down into sphingosine by ceramidases, or can be glycosylated to form HexCer. HexCer can subsequently be built upon to form complex glycolipids, including LacCer and sulfatide. Sphingosine is then recycled back into ceramide or phosphorylated by SPHK1 or SPHK2 into S1P. S1P is converted back into sphingosine or irreversibly broken down into hexadecanal and ethanolamine phosphate.

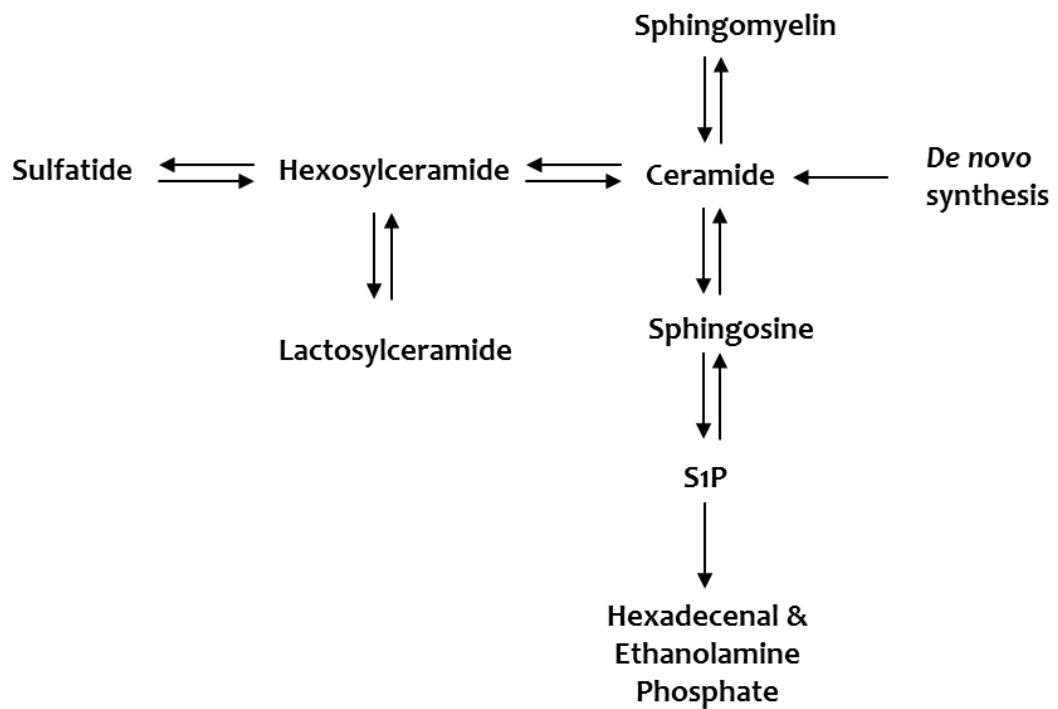


Figure 3.1 Schematic Diagram of the Sphingolipid Pathway

Although previous studies on clinical samples have shown important sphingolipid alterations, the scope was limited to specific metabolites, enzymes and/or receptors. In addition, experimental therapeutics were developed based on the aforementioned studies, and therefore may have missed potential targets. In order to move sphingolipidomics into the forefront of glioma targeted therapies, an adequate understanding of changes in the pathway is required. This is vital, as the pathway has a rheostat mechanism, thereby changes in one metabolite have a knock-on effect onto other metabolites with biological consequences [53].

3.1.1 Hypothesis and Aims

Working hypothesis for this chapter:

1. Sphingolipid metabolism in gliomas, specifically GBM, is altered compared to NGM, favouring the production of S1P.
2. Targeted enzyme gene expression in the sphingolipid pathway will support an S1P increase over precursor metabolites, such as ceramide and sphingosine.

The overall aim of this chapter is to examine the baseline sphingolipid metabolism in NGM, in addition to AII, AIII, and GBM using LC-MS/MS and RT-PCR.

The specific aims of this chapter:

1. To examine the ceramide-S1P balance between NGM and gliomas.
2. To identify other sphingolipids common in brain, and establish the levels in NGM and gliomas, specifically SM, HexCer, sulfatide, and LacCer in addition to the ceramide-S1P axis.
3. To examine the relationship between enzyme expression and metabolite levels in the ceramide-S1P axis.

3.2 Results

3.2.1 Sphingolipid Levels in Normal and Glioma Tissues

NGM and glioma tissue samples were processed and analysed as discussed previously (see Chapter 2.2). The heat map, in Figure 3.2, indicates the changes in each sphingolipid class as a mean fold change when compared to NGM. For sphingolipids with several chain lengths analysed, the total sum of the chain lengths is represented in the respective class (SM, HexCer, LacCer, sulfatide, and ceramide). Overall, there is a reduction in HexCer, sulfatide, and ceramide, which is accompanied by an increase in LacCer and S1P for GBM tissue compared to NGM.

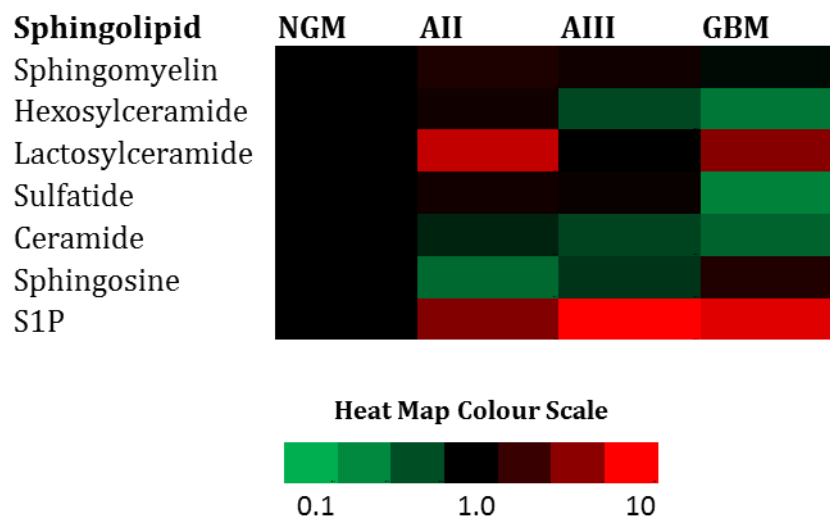


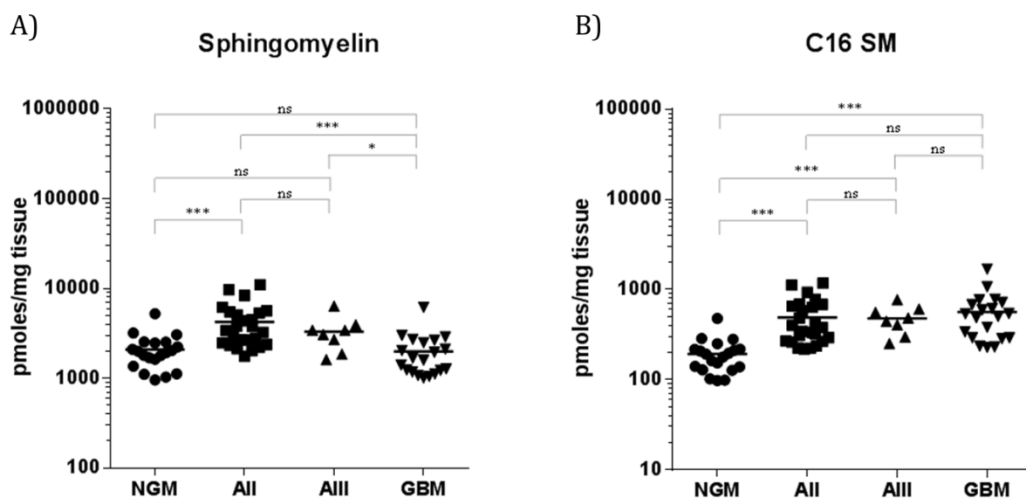
Figure 3.2 Sphingolipids in NGM, AII, AIII, and GBM

The heat map represents the various sphingolipids for each tissue group. Colour scheme represents the mean fold change in the tissue groups, as indicated on the scale, for each sphingolipid class adjusted to NGM.

3.2.1.1 Sphingomyelin Levels in Normal and Glioma Tissues

SM levels in the different tissue groups are illustrated in Figure 3.3. Total SM, representing the sum of all SM chain lengths, was quantified as shown in Figure 3.3.A. AII and AIII samples had similar levels of total SM. Equally, NGM and GBM had similar levels of total SM. SM was significantly elevated in both AII and AIII samples compared to either of NGM and GBM samples.

The most abundant chain lengths, listed in Figure 3.3.B-D, include C16, C18, and C24:1. C16 SM (see Figure 3.3.B) was similar between the various glioma grades, but was significantly elevated in all gliomas compared to NGM. In contrast, C18 SM (see Figure 3.3.C) was similar between NGM with either AII or AIII samples, but was significantly reduced in GBM compared to either NGM or AII samples. Of interest, C24:1 SM showed the same pattern as total SM, whereby AII and AIII samples had significantly higher levels than NGM or GBM.



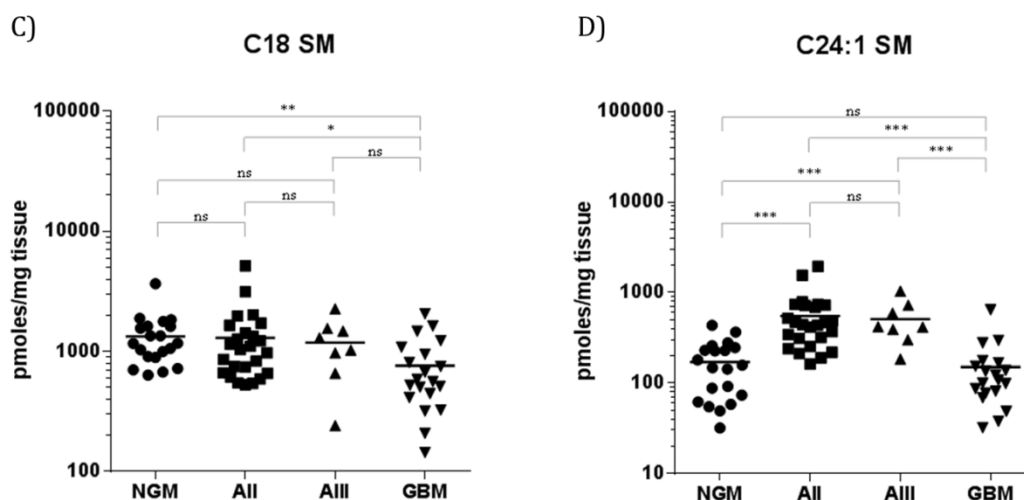


Figure 3.3 Spingomyelin Levels in NGM, AII, AIII, and GBM

(A) Levels of total SM are presented in the scatter plot for each individual sample. (B-D) The three most common SM chain lengths are represented as scatter plots for C16 SM (B), C18 SM (C), and C24:1 SM (D). All values in the scatter plots represent the absolute quantification in pmoles adjusted to tissue weight (mg). *p-value <0.05, **p-value <0.01, ***p-value <0.001, ns = not significant.

3.2.1.2 Hexosylceramide Levels in Normal and Glioma Tissues

HexCer is an important precursor for complex glycolipids. Although there were similar levels of total HexCer between NGM and AII samples, there was a trend decrease in AIII samples, and a significant reduction in GBM compared to NGM and AII samples. Interestingly, with regards to C16 HexCer, all glioma samples had significantly higher levels than NGM. C18 HexCer was relatively similar between all groups, with the exception of a significant reduction in levels for GBM compared to AII samples. C24:1 HexCer (see Figure 3.4.D), the most abundant HexCer chain length, had the same reduction pattern as total HexCer in Figure 3.4.A.

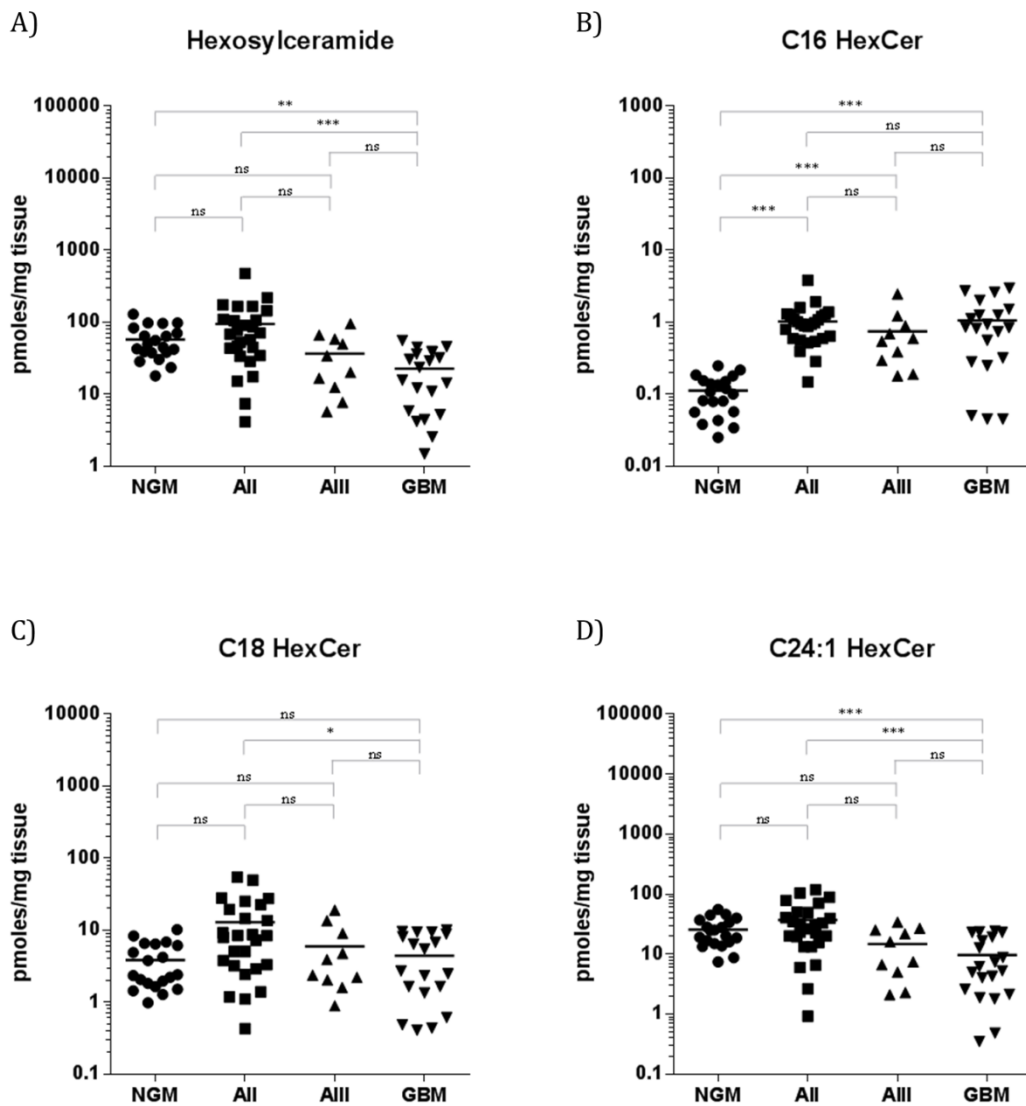


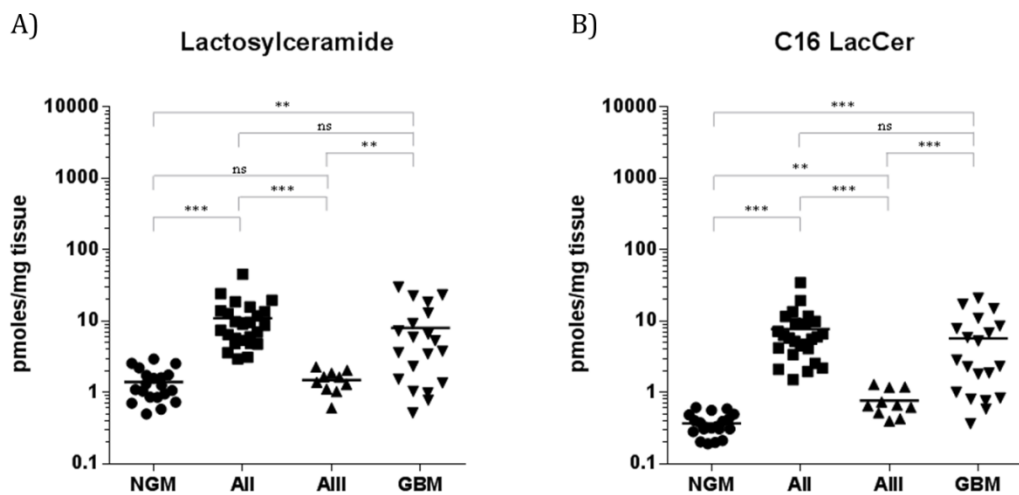
Figure 3.4 Hexosylceramide Levels in NGM, AII, AIII, and GBM

(A) Levels of total HexCer are presented in the scatter plot for each individual sample. (B-D) The three most common HexCer chain lengths are represented as scatter plots for C16 HexCer (B), C18 HexCer (C), and C24:1 HexCer (D). All values in the scatter plots represent the absolute quantification in pmoles adjusted to tissue weight (mg). *p-value <0.05, **p-value <0.01, ***p-value <0.001, ns = not significant.

3.2.1.3 Lactosylceramide Levels in Normal and Glioma Tissues

Total LacCer levels were significantly increased in AII and GBM samples compared to NGM and AIII samples, as evident in Figure 3.5.A. NGM and AIII samples were

similar in LacCer content, and equally AII and GBM samples had relatively similar levels. Of note, AII samples were more clustered together, while GBM samples had a larger distribution of LacCer levels between the samples. However, C16 LacCer was significantly elevated in all glioma samples compared to NGM, and AII and GBM samples had significantly higher levels than AIII samples. Having said that, the GBM samples had a wider spread than AII samples for C16 LacCer, whereby some samples overlapped with the distribution of AIII samples. C18 LacCer levels were significantly increased in AII samples only compared to all other groups. In contrast, C24:1 LacCer levels were significantly reduced in AIII samples only compared to NGM and AII samples.



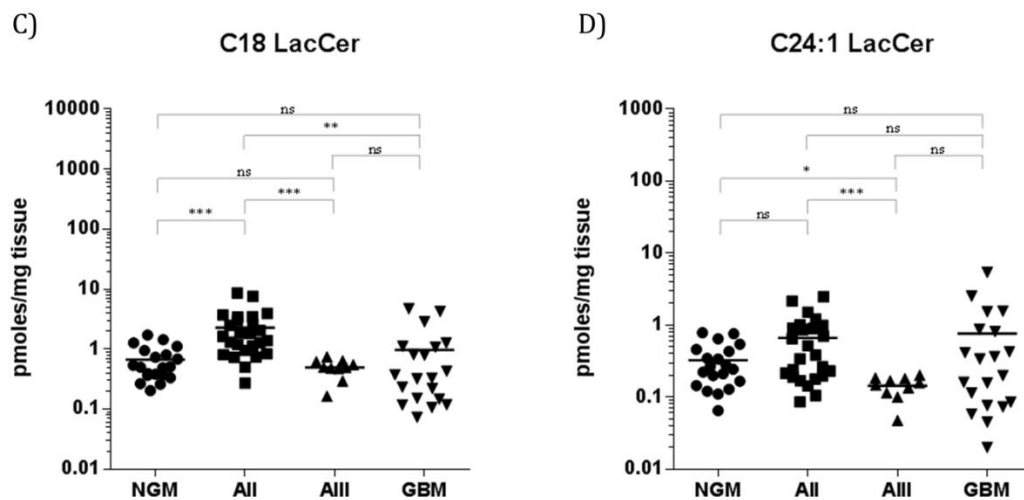


Figure 3.5 Lactosylceramide Levels in NGM, AII, AIII, and GBM

(A) Levels of total LacCer are presented in the scatter plot for each individual sample. (B-D) The three most common LacCer chain lengths are represented as scatter plots for C16 LacCer (B), C18 LacCer (C), and C24:1 LacCer (D). All values in the scatter plots represent the absolute quantification in pmoles adjusted to tissue weight (mg). *p-value <0.05, **p-value <0.01, ***p-value <0.001, ns = not significant.

3.2.1.4 Sulfatide Levels in Normal and Glioma Tissues

Sulfatide levels, as depicted in Figure 3.6.A, were equal between NGM, AII and AIII samples, but significantly reduced in GBM compared to all three groups independently. C16 sulfatide, as seen in Figure 3.6.B, was increased significantly in AII and AIII samples compared to NGM. Moreover, AIII samples were significantly higher in C16 sulfatide compared to GBM. Of note, GBM and NGM had similar C16 sulfatide levels, but the spread of GBM samples was wide, with several samples well below or above most NGM samples. In contrast, C18 sulfatide was relatively similar amongst all groups. C24:1 sulfatide was only significantly reduced in GBM samples compared to NGM or AII samples.

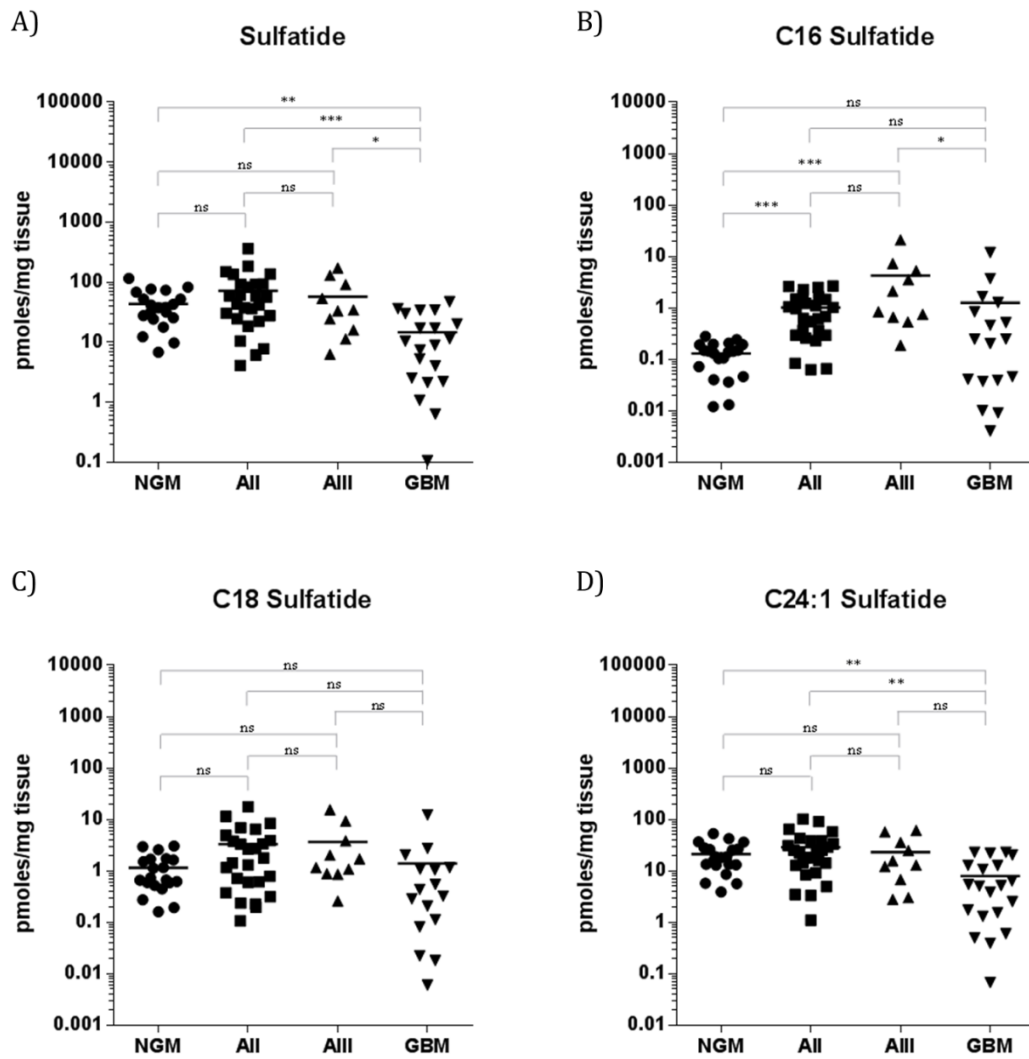
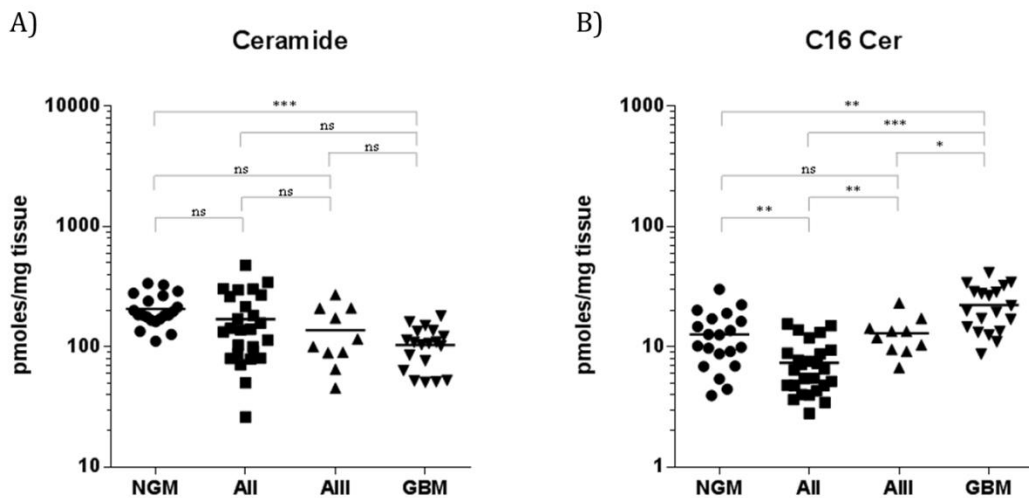


Figure 3.6 Sulfatide Levels in NGM, AII, AIII, and GBM

(A) Levels of total sulfatide are presented in the scatter plot for each individual sample. (B-D) The three most common sulfatide chain lengths are represented as scatter plots for C16 sulfatide (B), C18 sulfatide (C), and C24:1 sulfatide (D). All values in the scatter plots represent the absolute quantification in pmoles adjusted to tissue weight (mg). *p-value <0.05, **p-value <0.01, ***p-value <0.001, ns = not significant.

3.2.1.5 Ceramide Levels in Normal and Glioma Tissues

Ceramide is a central metabolite in the sphingolipid pathway. Total ceramide, present at levels approximately 10% of total SM in NGM, was progressively reduced as glioma grade increased. Although there was no statistical difference between NGM and AII or AIII samples, a trend in ceramide reduction is apparent in Figure 3.7.A, with a significant reduction in ceramide content when comparing GBM to NGM. More importantly, the three abundant ceramide chain lengths in Figure 3.7.B-D illustrate divergent shifts. C16 ceramide was significantly lower in AII samples compared to NGM or AIII samples, while GBM had significantly high levels compared to all groups. In contrast, C18 ceramide was significantly reduced as histological grade increased compared to NGM. C24:1 ceramide had similar levels among all four groups.



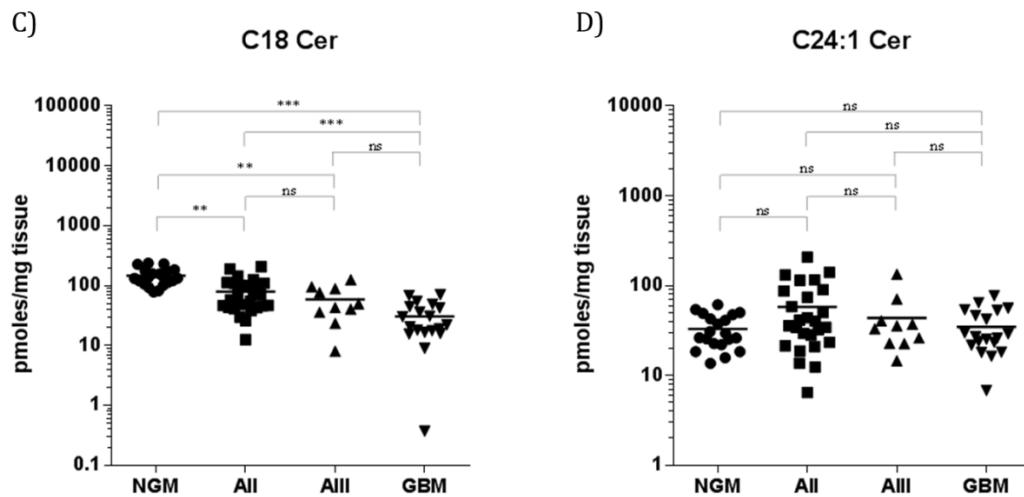


Figure 3.7 Ceramide Levels in NGM, AII, AIII, and GBM

(A) Levels of total ceramide are presented in the scatter plot for each individual sample. (B-D) The three most common ceramide chain lengths are represented as scatter plots for C16 ceramide (B), C18 ceramide (C), and C24:1 ceramide (D). All values in the scatter plots represent the absolute quantification in pmoles adjusted to tissue weight (mg). *p-value <0.05, **p-value <0.01, ***p-value <0.001, ns = not significant.

The relationship between C16 and C18 ceramide levels is outlined in Figure 3.8 for each group. C18 ceramide was noted as the independent measure, and C16 ceramide as the dependent measure for the purpose of the spearman correlation analysis only. In NGM, as C18 ceramide levels increased, C16 ceramide increased as well. The significant positive correlation between the two ceramide chain lengths was maintained in AII samples as well. However, in AIII samples and GBM, the relationship between C16 and C18 ceramide was not significant. The levels of C18 ceramide, as noted in Figure 3.7.C previously, was clearly reduced as histological grade increased. Similar to Figure 3.7.B, C16 ceramide levels were lower in NGM, AII, and AIII samples compared to GBM.

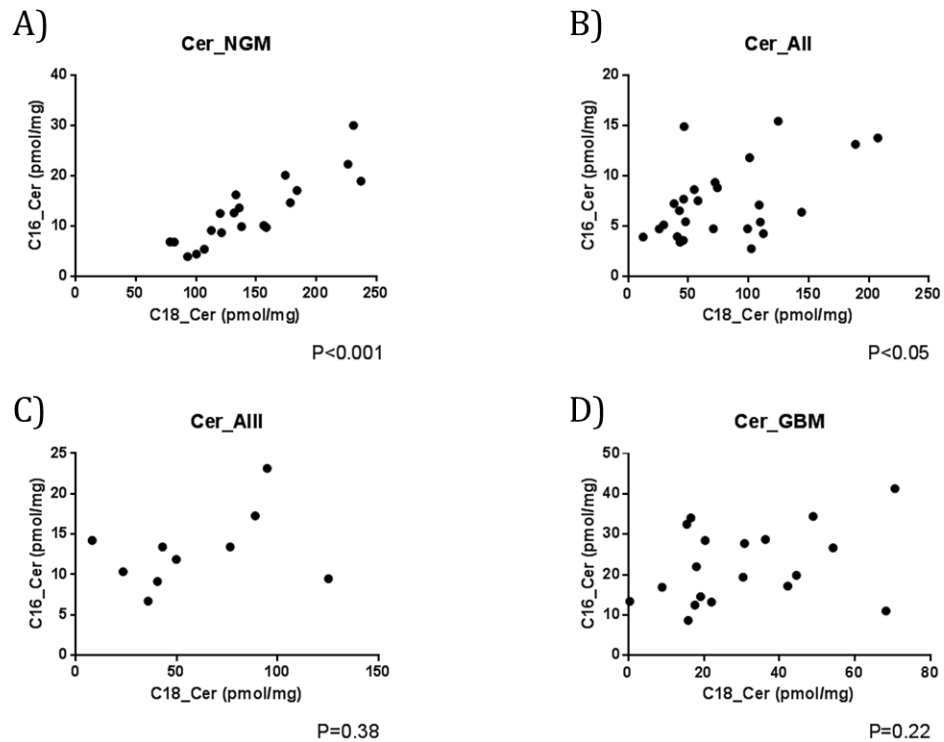


Figure 3.8 Balance between C16 Ceramide and C18 Ceramide in NGM, AII, AIII and GBM

(A-D) Bivariate correlation between C16 ceramide and C18 ceramide in NGM (A), AII (B), AIII (C), and GBM (D). Data points represent the absolute levels for each sample in pmoles adjusted to weight (mg). P-values were determined using a spearman correlation.

3.2.1.6 Sphingosine Levels in Normal and Glioma Tissues

Sphingosine, the precursor to S1P, illustrates a step-wise gradient change between the glioma groups. Unexpectedly, AII samples had significantly lower sphingosine compared to NGM. Sphingosine trended to increase in AIII samples compared to AII samples, and was significantly elevated in GBM compared to either AII or AIII samples. However, NGM and GBM did not statistically differ in sphingosine levels.

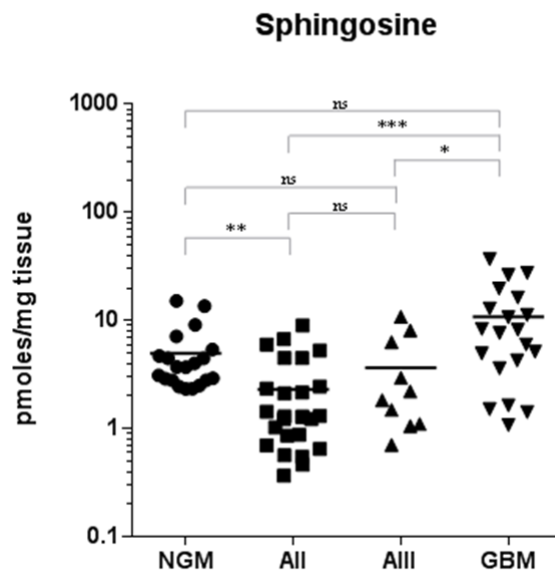


Figure 3.9 Sphingosine Levels in NGM, AII, AIII, and GBM

Levels of sphingosine are presented in the scatter plot for each individual sample. All values in the scatter plots represent the absolute quantification in pmoles adjusted to tissue weight (mg). *p-value <0.05, **p-value <0.01, ***p-value <0.001, ns = not significant.

3.2.1.7 S1P Levels in Normal and Glioma Tissues

S1P, present at levels less than 5% of sphingosine in NGM, was significantly elevated in all glioma samples when compared to NGM. Although AII samples had significantly higher levels of S1P than NGM, the spread of S1P levels was wide, with a few samples falling below the level of all NGM samples. In contrast, AIII samples and GBM were uniform in distribution, and 26 out of 30 samples (87%) had higher S1P levels than NGM. There were no differences between GBM with either of AII or AIII samples, but AIII samples had significantly higher levels of S1P than AII samples.

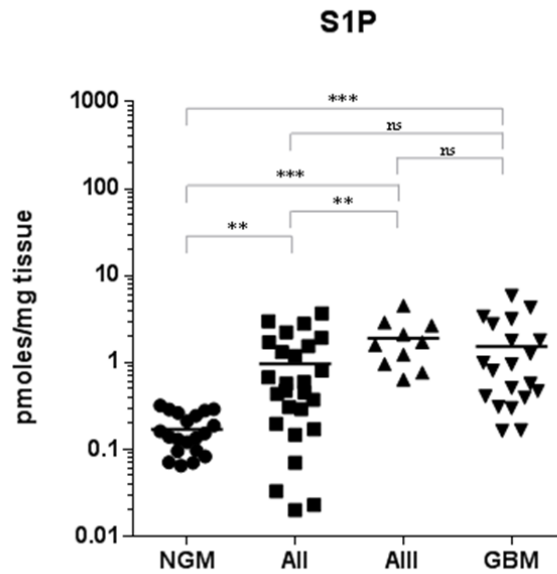


Figure 3.10 S1P Levels in NGM, AII, AIII, and GBM

Levels of S1P are presented in the scatter plot for each individual sample. All values in the scatter plots represent the absolute quantification in pmoles adjusted to tissue weight (mg). *p-value <0.05, **p-value <0.01, ***p-value <0.001, ns = not significant.

3.2.2 Sphingolipid Enzymes Expression in Normal and Glioma Tissues

Enzyme expression was determined through absolute quantification and normalised to GAPDH or 18S. Figure 3.11 contains an overview of the enzymes analysed, their position in sphingolipid metabolism, and a heat map expression with the mean fold change adjusted to NGM. The heat map is arranged in a streamlined order, commencing with enzymes responsible for forming ceramide, followed by enzymes that catabolise ceramide, then enzymes responsible for forming S1P, and finally enzymes that recycle or catabolise S1P. A total of 15 enzymes in the pathway were measured for gene expression, but only 14 are listed in the heat map as *ASAH2* was below the limit of detection.

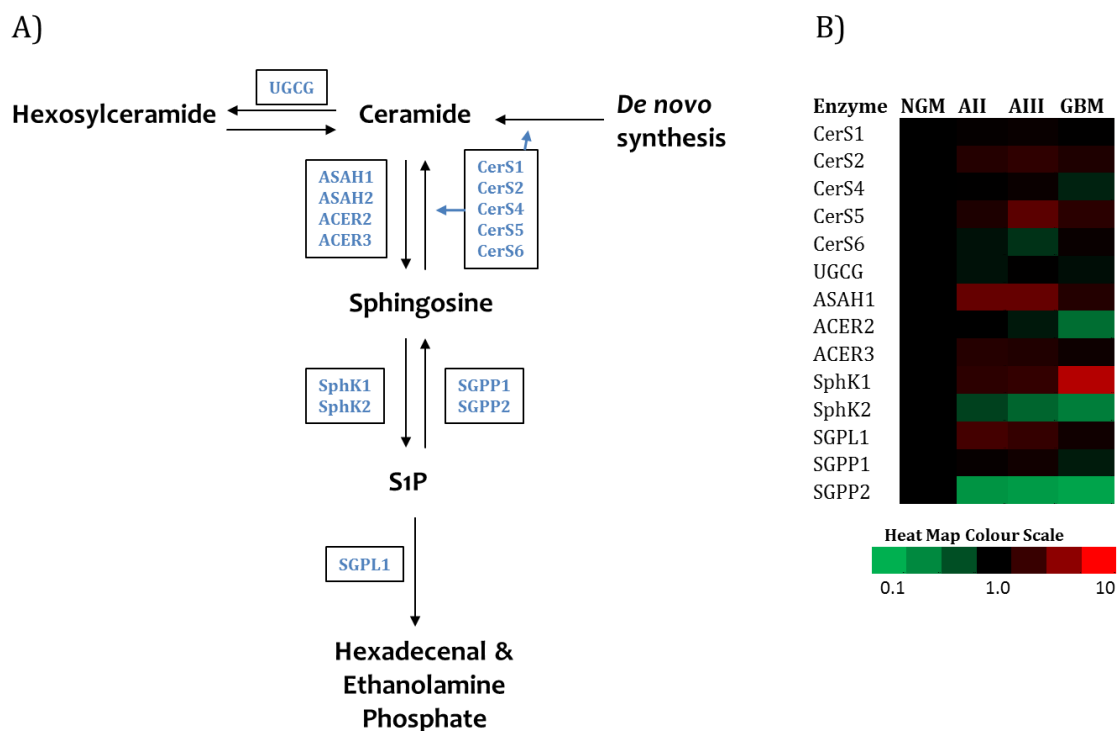


Figure 3.11 Sphingolipid Enzymes Expression in NGM, AII, AIII, and GBM

(A) Schematic diagram of the sphingolipid pathway. All enzymes listed were analysed. (B) Heat map representing the various sphingolipid enzymes for each tissue group. Colour scheme represents the mean fold change in the tissue groups, as indicated on the scale, for each enzyme adjusted to NGM. Data presented is normalised to 18S (similar pattern with GAPDH).

3.2.2.1 Ceramide Synthases in Normal and Glioma Tissues

Ceramide formation is contributed by six ceramide synthases. CERS3 is not expressed in brain tissue, and was therefore excluded from the gene expression analysis. Each ceramide synthase has a preferential carbon chain length (N-acyl), hence regulating specific ceramides, but overlap (as outlined in Table 3.1) in synthesis occurs [160].

Table 3.1 List of Ceramide Synthases and Target Ceramide Chain Length

Ceramide Synthase	Preferential Chain Length
CerS1	C18
CerS2	C22, C24, C26
CerS3	C18, C24, >C26
CerS4	C18, C20
CerS5	C14, C16
CerS6	C14, C16

Scatter plots for each ceramide synthase are outlined in Figure 3.12. CERS1 synthesises C18 ceramide, while CERS4 synthesises C18 and C20 ceramide. CERS1 expression was similar among the four groups. Conversely, C18 ceramide target was significantly reduced as grade increased as previously described. CERS4 was relatively stable across all four groups, except for a significant reduction in expression for GBM samples compared to AIII samples only. C20 ceramide target was significantly reduced in all glioma samples equally compared to NGM. CERS2, synthesising C22 and C24 ceramide, was significantly upregulated in all glioma samples equally in comparison to NGM. C22 ceramide target was significantly upregulated in AIII and GBM samples in comparison to AII samples only, while C24 ceramide target was significantly upregulated in AII and GBM samples compared to NGM and AIII samples only. Finally, CERS5 and CERS6 synthesise C16 ceramide. In all glioma groups, CERS5 was significantly upregulated in comparison to NGM. There were no differences between the glioma groups for CERS5 expression. In contrast, CERS6 remained stable across all four groups. C16 ceramide target was significantly reduced in AII samples compared to NGM, and increased significantly with grade as previously discussed.

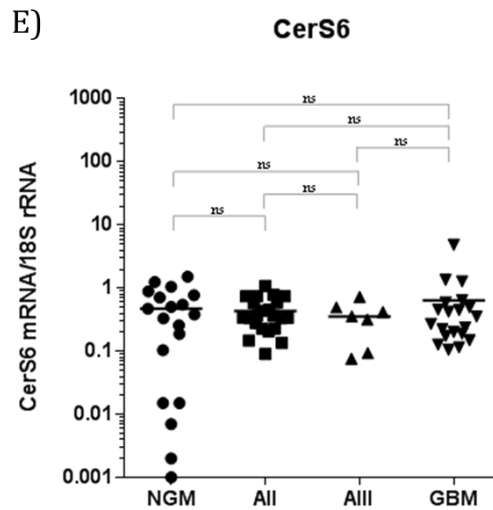


Figure 3.12 Ceramide Synthases Expression in NGM, AII, AIII, and GBM

(A-E) Absolute quantification of gene expression adjusted to 18S for the various ceramide synthases as indicated: CERS1 (A), CERS2 (B), CERS4 (C), CERS5 (D), and CERS6 (E). *p-value <0.05, **p-value <0.01, ***p-value <0.001, ns = not significant.

3.2.2.2 Ceramide Conversion in Normal and Glioma Tissues

Ceramide can be converted to several sphingolipids, but the focus presented herein is the conversion of ceramide to HexCer through the activity of UDP-glucose ceramide glucosyltransferase (UGCG) (Figure 3.13.A), or the conversion to sphingosine through the activity of ceramidases (Figure 3.13.B-D). UGCG was relatively stable between all groups, even though NGM had a wide-spread gene expression compared to gliomas. *ASAH1* was significantly upregulated in all gliomas compared to NGM. More specifically, AII and AIII samples had a significantly higher *ASAH1* expression than GBM. In contrast, alkaline ceramidase 2 (*ACER2*) was relatively stable between NGM, AII and AIII samples, but was significantly down regulated in GBM compared to NGM. Alkaline ceramidase 3 (*ACER3*) was significantly upregulated in AII samples compared to NGM and GBM only, which were both at similar levels of gene expression. Of note,

alkaline ceramidase 1 (ACER1) is not expressed in brain tissue, hence was excluded from the analysis.

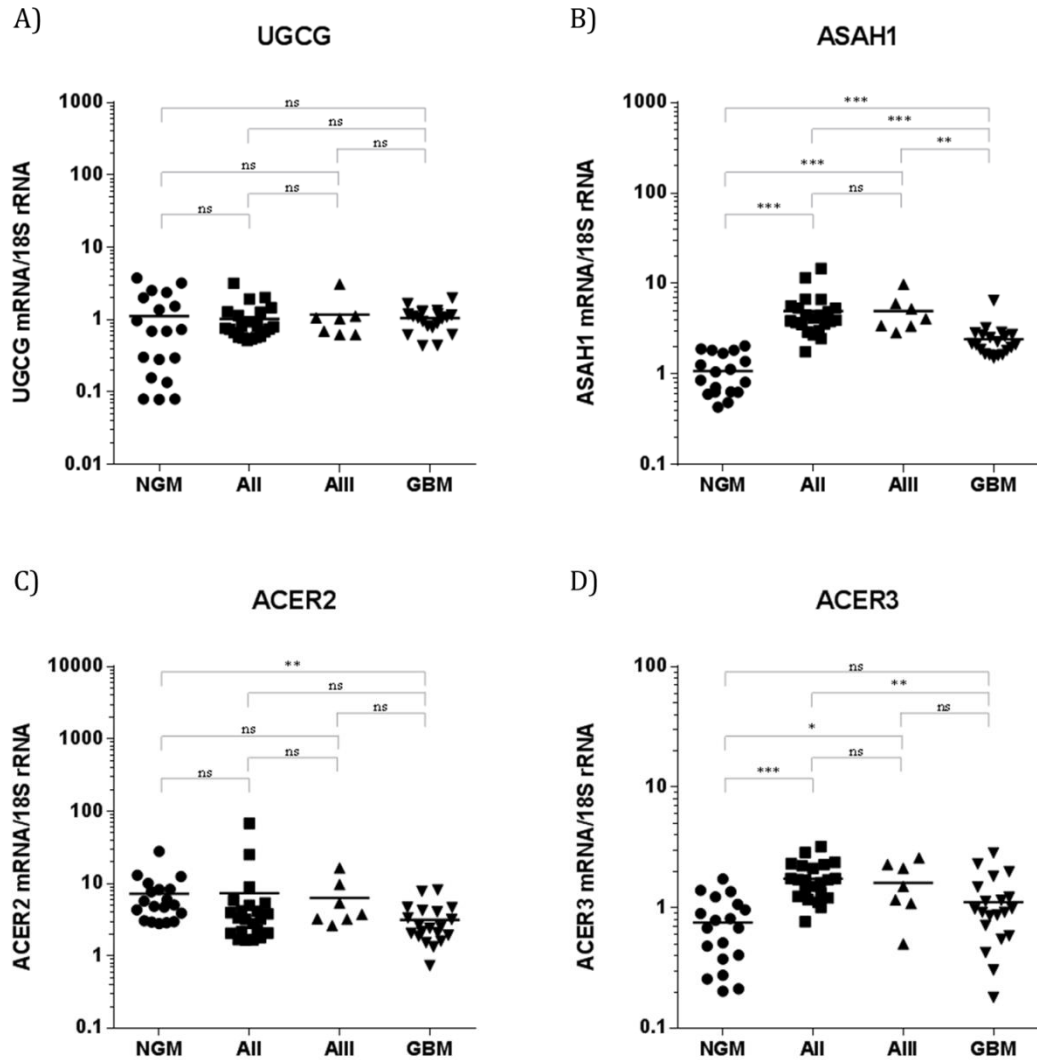
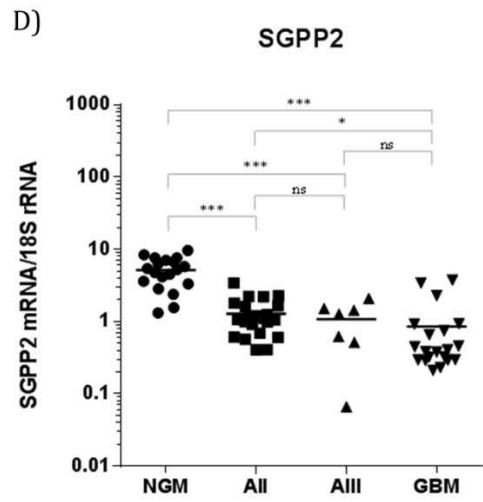
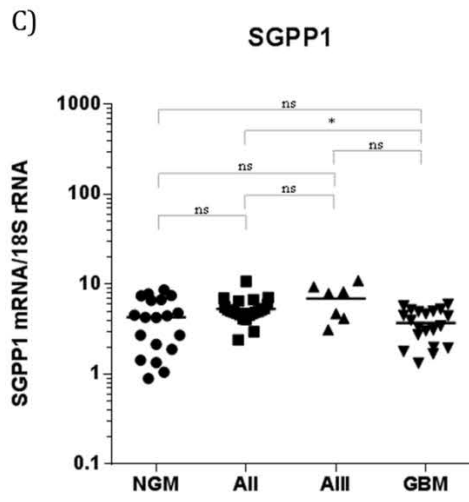
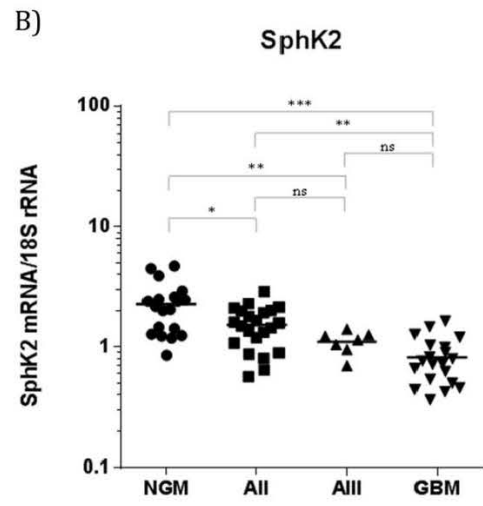
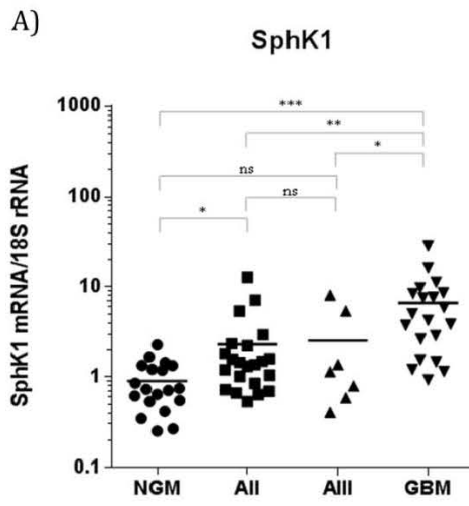


Figure 3.13 Ceramide Glycosylation and Ceramidase Enzymes Expression in NGM, AII, AIII, and GBM

(A -D) Absolute quantification of gene expression adjusted to 18S for UGCG (A), ASAH1 (B), ACER2 (C), and ACER3 (D). *p-value <0.05, **p-value <0.01, ***p-value <0.001, ns = not significant.

3.2.2.3 S1P Formation and Catabolism in Normal and Glioma Tissues

S1P formation and breakdown is controlled by multiple enzymes, as outlined in Figure 3.11.A. Phosphorylation of sphingosine to S1P is catalysed through SPHK1 or SPHK2. SPHK1 (Figure 3.14.A) illustrated a significant upregulation in AII and AIII samples compared to NGM. Moreover, GBM samples were further upregulated in comparison to NGM, AII, and AIII samples. In contrast, SPHK2 (Figure 3.14.B) was significantly down regulated in AII samples compared to NGM. A trend reduction in AIII samples was apparent when compared to AII samples. GBM samples illustrated a significant reduction in SPHK2 expression compared to NGM and AII samples. Following S1P formation, enzymes can either catabolise or recycle S1P. Recycling S1P back into the sphingolipid pathway occurs through SGPP1 or SGPP2. All samples had similar expression of SGPP1 (Figure 3.14.C), with the exception of GBM, which was significantly down regulated in SGPP1 expression when compared to AII samples. Moreover, SGPP2 (Figure 3.14.D) was significantly down regulated in all glioma samples in comparison to NGM, and was significantly down regulated in GBM compared to AII samples. SGPL1 (Figure 3.14.E) irreversibly breaks down S1P into hexadecenal and ethanolamine phosphate. All glioma groups upregulated SGPL1 significantly in comparison to NGM; specifically, AII and AIII samples had similar expression of SGPL1, but both were significantly upregulated in comparison to GBM.



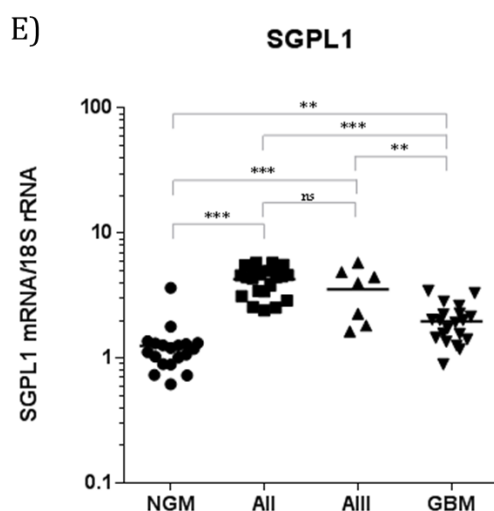


Figure 3.14 S1P-Related Enzymes Expression in NGM, AII, AIII, and GBM

(A-E) Absolute quantification of gene expression adjusted to 18S for the various S1P-related enzymes as indicated: SPHK1 (A), SPHK2 (B), SGPP1 (C), SGPP2 (D), and SGPL1 (E). *p-value <0.05, **p-value <0.01, ***p-value <0.001, ns = not significant.

Examining the relationship between metabolites and enzymes assists in understanding changes occurring in tandem. In Table 3.2, a correlation matrix identified the positive, negative, and neutral relationships between all components surrounding S1P formation. Spearman correlations were applied because the data was not normally distributed. A positive correlation indicated that measurements move in the same direction, while a negative correlation indicated that measurements move in opposite directions. A neutral relationship is not significant. At the metabolite level, sphingosine and S1P have a significant positive correlation. S1P forming enzyme, SPHK1, has a significant positive correlation with S1P as expected, but interestingly, SPHK2 has a significant negative correlation with S1P. Additionally, SGPP2, which recycles S1P into sphingosine, has a significant negative correlation with S1P.

Table 3.2 Correlations between S1P-Related Measurements

	SPH	SphK1	SphK2	S1P	SGPP1	SGPP2	SGPL1
SPH	1.000						
SphK1	0.26*	1.000					
SphK2	-0.35**	-0.42***	1.000				
S1P	0.31**	0.38**	-0.44***	1.000			
SGPP1	-0.33**	0.17	0.26*	0.16	1.000		
SGPP2	-0.02	-0.38**	0.63***	-0.41***	0.24	1.000	
SGPL1	-0.40***	0.23	-0.08	0.39**	0.44***	-0.27*	1.000

* p-value < 0.05, ** p-value < 0.01, *** p-value < 0.001

In a multivariate model, the correlation of enzyme expression to metabolite levels per sample was tested as indicated in Table 3.3. The model examined the effect of SPHK1 and SPHK2 to yield S1P, both independently and when combined with sphingosine. The reverse reaction, S1P dephosphorylation by SGPP1 and SGPP2 to yield sphingosine, was also examined in the same manner. Grade was adjusted for in the model, as most measurements were significantly different between the grades as previously stated. Measurements were divided into low and high based on their median, which was used to generate the mean values for the metabolite examined. Sphingosine, when divided into low and high, was significantly predictive of S1P mean levels. Unexpectedly, SPHK1 and SPHK2 independently did not successfully predict S1P levels. Furthermore, the interaction of sphingosine with either of SPHK1 or SPHK2 was not predictive of S1P levels. For the reverse reaction, S1P was significantly predictive of sphingosine mean levels. SGPP1 and SGPP2, however, were not predictive of sphingosine levels either independently or in combination with S1P.

Table 3.3 Mean (95% CI) Values of Sphingosine and S1P Measurements According to Median Levels of SPHK1, SPHK2, SGPP1, and SGPP2 (N=67)

	S1P				Sphingosine			
	N	Mean	95% CI	P	N	Mean	95% CI	P
Sphingosine				0.01*				
Low	33	0.70	(0.31-1.09)					
High	34	1.43	(1.04-1.81)					
SPHK1				0.14				
Low	33	0.85	(0.44-1.26)					
High	34	1.30	(0.89-1.71)					
SPHK2				0.23				
Low	33	1.24	(0.84-1.63)					
High	34	0.86	(0.41-1.31)					
Sphingosine *SPHK1				0.54				
Low, Low	19	0.60	(0.11-1.09)					
Low, High	14	0.82	(0.25-1.40)					
High, Low	14	1.11	(0.49-1.74)					
High, High	20	1.67	(1.14-2.20)					
Sphingosine *SPHK2				0.21				
Low, Low	12	0.64	(0.05-1.23)					
Low, High	21	0.68	(0.17-1.20)					
High, Low	21	1.67	(1.17-2.16)					
High, High	13	1.06	(0.43-1.69)					
S1P								0.007**
Low					34	2.56	(-0.07-5.20)	
High					33	7.79	(5.55-10.0)	
SGPP1								0.32
Low					33	6.38	(4.02-8.74)	
High					34	4.79	(2.57-7.01)	
SGPP2								0.88
Low					34	5.70	(3.05-8.36)	
High					33	5.38	(2.80-7.96)	
S1P*SGPP1								0.46
Low, Low					21	3.19	(0.15-6.22)	
Low, High					13	1.58	(-2.05-5.20)	
High, Low					12	10.2	(6.61-13.8)	
High, High					21	6.46	(3.75-9.17)	
S1P*SGPP2								0.44
Low, Low					12	2.00	(-2.02-6.02)	
Low, High					22	3.69	(-1.56-8.94)	
High, Low					22	8.04	(4.89-11.2)	
High, High					11	6.35	(2.35-10.4)	

* p-value < 0.05, ** p-value < 0.01, *** p-value < 0.001

3.3 Discussion

Omic technologies are exponentially unlocking the complexities of molecular aberrations that occur in a cancerous cell. Identifying the differences between cancer and normal tissue is an important step in understanding the bigger picture. A clearer characterisation of DNA mutations in gliomas and other cancers has been possible with the revolution in sequencing technologies. The documentation of oncogenic changes though is taking place at multiple levels, including post transcriptional regulation, post translational modifications, and epigenetic influences, thus representing some of the complex layers in tumour biology. As a result, focusing only on mutational gains and losses may not be sufficient in developing therapeutically viable targets. Moreover, alterations in tumour metabolism are well documented, with a focus on an increase in glycolytic activity as a hallmark of cancer [161]. Metabolism though is not only characterised by carbohydrates, as lipid metabolism is also an important component of cellular regulation. Of interest, alteration in lipid metabolism can promote glycolytic activity [162]. Furthermore, at the sphingolipid level, only ceramide dysregulation in gliomas has been documented [163]. Additionally, a pathway centric approach has never been presented in any cancer for sphingolipid metabolism. In this context, we present a blue-print for all the sphingolipid changes, complemented with a focused enzymatic screen, between NGM and various glioma grades.

This chapter focuses on identifying the sphingolipid pathway changes at the metabolite level. In saying that, a discussion on the cohorts utilised is relevant to rationalise the potential meaning of any changes identified, and the limitations when interpreting the datasets. NGM samples obtained were from post mortem tissues, while AII, AIII, and

GBM samples were fresh frozen. Although post mortem tissue may be associated with lipid degradation, a study examining lipids in rat spinal cord found minimal effects for autolysis on lipid degradation within a 4 hour window [164]. More recently, a study by Yao *et al.* examined lipids in schizophrenic and control patients, with varying post mortem intervals (PMI), and found that there was no association of PMI with their lipid analysis [165]. Moreover, the normal control selected for the study was grey matter tissue as opposed to white matter tissue, since white matter contains a higher abundance of sphingolipids due to myelin. Myelin does not reflect the composition of gliomas, although gliomas may invade white matter. To account for the difference in tissue storage conditions or potential differences in tissue composition, we have included lower grade gliomas (i.e. AII) to compare with GBM as an added control, thus emphasising that sphingolipid changes are specific to the tumour cells and not to the microenvironment. Sample size is relatively similar among NGM (n=20), AII (n=26), and GBM (n=20), but AIII (n=10) is a significantly smaller cohort. Therefore, interpretation of changes in this group should be taken with caution, as the low numbers reduce precision of the data. Finally, glioma samples, specifically GBM, were surgically resected and have not been exposed to chemotherapy or radiotherapy to the best of our knowledge. This restricts the interpretation of sphingolipid alteration to a pre-treatment setting, excluding the effect of surgery. As a result, the current sphingolipid profile described cannot be assumed to represent recurrent tumours that have been exposed to multiple therapies. This could be examined in future studies to assess the effect of chemotherapy and radiotherapy on tumour sphingolipid metabolism and associated consequences.

SM, the most abundant sphingolipid, is an important component of myelin. In our cohort groups, AII and AIII samples had higher levels of total SM than NGM and GBM, which were similar in levels. The difference in total SM levels is due to the higher abundance of very long chain SMs, such as C24:1 in AII and AIII samples. This may be the result of more myelin incorporated in our samples, or a unique characteristic of low grade gliomas that increase very long chain SMs in AII, and as it progresses into an AIII gradually reduces SM levels, before returning to normal levels in GBM. Of note, the higher level of very long chain SMs in AII and AIII samples is also mirrored in very long chain ceramides. Alternatively, the difference may be due to analysing samples on the LC-MS/MS on different days. Having said that, rigorous quality control is factored into the experimental design through the use of internal and external standards for each run. Moreover, this possibility is less likely to be the case, as the most abundant SM chain length, C18 SM, is equal between NGM, AII, and AIII samples, although significantly reduced in GBM compared to NGM or AII samples. NGM and GBM samples were analysed concurrently, therefore experimental setup errors would not account for differences in C18 SM chain lengths. Additionally, when examining C16 SM, it is significantly increased in all glioma samples equally when compared to NGM. This supports the notion that differences in SM chain lengths between all groups are most probably due to true biological or tissue-composition differences (i.e. malignancy-related or myelin incorporation).

HexCer, combining GlcCer and GalCer, is significantly reduced in GBM. GlcCer and GalCer have the same mass, fragment mass, and elution profile for a gradient elution; therefore, it is difficult to resolve the difference between both compounds using a C8 column for the LC-MS/MS run. However, GlcCer is the precursor to LacCer, and

GalCer is the precursor to sulfatide. Since LacCer is increased in GBM, and sulfatide is reduced in GBM, then it is likely that the reduction in HexCer is due to a reduction in GalCer. An increase in GlcCer is plausible, to account for a significant increase in LacCer; however, to prove this definitively would require the separation of GlcCer and GalCer using a silica column and an isocratic (i.e. single continuous mobile phase) elution profile to give a 0.5-1 min separation between both sphingolipids [166]. For the purposes of our study, identifying and quantifying sphingolipids using the current methodology without the need to further separate groups (i.e. HexCer) is sufficient to answer key questions on sphingolipid composition in NGM and gliomas.

HexCer, associated with oligodendrocytes and Schwann cells due to myelin composition, is reduced in GBM samples compared to NGM and AII samples. Moreover, AIII samples have a trend reduction in HexCer levels compared to NGM. The reduction in HexCer levels in high grade gliomas may be contributed in part by the cellular composition of these tumours. As high grade astrocytomas have a rapid proliferation of mutated astrocyte-derived cells, the normal cytoarchitecture is replaced and destroyed. NGM, although it does not contain white matter, retains a balance between the various glial cells, which include oligodendrocytes. AII samples have a lower proliferation rate for neoplastic astrocytes compared to AIII and GBM samples [5]. Having said that, C16 HexCer is significantly elevated in all gliomas in comparison to NGM, which may reflect the increase noted in C16 SM causing a downstream increase in successive metabolites.

Following from HexCer, specifically GlcCer, LacCer is elevated in absolute levels and percentage compositions in specifically AII samples and GBM. AIII samples are

similar to NGM, but C16 LacCer is significantly elevated in AIII samples as well compared to NGM. Similar to HexCer, the increase in C16 LacCer may reflect upstream changes as opposed to a gain of function specific to LacCer. Of interest though, LacCer promotes cell migration of smooth muscle cells in the context of vascular disease [167]. LacCer has also been shown to interact with VEGF and induce angiogenesis *in vitro* and *in vivo* [61], therefore, an increase in C16 LacCer may have a role in promoting or supporting glioma-induced angiogenesis. The stark difference though in total LacCer levels between AIII samples compared to AII and GBM samples is difficult to explain. However, the AIII sample cohort is unequal in size compared to the other cohorts, therefore interpretation of absolute differences for AIII samples should be taken in context of the other cohorts, and further repeated measures would be required to ensure the validity of the AIII samples results.

Sulfatide, similar to HexCer, is an important component of myelin, forming 4% of total myelin lipid by mass [168]. In addition to being abundant in oligodendrocytes and Schwann cells, sulfatide is also present in astrocytes and neurons, albeit small amounts [169, 170]. As presented previously, HexCer has a trend reduction in AIII samples compared to NGM and AII samples, and a significant reduction in GBM samples compared to NGM and AII samples. Sulfatide has the same pattern, with the added significant reduction in sulfatide for GBM compared to AIII samples. The differences noted are likely due to the changing cellular balance, with a significant increase in astrocyte content in comparison to myelinating cells, such as oligodendrocytes. The possibility of a functional effect is plausible, as sulfatide binds to adhesion molecules P-selectin and L-selectin, inducing migration of immune cells [171]. Moreover, a mixture of literature reports an elevation of sulfatide in some cancers, and a reduction in other

cancers [172]. In our glioma cohort, sulfatide is reduced overall, with the exception of C16 sulfatide. As noted previously, C16 is elevated in SM, HexCer and LacCer. The elevation in C16 sulfatide is most likely due to an increase in C16 synthesis and incorporation into the sphingolipid pathway.

Ceramide reduction in glioma, identified previously [163], is reduced further as the histological grade is increased. This reduction is accounted by the loss of the most abundant ceramide chain length, namely C18 ceramide. Since ceramide is a known pro-apoptotic metabolite [80], regulator of cell polarity [173] and stem cell differentiation [174, 175], a reduction in this central metabolite has potential biological consequences, including a reduction of cellular stress in gliomas, and maintenance of a stem cell phenotype. Importantly though, as previously mentioned regarding C16 accumulation, C16 ceramide is also elevated, though only significantly upregulated in GBM compared to NGM, as opposed to all glioma groups. There is a notable increase in C16 ceramide as glioma grade increases. Again, the increase in C16 ceramide could simply be due to an increase in C16 fatty acid (palmitate) incorporation into the sphingolipid metabolic pathway, and the observations on increased sphingolipids with C16 acyl chains are downstream consequences. However, there is a concept known as “many ceramides”, where each ceramide chain length has a different biological action as reviewed recently by Hannun and Obeid [176]. Ceramide is understood to be composed of multiple entities that are interconnected and function differently within the cellular compartment it localises. This complexity cannot be addressed in the data we present, but interesting and valid changes can be noted. When examining the relationship between C16 and C18 ceramide, a clear positive correlation is observed in NGM, which is maintained for AII samples, but is lost in AIII and GBM samples. The balance between C16 and C18

ceramide is biologically important: C18 ceramide has been specifically implicated as a pro-apoptotic metabolite [82, 85], and a potential predictive marker for chemotherapy response in head and neck squamous cell carcinomas (HNSCC) [177]; in contrast, C16 ceramide is described as a protective ceramide against cellular endoplasmic reticulum (ER) stress in HNSCC, thereby facilitating tumour growth *in vivo* [82, 83]. Within our dataset, C18 ceramide is progressively reduced as a function of glioma grade, while C16 ceramide is significantly increased, thereby creating a protective environment for gliomas to survive and resist apoptotic stimuli. This is achieved by the suppression of apoptotic stimuli coupled with protection from cellular ER stress. These features may not be unique to gliomas, but possibly a common alteration in tumourigenesis, as this specific imbalance has been noted previously in HNSCC [86]. More importantly though, the layered complexity in ceramides and the concept of ‘interconnectedness’ implies that the shift in ceramide chain lengths does not end there, and has further knock-on effects to further elements in the sphingolipid pathway.

The reduction in ceramide is followed by an elevation in sphingosine in GBM compared to AII and AIII samples. Unexpectedly, levels between GBM and NGM were similar. Since ceramide was lower in GBM and S1P was higher compared to NGM, sphingosine, an intermediate metabolite, would have been expected to be higher in GBM compared to NGM. To account for the similar levels, sphingosine is likely to be rapidly interconverted to S1P or ceramide, which is supported by SPHK1, CERS2, and CERS5 overexpression. Moreover, the pattern of change for sphingosine between the four groups is similar to that of C16 ceramide. Although sphingosine is noted as a pro-apoptotic metabolite [178], the elevation in GBM compared to AII and AIII samples may reflect the drive of the rheostat pathway away from ceramide and towards S1P.

This is supported by the multivariate modelling, whereby high sphingosine levels significantly predicted high S1P levels. In contrast to ceramide, S1P, a known pro-proliferative [103, 179, 180], anti-apoptotic [65], and pro-angiogenic [153, 181] lipid mediator is elevated in all gliomas compared to NGM. The bioactive signalling of S1P is evidently enhanced in gliomas, and consequently its pleiotropic activity likely supports these tumours by evading apoptosis and stimulating angiogenesis as possible outcomes.

The enzymatic screen, mirroring most metabolomic changes observed, provides an insight to pivotal enzymes that have altered expression within the ceramide-S1P axis. When considering ceramide species, ceramide synthases are crucial in understanding the complex regulation, redundancies in the pathway and compartmentalized activity for *de novo* or salvage pathways in ceramide synthesis [160, 182]. With our dataset, we identify an upregulation of CERS5 but not CERS6, which is likely responsible for the elevated C16 ceramide levels in GBM. In contrast, CERS1, the key enzyme for C18 ceramide synthesis is relatively stable between NGM and gliomas. Since C18 ceramide is reduced as a function of glioma grade, and C18 ceramide is a specific product of CERS1 activity, the stability of this gene between the cohorts is unexpected. Potentially, proteasome-mediated degradation of the enzyme could explain this, as previously reported [183], such that CERS1 enzyme is degraded resulting in a reduction in C18 ceramide levels despite normal gene expression. Alternatively, a shift in the catabolic processing may account for the reduction in C18 ceramide specifically and ceramides in general to sphingosine. This is supported by an upregulation in ceramidases, namely acidic ceramidase (ASAH1) and alkaline ceramidase (ACER3). Moreover, the phosphorylation of sphingosine to S1P is catalysed by SPHK1, which is

significantly upregulated in the gliomas, and the reverse reaction catalysed by SGPP2 is significantly down regulated as well, indicating a predisposition towards enhancing S1P signalling in gliomas in comparison to NGM. Of note, SPHK2 which also phosphorylates sphingosine to S1P is down regulated significantly in gliomas, and illustrates a step-wise reciprocal pattern with SPHK1, whereby as SPHK1 increases there is a reduction in SPHK2, suggesting a negative feedback mechanism. Recently, in a model of colitis-associated cancer, *SPHK2*^{-/-} mice showed a significant overexpression of SPHK1, and an increase in S1P levels, suggesting that SPHK2 down regulation amplifies S1P levels through upregulating SPHK1 [184].

When examining the associations between the enzymes forming or catabolising S1P, many associations were significant within the results. In contrast, the modelling for conversion of sphingosine to S1P, and the reverse reaction, did not yield significant results for enzyme predictions. Having said that, the metabolites were closely associated, whereby if sphingosine was elevated, then S1P would be elevated, and vice versa. That association is linked with tissue grade, and adds emphasis that alteration in sphingolipid metabolism is interlinked with cancer formation and progression. However, the discrepancy between the correlation matrix and the multivariate analysis raises a few issues. First, the adjustment for grade, although statistically valid, may overshadow the basic biology, hence modelling enzymes and metabolites might be more appropriately examined in a homogenised group of samples. Second, our sample number was relatively small, and a larger cohort would increase the power to examine more variables. Third, since our data represents a single time point, dynamic changes were unaccounted for in the model; therefore, a suitable design including flux might address this limitation. In our attempt to model this pathway with our current data, we

identified a strong association between sphingosine and S1P, independent of tissue grade, but were unsuccessful in identifying the enzyme predictions for metabolite levels with the aim of further emphasising critical enzymes in the pathway.

In summary, the changes observed in metabolites, and even at the chain length, are an important confirmation that the sphingolipid rheostat is relevant to gliomas, and indicate potential changes in cellular differentiation status, apoptotic sensitivity, and angiogenesis as a result. In the following chapter, the functional significance will be investigated for the significant reduction in ceramide and increase in S1P for GBM samples.

Chapter 4: Assessing the Functional Effects of ASAH1 and SPHK1 Reduction in GBM cells

4.1 Introduction

Aberrant sphingolipid metabolism, as presented in the previous chapter and supported by the literature holds great potential to be modulated by targeting key enzymes in the pathway. The selection of the therapeutic targets is based on the degree of enzyme dysregulation, the target metabolite of interest, and the therapeutic potential. Each sphingolipid group presented has a degree of dysregulation, but our target metabolites of interest are ceramide and S1P due to their opposing biological properties, and their rheostat nature. Our metabolite data clearly demonstrated a reduction in ceramide for GBM, hence overexpression of ceramidases (i.e. ASAH1) that catabolise ceramide make an attractive target. Similarly, with a significant increase in S1P, overexpressed sphingosine kinases (i.e. SPHK1) that form S1P will also be targeted. Additionally, the combination of simultaneously inhibiting overexpressed ASAH1 and SPHK1 will be evaluated herein.

4.1.1 ASAH1

N-acylsphingosine amidohydrolase, also known as ASAH1, is a lysosomal enzyme that degrades ceramide into sphingosine. ASAH1 was first purified into apparent homogeneity in 1995 [185]. The gene, located on chromosome 8, contains 14 exons and 13 introns. An inherited deficiency in this enzyme leads to Farber Disease (FD), whereby ceramide accumulates in the lysosomes, and manifests clinically through painful nodule formation in the joints, hoarseness, growth retardation, and death by 2-3 years of age [186].

ASAH1 is one of five ceramidase enzymes, which hydrolyse ceramide into sphingosine [187]. Different stimuli induce ceramidases expression, including: cytokines (i.e. TNF α , IL-1 β), dexamethasone, chemotherapy (i.e. doxorubicin), and γ -radiation amongst other stimuli. ASAH1 has an optimum pH of 4.5, and a substrate preference for C6 to C16 ceramide [187]. Since ceramide is involved in cell growth arrest and apoptosis, ASAH1 is thought to mediate resistance to therapies in various cancers. Indeed, in the U87MG glioma cell line with a functional p53, overexpression of ASAH1 was induced by γ -radiation, and inhibition of ASAH1 with *N*-oleoylethanolamine resulted in ceramide accumulation and sensitisation to γ -radiation [188]. Additionally, ASAH1 has been shown to be overexpressed in prostate cancer [189], thereby protecting cells from TNF-induced apoptosis and mediating resistance to chemotherapy [190, 191]. In breast cancer, overexpression of ASAH1 correlated with tumour size and oestrogen receptor status [192]. Furthermore, stimulation of ASAH1 in MCF-7 breast cancer cells induced cellular proliferation [193], while in A375 melanoma cells, overexpression resulted in resistance to dacarbazine, a chemotherapeutic agent [194].

Since ASAH1 is overexpressed in gliomas, as presented in chapter 3, silencing this enzyme with a subsequent increase in ceramide should affect cellular progression.

4.1.2 SPHK1

SPHK1 has been described in Chapters 1 and 3, however in brief SPHK1 is overexpressed in a number of cancers, and more importantly, correlated with poor survival outcome in two independent studies in GBM [133, 134]. Moreover, overexpression of SPHK1 correlated with an increase in tumour grade progression from AII, to AIII, to GBM [133]. Furthermore, S1P generated by SPHK1 has been shown to induce tumour angiogenesis in breast cancer cells *in vitro* and *in vivo* [142, 153], and glioma cells, which was insufficiently blocked by VEGF inhibition [142]. The clinical correlations and pro-angiogenic tumour phenotype, along with the elevated S1P levels in GBM, strongly suggest SPHK1 is an important target to modulate. The effect of SPHK1 modulation using siRNA and pharmacological inhibition will be presented in the context of this chapter.

4.1.3 Hypothesis and Aims

Working hypothesis for this chapter:

1. The ceramide-S1P axis can be regulated by targeting key overexpressed sphingolipid enzymes; specifically, ceramide can be increased by inhibiting ASAH1, and S1P can be reduced by inhibiting SPHK1.
2. Regulating the ceramide-S1P axis will affect biological processes, thereby creating an unfavourable environment for cancer growth and progression.

The overall aim of this chapter is to examine the functional consequences of manipulating two overexpressed enzymes, ASAH1 and SPHK1, in GBM sphingolipid metabolism.

The specific aims of this chapter:

1. To examine the metabolite changes as a result of down regulating ASAH1 and SPHK1.
2. To examine proliferation, clonogenicity, and angiogenesis in the context of altering sphingolipid metabolism.
3. To examine the specific effect of bulk S1P reduction, using pharmacological inhibitors, on tumour proliferation and angiogenesis.

4.2 Results

In order to establish which cell line to examine for functional *in vitro* assays, the expression of ASAH1 and SPHK1 was analysed in a panel of immortalised GBM cell lines, and patient derived GBM (PDG) cell lines. In tandem, the ceramide-S1P axis was quantified in the immortalised GBM cell line panel. Two cell lines, one immortalised and one PDG cell line, were then selected for siRNA knockdown experiments. Successful knockdown of ASAH1 and SPHK1 was verified for gene expression, in both cell lines, and sphingolipid changes (immortalised cell line only). Functional work on cellular proliferation, clonogenicity, and angiogenesis were examined in the context of ASAH1 and SPHK1 silencing. Finally, pharmacological inhibition of SPHK1 activity and the consequences for proliferation and angiogenesis were examined in collaboration with researchers in Dr. Don's group (Qiao Qiao & Azadeh Matin).

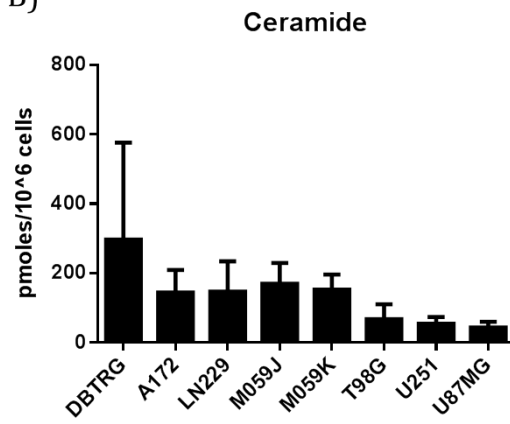
4.2.1 Ceramide, Sphingosine, and S1P Levels in GBM Cell Lines

A simple schematic diagram outlining the ceramide-S1P axis and the relation of the metabolites with ASAH1 and SPHK1 enzymes is illustrated in Figure 4.1.A. The immortalised cell lines listed in Figure 4.1 were originally derived from primary high grade gliomas, with the exception of DBTRG, which was derived from a recurrent GBM. As evident in Figure 4.1.B, ceramide content is highest in DBTRG by almost 2-fold compared to most cell lines, and in some cases 3-fold. Similarly in Figure 4.2.C and Figure 4.2.D, DBTRG has high levels of sphingosine and S1P. Interestingly, U251 has low levels of ceramide, sphingosine, and S1P compared to the other cell lines. In contrast, U87MG has low levels of ceramide and sphingosine, but high levels of S1P.

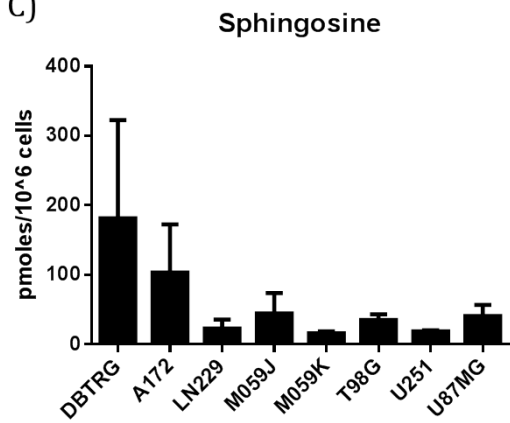
A)



B)



C)



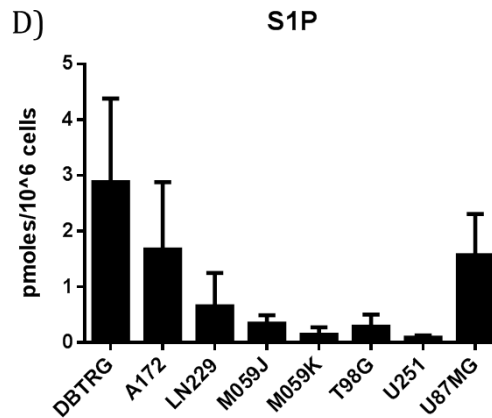


Figure 4.1 Ceramide-Sphingosine-S1P Levels in Immortalised GBM Cell Lines

(A) Schematic diagram of the ceramide-S1P rheostat axis. (B-D) Levels of ceramide, sphingosine, and S1P are presented in the bar graphs for each cell line (n=3) as mean +/- standard deviation (SD). All values represent the absolute quantification in pmoles adjusted to 10⁶ cells.

Levels of C16 ceramide, as seen in Figure 4.2.A, mirror total ceramide for the cell lines. Moreover, C16 ceramide contributes to the majority of ceramide content. In contrast, C18 ceramide follows a similar trend as sphingosine for cell-to-cell variation. Interestingly, C18 ceramide constituted only a small percentage of ceramide content for all cell lines. The relationship between C16 and C18 ceramide, as examined with a Pearson's correlation, was identified as a significantly positive correlation, therefore an increase in C18 ceramide would be accompanied by an increase in C16 ceramide, and vice versa.

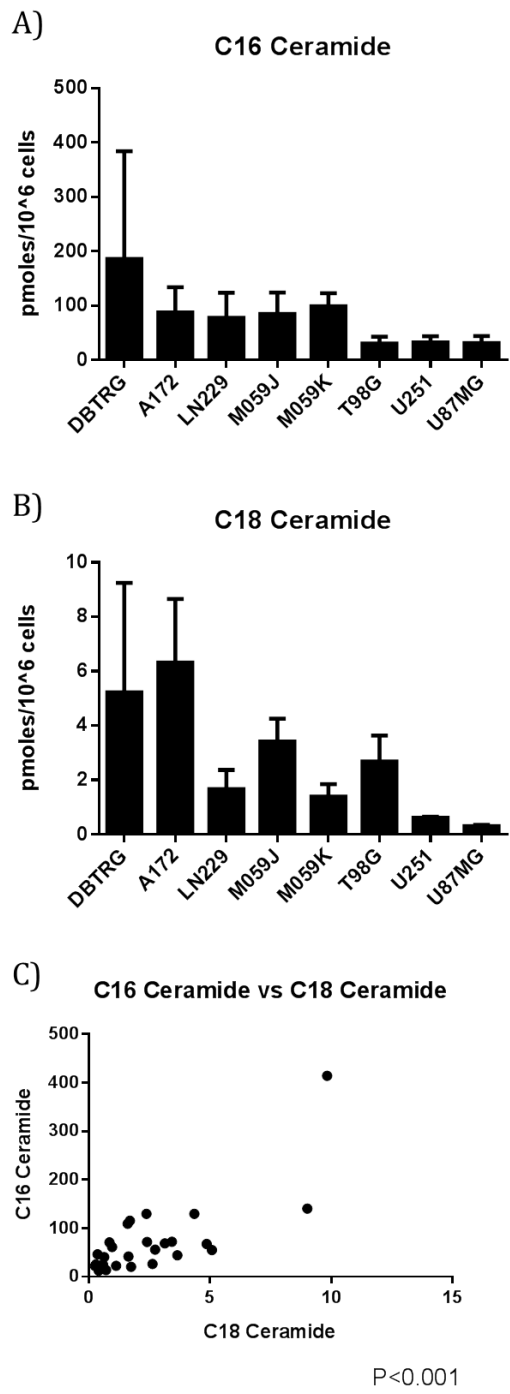
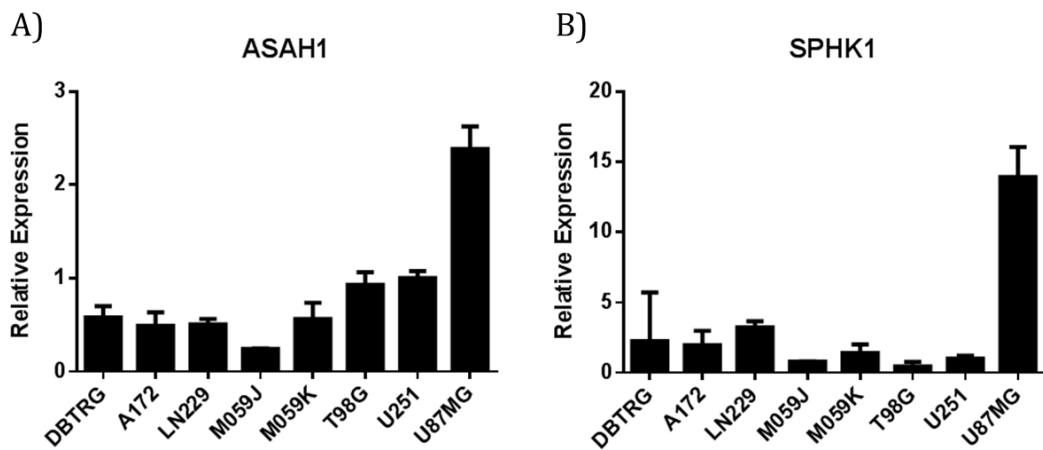


Figure 4.2 C16 and C18 Ceramide Levels in Immortalised GBM Cell Lines

(A-B) Levels of C16 and C18 ceramide are presented in bar graphs for each cell line as mean +/- SD (n=3). (C) Pearson correlation between C16 and C18 ceramide in cell lines was used to determine the p-value as indicated. All values represent the absolute quantification in pmoles adjusted to 10⁶ cells.

4.2.2 ASAH1 and SPHK1 Relative Gene Expression in GBM Cell Lines

Gene mRNA expression for ASAH1 and SPHK1 in a panel of immortalised GBM cell lines is illustrated in Figure 4.3.A-B. Surprisingly, the recurrent cell line, DBTRG, had baseline levels of ASAH1 and SPHK1 in comparison to the immortalised cell lines. Moreover, U87MG cells had the highest expression of both ASAH1, by 2- to 3-fold, and SPHK1, by 5- to 10-fold, relative to the panel. U251 had moderate ASAH1 expression, but low SPHK1 expression in comparison to the panel. Figure 4.3.C-D includes recurrent PDG cell lines (G1, G13, and G28) and primary (treatment naive) PDG cell lines (BAH1, HW1, PB1, RN1, and WK1). The expression of both enzymes is variable amongst the panel of PDG cells. ASAH1 was expressed highly in WK1, while SPHK1 was expressed highly in G1, a recurrent cell line, and RN1, a primary cell line, compared to the panel.



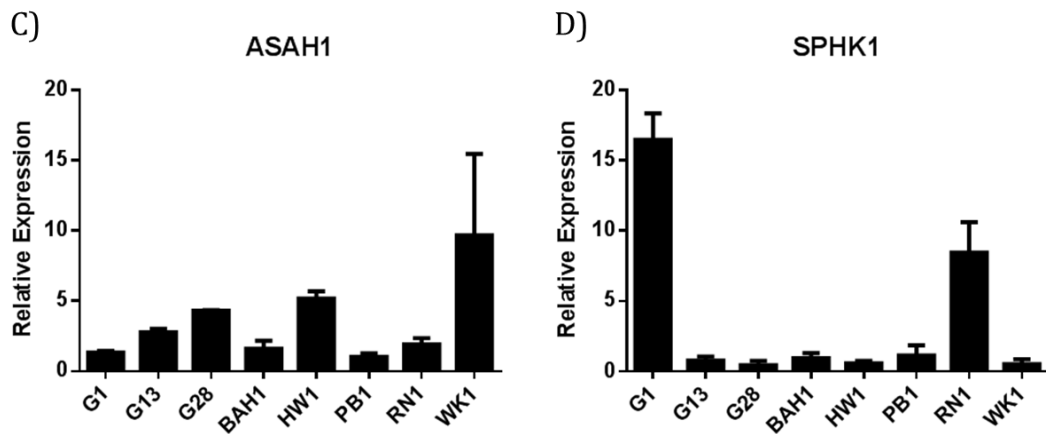


Figure 4.3 ASAHI and SPHK1 Relative Gene Expression in GBM Cell Lines

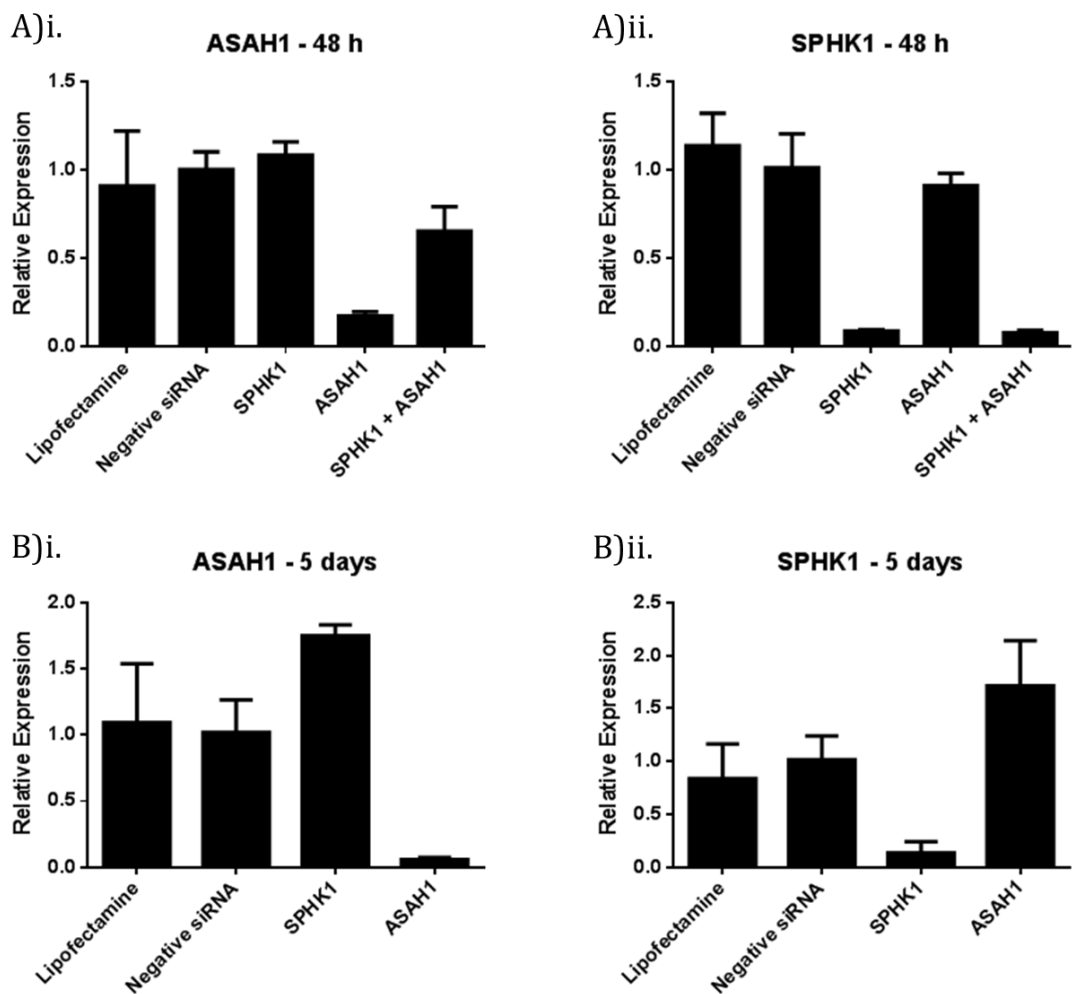
(A-B) Relative gene expression for ASAHI and SPHK1 in a panel of immortalized cell lines compared to U251. (C-D) Relative gene expression for ASAHI and SPHK1 in a panel of primary PDG cell lines compared to PB1. Gene expression is normalised to 18S rRNA, and expressed as mean +/- SD for triplicate measurements.

4.2.3 ASAHI and SPHK1 Knockdown Validation

Based on the gene expression data for the immortalised cell lines, U87MG was selected for further functional work, due to the high ASAHI and SPHK1 expression. As for the PDG cell lines, RN1 was selected for further functional work, due to the high SPHK1 expression, although ASAHI was only moderately expressed in comparison to the panel. Recurrent cell lines were not selected, as the tissue work conducted in chapter 3 was primarily newly diagnosed gliomas with no prior exposure to chemotherapy or radiotherapy, therefore only cell lines derived from primary gliomas were deemed appropriate.

U87MG cells were transfected with siRNA to SPHK1 and ASAHI mRNA expression of the targets assessed after 48 h (Figure 4.4.A), 5 days (Figure 4.4.B), and 8 days

(Figure 4.4.C). ASAHI was successfully knocked down after 48 h, and this was maintained throughout the time course of 8 days. The combination knockdown of SPHK1 + ASAHI at 48 h partially reduced ASAHI expression. SPHK1 was also successfully knocked down at 48 h, and remained reduced in expression at 5 days, but is re-expressing at near-normal expression by 8 days. The combination knockdown of SPHK1 + ASAHI at 48 h reduced SPHK1 expression.



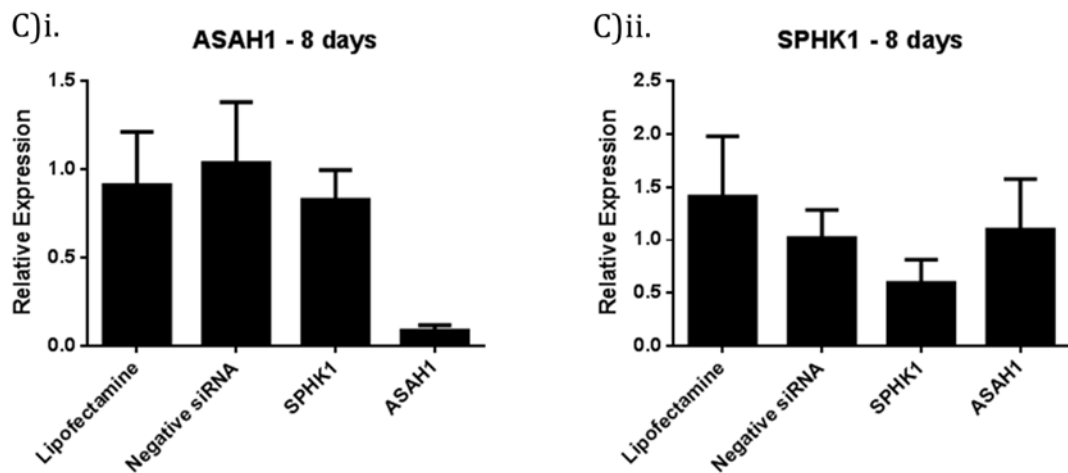
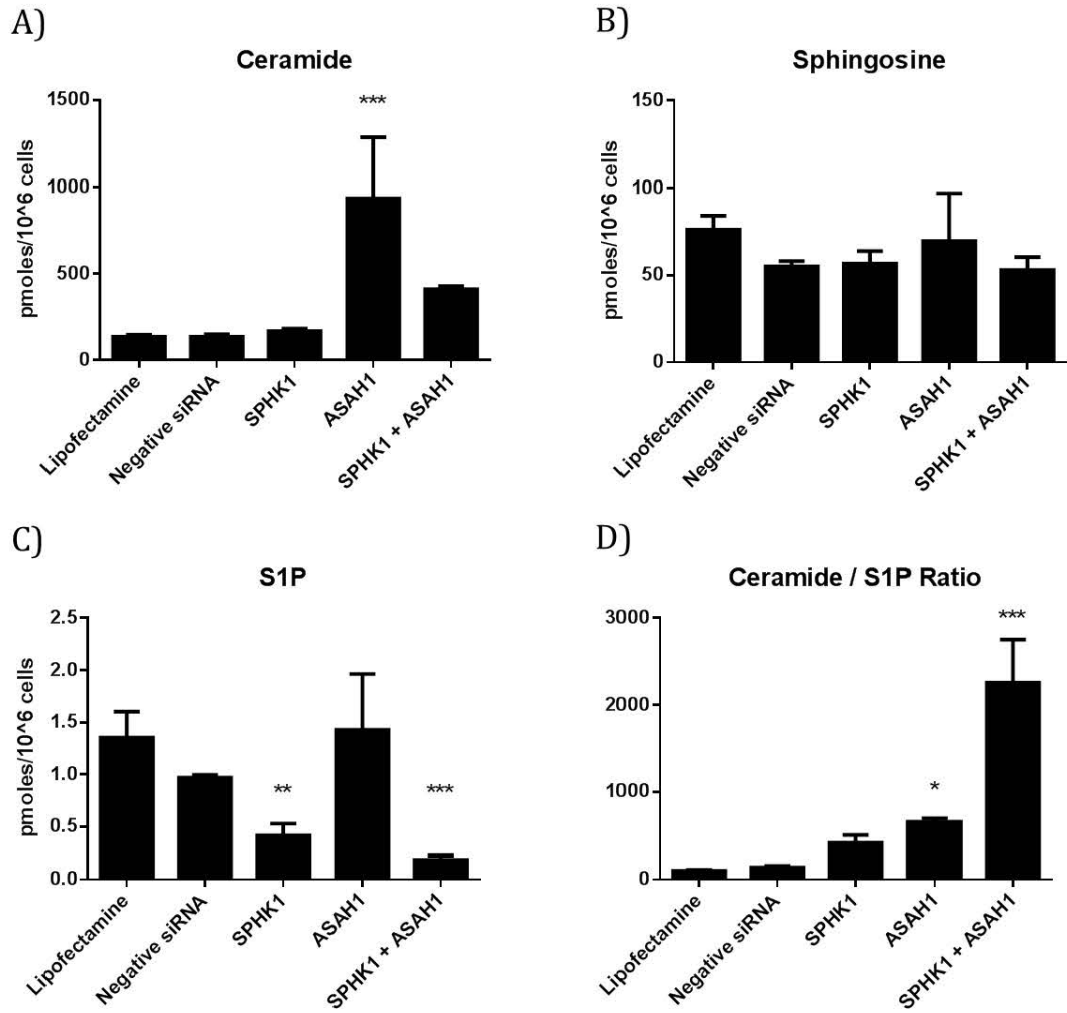


Figure 4.4 Gene Expression Analysis Post ASAHI and SPHK1 Knockdown in U87MG Cells

(A-C) Relative gene expression for ASAHI (i) and SPHK1 (ii) in the U87MG cell line at 48 h (Ai, Aii), 5 days (Bi, Bii), and 8 days (Ci, Cii) following transfection as indicated in each group. Negative siRNA is a non-targeting siRNA control. Gene expression is normalised to 18S rRNA, and expressed as mean +/- SD for triplicate measurements (n=2 for A, n=1 for B and C).

Following the knockdown of ASAHI and SPHK1 in U87MG, sphingolipid analysis was performed to assess the impact on the ceramide-S1P axis at 72 h, as shown in Figure 4.5. Ceramide levels were unaffected following SPHK1 silencing, but ASAHI reduction resulted in the significant accumulation of ceramide. The combination of SPHK1 + ASAHI also enhanced ceramide accumulation, but not significantly. Sphingosine levels, surprisingly, were unaffected by either or both of ASAHI and SPHK1 reduction. S1P, following SPHK1 reduction was significantly reduced, but unaffected by ASAHI reduction. The combination of SPHK1 + ASAHI also resulted in a reduction in S1P levels. A ratio, illustrating the amount of ceramide relative to S1P identified the combination treatment as having the most significant impact on the rheostat balance, followed by ASAHI reduction, and a trend increase in the ceramide to S1P ratio with SPHK1 reduction. Of note, elevation of ceramide, following ASAHI or

the combination of SPHK1 + ASAH1, was evident in all chain lengths, with both C16 and C18 ceramide accumulating as seen in Figure 4.5.E-F.



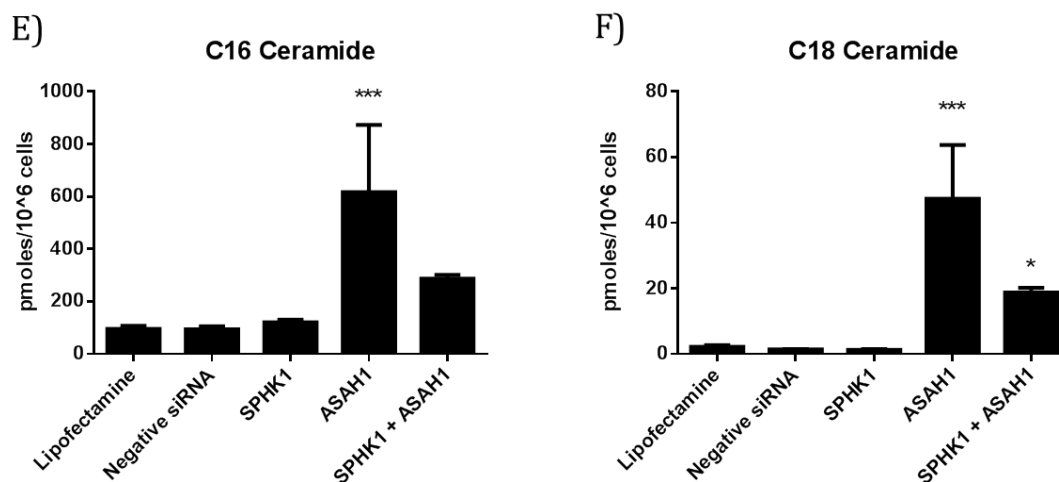


Figure 4.5 Spingolipid Analysis Post ASA1 and SPHK1 Knockdown in U87MG Cells

Levels of ceramide (A), sphingosine (B), S1P (C), C16 ceramide (E), and C18 ceramide (F) are presented in bar graphs for the U87MG cell line as mean \pm SD (n=3) following transfection for 72 h. (D) Ratio of ceramide/S1P is presented in a bar graph representing the relative amounts of metabolites in each condition. Metabolite values represent the absolute quantification in pmoles adjusted to 10^6 cells. Statistical significance was determined with an ANOVA and Dunnett's post hoc test, comparing each transfection with Lipofectamine. *p-value <0.05, **p-value <0.01, ***p-value <0.001.

Knockdown of ASA1 and SPHK1 were also performed for 72 h in the PDG line, RN1 (Figure 4.6). Similar to U87MG knockdowns, ASA1 and SPHK1 + ASA1 siRNAs successfully reduced ASA1 expression in the RN1 cell line. Moreover, SPHK1 and SPHK1 + ASA1 siRNAs successfully reduced SPHK1 expression as well compared to controls.

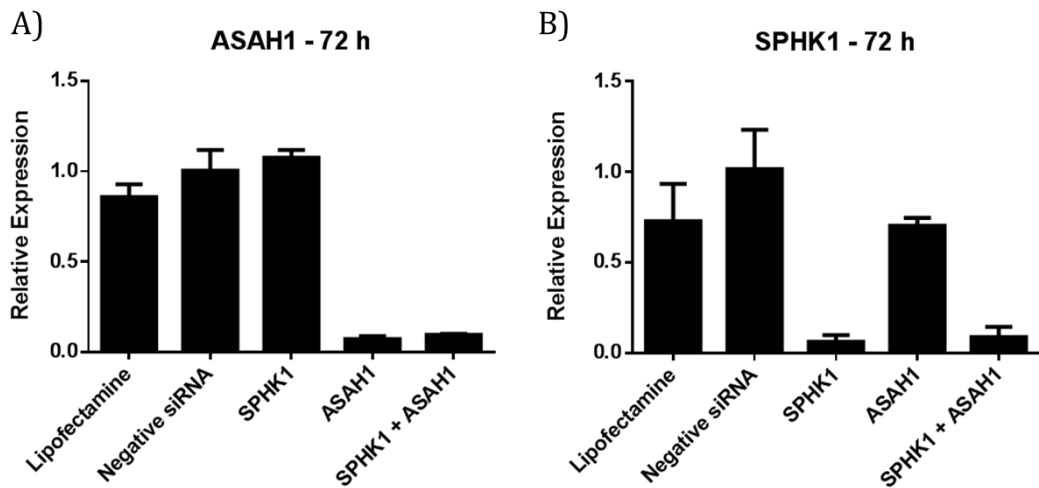


Figure 4.6 Gene Expression Analysis Post ASAHI and SPHK1 Knockdown in RN1 Cells

(A-B) Relative gene expression for ASAHI (A) and SPHK1 (B) in the RN1 cell line at 72 h following transfection as indicated in each group. Gene expression is normalised to 18S rRNA, and expressed as mean +/- SD for triplicate measurements (n=2).

4.2.4 Functional Consequences of SPHK1 and ASAHI Knockdown

Following the validation of ASAHI and SPHK1 knockdown, three *in vitro* assays (proliferation, clonogenicity, and angiogenesis) were examined to assess the effect of inhibiting either or both enzymes in the sphingolipid pathway. Proliferation was assessed for 96 h in U87MG cells. Viable cells, staining negative for propidium iodide (PI), were assessed with flow cytometry cell counting. SPHK1 knockdown significantly reduced proliferation of U87MG cells, while ASAHI knockdown had no effect on proliferation. The combination of SPHK1 + ASAHI knockdown had a negative trend reduction in U87MG proliferation as indicated in Figure 4.7.A. RN1 cells were assessed for proliferation at 10 days. Similar to U87MG cells, SPHK1 knockdown significantly reduced proliferation of RN1 cells, while ASAHI knockdown

had no effect. However, the combination knockdown also significantly reduced proliferation of RN1 cells.

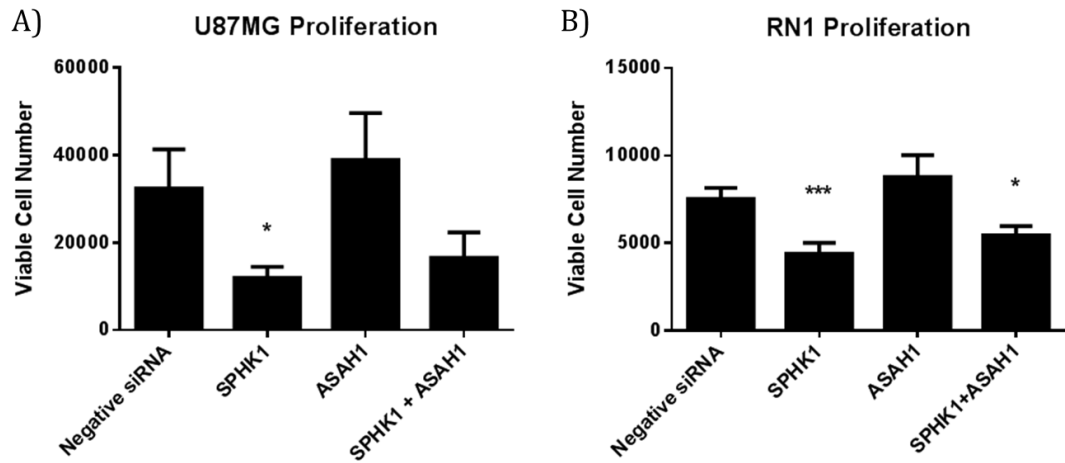


Figure 4.7 Effect of SPHK1 and ASA11 Knockdown on Proliferation in U87MG and RN1 Cells

(A-B) Relative viable cell numbers for U87MG (A) and RN1 (B) cell lines at 96 h and 10 days, respectively, following transfection with the indicated siRNA. Relative viable cells, determined with cell counting and PI staining, are expressed as mean \pm SD for triplicate (A) or quadruplicate transfections (B). Statistical significance was determined with an ANOVA and Dunnett's post hoc test, comparing each transfection with negative siRNA. *p-value <0.05, ***p-value <0.001. Note: experiment performed in conjunction with Qiao Qiao.

Clonogenicity assesses the ability of single cells to form their own colonies, which tumours, and specifically stem cells, are capable of forming. RN1 was assessed for clonogenicity at day 14 following transfection with the indicated siRNAs (see Figure 4.8). SPHK1 knockdown significantly reduced RN1 colony formation, while ASA11 had no significant affect, and the combination had a negative trend reduction in colony formation. Representative images for colonies, stained with 0.5% crystal violet and quantified with ImageJ, include negative siRNA (i), SPHK1 (ii), ASA11 (iii), and SPHK1 + ASA11 (iv) as presented below. SPHK1 (ii) has clearly lower colonies formed than the other groups as per the visual representation.

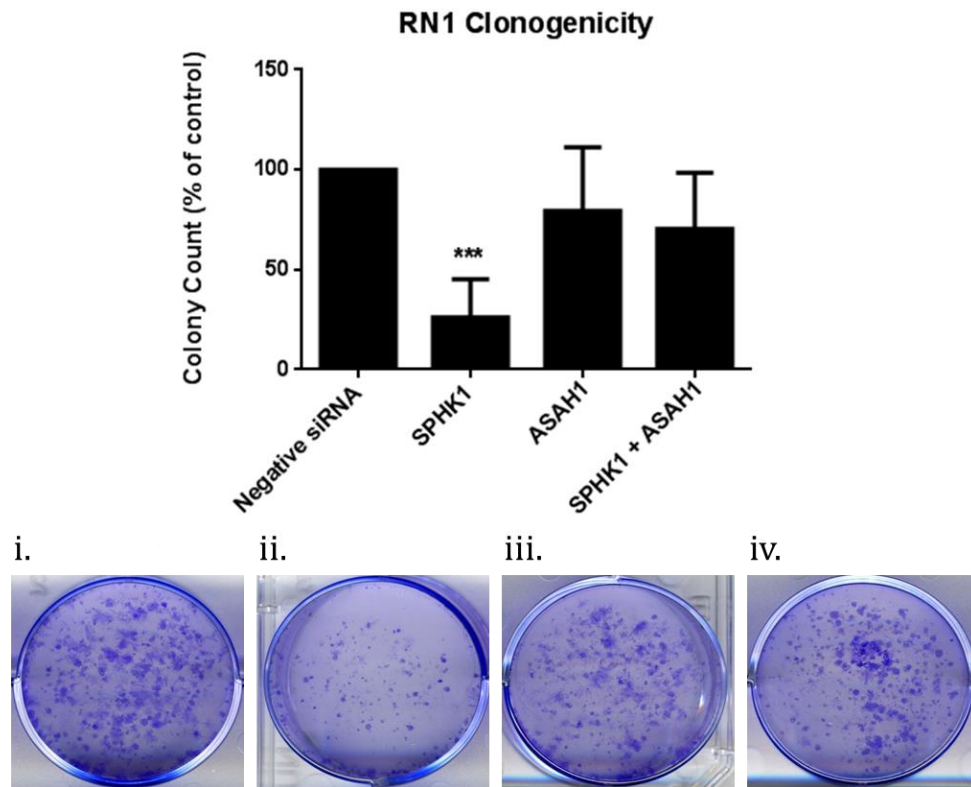
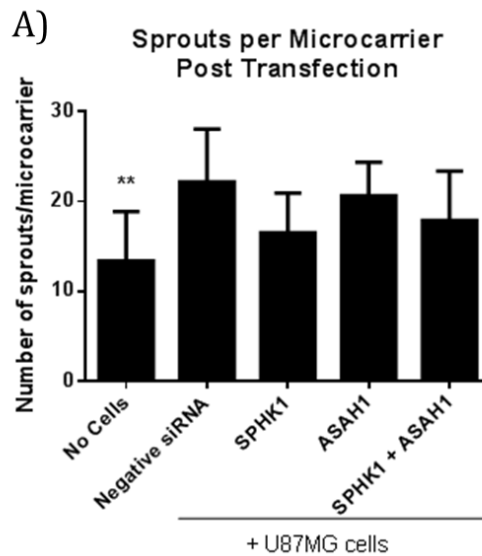


Figure 4.8 Effect of SPHK1 and ASAH1 Knockdown on Clonogenicity in RN1 Cells

RN1 colony counts, 14 days after transfection with the indicated siRNA, are expressed as a percentage of control. Colony counts percentage, as identified with ImageJ, is expressed as mean \pm SD for quadruplicate transfections. Representative images of negative siRNA (i), SPHK1 (ii), ASAH1 (iii), and SPHK1+ASAH1 (iv) for colony formation are presented. Statistical significance was determined with an ANOVA and Dunnett's post hoc test, comparing each transfection with negative siRNA. ***p-value <0.001.

Angiogenesis, a hallmark of many solid tumours [161], was assessed using a co-culture method as described in Chapter 2.5.7. Briefly, Human Microvascular Endothelial Cell line (HMEC-1) cells were grown on microcarriers and embedded into a fibrin gel. U87MG cells were seeded on top, but were transfected for 72 h prior to seeding (see Figure 4.9). A “no cells” control, where no U87MG cells are seeded on top of HMEC-1 bound to microcarriers, was added to each experiment to account for background sprouting as indicated in Figure 4.9. The angiogenesis assay was quantified for the numbers of sprouts per microcarrier (A), average sprout length (B), and percentage of

sprouts greater than 100 μm in length (C). The “no cell” control was significantly lower in all three categories compared to the negative siRNA. Only SPHK1 knockdown of U87MG cells resulted in a significant reduction of the average sprout length and percentage of sprouts greater than 100 μm in length, while the number of sprouts per microcarrier illustrated a trend reduction in comparison to the negative siRNA. In contrast, ASAH1 and the combination of SPHK1 + ASAH1 did not affect U87MG induced angiogenesis for HMEC-1 cells, despite a trend reduction in the percentage of sprouts greater than 100 μm in length.



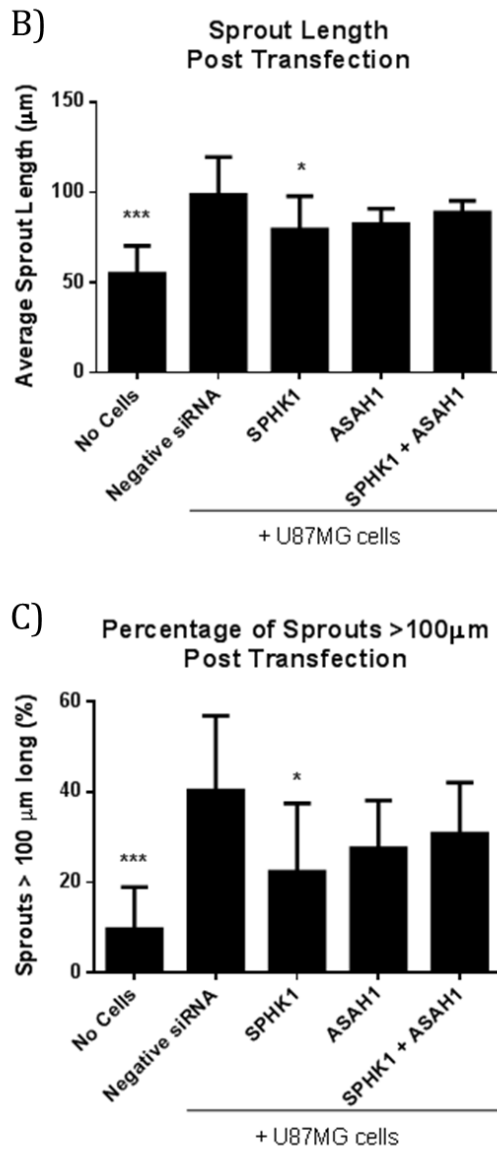


Figure 4.9 Effect of SPHK1 and ASAH1 Knockdown on Angiogenesis in Co-cultured U87MG and HMEC-1 Cells

(A-C) U87MG induced angiogenesis is quantified for the number of HMEC-1 sprouts per microcarrier (A), average sprout length (B), and percentage of sprouts greater than 100 µm in length (C). Each bar graph represents the mean +/- SD of two independent experiments, with a range of 4-8 microcarriers analysed per experiment following 7 days post transfection of U87MG cells. Seeding of U87MG cells with HMEC-1 cells bound to microcarriers was at 72 h post transfection, and lasted for 4 days. Media was replenished every 48 h. Statistical significance was determined with an ANOVA and Dunnett's post hoc test, comparing each transfection with negative siRNA. *p-value <0.05, **p-value <0.01, ***p-value <0.001.

4.2.5 Pharmacological Inhibition of SPHK1

In support of the siRNA work, selective drug inhibition is key in illustrating that functional consequences are not due to off-target effects, but specifically as a result of target modulation. In this context, SPHK1 was selectively targeted using a nanomolar potency inhibitor, SKI-1a, recently published [195]. Additionally, a stereoisomer control for SPHK1 inhibition, SKI-1b, which is two orders of magnitude [or 100-fold] less potent as a SPHK1 inhibitor, was used to illustrate the specificity of SKI-1a. ASAH1 was not selected for drug inhibition due to the lack of a suitably potent, selective, and cell-permeable inhibitor.

The changes in S1P (A), sphingosine (B), and ceramide (C) as a result of SPHK1 drug inhibition in U87MG cells are shown in Figure 4.10. SKI-1a, and not SKI-1b, dose-dependently reduced cellular S1P content significantly in U87MG cells, reaching statistical significance at 300 nM. In contrast, SKI-1a, and not SKI-1b, resulted in significant accumulation of sphingosine at 1000 nM, and the significant accumulation of ceramide at 300 nM in U87MG cells.

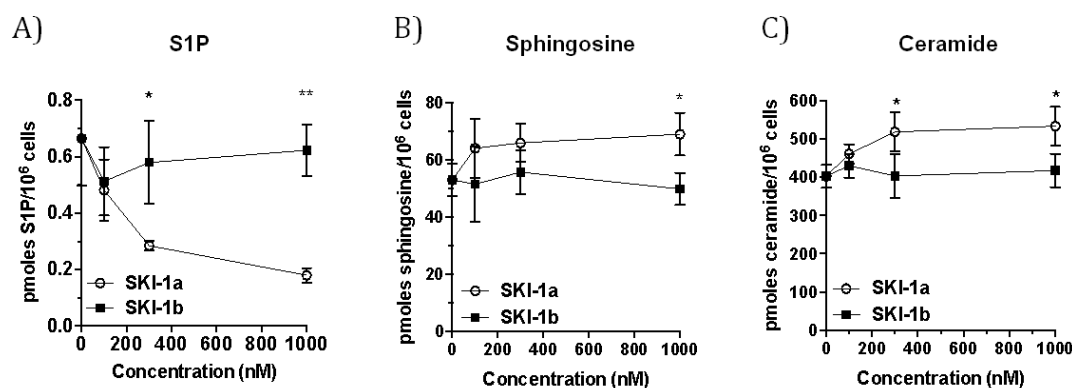


Figure 4.10 S1P, Sphingosine, and Ceramide Levels Post SPHK1 Drug Inhibition in U87MG Cells

(A-C) Levels of S1P (A), sphingosine (B), and ceramide (C) in U87MG cells following 72 h treatment with SKI-1a or 1b at indicated concentrations. Results are mean \pm SD derived from triplicate treatments. Statistical significance was determined using a 2-way ANOVA and Bonferroni's post hoc test to compare SKI-1a to 1b. *p-value <0.05, **p-value <0.01, ***p-value <0.001. Note: experiment performed in conjunction with Dr. Don.

4.2.6 Effect of SPHK1 Drug Inhibition on Proliferation

U87MG, RN1, HMEC-1 cells were treated with SKI-1a or SKI-1b for 7 days with 100 nM, 300 nM, or 1000 nM. Proliferation was assessed with an MTT assay (described in Chapter 2.5.4). U87MG cellular proliferation was not affected by either SKI-1a or SKI-1b, though at 1000 nM there was a trend reduction in viable cells for both compounds. Similarly, RN1 cellular proliferation was not affected by either drug, but at 1000 nM a more pronounced trend reduction in viable cells was apparent for both compounds. Finally, HMEC-1 cells were not affected, even at the higher dose of 1000 nM, by either compound. This data contrasts the siRNA proliferation data presented previously.

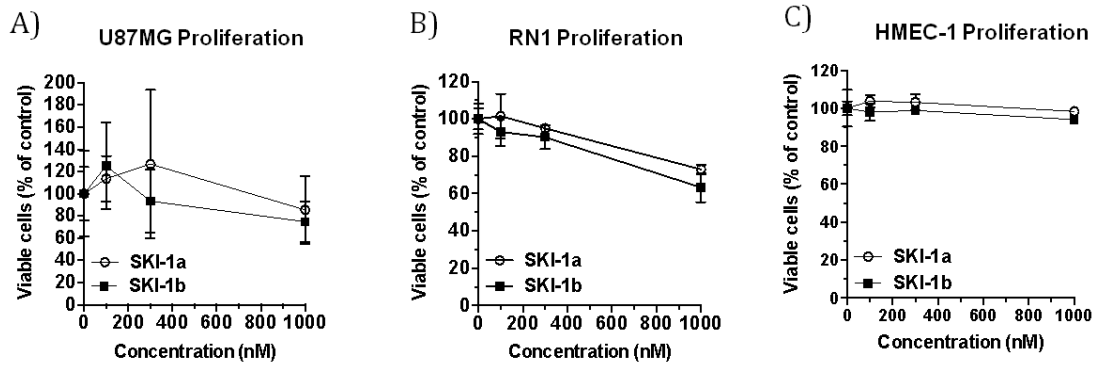


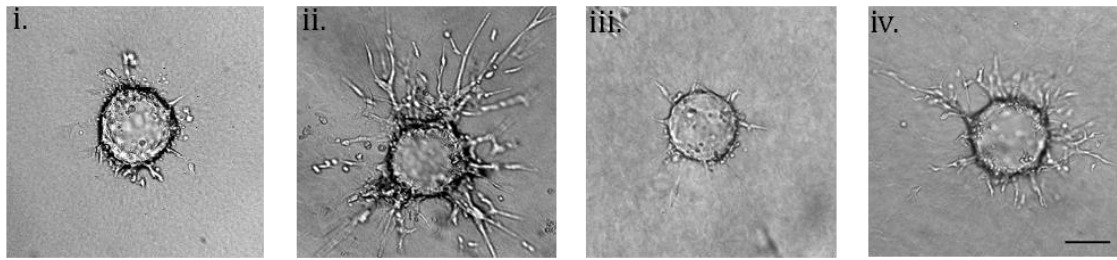
Figure 4.11 Effect of SPHK1 Drug Inhibition on Proliferation in U87MG, RN1, and HMEC-1 Cells

(A - C) Effect of SKI-1a and 1b on proliferation of U87MG (A), RN1 (B), and HMEC-1 (C) cells was assessed after 7 days by MTT assay. Results are mean \pm SD derived from two independent experiments. Statistical significance was determined using a 2-way ANOVA and Bonferroni's post hoc test to compare SKI-1a to 1b. *p-value <0.05, **p-value <0.01, ***p-value <0.001. Note: experiment performed by Azadeh Matin.

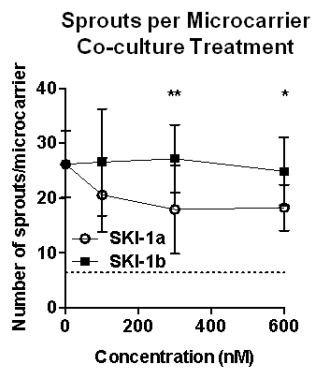
4.2.7 Anti-angiogenic Effect of SPHK1 Drug Inhibition

U87MG cells were co-cultured with HMEC-1 bound to microcarriers, and treated with different doses of SKI-1a or SKI-1b for 4 days. Representative images of HMEC-1 cells sprouting from a microcarrier for the following seeding conditions: no U87MG cells (i), U87MG + vehicle (ii), U87MG + 300 nM SKI-1a (iii), and U87MG + 300 nM SKI-1b (iv) are shown in Figure 4.12.A. Quantification of number of sprouts per microcarrier (B), average sprout length (C), and percentage of sprouts greater than 100 μ m in length (D) were assessed. SKI-1a, at 100 nM, had a trend reduction in all three parameters. Moreover, doses of 300 nM and 600 nM showed a significant reduction in all three parameters for SKI-1a compared to SKI-1b. Average sprout length and percentage of sprouts greater than 100 μ m in length progressively reduced as SKI-1a dosage increased, while SKI-1b had an insignificant impact on the *in vitro* angiogenic process.

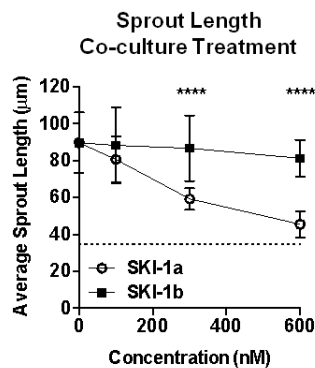
A)



B)



C)



D)

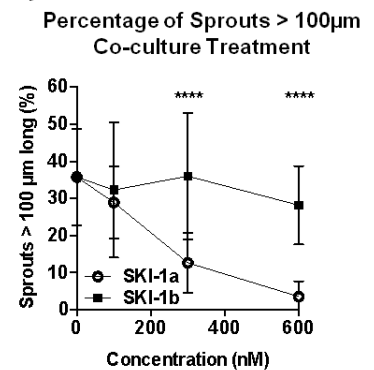


Figure 4.12 Effect of SPHK1 Drug Inhibition on Angiogenesis in Co-cultured U87MG and HMEC-1 Cells

(A) Representative images for HMEC-1 cells bound microcarriers treated with no U87MG cells (i), U87MG + vehicle (ii), U87MG + 300 nM SKI-1a (iii), or U87MG + 300 nM SKI-1b (iv). Scale bar equals 100 μm . (B-D) U87MG induced angiogenesis is quantified for the number of HMEC-1 sprouts per microcarrier (B), average sprout length (C), and percentage of sprouts greater than 100 μm in length (D). Each value represents the mean \pm SD of three independent experiments, with approximately 6-10 microcarriers analysed per experiment following 4 days of co-culture treatment at the indicated concentrations. The negative control of HMEC-1 bound microcarriers with no U87MG cells is indicated as a dotted line on the graphs. Statistical significance was determined using a 2-way ANOVA and Bonferroni's post hoc test to compare SKI-1a to 1b. *p-value <0.05, **p-value <0.01, ****p-value <0.0001. Note: experiment performed in conjunction with Azadeh Matin.

The co-culture treatment with SKI-1a or SKI-1b may be affecting either or both of U87MG and HMEC-1 cells. Therefore, U87MG cells were pre-treated for 48 h with SKI-1a or SKI-1b at 500 nM, and the conditioned media, which includes the respective drug treatments, was added for 4 days to HMEC-1 cells bound to microcarriers as indicated in Figure 4.13. Conditioned media from U87MG cells treated with SKI-1a

produced a significant reduction on sprouts per microcarrier, average sprout length, and percentage of sprouts greater than 100 μm in length, while SKI-1b had no effect compared to the vehicle-treated conditioned media. S1P, at 100 nM, was added directly to the co-culture with treated conditioned media. The addition of S1P into conditioned media from U87MG cells treated with SKI-1a had a significant impact in rescuing HMEC-1 sprouting, while the addition of S1P to the SKI-1b condition had no significant effect in further promoting sprouting of HMEC-1 cells.

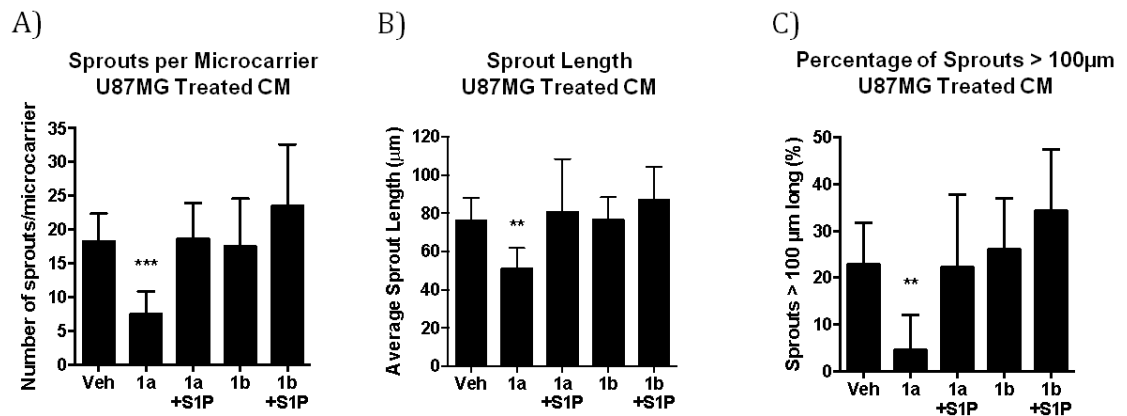


Figure 4.13 Effect of SPHK1 Drug Inhibition on Angiogenesis in Co-cultured U87MG Treated CM and HMEC-1 Cells

(A-C) Number of HMEC-1 sprouts per microcarrier (A), average sprout length (B), and percentage of sprouts greater than 100 μm in length (C) were determined for HMEC-coated microcarriers cultured for 4 days in conditioned medium taken from U87MG cells treated with vehicle (Veh), 500 nM SKI-1a (1a), or 500 nM SKI-1b (1b). S1P (100 nM) was added directly to the angiogenesis assay where indicated. Results shown are mean \pm SD derived from a minimum of ten microcarriers per condition. Statistical significance was determined using an ANOVA and Dunnett's post hoc test comparing each treatment to the vehicle control. *p-value <0.05, **p-value <0.01, ***p-value <0.001. Note: experiment performed in conjunction with Azadeh Matin.

To examine the effect of SKI-1a on HMEC-1 cells directly, conditioned media from untreated U87MG cells was added to the co-culture angiogenesis assay. HMEC-1 cells bound to microcarriers were treated with vehicle or SKI-1a for 4 days. Sprouting

induced by U87MG conditioned media was not affected by SKI-1a for all three parameters, as shown in Figure 4.14.A-C.

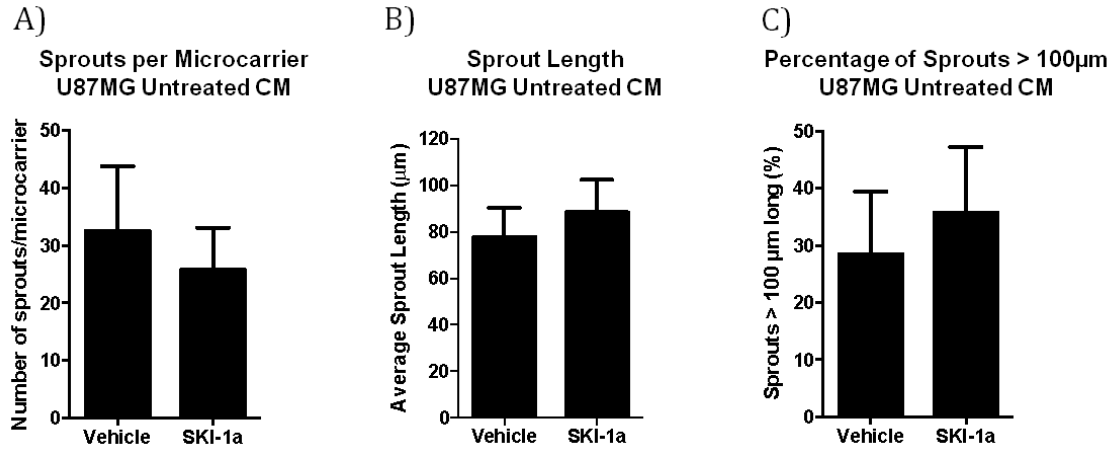


Figure 4.14 Effect of SPHK1 Drug Inhibition on Angiogenesis in Co-cultured U87MG Untreated CM and HMEC-1 Cells

(A-C) Number of sprouts per microcarrier (A), average sprout length (B), and percentage of sprouts greater than 100 µm in length (C) were determined for HMEC-1 bound microcarriers cultured for 4 days in U87MG conditioned medium and treated with vehicle or 500 nM SKI-1a. No statistical significance was identified between vehicle control and SKI-1a using unpaired t-tests.

4.3 Discussion

The work presented in this chapter subdivides into three main areas for discussion. First, sphingolipid analysis and enzyme expression for the cell line panel and knockdown validation established the experimental platform. Second, siRNA silencing to assess proliferation, clonogenicity, and angiogenesis provided the functional relevance of pathway modulation in limiting tumour progression. Third, drug testing with a selective potent inhibitor for SPHK1 confirmed the siRNA functional work and sets the focus for *in vivo* experiments.

4.3.1 Cell Line Screen and Knockdown Validation

The sphingolipid profile for the cell lines, although focused on the ceramide-sphingosine-S1P axis only, contained interesting sphingolipid changes that in some cases were comparable to the GBM tissue data in chapter 3, and in other cases were non-representative of clinical disease profile. Ceramide levels in the recurrent cell line, DBTRG, were higher than the immortalised cell lines derived from treatment naive high grade gliomas. Although our GBM tissue data presented included only newly diagnosed GBMs that were treatment naive, tissue from recurrent GBMs were assessed, and had higher levels of ceramide compared to treatment naive GBMs. The data was not presented, as the cohort of recurrent GBMs was less than 5 samples, therefore conclusions drawn from that sample size may be misleading. Higher ceramide levels in recurrent tissue samples or cell lines derived from recurrent tumours is plausible, because ceramide accumulation can be induced through chemotherapy, radiotherapy,

hypoxia, and other cellular stress causing agents [196]. However, the permanency of high ceramide levels, created through *de novo* synthesis or SM hydrolysis, is unknown.

Of interest, the levels of C16 and C18 ceramide in GBM cell lines compared to GBM tissues were different in percentage composition; C16 ceramide was the main contributor for total ceramides in cell lines, while C18 ceramide was the main contributor for total ceramides in GBM tissue. The low C18 ceramide and high C16 ceramide in our GBM cell lines may reflect a characteristic of cells grown artificially, as opposed to a functional consequence. However, in a study examining HNSCC compared to adjacent normal tissue, C18 ceramide was reduced significantly in the carcinoma samples, while C16 ceramide was increased. Moreover, when C18 ceramide was increased 2-fold by over expressing CERS1, previously known as LAG1, cellular proliferation was reduced by 70-80% [86]. Since C18 ceramide induces caspase activation and reduces tumour growth, while C16 ceramide protects against endoplasmic reticulum (ER) stress thereby promoting tumour survival [82], it is plausible that the low levels of C18 ceramide, and equally, high levels of C16 ceramide support the tumour cells. Alternatively, the low levels of C18 ceramide may reflect rapid conversion to downstream metabolites, such as sphingosine and S1P.

Sphingosine, previously noted to account for 5-10% of ceramide content in NGM and glioma samples, illustrated extremely high levels in GBM cell lines, accounting for approximately 50% of ceramide content. S1P levels however, were at concentration levels similar to GBM tissue samples, although exact conversion is not an accurate measure as tissue samples were adjusted per mg, while cells lines were adjusted per 10^6

cells. S1P levels were variable among the immortalised cell lines, with the highest levels present in DBTRG, A172 and U87MG cells.

ASAH1 and SPHK1 gene expression did not reflect the variation in metabolites. For example, U87MG had the highest expression of ASAH1, and relatively low ceramide levels, which should result in higher sphingosine levels. However, sphingosine was relatively low in U87MG, which may be explained by the 5- to 10-fold increase in SPHK1 that manifests with high S1P levels. In contrast, DBTRG has similar ASAH1 and SPHK1 expression to the other cells lines, yet has high ceramide, sphingosine, and S1P levels in comparison. The inconsistency between gene expression predicting metabolite levels underscores the complexity of the sphingolipid pathway, and the influence multiple enzymes have on a single metabolite. As discussed earlier, S1P levels are directly controlled by multiple enzymes, including sphingosine kinases, S1P phosphatases, and S1P lyase. Therefore predicting levels based on the expression of one enzyme is likely to be overly simplistic. Having said that, enzyme knockdown of ASAH1 or SPHK1 had profound effects on ceramide and S1P levels respectively, therefore the contribution of both enzymes to metabolite levels is evident.

The PDG cell line panel also showed variable expression of ASAH1 and SPHK1. The cell lines: WK1, HW1 and G28 had the highest ASAH1 expression, while G1 and RN1 had the highest SPHK1 expression. Selection of cells lines was determined based on SPHK1 expression, which is an unfavourable prognostic marker for survival in GBM, and correlated with increased glioma grade progression, therefore clinically relevant [133, 134]. As a result, U87MG was chosen for functional analysis for the

immortalised cell lines. Additionally, a primary PDG cell line was selected instead of a recurrent PDG cell line; hence RN1 was studied for siRNA functional experiments.

Reducing ASAH1 mRNA levels resulted in a further increase in ceramide levels compared to control cells. Both C16 and C18 ceramide were significantly elevated demonstrating no effect of the reduced ASAH1 levels on preferentially increasing one ceramide chain length over another. In contrast, knockdown of SPHK1 led to the significant reduction of S1P levels, with no evidence of sphingosine or ceramide accumulation. Dual knockdown of both SPHK1 and ASAH1 resulted in an increase in ceramide levels (significant though not as pronounced), and a reduction in S1P. Of note, control levels for ceramide and S1P differ for U87MG cells between the siRNA and the drug inhibitor experiments, which may be due to the different treatments applied (lipofectamine vs DMSO). Alternatively, the experiment may reflect the variation between individuals in cell pipetting prior to cell counting. Importantly, both experiments have been adequately controlled for the specific hypotheses examined.

Although gene expression was examined at 48 h, metabolites were examined at 72 h to allow for the gene silencing effects to translate at the metabolite level. The apparent compensatory increase of SPHK1 for ASAH1 knockdown, and ASAH1 for SPHK1 knockdown was not significant at 5 days, and therefore will unlikely effect metabolite levels. The time course assessed the length of time gene silencing was maintained to inform the design time for functional assays. The clonogenic experiment has expanded beyond our time course, and the transient gene silencing is unlikely to be maintained for 14 days. However, the purpose of the experiment is to assess the initial impact of gene

silencing on colony formation, and the added length of time allowed the separation of the groups as indicated in Figure 4.8.

4.3.2 Proliferation, Clonogenicity, and Angiogenesis in siRNA Experiments

There was decreased proliferation for U87MG cells, and decreased proliferation and clonogenicity for RN1 cells following SPHK1 silencing, which is supported by other studies [130, 197-199]. Several mechanisms have been suggested for SPHK1 in promoting cancer cell proliferation. In a study examining breast cancer cells, MCF-7, SPHK1 induced proliferation through an oestrogen-dependent mechanism, which involved the activation of extracellular signal-related kinases (ERK1/2). As a result, activator protein 1 (AP-1) was enhanced, leading to cyclin D1 activation, hence an increase in proliferation. The same cells had no effect on Akt induced cellular proliferation [200]. In contrast, another study examining 1321N1 human astrocytoma cells illustrated that TNF- α induced proliferation through several mechanisms including ERK and Rho activation, but signalling via SPHK1 mediated activation of the PI3K/Akt pathway and cyclin D [201]. In a third study, EGFRvIII stably transfected in a glioma cell line (U251-E18) showed increased SPHK1 activity, which partially enhanced ERK signalling to increase proliferation [198]. Since GBMs harbour multiple mutations, induction via SPHK1 may be through different growth factors and pathways, and downstream activators are likely to be cell type dependent.

ASAH1 knockdown though had no impact on the proliferation of either U87MG or RN1 cells. Although ASAH1 resulted in the accumulation of ceramide, a pro-apoptotic metabolite, the lack of chain length specificity could result in the null effect observed. As indicated in the knockdown validation for ASAH1, both C16 and C18 ceramide

were increased significantly. Alternatively, the GBM cell lines might not be sensitive to ceramide accumulation in their lysosomes. The combination had a trend reduction in proliferation for U87MG, and a significant reduction in proliferation for RN1 cells. This effect was likely mediated through SPHK1 knockdown, and not due to a shift in ceramide-S1P balance, which also occurs for ASAH1 knockdown, yet with no effect on proliferation. Specific ASAH1 pharmacological inhibitors, at nanomolar potency, have been recently identified, and should be examined in future experiments to inform our current siRNA data [202].

Silencing SPHK1 affected angiogenesis activity significantly. The effect may be mediated through a reduction in secreted extracellular S1P, which has been shown to modulate sprout formation. Alternatively, SPHK1 knockdown has been shown to affect proliferation, and may account for an apparent reduction in HMEC-1 sprouting as a result of fewer U87MG cells stimulating the process. ASAH1 knockdown and the combination knockdown did not significantly reduce the angiogenic stimulation of U87MG cells. Although the combination knockdown successfully reduced S1P levels equally as SPHK1 knockdown at 72 h, the angiogenesis assay was commenced following 72 h of transfection and lasted for 4 days. Given that the combination knockdown had only half the siRNA dose as the single knockdown, and the time course for SPHK1 gene expression began to re-express at day 5 in the single knockdown, it is possible that the combination knockdown did not efficiently reduce S1P levels throughout the assay timeline. Based on the current literature, S1P is known to have pro-angiogenic properties [203]. Moreover, S1P generated from SPHK1 is crucial for vascular and neural development. Embryos lacking both SPHK1 and SPHK2 had widespread cranial haemorrhages [87]. Furthermore, *S1P1*^{-/-} mice have a similar

phenotype as the *SPHK1*^{-/-} *SPHK2*^{-/-} mice, suggesting the pro-angiogenic effect of S1P is partly dependent on S1P₁ signalling [204, 205]. Finally, SPHK1 down regulation in glioma cell lines reduced extracellular S1P levels, and consequently reduced endothelial tube formation *in vitro* [142]. Taken together, the effect of S1P in angiogenesis is justifiable, but the potential anti-proliferative effect of SPHK1 silencing alongside the minimal effect SPHK1 + ASAH1 silencing had on the angiogenesis assay raises a few questions. To resolve this, specific pharmacological inhibition of SPHK1 activity was examined in the context of proliferation and angiogenesis.

4.3.3 SPHK1 Drug Inhibition and Functional Effects

The selective SPHK1 inhibitor, SKI-1a, has a K_i of 100 nM [195]. The stereoisomer, SKI-1b, is 100-fold less potent as a SPHK1 inhibitor, hence acting as a control compound. As expected, SKI-1a but not SKI-1b dose-dependently reduced S1P levels in U87MG cells, although no effect on cell proliferation was observed. This is supported by a previous study demonstrating that this inhibitor does not affect cancer cell proliferation [195]. The SPHK1 inhibitor, PF-543 (K_i of 3.6 nM and 100-fold more selective for SPHK1 over SPHK2), also had no effect on cancer cell proliferation [206]. However, those studies did not identify an accumulation of ceramide as a consequence of SPHK1 inhibition. Additionally, our treatments were performed with 10% FBS, which contains S1P, thus potentially masking the anti-proliferative effects. Moreover, S1P in serum is partly dephosphorylated by cells, and taken up as sphingosine [207], hence contributing to intracellular sphingolipids and may explain the accumulation of ceramide, since intracellular SPHK1 is inhibited. Having said that, the new generation of highly selective SPHK1 inhibitors are in contrast to previous SPHK1 inhibitors that

have shown an effect on cellular proliferation [143, 208]. This is likely due to off-target effects, since higher concentrations of previous SPHK1 inhibitors, in the micromolar range, were required to reduce S1P levels, while the new SPHK1 inhibitors are much more potent and therefore likely to be much more selective [195, 206]. Moreover, previous SPHK1 inhibitors have the long-chain base structure, which are toxic to cells especially at micromolar concentrations [195, 206]. Interestingly, SPHK1 silencing in MCF-7 breast cancer cells reduced proliferation, but was independent of S1P signalling via S1P receptors [200]. Given the recent literature and current results, specifically the targeted drug inhibition of SPHK1, we may conclude that GBM cell proliferation, specifically U87MG and RN1 cells, was not directly dependent on bulk S1P production, but further serum deprivation experiments are required to ensure data is not confounded by other variables. The conflicting data between our SPHK1 drug inhibition and siRNA data, for U87MG and RN1 cells, may suggest that siRNA treatment inhibits non-catalytic functions of SPHK1, thus contributing to the reduced proliferation observed. For example, SPHK1 has been shown to increase Bim, a pro-apoptotic protein, when targeted by siRNA [144]. Additionally, SPHK1 signals via ERK to increase proliferation under hypoxic conditions, therefore siRNA targeting results in a reduced proliferative effect [145]. These examples illustrate that SPHK1 siRNA treatment may modulate other biological pathways, thereby reducing cellular proliferation independent of S1P production.

S1P, a potent angiogenic factor, has a role in tumour angiogenesis as established using both genetic and pharmacological approaches [108, 153, 209]. The number of sprouts, average sprout length, and the proportion of long sprouts were reduced at 100 nM of SKI-1a, and significantly reduced at 300 nM of SKI-1a compared to SKI-1b. The

reduction in early angiogenesis correlated well with the concentration needed to block S1P production by U87MG cells. Importantly, SKI-1a and SKI-1b had no effect on HMEC-1 proliferation at concentrations up to 1000 nM; therefore, the observed effects indicate that SPHK1 activity is required for the transfer of angiogenic signals from GBM cells to co-cultured endothelial cells.

To test whether SPHK1 activity in U87MG cells or HMEC-1 cells, or both, was required for angiogenesis, we added conditioned medium taken from U87MG cells to HMEC-1 cells on microcarriers and assessed sprouting in the presence or absence of SKI-1a. Angiogenic sprouting was inhibited in conditioned medium taken from U87MG cells that had been treated with SKI-1a; but not when SKI-1a was added to the assay after collecting conditioned medium from untreated U87MG cells, indicating that SPHK1 activity in U87MG but not HMEC-1 cells was necessary to induce angiogenic behaviour in the co-culture system. Moreover, endothelial sprouting in conditioned medium taken from U87MG cells treated with SKI-1a was rescued by the addition of 100 nM S1P; strongly suggesting that S1P secreted by U87MG cells into the conditioned medium is an essential co-factor for endothelial sprouting. Interestingly, work done in Dr. Don's lab examining the effect of SKI-1a and SKI-1b on angiogenic cytokines in conditioned medium from U87MG cells following treatment suggests that there was no interaction with SPHK1 activity inhibition. The expression of 55 different angiogenic cytokines were analysed using an antibody array, and secretion of angiogenic factors including VEGF, uPA, and IL-8 by the U87MG cells were clearly evident and unchanged with SKI-1a or 1b treatment. A VEGF ELISA confirmed the lack of effect of SKI-1a treatment on secreted VEGF levels, indicating that bulk S1P

reduction affected *in vitro* angiogenesis independent of the secretion of angiogenic factors such as VEGF.

Our results are in agreement with recent studies demonstrating anti-angiogenic effects after the addition of SPHK1 inhibitors [153]. An essential role for S1P, signalling through endothelial cell S1P₁ receptors, in tumour angiogenesis has been demonstrated previously [108], and an anti-S1P monoclonal antibody was shown to inhibit tumour angiogenesis [209].

In conclusion, ASAH1 and SPHK1 have variable expression between glioma cells lines, and did not correlate accurately with sphingolipid levels. ASAH1 silencing resulted in the non-preferential accumulation of C16 and C18 ceramide. SPHK1 silencing resulted in the reduction of S1P, proliferation, clonogenicity, and angiogenesis. SPHK1 activity was inhibited using a selective and potent SPHK1 inhibitor and angiogenesis was significantly inhibited. Recently, anti-VEGF therapies were shown to improve the quality of life and progression free survival in GBM, but do not significantly enhance overall survival [44, 45]. Combining anti-VEGF treatments with inhibition of S1P synthesis could enhance the potency of anti-angiogenic therapies in GBM and other highly vascular tumours. The current data, from the literature and experimental work presented here, provide important evidence supporting inhibition of S1P synthesis as a therapeutic target in cancer, and point to a new target for anti-angiogenic therapy in GBM.

Chapter 5: Examining Sphingolipids in GBM Tissue and Plasma

5.1 Introduction

The previous two chapters focused on two key concepts. Firstly, the focus was to establish whether sphingolipids are altered in gliomas compared to normal grey matter (NGM), and secondly, to assess the functional consequences for specific imbalances in the pathway. Our current data shows that sphingolipid metabolism is clearly altered in gliomas. The localised changes identified support and promote tumour growth, through reducing anti-apoptotic factors and increasing pro-angiogenic factors. However, the relationship of the observed changes to clinical and genetic factors remains unanswered. Given the paucity of lipid-related data in GBM, we sought to clarify the potential clinical correlations for sphingolipid changes in GBM by addressing three key aspects: genetic mutations interacting with the sphingolipid pathway [210], plasma sphingolipids [153, 211-213], and correlation with clinical outcome [133, 134, 177].

Figure 5.1 provides a schematic diagram outlining the correlations investigated in this chapter. Key mutations in driver cancer genes and their association with metabolites is a growing research area. Moreover, the genetic code can only predict a static image of metabolism [214], with no consideration of environmental influences. Additionally, each omic dataset provides a portion of the biological picture [215]. By combining the cellular genetic code, with a snapshot of biological metabolism, new relationships and

interactions can be established [210]. Furthermore, addressing the correlation of sphingolipids in GBM tissue and GBM plasma is potentially useful, especially if plasma sphingolipids are informative of tissue changes. Importantly, examining plasma sphingolipid levels in GBM patients and normal healthy controls is a novel dataset, which may pinpoint a specific dysregulation, and establishes a baseline measure for GBM plasma levels against normal levels. Two previous studies in ovarian and breast cancer have shown higher levels of S1P in patient plasma and serum, respectively, compared to normal healthy controls [153, 211]. However, no direct correlations between tissue levels and circulating levels were examined. Finally, the association of the sphingolipid pathway with survival has been illustrated in several studies. As mentioned previously, SPHK1 overexpression has been shown to correlate unfavourably with survival in two independent studies [133, 134], yet no data regarding S1P and survival has been reported. Moreover, plasma sphingolipids may have a role as predictive markers of therapy, as has been shown for C18 ceramide in HNSCC [177].

Study Design

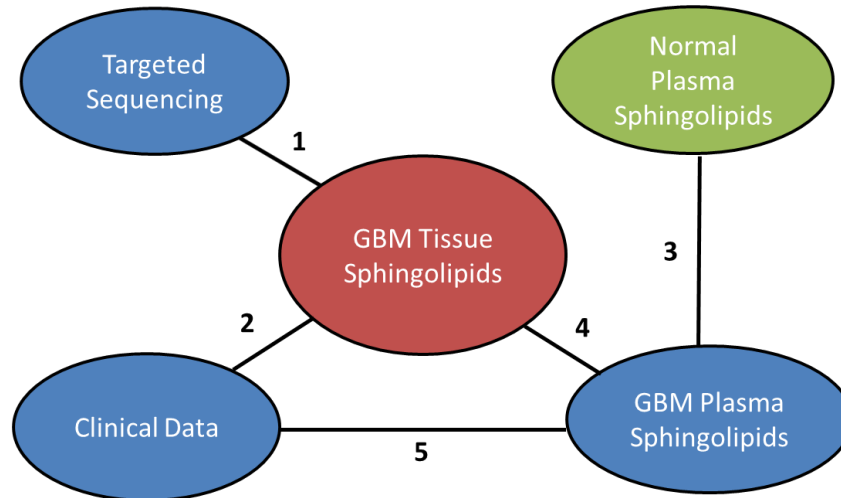


Figure 5.1 Design Overview Examining GBM Sphingolipids with Several Factors

This is the study overview for the factors being assessed in relation to tissue and plasma sphingolipids. The numbers (1-5) reflect the order of result presentation within this chapter.

5.1.1 Hypothesis and Aims

Working hypothesis for this chapter:

1. Sphingolipid changes in GBM are likely to be influenced by specific genetic mutations that support tumourigenesis.
2. The sphingolipid levels in GBM plasma will be elevated compared to normal plasma levels, and will reflect GBM tissue changes for diffusible factors.
3. Sphingolipids in GBM tissue and plasma may have a role as potential biomarkers.

The overall aim of this chapter is to examine the relationship between sphingolipids in tissue with known genetic mutations in GBM, plasma sphingolipids, and clinical markers.

The specific aims of this chapter:

1. To examine the relationship between sphingolipids in GBM tissue and mutations in key cancer genes.
2. To examine sphingolipids in plasma from GBM patients and normal age-matched controls.
3. To examine the correlation between sphingolipids in GBM tissue with matched plasma samples.
4. To examine the correlation between sphingolipids in GBM tissue and plasma with survival outcomes.

5.2 Results

This section is subdivided into a brief review of the clinical cohort examined and patient survival outcome, followed by correlations between GBM tissue sphingolipids with known genetic mutations in the cohort and clinical associations. Thereafter, matched GBM tissue and plasma sphingolipids are examined. Finally, GBM plasma sphingolipids are assessed with normal control plasma sphingolipids and survival outcome.

5.2.1 Clinical Cohort Overview

Table 5.1 provides an overview of the clinical composition of the GBM cohort examined in this study.

Table 5.1 Clinical Cohort Characteristics

Summary	
N	
Primary GBM Tissue	47
GBM Plasma (matched)	47 (43)
Normal Control Plasma	21
Age	
Median (years)	64
Control Median (years)	58
Survival	
Median (months)	11.4
Average (months)	12.4
Time to Radiotherapy	
Median (days)	40
Completed Chemotherapy and Radiotherapy	68.6%
MGMT Methylation	27.1%

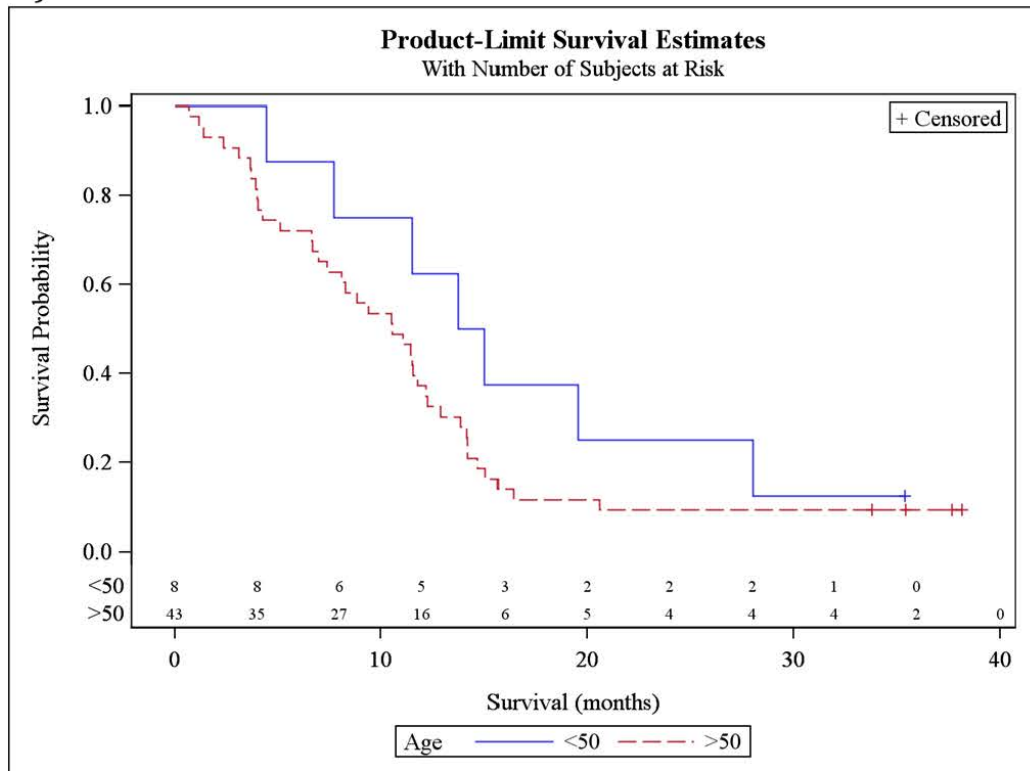
Briefly, the cohort investigated comprised 47 primary GBM tissues and 47 GBM plasmas, of which 43 were matched with tissue samples. Normal plasma controls (n=21) were age-matched with the GBM cohort. The median age of the GBM patients was 64 years, with a median survival of 11.4 months. Of note, a third of patients had either not completed concurrent chemotherapy and radiotherapy, or received only one treatment modality in addition to surgery. *MGMT* promoter methylation was found in approximately a quarter of the cohort.

5.2.2 Clinical Outcomes

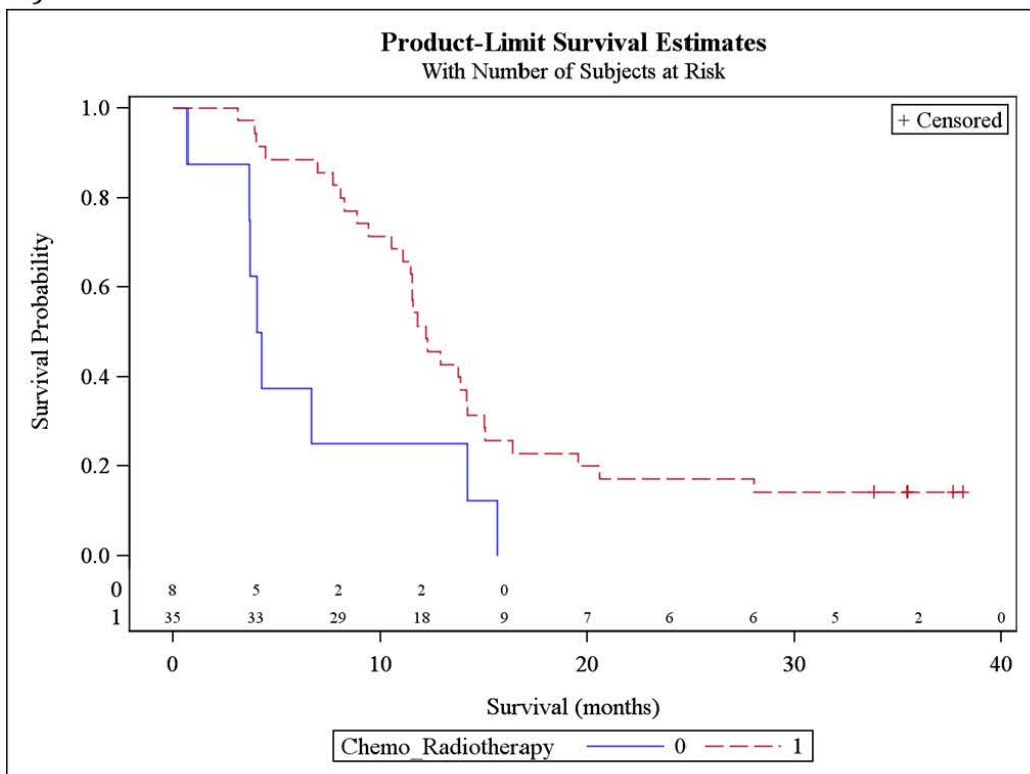
Kaplan Meier survival analysis and Log-Rank p-values were used to examine clinical factors, sphingolipids in tissue and plasma for the GBM patients. Hazard ratios (HR) were determined using a cox proportional hazard regression model. Of note, all survival graphs include the number of patients in each group and the attrition over the course of 40 months.

Kaplan Meier curves for three clinical characteristics previously known to affect survival (age, treatment and *MGMT* methylation) are presented in Figure 5.2.A-C. Patient age was categorised into two groups: (1) patients younger than 50 (n=8) and (2) patients older than 50 years (n=43) [28]. There was no significant difference between both age groups in our cohort. Patients completing the treatment regimen of concurrent chemotherapy and radiotherapy (n=35) showed a survival benefit compared to those patients who had an interrupted or incomplete course of treatment (n=8, p-value <0.05, HR = 0.38). *MGMT* methylation, denoted as 1 in Figure 5.2.C, trended towards significance, with a survival advantage appearing after 13 months, and a 50% reduction in HR.

A)



B)



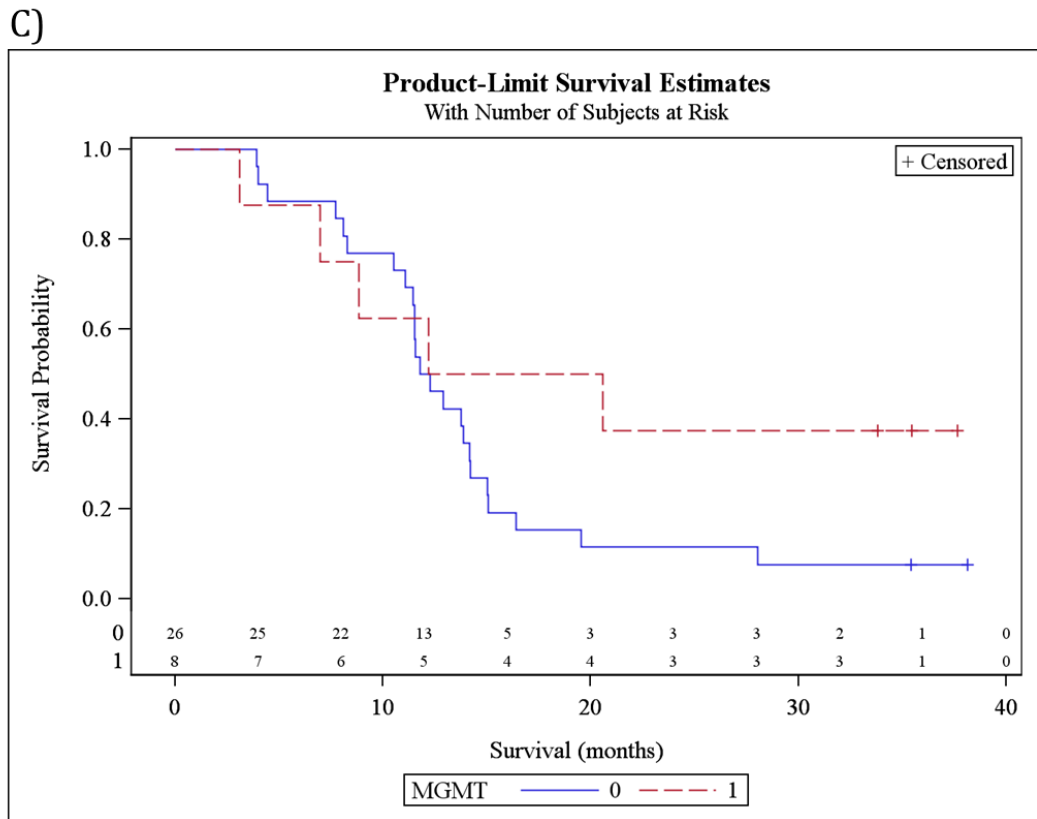


Figure 5.2 Survival Outcomes of Cohort Clinical Characteristics

(A-C) Kaplan Meier graphs for age, completed chemotherapy and radiotherapy, and MGMT methylation are presented above. Log-Rank p-value, hazard ratio, and 95% HR confidence interval (CI) for each graph, and legend where appropriate, are presented herein. (A) P-value = 0.22, HR = 0.61, 95% HR CI = 0.27-1.37. (B) P-value <0.05*, HR = 0.38, 95% HR CI = 0.17-0.84. Legend: 0 = incomplete treatment, 1 = complete treatment. (C) P-value = 0.17, HR = 0.50, 95% HR CI = 0.19-1.34. Legend: 0 = unmethylated *MGMT* promoter, 1 = methylated *MGMT* promoter.

5.2.3 Correlating Sphingolipids with Mutations in GBM

Ion Torrent sequencing was used to identify mutations in “known” cancer genes. Non-synonymous mutations in 20 different cancer genes were identified in at least one GBM specimen and are presented in Table 5.2. The commonest oncogenic-related mutations, involving more than 10% of patients, were found to occur at *EGFR*, *KDR*, *KIT*,

PIK3CA, *PTEN*, and *TP53*. Of note, no *IDH1* mutations were present in the primary GBM cohort.

Table 5.2 Non-Synonymous Gene Mutations in GBM Cohort

Gene	Mutation Frequency (%)
ATM	6.8
CDH1	2.3
CDKN2A	6.8
EGFR	18.2
FGFR3	4.5
FIP1L1	2.3
PDGFRA	2.3
FTL3	2.3
JAK3	4.5
KDR	40.9
KIT	25.0
MET	6.8
MPL	2.3
NRAS	2.3
PIK3CA	20.5
PTEN	27.3
PTPN11	2.3
RB1	6.8
STK11	4.5
TP53	22.7

The six mutated genes highlighted in Table 5.2 were correlated with sphingolipid metabolite levels. Other oncogenic-related mutations were not correlated with metabolites to avoid false positive associations due to a small number effect [216, 217]. GBM specimens positive for mutations within the extracellular domain (EC) of EGFR correlated with specific chain length ceramides (Figure 5.3). C16 and C22 ceramide were significantly elevated in *EGFR* mutant (mt) samples compared to *EGFR* wild-type (wt). In contrast, C18 ceramide, and collectively all ceramides combined, were similar

between *EGFR* mt (median = 58.61 pmol/mg, 95% CI = 55.41-103.7 pmol/mg) and *EGFR* wt samples (median = 116.5 pmol/mg; 95% CI = 65.61-139.4 pmol/mg; p-value = 0.43). No associations were observed with ceramide-S1P sphingolipids when categorised according to the mutations in the other five genes.

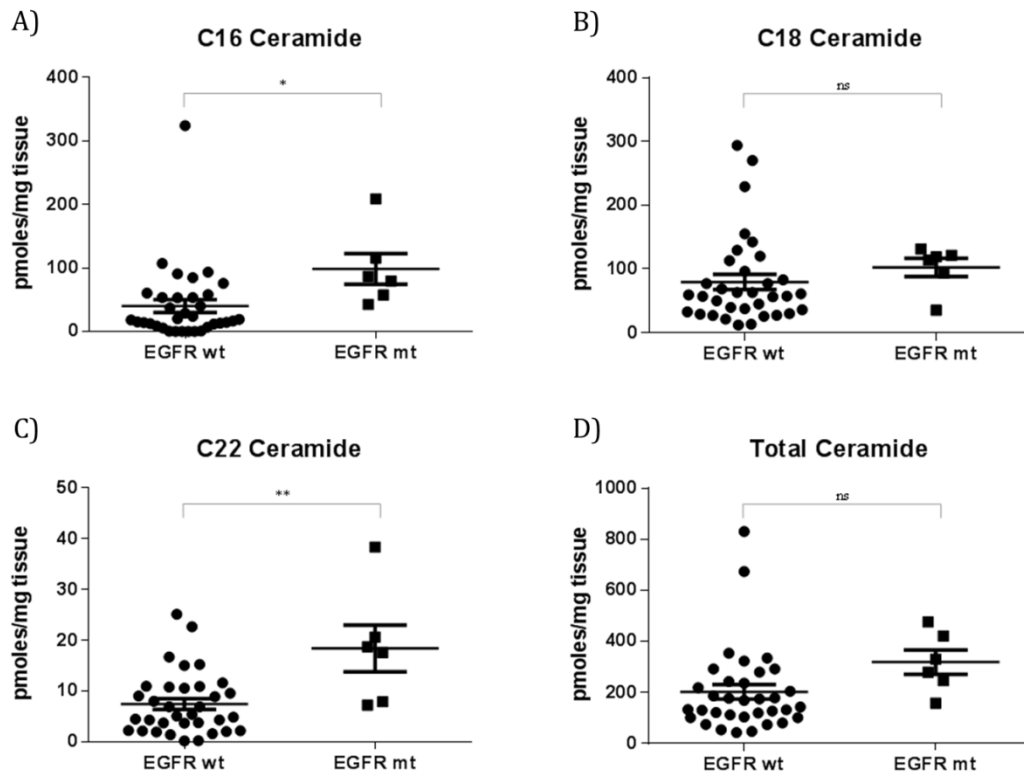


Figure 5.3 Ceramide Levels in *EGFR* Wild-Type (wt) and Mutant (mt) GBM Tissues

(A-D) Levels of C16 ceramide, C18 ceramide, C22 ceramide, and total ceramide are presented in the scatter plot for each individual sample. All values in the scatter plots represent the absolute quantification in pmoles adjusted to tissue weight (mg). *p-value<0.05, **p-value <0.01, ns=not significant.

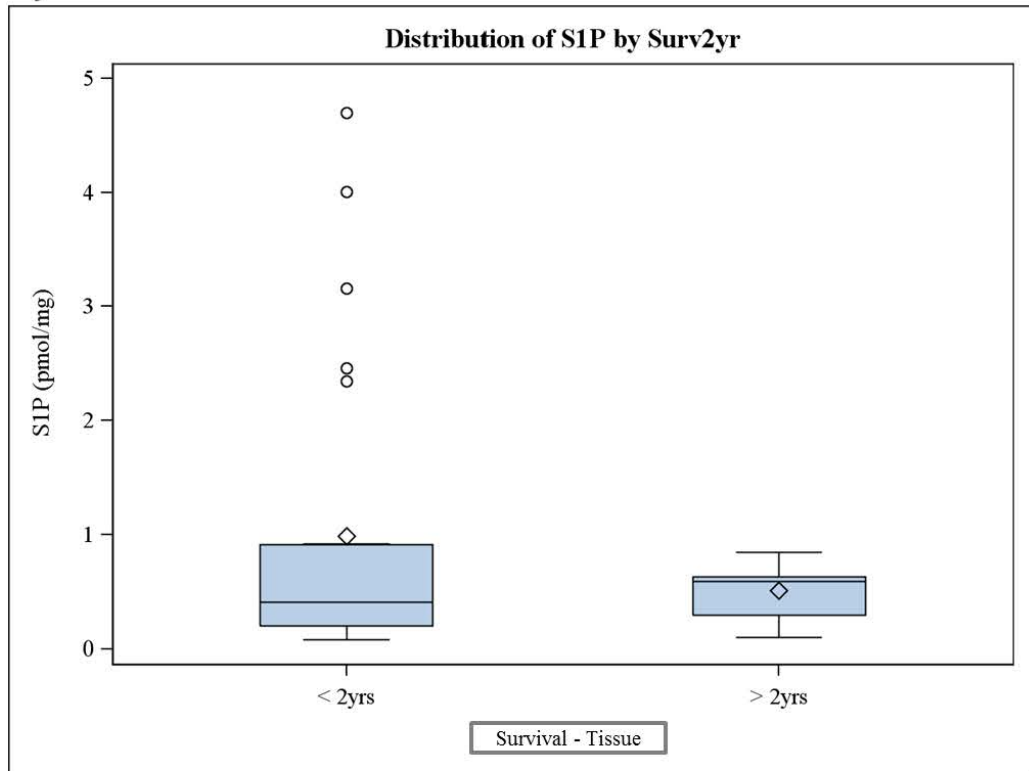
5.2.4 Sphingolipids in GBM Tissue and Survival

The level of different sphingolipid metabolites, within the ceramide-S1P axis, was correlated with patient overall survival. The only metabolite to show correlation with

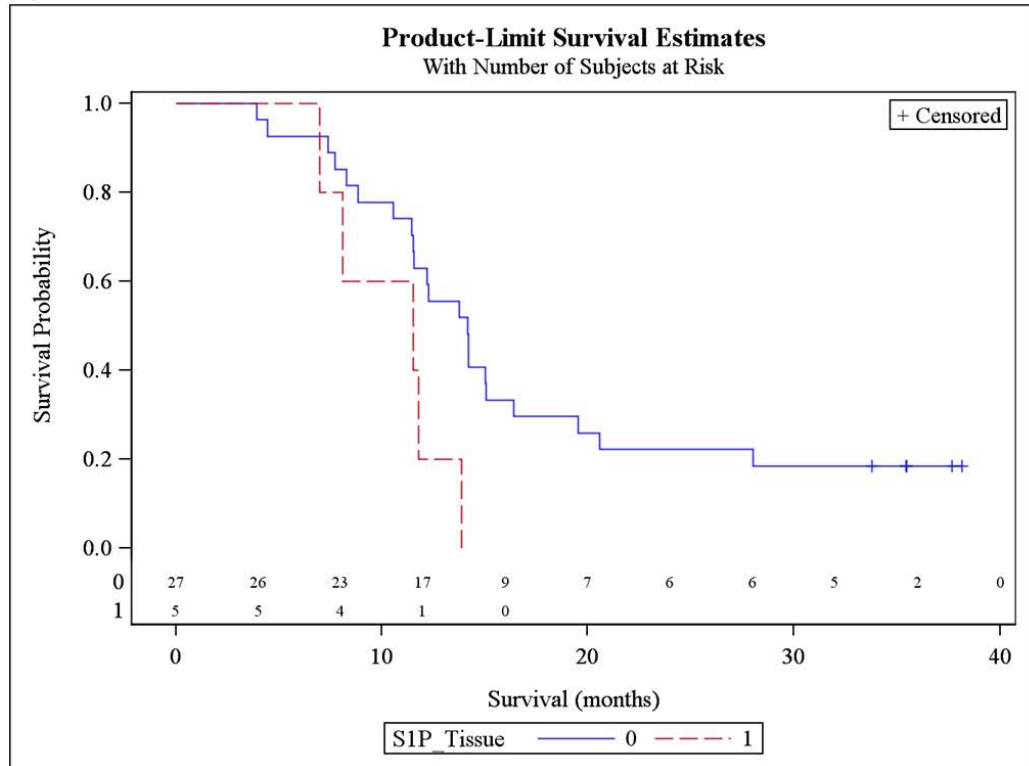
survival outcome was S1P (Figure 5.4). The data was dichotomised into two groups according to overall survival times: short term survivors (STS), defined as patients surviving less than 2 years, and long term survivors (LTS), which was defined as patients surviving more than 2 years [26]. Although there was no significance (as evidenced by the confidence interval overlap), high levels of S1P above 1pmol/mg were not found in any LTS.

To determine the effect of S1P levels on patient survival, we grouped S1P into low levels (denoted as 0), and high levels (denoted as 1) based on a ROC curve cut-off of 1.0 pmol/mg, as described previously in the methods section (Chapter 2.7). A Kaplan Meier survival curve, shown in Figure 5.4.B, illustrates that S1P in tissue has an effect on patient survival, which was statistically significant (Log-Rank p-value <0.05; HR of 2.93). Of interest, when MGMT status was categorised according to high or low S1P levels, a strong interaction between both MGMT and S1P was observed for predicting survival outcome, as shown in Figure 5.4.C. Specifically, MGMT methylation and low S1P levels correlated with a good survival outcome, while MGMT methylation and high S1P levels correlated with a poor survival outcome (HR = 0.13). In contrast, unmethylated MGMT correlated with a poor survival outcome irrespective of S1P levels (HR = 1.01).

A)



B)



C)

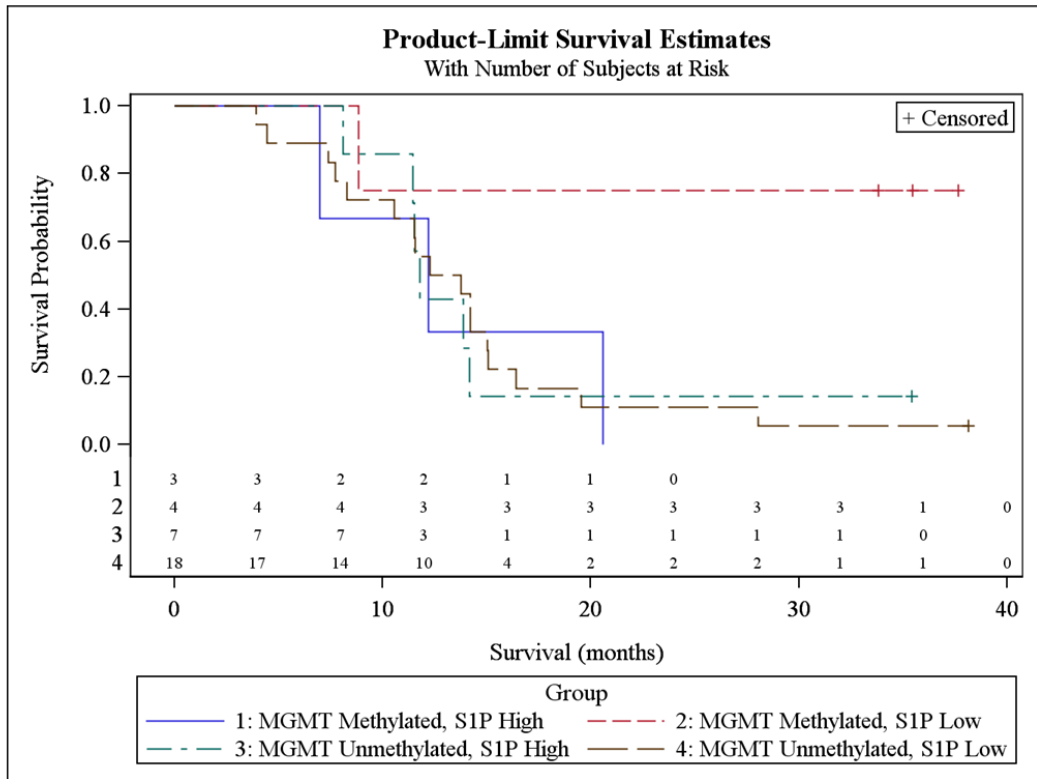


Figure 5.4 Survival Outcome of S1P in GBM Tissue

(A) Distribution of S1P in GBM tissue for STS (n=25) and LTS (n=6) in a box-and-whisker plot. (B-C) Kaplan Meier graphs for S1P in GBM tissue and for MGMT categorisation with S1P are presented above. Log-Rank p-value, HR, 95% HR CI, and legend where appropriate are presented herein. (B) P-value <0.05*, HR = 2.93, 95% HR CI = 1.03-8.33. Legend: 0 = low S1P, 1 = high S1P. (C) HR for high/low S1P with MGMT unmethylated = 1.0, 95% HR CI = 0.39-2.58; HR for high/low S1P with MGMT methylated = 0.13, 95% HR CI = 0.01-1.27.

5.2.5 Sphingolipids in GBM Plasma and Normal Plasma

The levels of S1P, sphingosine, ceramide, and SM for GBM and normal plasma are presented in Figure 5.6. S1P, ceramide and SM were significantly elevated in GBM plasma compared to normal age-matched controls, while sphingosine was significantly lower. Of note, HexCer and LacCer, which are relatively abundant components of plasma, and sulfatide, were not altered significantly between GBM plasma and controls.

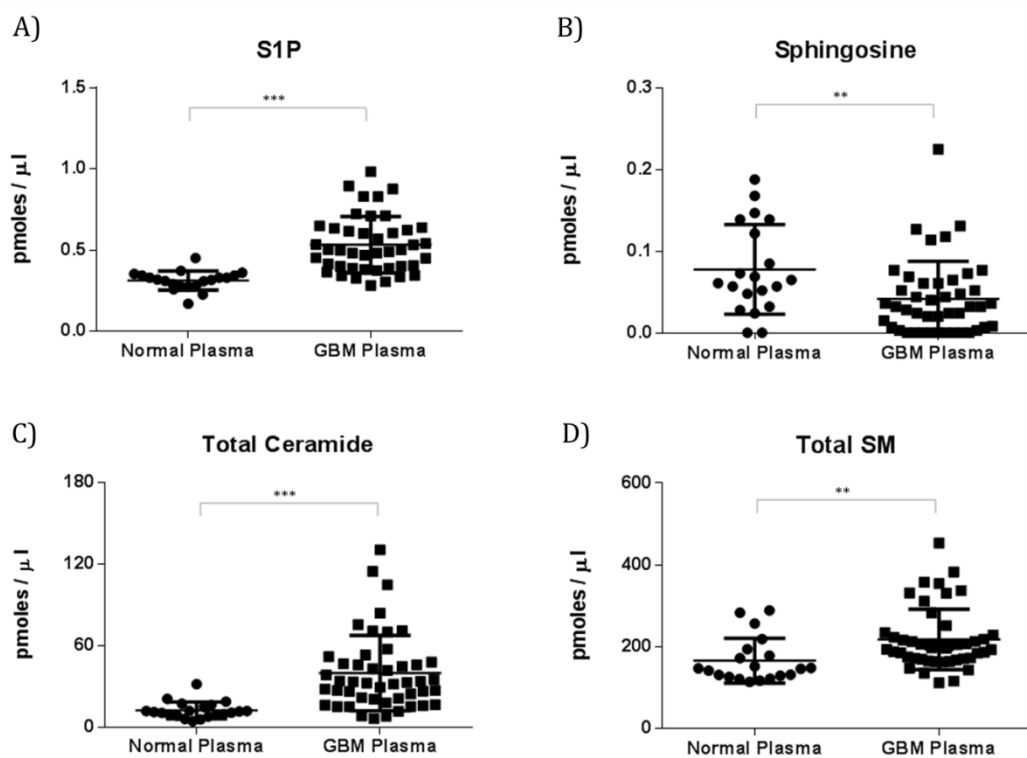


Figure 5.5 SM-Ceramide-Sphingosine-S1P Levels in GBM and Normal Plasma

(A-D) Levels of SM, ceramide, sphingosine, and S1P are presented in the scatter plot for each individual sample. All values in the scatter plots represent the absolute quantification in pmoles adjusted to plasma volume (μ l). **p-value <0.01, ***p-value <0.001.

5.2.6 Sphingolipids in GBM Tissue and GBM Plasma

A summary of the sphingolipid measurements for all patient tissue samples is presented in Table 5.3. The data was dichotomised into STS and LTS, as indicated previously. The STS group of patients, on average, showed higher sphingolipid levels when compared to the LTS patients, though this was not statistically significant.

Table 5.3 Summary of Sphingolipids in GBM Tissue

Sphingolipid (pmol/mg)	Short Term Survivors	Long Term Survivors	Unpaired T-tests
Sphingomyelin	858.2 +/- 670.0	669.3 +/- 270.5	P-value = 0.51
Hexosylceramide	38.5 +/- 66.3	16.0 +/- 17.8	P-value = 0.42
Lactosylceramide	12.9 +/- 16.6	11.2 +/- 12.9	P-value = 0.81
Sulfatide	107.1 +/- 200.6	30.1 +/- 40.4	P-value = 0.36
Ceramide	202.9 +/- 135.4	133.4 +/- 63.2	P-value = 0.28
Sphingosine	9.6 +/- 5.7	7.8 +/- 6.7	P-value = 0.50
S1P	1.0 +/- 1.3	0.5 +/- 0.3	P-value = 0.38

No correlations were observed between GBM tissue sphingolipids and plasma sphingolipids as presented in Figure 5.5.

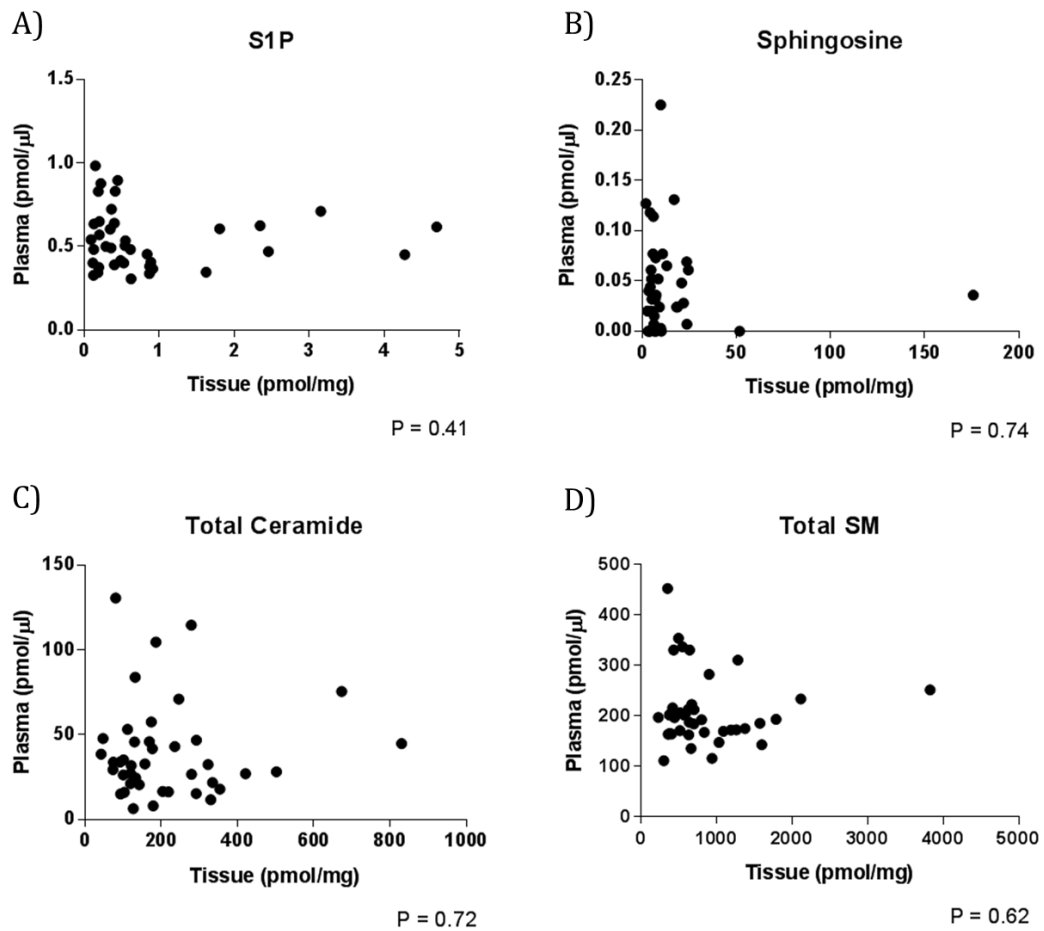


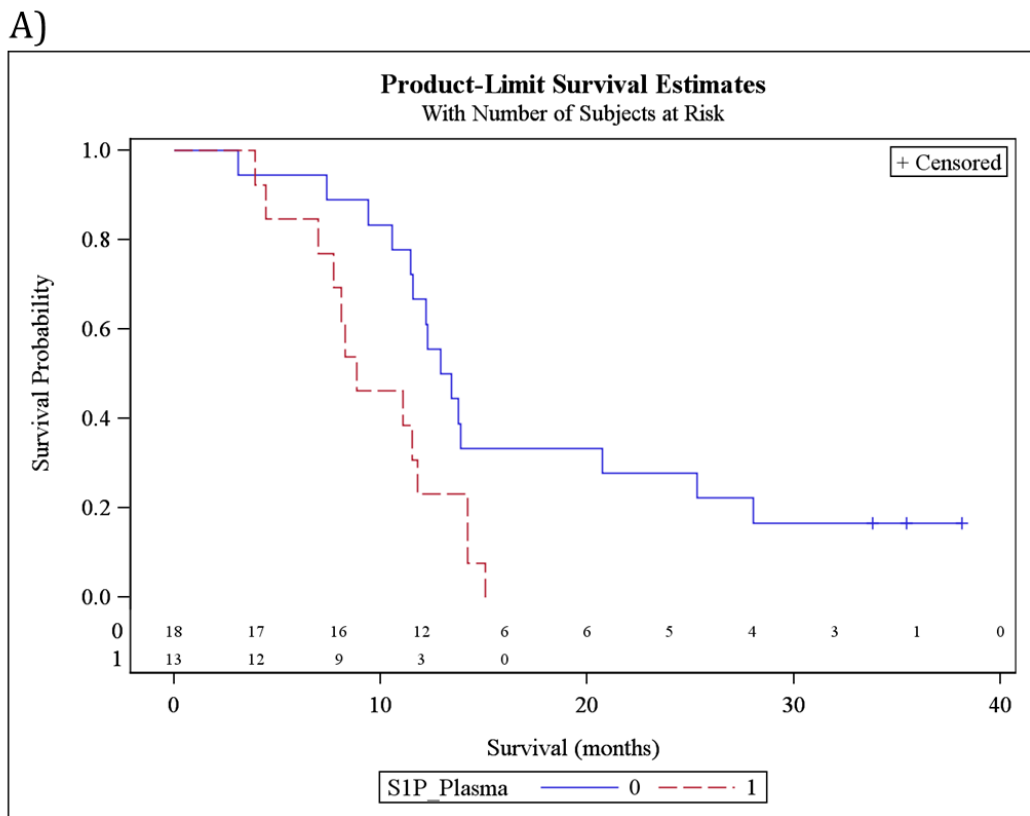
Figure 5.6 Correlations between GBM Tissue and Plasma Sphingolipids

(A-D) Correlation of S1P, sphingosine, ceramide, and SM are presented in the scatter plot for each individual sample. All values in the scatter plots represent the absolute quantification in pmoles adjusted to tissue weight (mg) or plasma volume (μ l).

5.2.7 Sphingolipids in GBM Plasma and Survival

Similar to the GBM tissue analysis with survival, the focus for GBM plasma sphingolipids was the ceramide-S1P axis, with only S1P data illustrating a significant difference in survival. S1P measurements in the plasma (taken from the patient pre-operatively or post-operatively) were categorised into low levels (denoted as 0) or high levels (denoted as 1) based on a ROC curve cut-off of 0.54 pmol/ μ l, as described in the

methods section (Chapter 2.7). Low levels of S1P in plasma were significantly correlated with a good survival outcome, while high levels of S1P in plasma correlated with a poor survival outcome (HR = 2.56), as shown in Figure 5.7.A. Some plasma samples (n=10) were taken from patients after concurrent chemotherapy and radiotherapy treatment. We performed an analysis of S1P and survival in this subgroup (Figure 5.7.B). A significant correlation between low S1P levels and survival was observed (Log-Rank p-value <0.05), with a HR of 6.07.



B)

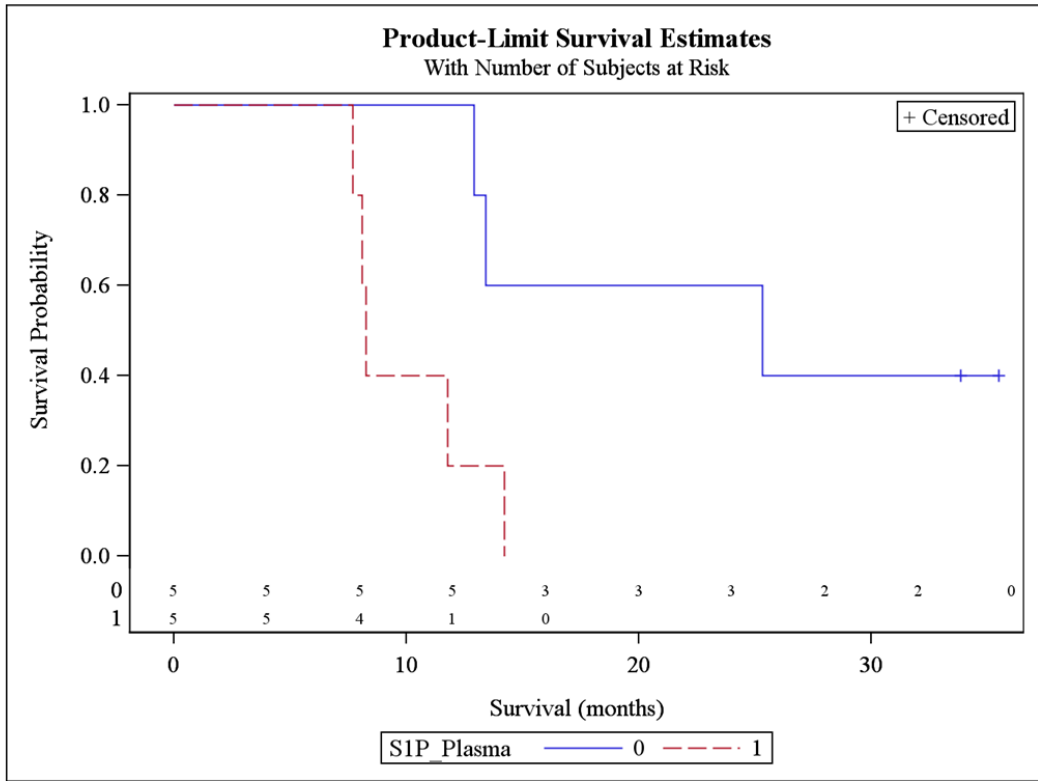


Figure 5.7 Survival Outcome of S1P in GBM Plasma

(A-B) Kaplan Meier graphs for S1P in plasma, and S1P in plasma post treatment are presented above. Log-Rank p-value, HR, 95% HR CI, and legend for each graph are presented herein. (A) P-value <0.05*, HR = 2.56, 95% HR CI = 1.15-5.68. (B) P-value <0.05*, HR = 6.07, 95% HR CI = 1.12-32.82. Legend: 0 = low S1P, 1 = high S1P.

5.3 Discussion

The translation of sphingolipids, as potential biomarkers, into clinical practice requires examining clinical cohorts and identifying the relevance of this pathway in GBM. Building upon the data presented in chapters 3 and 4, our objective herein was to examine correlations between GBM tissue sphingolipids with known oncogenes. In addition, the sphingolipid levels in plasma from GBM patients had not been examined previously. We obtained plasma from both GBM patients and an aged-matched population of healthy controls to determine the potential prognostic value of these lipids.

The genetic composition of the GBM cohort represented is dominated by *EGFR*, *TP53*, *PTEN*, *PIK3CA*, *KDR*, and *KIT* mutations. Rare *PDGFRA* and no *IDH1* mutations were identified, therefore, the proneural GBM subtype was unlikely to be represented within our cohort [24]. The proneural subtype, which forms less than 10% of primary GBMs, and is primarily a secondary GBM clinically, may or may not have correlations with the sphingolipid pathway, and is a question unanswered in our cohort.

MGMT methylation was identified in 27% of our cohort, which has been reported at a similar rate [218]. However, no survival advantage was predicted for concurrent chemotherapy and radiotherapy, which is also reported previously [9, 35]. This may reflect our small cohort sample of 32 patients. The reduction in samples was due to eliminating patients with incomplete treatment, reflecting the lower median survival of 11.4 months, therefore adjusting a potential confounder [9, 34]. Additionally, complete surgical resection and the Karnofsky score are two vital clinical factors that cannot be accounted for in our cohort, and both have been shown to affect survival [28, 32, 33].

Notably though, MGMT methylation appeared to correlate with a survival advantage after 13 months with a HR of 0.5.

The combination of genetics and biochemistry is a powerful tool in understanding another layer of disease pathophysiology, which has potential consequences for treatment targeting. The association of *EGFR* mutations with C16 and C22 ceramide is an interesting observation. *EGFR* mutations targeted in clinical trials have been unsuccessful, and this was partly attributed to the drug (erlotinib) targeting mutations in the kinase domain, typical of lung cancer, while GBM mutations for *EGFR* are commonly in the extracellular domain [219]. C16 and C22 ceramide protect against ER-induced stress [182], and may present an added challenge in therapeutic resistance of GBMs targeted by a new generation of *EGFR* inhibitors. Moreover, our initial screen of the CERS enzymes identified an upregulation in CERS5 and CERS2, which were responsible for the generation of C16 and C22 ceramide, respectively. Furthermore, similar levels of C18 ceramide, a pro-apoptotic metabolite, between *EGFR* mt and *EGFR* wt samples supports the changes observed are chain length specific, and ceramides as a whole are not increased. Previously, *EGFR* mutations in tissue samples have been shown to increase fatty acid synthesis, through activating sterol regulatory element-binding protein 1 (SREBP-1), which was inhibited by treatment with lapatinib, an *EGFR* inhibitor [220]. SREBP-1 activation resulted in an increase in fatty acid synthesis. Importantly, blocking fatty acid synthesis *in vitro* and *in vivo* for GBM models resulted in a decrease of tumour growth and an increase in cell death for *EGFR* mutated cell lines [220, 221]. Recently, SREBP-1 has been shown to protect against lipotoxicity for various GBM cancer cells, and a loss of desaturase activity mediated by stearoyl-CoA desaturase 1 (SCD1) resulted in reduced SREBP-1

activity, and a reduction in cell growth and viability [222]. Of note, SREBP-1, a transcription factor regulating sterol synthesis, is co-regulated with sphingolipids [223, 224], with a previous study identifying an increase in ceramide correlates with an increase in precursor SREBP, but a reduction in mature SREBP in hamster ovary cells [225]. Our observations of *EGFR* mt and specific ceramide upregulation requires further validation, but opens new questions into the interaction of sphingolipids with unknown gene mutations driving tumourigenesis.

Circulating sphingolipids are important, because they can be easily obtained and readily processed for mass spectrometry measurements, therefore clinical utility would be more promising if the profile in blood corresponds with clinical end-points. We established that circulating levels of S1P, ceramide, and SM were elevated in GBM plasma compared to normal plasma. Sphingosine, however, was reduced, and may reflect the rapid interconversion of sphingosine into either S1P or ceramide. Of interest, Hex, LacCer, and sulfatide were unaltered, suggesting a specific activation of SM to S1P activity. The correlation between all tissue sphingolipids and plasma sphingolipids though was not significant. One potential explanation is that circulating sphingolipid levels were not elevated because of local production of tumour S1P; instead it may reflect a systemic response for tumour formation. The role of systemic S1P can depress the immune mediated response, and support tumour growth by polarising macrophages towards an anti-inflammatory phenotype [226, 227]. Additionally, in a mouse model of breast cancer, circulating S1P levels were significantly higher as a result of tumour initiation, and a SPHK1 inhibitor reduced both tumour growth and circulating S1P levels [153]. One missing clinical parameter though is a volumetric analysis for GBM

samples through MRI scans, which may illustrate a correlation between tumour size and circulating S1P levels.

Survival is a clinically crucial end-point, which all new biomarkers and treatment modalities are measured against. The translation of biomarkers in the field of cancer from identification to clinical practice is limited [228, 229]. Our approach was to focus on metabolites of biological interest, and assess their potential as predictors of survival, as opposed to screening all metabolites. Ceramides did not yield any positive results in tissue or plasma, yet it would be a potential candidate for following patients over a treatment time course as has been shown previously in HNSCC. In a phase II clinical trial, patients with recurrent HNSCC were treated with two chemotherapeutic agents, gemcitabine and doxorubicin, and serial blood sample analysis identified higher C18 ceramide levels with stable disease or remission, compared to C18 ceramide levels with progressive disease [177]. S1P, on the other hand, showed a significant prognostic association in tissue, but the spread of data for the STS and LTS groups indicated that S1P has poor sensitivity at differentiating between both groups. Of note, S1P metabolism is a dynamic process regulated by several enzymes, hence our measurements only reflect a snapshot for time after surgical resection. Thus, a larger cohort is needed to confirm if high levels of S1P are associated with a poor survival outcome. Previous studies with SPHK1 illustrated a poor survival outcome with enzyme overexpression, which our data supports at the metabolite level, though the 95% HR CI was 1.03-8.33, further emphasising the need for repeated measures and validation to establish clinical utility. Interestingly, S1P had a strong interaction with MGMT methylation. S1P has been shown to modulate epigenetic factors, including histone deacetylases [109], but an interaction with MGMT methylation in a clinical

setting is a novel observation, and low levels of S1P with only MGMT methylation seem to confer a 90% reduction in HR. The mechanism for that interaction is unclear, and our data would require validation in an independent cohort prior to investigating potential pathway links. Finally, S1P in plasma illustrated promising results, whereby elevated levels associate unfavourably with survival, and that was even more pronounced in the subgroup analysis for post chemotherapy and radiotherapy patients.

With the current data, we identified ceramides, specifically C16 and C22 ceramide, were increased in EGFR mutated GBM samples, which may provide added resistance to therapy. Additionally, we established that the SM-ceramide-sphingosine-S1P axis is activated in GBM plasma compared to normal plasma. This increase in specific circulating sphingolipids does not appear to be as a direct result of local S1P tumour production, and may represent a systematic immune mediated response. For our survival analysis, S1P in tissue has potential prognostic value, and a strong interaction with MGMT methylation, while circulating S1P has potential prognostic and predictive value. Importantly, this requires further validation in an independent cohort with complete clinical data and genetic characterisation to adjust for potential confounders. Finally, the use of serial samples for monitoring possible treatment-related changes in circulating sphingolipids would be novel for GBM research.

Chapter 6: Summary & Future

Directions

GBM, a disease with the highest burden on society [13], has a poor track record for therapy response, despite aggressive surgery, radiotherapy, and chemotherapy. Consequently, targeted therapies form a fourth line aimed at neutralising overexpressed factors or mutated genes and their associated signalling pathways. However, over the past decade, many clinical trials with targeted drug therapies have failed to add any benefit to patient survival, which begs the question “why has this treatment paradigm been unable to succeed?” Most targeted therapies in GBM are protein or gene centric [14]. Lipids on the other hand, are gradually being recognized as important targets for disease modulation as their biological roles are being uncovered. There are six lipid families in mammalian cells, of which, sphingolipids form an integral component of cell membranes and important transducers and effectors of cell signalling. Most current literature has focused on sphingolipid dysregulation in the context of the enzymes and associated receptors. In addition, no comprehensive data for sphingolipid alterations has been identified from human tissue studies.

With the accessibility and availability of high-throughput mass spectrometry techniques, examining lipids has become less daunting and more practically feasible; therefore, I investigated the fundamental question of whether the sphingolipid metabolites, and not only enzymes in the pathway, are altered. I measured numerous

sphingolipid metabolites in NGM, AII, AIII, and GBM human tissue samples using LC-MS/MS to determine absolute sphingolipid levels. In conjunction, I used qRT-PCR to determine gene expression for enzymes involved in the ceramide-S1P rheostat pathway. Several important observations can be concluded from this analysis. Ceramide, a key metabolite in the pathway, is significantly down regulated in gliomas compared to NGM. This has been reported previously [163], but I specifically identified C18 ceramide, an important pro-apoptotic mediator, as the main chain length ceramide reduced. Interestingly, C16 ceramide, an important anti-apoptotic mediator, was increased in GBM compared to NGM. The imbalance between C16 and C18 ceramide, identified in HNSCC previously [86], adds another level of complexity to a dysregulated pathway, whereby different chain lengths within the same metabolite are altered, leading to a change in phenotypic response to therapy. Increasing ceramide levels as a potential therapeutic approach to cancer has been suggested [69, 230-233], but so far no positive clinical outcome has been reported for this approach [234]. Since C16 and C18 ceramide levels are positively correlated in NGM, and the correlation is uncoupled in GBM, future studies may benefit the clinical paradigm by examining this context. For example, most therapies aim to increase ceramide levels indiscriminate of the ceramide chain length, but with our current data and the literature, this does not appear to be a potent method at inducing proliferation arrest or apoptosis. *In vitro* work can establish a comparison between ceramide generation as a whole or increasing specific chain lengths to yield better results as an adjunct to chemotherapy or radiotherapy. Although this has been examined for C16 and C18 ceramide in HNSCC, it is important to note that the enzymatic changes observed underlying the ceramide changes are different than our results. In HNSCC, CERS6 increase results in the

accumulation of C16 ceramide [82, 235], while our data suggests CERS5 increase results in the accumulation of C16 ceramide. CERS1, on the other hand, is reduced in HNSCC, accounting for the reduction in C18 ceramide [86], while CERS1 in our dataset is similar in expression, though we have yet to investigate the post translational modification of the protein which has been attributed to reduce C18 ceramide as well [183]. Another important observation is the elevated levels of C16 fatty acids, also referred to as palmitic acid, for SM, HexCer, LacCer, and sulfatide in GBM samples compared to NGM. The functional relevance of accumulating C16 fatty acids throughout the entire sphingolipid pathway in GBM samples, as per our data, is unknown, and should be investigated in future work. The likely targets for increased C16 fatty acids are upstream of sphingolipid synthesis, hence implicating the *de novo* pathway. A general screen for gene expression of enzymes controlling C16 fatty acid incorporation into the pathway, comparing NGM and gliomas, would be a suitable initial experiment.

In addition to the ceramide changes observed, I observed ceramidases, specifically ASAH1 to be upregulated in gliomas when compared to NGM. An increase in the catabolism of ceramide into sphingosine is followed by a significant upregulation in SPHK1 and down regulation of SPHK2 in glioma samples. Moreover, the reverse reaction of S1P conversion back into sphingosine is down regulated in gliomas compared to NGM for SGPP2. The increased expression of ASAH1 and SPHK1 in cancer is well documented in the literature, but the down regulation of SPHK2 and SGPP2 in human tissue samples has not been stated previously. There are several points the qRT-PCR data provides. First, an increase in catabolic activity of ceramides may explain the significant reduction in C18 ceramide in the absence of any change for

CERS1. Second, the upregulation of multiple enzymes responsible for ceramide conversion to sphingosine, then sphingosine conversion to S1P, in tandem with a down regulation of the reverse reaction, supports the concept of a shift in the ceramide-S1P rheostat in favour of S1P, and at the expense of ceramide. Third, the down regulation of SPHK2 coupled with an upregulation of SPHK1 as glioma grade increases compared to NGM, suggests an interplay between these two enzymes which form S1P in different cellular compartments. In recent literature, *SPHK2*^{-/-} mice have been shown to have higher circulating S1P in blood compared to wild-type and *SPHK1*^{-/-} mice [236]. Moreover, in an animal model of chronic colitis leading to colitis associated cancer, *SPHK2*^{-/-} mice resulted in a significant increase in S1P serum and tissue levels, SPHK1 expression, and colitis severity in comparison to wild-type mice [184]. Therefore, although most research has emphasized SPHK1 upregulation, future work should examine the feedback loop that drives SPHK1 as SPHK2 is reduced, in addition to identifying the factors that drive SPHK2 reduction in the process. Fourth, SGPP2 down regulation is a novel finding, and may or may not contribute significantly to S1P levels in the context of SPHK1 overexpression. As a result, future work would be useful in determining SGPP2 protein expression to confirm the qRT-PCR findings, followed by functional work aimed at over expressing SGPP2 in a GBM cell line to identify the effect on S1P levels and the related biological consequences implicated in S1P signalling.

S1P, a potent secondary messenger with pleiotropic activity, is clearly increased in glioma samples compared to NGM. This is the first documented observation for S1P elevation in any human cancer samples. Given the context of the enzymatic changes and metabolite changes described, this was a complementary finding. Moreover,

previous *in vitro* and *in vivo* experiments have illustrated an elevation in S1P for cancer samples compared to controls. Our data, through this integrated pathway approach, adds to that pool of knowledge, and further reaffirms the hypothesis that the ceramide-S1P axis is shifted in GBM, favouring S1P. In saying that, the findings outlined should not be confined to lab-based testing only, but should be examined in a clinical setting to identify potential translational benefits in the future. Recently, a method to examine intra-operative glioma samples for metabolites using ambient mass spectrometry provided a clear diagnostic clinical utility, and an aid to assessing tumour margins [237, 238]. The lipid results for the imaging mass spectrometry corresponded to the neuropathological diagnosis for various brain tumours and grades, providing the data within near-real time. This novel approach is an example of similar work that can be conducted, though with a targeted sphingolipid profile, to assess the diagnostic potential of this pathway. One non-invasive method would be to utilise magnetic resonance spectroscopy (MRS) clinically, and additionally nuclear magnetic resonance (NMR) in the lab. Through collaborative work, we know that S1P, the least abundant metabolite in tissue, can be measured by NMR. NMR though is more effective at identifying and measuring S1P due to the higher resolution, sample homogeneity, and the lack of interfering noise from the surrounding tissue and cranial vault. Conversely, MRS may not be capable of measuring low abundant sphingolipids, though this has not been performed to the best of our knowledge. In saying so, sphingomyelin, the most abundant sphingolipid in the brain, can be measured using MRS, and with the information of high C16 SM levels in glioma samples compared to NGM, it would be worthwhile investigating that relationship along with other metabolites in a patient setting. Currently, there is no literature on sphingolipid analysis using any of these

techniques; therefore examining these lipids in a non-invasive process would be novel, challenging, and potentially useful clinically for the simple differentiation of tumour versus normal tissue, which is a major issue when evaluating tumour recurrence post operatively.

I examined the functional consequences of low ceramide levels and high S1P levels, through targeting two key enzymes that were overexpressed in our qRT-PCR analysis: ASAH1 and SPHK1. The work was divided into three main components: identifying the metabolite changes following ASAH1 and SPHK1 knockdown, defining the functional effects through proliferation, clonogenicity, and angiogenesis, and finally, examining the effect of SPHK1 drug inhibition for proliferation and angiogenesis.

ASAH1 silencing resulted in a significant accumulation of ceramide levels, without discriminating between C16 or C18 ceramide. SPHK1 silencing resulted in a significant reduction of S1P levels. The combination knockdown of both enzymes reduced S1P levels and increased ceramide levels. Hence, the cell line model was sufficient to examine S1P modulation, but was limited in examining ceramide accumulation; thus future work would examine the accumulation of specific ceramide chain lengths through a double knockout of ASAH1 and CERS5, to control for C16 ceramide accumulation, while increasing C18 ceramide levels.

The functional assessment of ASAH1 and SPHK1 knockdown was assessed in the context of proliferation, clonogenicity, and angiogenesis. ASAH1 knockdown had no effect on the three assays described, and the combination knockdown had a partial effect on reducing proliferation and clonogenicity, which is likely due to SPHK1 knockdown. However, given the indiscriminate elevation of C16 and C18 ceramide, and the

limitation of the model for exhibiting a similar *in vivo* profile, the results should be taken cautiously, and cannot rule out specific functional effects when controlling the ceramide chain length accumulated intracellularly. SPHK1 knockdown had a significant effect on reducing proliferation and clonogenicity. Additionally, SPHK1 knockdown resulted in a reduction of U87MG-induced angiogenesis. Although the data is supported by the literature for the role of S1P in promoting angiogenesis, it is difficult to discern whether the reduction in U87MG-induced angiogenesis in our model was affected partly by a reduction in U87MG proliferation, even though we attempted to control for that variable by equal cell seeding following a 72 h knockdown.

As a result, SPHK1 inhibition using a new nanomolar potent drug, SKI-1a, was assessed for metabolite changes, effect on proliferation and angiogenesis to further confirm our siRNA data. SKI-1a illustrated a dose-dependent inhibition of S1P, while the stereoisomer control, SKI-1b, did not have a significant effect on reducing S1P levels. Interestingly, SKI-1a and SKI-1b had no effect on the proliferation of U87MG, RN1, or HMEC-1 cell lines. This is consistent with previous reports [195, 206], and adds to the controversy of the anti-proliferative activity of SPHK1 inhibition. Concisely, siRNA inhibition may affect proliferation due to non-catalytic inhibition of SPHK1. The new generation of SPHK1 pharmacological inhibitors support this argument, as depletion of S1P has no correlation with an anti-proliferative effect. Older generation of SPHK1 inhibitors do not support this argument, but it should be noted that they are less selective, more toxic at micromolar concentrations, and our stereoisomer control, SKI-1b, had no effect on S1P depletion yet has the same effect on cellular proliferation as SKI-1a. S1P depletion, however, significantly reduced U87MG-induced angiogenesis in a dose-dependent manner. Moreover, the effect was localised

to U87MG release of S1P only, and not HMEC-1 endothelial cells. This distinction was identified through a series of conditioned media experiments, suggesting GBM cells utilise S1P to recruit endothelial cells and form new blood vessels. Of interest, this process was independent of VEGF levels, which is an important clinical target for controlling GBM-induced angiogenesis. Recently, a study examining a biomimetic model for angiogenesis *in vitro* described VEGF and S1P as two vital modulators for angiogenesis mediating filopodial formation [46]. Our current data, from the siRNA and pharmacological inhibition experiments, suggest that the elevated levels of S1P identified in GBM tissue likely contributes to inducing angiogenesis by co-opting neighbouring endothelial cells, and thereby indirectly promoting cellular proliferation and survival. The data opens the possibility for two different future projects. One potential project would be to examine the efficacy of S1P depletion *in vivo* on GBM-induced angiogenesis and growth using a stable new generation SPHK1 inhibitor. These inhibitors for *in vivo* work are currently being tested for pharmacokinetics, pharmacodynamics, and safety dosing. The second project would examine the combinatorial effect of S1P and VEGF inhibition on reducing GBM-induced angiogenesis *in vitro* and *in vivo*, with the aim to prolong survival as a primary endpoint.

Moving from the profiling and functional assays, we assessed the correlations of sphingolipids in GBM tissue with three key components: known genetic mutations in GBM, matched plasma sphingolipids, and survival. The importance of establishing these parameters is to inform potential translation for clinical application, mainly biomarker work.

Through the targeted genetic sequencing, six gene missense mutations were present in more than 10% of the cohort, and were therefore sufficient for analysis with sphingolipid changes [217]. Interestingly, *EGFR* mutations affected specific ceramide chain lengths, namely C16 and C22 ceramide, which were significantly elevated compared to *EGFR* wild-type. In contrast, C18 ceramide was similar between both groups. The ceramides upregulated are anti-apoptotic ceramides, which are formed through the activity of CERS5 and CERS2, respectively [82, 239]. Both CERS2 and CERS5 were upregulated in our qRT-PCR screen, presented in Chapter 3, and notably, a double siRNA knockdown of both enzymes in MCF-7 breast cancer cell lines resulted in an ER stress response [182]. Future work would require confirming the association of *EGFR* mutation with the ceramide chain length changes in a separate tissue cohort, and to examine *in vitro* associations for *EGFR* mutated and wild-type cells with various ceramide chain lengths, and their biological consequences.

GBM plasma was examined with normal control plasma to establish whether sphingolipids were altered in plasma samples in the context of cancer. In support of this, literature for ovarian and breast cancer identify an increase in circulating S1P levels in comparison with normal controls [153, 211]. The generalised upregulation of circulating sphingolipids in our GBM plasma samples may potentially have a pathophysiological role or simply a surrogate reflection for sphingolipid changes, which should be examined further to explain these changes. Furthermore, our data suggests that sphingolipids in GBM tissue have no correlation with circulating sphingolipids, thus, although S1P, for example, was elevated in cancer tissue samples and circulating plasma or serum, the changes in circulating S1P do not inform the tissue S1P changes.

Survival analysis can be affected by multiple variables, therefore we attempted to control for all known factors that can affect survival outcome prior to evaluating sphingolipids in tissue and plasma with patient survival. The significant findings are centred upon S1P in tissue and plasma. In tissue, high levels of S1P were a poor predictor of survival for patients. Surprisingly, S1P levels illustrated a strong interaction with MGMT methylation, whereby low levels of S1P combined with MGMT methylation resulted in improved survival. This is the first observation of a lipid interacting with an epigenetic process, which has strong clinical association to treatment; therefore, future work would require the validation of this observation, and if the interaction is confirmed, should be further examined to understand the mechanistic link between MGMT methylation and S1P levels. Finally, S1P in plasma, although not directly correlated with S1P in tissue, has a significant association with poor survival if elevated. In a subgroup analysis for post concurrent chemotherapy and radiotherapy, plasma S1P was very significantly associated with survival outcome. The S1P plasma results are promising, and would certainly require validation in a cohort with regular matched plasma interval sampling from time of diagnosis onwards to outline the prognostic and predictive potential of S1P.

In conclusion, I have demonstrated through this thesis that the sphingolipid pathway in GBM is dysregulated, and illustrated for the first time that S1P is elevated in human cancer samples. Moreover, the increase in S1P provides a favourable pro-angiogenic microenvironment for GBM growth. Clinically, the sphingolipid alterations correlate with *EGFR* mutation, interact with MGMT methylation, and may have a biomarker role. With this thesis, I have added to the knowledge base for the lipid paradigm in GBM, thereby illuminating the importance of this pathway, which is currently not

targeted clinically in this disease, and contributed to the understanding of one of the many faces of GBM biology.

References

1. Azevedo, F.A., L.R. Carvalho, L.T. Grinberg, J.M. Farfel, R.E. Ferretti, R.E. Leite, W. Jacob Filho, R. Lent, and S. Herculano-Houzel, *Equal numbers of neuronal and nonneuronal cells make the human brain an isometrically scaled-up primate brain*. J Comp Neurol, 2009. **513**(5): p. 532-41.
2. Smith, K., *Neuroscience: Settling the great glia debate*. Nature, 2010. **468**(7321): p. 160-2.
3. Kettenmann, H. and A. Verkhratsky, *Neuroglia: the 150 years after*. Trends Neurosci, 2008. **31**(12): p. 653-9.
4. Sofroniew, M.V. and H.V. Vinters, *Astrocytes: biology and pathology*. Acta Neuropathol, 2010. **119**(1): p. 7-35.
5. Burger, P.C., B.W. Scheithauer, and F.S. Vogel, *Surgical Pathology of the Nervous System and its Coverings*. 4th ed. 2002, Philadelphia: Churchill Livingstone.
6. Louis, D.N., W.K. Cavenee, H. Ohgaki, and O.D. Wiestler, *WHO Classification of Tumours of the Central Nervous System*. 4th ed. Vol. 1. 2007, Lyon, France: IARC Press.
7. McLendon, R.E. and E.C. Halperin, *Is the long-term survival of patients with intracranial glioblastoma multiforme overstated?* Cancer, 2003. **98**(8): p. 1745-1748.
8. Krex, D., B. Klink, C. Hartmann, A. von Deimling, T. Pietsch, M. Simon, M. Sabel, J.P. Steinbach, O. Heese, G. Reifenberger, M. Weller, G. Schackert, and f.t.G.G. Network, *Long-term survival with glioblastoma multiforme*. Brain, 2007. **130**(10): p. 2596-2606.
9. Stupp, R., M.E. Hegi, W.P. Mason, M.J. van den Bent, M.J. Taphoorn, R.C. Janzer, S.K. Ludwin, A. Allgeier, B. Fisher, K. Belanger, P. Hau, A.A. Brandes, J. Gijtenbeek, C. Marosi, C.J. Vecht, K. Mokhtari, P. Wesseling, S. Villa, E. Eisenhauer, T. Gorlia, M. Weller, D. Lacombe, J.G. Cairncross, R.O. Mirimanoff, R. European Organisation for, T. Treatment of Cancer Brain, G. Radiation Oncology, and G. National Cancer Institute of Canada Clinical Trials, *Effects of radiotherapy with concomitant and adjuvant temozolomide versus radiotherapy alone on survival in glioblastoma in a randomised phase III study: 5-year analysis of the EORTC-NCIC trial*. Lancet Oncol, 2009. **10**(5): p. 459-66.
10. Jung, K.W., H. Yoo, H.J. Kong, Y.J. Won, S. Park, and S.H. Lee, *Population-based survival data for brain tumors in Korea*. J Neurooncol, 2012. **109**(2): p. 301-7.

11. Wen, P.Y. and S. Kesari, *Malignant Gliomas in Adults*. N Engl J Med, 2008. **359**(5): p. 492-507.
12. Hoelzinger, D.B., T. Demuth, and M.E. Berens, *Autocrine Factors That Sustain Glioma Invasion and Paracrine Biology in the Brain Microenvironment*. J Natl Cancer Inst, 2007. **99**: p. 1583-93.
13. Burnet, N.G., S.J. Jefferies, R.J. Benson, D.P. Hunt, and F.P. Treasure, *Years of life lost (YLL) from cancer is an important measure of population burden--and should be considered when allocating research funds*. Br J Cancer, 2005. **92**(2): p. 241-5.
14. Huse, J.T. and E.C. Holland, *Targeting brain cancer: advances in the molecular pathology of malignant glioma and medulloblastoma*. Nat Rev Cancer, 2010. **10**(5): p. 319-31.
15. Schwartzbaum, J., B. Ding, T.B. Johannesen, L.T. Osnes, L. Karavodin, A. Ahlbom, M. Feychting, and T.K. Grimsrud, *Association between prediagnostic IgE levels and risk of glioma*. J Natl Cancer Inst, 2012. **104**(16): p. 1251-9.
16. Sherer, H., *Cerebral astrocytomas and their derivatives*. Am J Cancer, 1940(40): p. 159-98.
17. Fisher, J.L., J.A. Schwartzbaum, M. Wrensch, and J.L. Wiemels, *Epidemiology of brain tumors*. Neurol Clin, 2007. **25**(4): p. 867-90, vii.
18. Ohgaki, H., P. Dessen, B. Jourde, S. Horstmann, T. Nishikawa, P.L. Di Patre, C. Burkhard, D. Schuler, N.M. Probst-Hensch, P.C. Maiorka, N. Baeza, P. Pisani, Y. Yonekawa, M.G. Yasargil, U.M. Lutolf, and P. Kleihues, *Genetic pathways to glioblastoma: a population-based study*. Cancer Res, 2004. **64**(19): p. 6892-9.
19. Nobusawa, S., T. Watanabe, P. Kleihues, and H. Ohgaki, *IDH1 mutations as molecular signature and predictive factor of secondary glioblastomas*. Clin Cancer Res, 2009. **15**(19): p. 6002-7.
20. Fujisawa, H., R.M. Reis, M. Nakamura, S. Colella, Y. Yonekawa, P. Kleihues, and H. Ohgaki, *Loss of heterozygosity on chromosome 10 is more extensive in primary (de novo) than in secondary glioblastomas*. Lab Invest, 2000. **80**(1): p. 65-72.
21. Noshmehr, H., D.J. Weisenberger, K. Diefes, H.S. Phillips, K. Pujara, B.P. Berman, F. Pan, C.E. Pelloski, E.P. Sulman, K.P. Bhat, R.G. Verhaak, K.A. Hoadley, D.N. Hayes, C.M. Perou, H.K. Schmidt, L. Ding, R.K. Wilson, D. Van Den Berg, H. Shen, H. Bengtsson, P. Neuvial, L.M. Cope, J. Buckley, J.G. Herman, S.B. Baylin, P.W. Laird, and K. Aldape, *Identification of a CpG island methylator phenotype that defines a distinct subgroup of glioma*. Cancer Cell, 2010. **17**(5): p. 510-22.

22. Ohgaki, H. and P. Kleihues, *The definition of primary and secondary glioblastoma*. Clin Cancer Res, 2013. **19**(4): p. 764-72.
23. Phillips, H.S., S. Kharbanda, R. Chen, W.F. Forrester, R.H. Soriano, T.D. Wu, A. Misra, J.M. Nigro, H. Colman, L. Soroceanu, P.M. Williams, Z. Modrusan, B.G. Feuerstein, and K. Aldape, *Molecular subclasses of high-grade glioma predict prognosis, delineate a pattern of disease progression, and resemble stages in neurogenesis*. Cancer Cell, 2006. **9**(3): p. 157-73.
24. Verhaak, R.G., K.A. Hoadley, E. Purdom, V. Wang, Y. Qi, M.D. Wilkerson, C.R. Miller, L. Ding, T. Golub, J.P. Mesirov, G. Alexe, M. Lawrence, M. O'Kelly, P. Tamayo, B.A. Weir, S. Gabriel, W. Winckler, S. Gupta, L. Jakkula, H.S. Feiler, J.G. Hodgson, C.D. James, J.N. Sarkaria, C. Brennan, A. Kahn, P.T. Spellman, R.K. Wilson, T.P. Speed, J.W. Gray, M. Meyerson, G. Getz, C.M. Perou, and D.N. Hayes, *Integrated genomic analysis identifies clinically relevant subtypes of glioblastoma characterized by abnormalities in PDGFRA, IDH1, EGFR, and NF1*. Cancer Cell, 2010. **17**(1): p. 98-110.
25. Van Meir, E.G., C.G. Hadjipanayis, A.D. Norden, H.-K. Shu, P.Y. Wen, and J.J. Olson, *Exciting New Advances in Neuro-Oncology: The Avenue to a Cure for Malignant Glioma*. CA Cancer J Clin, 2010. **60**(3): p. 166-193.
26. Colman, H., L. Zhang, E.P. Sulman, J.M. McDonald, N.L. Shooshtari, A. Rivera, S. Popoff, C.L. Nutt, D.N. Louis, J.G. Cairncross, M.R. Gilbert, H.S. Phillips, M.P. Mehta, A. Chakravarti, C.E. Pelloso, K. Bhat, B.G. Feuerstein, R.B. Jenkins, and K. Aldape, *A multigene predictor of outcome in glioblastoma*. Neuro Oncol, 2010. **12**(1): p. 49-57.
27. Rohle, D., J. Popovici-Muller, N. Palaskas, S. Turcan, C. Grommes, C. Campos, J. Tsoi, O. Clark, B. Oldrini, E. Komisopoulou, K. Kunii, A. Pedraza, S. Schalm, L. Silverman, A. Miller, F. Wang, H. Yang, Y. Chen, A. Kernytsky, M.K. Rosenblum, W. Liu, S.A. Biller, S.M. Su, C.W. Brennan, T.A. Chan, T.G. Graeber, K.E. Yen, and I.K. Mellinghoff, *An inhibitor of mutant IDH1 delays growth and promotes differentiation of glioma cells*. Science, 2013. **340**(6132): p. 626-30.
28. Curran, W.J., Jr., C.B. Scott, J. Horton, J.S. Nelson, A.S. Weinstein, A.J. Fischbach, C.H. Chang, M. Rotman, S.O. Asbell, R.E. Krisch, and et al., *Recursive partitioning analysis of prognostic factors in three Radiation Therapy Oncology Group malignant glioma trials*. J Natl Cancer Inst, 1993. **85**(9): p. 704-10.
29. Curran, W.J., Jr., C.B. Scott, A.S. Weinstein, L.A. Martin, J.S. Nelson, T.L. Phillips, K. Murray, A.J. Fischbach, D. Yakar, J.G. Schwade, and et al., *Survival comparison of radiosurgery-eligible and -ineligible malignant glioma patients treated with hyperfractionated radiation therapy and carmustine: a report of Radiation Therapy Oncology Group 83-02*. J Clin Oncol, 1993. **11**(5): p. 857-62.

30. Nelson, D.F., W.J. Curran, Jr., C. Scott, J.S. Nelson, A.S. Weinstein, K. Ahmad, L.S. Constine, K. Murray, W.D. Powlis, M. Mohiuddin, and et al., *Hyperfractionated radiation therapy and bis-chlorethyl nitrosourea in the treatment of malignant glioma--possible advantage observed at 72.0 Gy in 1.2 Gy B.I.D. fractions: report of the Radiation Therapy Oncology Group Protocol 8302*. Int J Radiat Oncol Biol Phys, 1993. **25**(2): p. 193-207.
31. Simpson, J.R., J. Horton, C. Scott, W.J. Curran, P. Rubin, J. Fischbach, S. Isaacson, M. Rotman, S.O. Asbell, J.S. Nelson, and et al., *Influence of location and extent of surgical resection on survival of patients with glioblastoma multiforme: results of three consecutive Radiation Therapy Oncology Group (RTOG) clinical trials*. Int J Radiat Oncol Biol Phys, 1993. **26**(2): p. 239-44.
32. Lacroix, M., D. Abi-Said, D.R. Fournay, Z.L. Gokaslan, W. Shi, F. DeMonte, F.F. Lang, I.E. McCutcheon, S.J. Hassenbusch, E. Holland, K. Hess, C. Michael, D. Miller, and R. Sawaya, *A multivariate analysis of 416 patients with glioblastoma multiforme: prognosis, extent of resection, and survival*. J Neurosurg, 2001. **95**(2): p. 190-8.
33. Stummer, W., H.J. Reulen, T. Meinel, U. Pichlmeier, W. Schumacher, J.C. Tonn, V. Rohde, F. Opperl, B. Turowski, C. Woiciechowsky, K. Franz, and T. Pietsch, *Extent of resection and survival in glioblastoma multiforme: identification of and adjustment for bias*. Neurosurgery, 2008. **62**(3): p. 564-76; discussion 564-76.
34. Stupp, R., W.P. Mason, M.J. van den Bent, M. Weller, B. Fisher, M.J. Taphoorn, K. Belanger, A.A. Brandes, C. Marosi, U. Bogdahn, J. Curschmann, R.C. Janzer, S.K. Ludwin, T. Gorlia, A. Allgeier, D. Lacombe, J.G. Cairncross, E. Eisenhauer, and R.O. Mirimanoff, *Radiotherapy plus concomitant and adjuvant temozolomide for glioblastoma*. N Engl J Med, 2005. **352**(10): p. 987-96.
35. Hegi, M.E., A.C. Diserens, T. Gorlia, M.F. Hamou, N. de Tribolet, M. Weller, J.M. Kros, J.A. Hainfellner, W. Mason, L. Mariani, J.E. Bromberg, P. Hau, R.O. Mirimanoff, J.G. Cairncross, R.C. Janzer, and R. Stupp, *MGMT gene silencing and benefit from temozolomide in glioblastoma*. N Engl J Med, 2005. **352**(10): p. 997-1003.
36. Folkman, J., *Tumor angiogenesis: therapeutic implications*. N Engl J Med, 1971. **285**(21): p. 1182-6.
37. Folkman, J., E. Merler, C. Abernathy, and G. Williams, *Isolation of a tumor factor responsible for angiogenesis*. J Exp Med, 1971. **133**(2): p. 275-88.
38. Senger, D.R., S.J. Galli, A.M. Dvorak, C.A. Perruzzi, V.S. Harvey, and H.F. Dvorak, *Tumor cells secrete a vascular permeability factor that promotes accumulation of ascites fluid*. Science, 1983. **219**(4587): p. 983-5.

39. Ferrara, N. and W.J. Henzel, *Pituitary follicular cells secrete a novel heparin-binding growth factor specific for vascular endothelial cells*. *Biochem Biophys Res Commun*, 1989. **161**(2): p. 851-8.
40. Presta, L.G., H. Chen, S.J. O'Connor, V. Chisholm, Y.G. Meng, L. Krummen, M. Winkler, and N. Ferrara, *Humanization of an anti-vascular endothelial growth factor monoclonal antibody for the therapy of solid tumors and other disorders*. *Cancer Res*, 1997. **57**(20): p. 4593-9.
41. Kabbinavar, F., H.I. Hurwitz, L. Fehrenbacher, N.J. Meropol, W.F. Novotny, G. Lieberman, S. Griffing, and E. Bergsland, *Phase II, randomized trial comparing bevacizumab plus fluorouracil (FU)/leucovorin (LV) with FU/LV alone in patients with metastatic colorectal cancer*. *J Clin Oncol*, 2003. **21**(1): p. 60-5.
42. Hurwitz, H., L. Fehrenbacher, W. Novotny, T. Cartwright, J. Hainsworth, W. Heim, J. Berlin, A. Baron, S. Griffing, E. Holmgren, N. Ferrara, G. Fyfe, B. Rogers, R. Ross, and F. Kabbinavar, *Bevacizumab plus irinotecan, fluorouracil, and leucovorin for metastatic colorectal cancer*. *N Engl J Med*, 2004. **350**(23): p. 2335-42.
43. Vredenburgh, J.J., A. Desjardins, J.E. Herndon, 2nd, J. Marcello, D.A. Reardon, J.A. Quinn, J.N. Rich, S. Sathornsumetee, S. Gururangan, J. Sampson, M. Wagner, L. Bailey, D.D. Bigner, A.H. Friedman, and H.S. Friedman, *Bevacizumab plus irinotecan in recurrent glioblastoma multiforme*. *J Clin Oncol*, 2007. **25**(30): p. 4722-9.
44. Friedman, H.S., M.D. Prados, P.Y. Wen, T. Mikkelsen, D. Schiff, L.E. Abrey, W.K. Yung, N. Paleologos, M.K. Nicholas, R. Jensen, J. Vredenburgh, J. Huang, M. Zheng, and T. Cloughesy, *Bevacizumab alone and in combination with irinotecan in recurrent glioblastoma*. *J Clin Oncol*, 2009. **27**(28): p. 4733-40.
45. Lai, A., A. Tran, P.L. Nghiemphu, W.B. Pope, O.E. Solis, M. Selch, E. Filka, W.H. Yong, P.S. Mischel, L.M. Liau, S. Phuphanich, K. Black, S. Peak, R.M. Green, C.E. Spier, T. Kolevska, J. Polikoff, L. Fehrenbacher, R. Elashoff, and T. Cloughesy, *Phase II study of bevacizumab plus temozolomide during and after radiation therapy for patients with newly diagnosed glioblastoma multiforme*. *J Clin Oncol*, 2011. **29**(2): p. 142-8.
46. Nguyen, D.H., S.C. Stapleton, M.T. Yang, S.S. Cha, C.K. Choi, P.A. Galie, and C.S. Chen, *Biomimetic model to reconstitute angiogenic sprouting morphogenesis in vitro*. *Proc Natl Acad Sci U S A*, 2013. **110**(17): p. 6712-7.
47. Tanimoto, T., Z.G. Jin, and B.C. Berk, *Transactivation of vascular endothelial growth factor (VEGF) receptor Flk-1/KDR is involved in sphingosine 1-phosphate-stimulated phosphorylation of Akt and endothelial nitric-oxide synthase (eNOS)*. *J Biol Chem*, 2002. **277**(45): p. 42997-3001.

48. Igarashi, J., P.A. Erwin, A.P. Dantas, H. Chen, and T. Michel, *VEGF induces SIP1 receptors in endothelial cells: Implications for cross-talk between sphingolipid and growth factor receptors*. Proc Natl Acad Sci U S A, 2003. **100**(19): p. 10664-9.
49. Jung, B., H. Obinata, S. Galvani, K. Mendelson, B.S. Ding, A. Skoura, B. Kinzel, V. Brinkmann, S. Rafii, T. Evans, and T. Hla, *Flow-regulated endothelial SIP receptor-1 signaling sustains vascular development*. Dev Cell, 2012. **23**(3): p. 600-10.
50. Thudichum, J.L.W., *A treatise on the chemical constitution of the brain*. 1884, Bailliere, Tindall, and Cox: London.
51. Fahy, E., S. Subramaniam, R.C. Murphy, M. Nishijima, C.R. Raetz, T. Shimizu, F. Spener, G. van Meer, M.J. Wakelam, and E.A. Dennis, *Update of the LIPID MAPS comprehensive classification system for lipids*. J Lipid Res, 2009. **50** Suppl(Supplement): p. S9-14.
52. Sabbadini, R.A., *Targeting sphingosine-1-phosphate for cancer therapy*. Br J Cancer, 2006. **95**(9): p. 1131-5.
53. Hannun, Y.A. and L.M. Obeid, *Principles of bioactive lipid signalling: lessons from sphingolipids*. Nat Rev Mol Cell Biol, 2008. **9**(2): p. 139-50.
54. Spiegel, S. and S. Milstien, *Sphingosine-1-phosphate: an enigmatic signalling lipid*. Nat Rev Mol Cell Biol, 2003. **4**(5): p. 397-407.
55. Pyne, N.J. and S. Pyne, *Sphingosine 1-phosphate and cancer*. Nat Rev Cancer, 2010. **10**(7): p. 489-503.
56. Christie, W.W. *The AOCS Lipid Library*. [Web Page] 2013 13/06/2013 [cited 2013 20/06/2013]; Available from: www.lipidlibrary.co.uk.
57. Quarles, R., Macklin, WB, Morell, P, *Myelin Formation, Structure and Biochemistry*, in *Basic Neurochemistry: Molecular, Cellular and Medical Aspects*. 2006, Elsevier, Inc. p. 51-71.
58. Zhao, L., S.D. Spassieva, T.J. Jucius, L.D. Shultz, H.E. Shick, W.B. Macklin, Y.A. Hannun, L.M. Obeid, and S.L. Ackerman, *A deficiency of ceramide biosynthesis causes cerebellar purkinje cell neurodegeneration and lipofuscin accumulation*. PLoS Genet, 2011. **7**(5): p. e1002063.
59. Imgrund, S., D. Hartmann, H. Farwanah, M. Eckhardt, R. Sandhoff, J. Degen, V. Gieselmann, K. Sandhoff, and K. Willecke, *Adult ceramide synthase 2 (CERS2)-deficient mice exhibit myelin sheath defects, cerebellar degeneration, and hepatocarcinomas*. J Biol Chem, 2009. **284**(48): p. 33549-60.
60. Ben-David, O., Y. Pewzner-Jung, O. Brenner, E.L. Laviad, A. Kogot-Levin, I. Weissberg, I.E. Biton, R. Pienik, E. Wang, S. Kelly, J. Alroy, A. Raas-

- Rothschild, A. Friedman, B. Brugger, A.H. Merrill, Jr., and A.H. Futerman, *Encephalopathy caused by ablation of very long acyl chain ceramide synthesis may be largely due to reduced galactosylceramide levels*. J Biol Chem, 2011. **286**(34): p. 30022-33.
61. Kolmakova, A., M. Rajesh, D. Zang, R. Pili, and S. Chatterjee, *VEGF recruits lactosylceramide to induce endothelial cell adhesion molecule expression and angiogenesis in vitro and in vivo*. Glycoconj J, 2009. **26**(5): p. 547-58.
 62. Coetzee, T., N. Fujita, J. Dupree, R. Shi, A. Blight, K. Suzuki, K. Suzuki, and B. Popko, *Myelination in the Absence of Galactocerebroside and Sulfatide: Normal Structure with Abnormal Function and Regional Instability*. Cell, 1996. **86**(2): p. 209-219.
 63. Van Brocklyn, J.R., N. Young, and R. Roof, *Sphingosine-1-phosphate stimulates motility and invasiveness of human glioblastoma multiforme cells*. Cancer Lett, 2003. **199**(1): p. 53-60.
 64. Donati, C. and P. Bruni, *Sphingosine 1-phosphate regulates cytoskeleton dynamics: implications in its biological response*. Biochim Biophys Acta, 2006. **1758**(12): p. 2037-48.
 65. Cuvillier, O., G. Pirianov, B. Kleuser, P.G. Vanek, O.A. Coso, S. Gutkind, and S. Spiegel, *Suppression of ceramide-mediated programmed cell death by sphingosine-1-phosphate*. Nature, 1996. **381**(6585): p. 800-3.
 66. Ohta, H., E.A. Sweeney, A. Masamune, Y. Yatomi, S. Hakomori, and Y. Igarashi, *Induction of apoptosis by sphingosine in human leukemic HL-60 cells: a possible endogenous modulator of apoptotic DNA fragmentation occurring during phorbol ester-induced differentiation*. Cancer Res, 1995. **55**(3): p. 691-7.
 67. Mencarelli, C. and P. Martinez-Martinez, *Ceramide function in the brain: when a slight tilt is enough*. Cell Mol Life Sci, 2013. **70**(2): p. 181-203.
 68. Huwiler, A. and U. Zangemeister-Wittke, *Targeting the conversion of ceramide to sphingosine 1-phosphate as a novel strategy for cancer therapy*. Crit Rev Oncol Hematol, 2007. **63**(2): p. 150-159.
 69. Reynolds, C.P., B.J. Maurer, and R.N. Kolesnick, *Ceramide synthesis and metabolism as a target for cancer therapy*. Cancer Lett, 2004. **206**(2): p. 169-180.
 70. Tani, M., M. Ito, and Y. Igarashi, *Ceramide/sphingosine/sphingosine 1-phosphate metabolism on the cell surface and in the extracellular space*. Cell Signal, 2007. **19**(2): p. 229-37.
 71. Ogretmen, B. and Y.A. Hannun, *Biologically active sphingolipids in cancer pathogenesis and treatment*. Nat Rev Cancer, 2004. **4**(8): p. 604-16.

72. Wymann, M.P. and R. Schneider, *Lipid signalling in disease*. Nat Rev Mol Cell Biol, 2008. **9**(2): p. 162-76.
73. Dbaibo, G.S., W. El-Assaad, A. Krikorian, B. Liu, K. Diab, N.Z. Idriss, M. El-Sabban, T.A. Driscoll, D.K. Perry, and Y.A. Hannun, *Ceramide generation by two distinct pathways in tumor necrosis factor alpha-induced cell death*. FEBS Lett, 2001. **503**(1): p. 7-12.
74. Coroneos, E., M. Martinez, S. McKenna, and M. Kester, *Differential regulation of sphingomyelinase and ceramidase activities by growth factors and cytokines. Implications for cellular proliferation and differentiation*. J Biol Chem, 1995. **270**(40): p. 23305-9.
75. Sentelle, R.D., C.E. Senkal, W. Jiang, S. Ponnusamy, S. Gencer, S.P. Selvam, V.K. Ramshesh, Y.K. Peterson, J.J. Lemasters, Z.M. Szulc, J. Bielawski, and B. Ogretmen, *Ceramide targets autophagosomes to mitochondria and induces lethal mitophagy*. Nat Chem Biol, 2012. **8**(10): p. 831-8.
76. Lacour, S., A. Hammann, S. Grazide, D. Lagadic-Gossmann, A. Athias, O. Sergent, G. Laurent, P. Gambert, E. Solary, and M.T. Dimanche-Boitrel, *Cisplatin-induced CD95 redistribution into membrane lipid rafts of HT29 human colon cancer cells*. Cancer Res, 2004. **64**(10): p. 3593-8.
77. Bieberich, E., *Ceramide signaling in cancer and stem cells*. Future Lipidol, 2008. **3**(3): p. 273-300.
78. Chalfant, C.E., Z. Szulc, P. Roddy, A. Bielawska, and Y.A. Hannun, *The structural requirements for ceramide activation of serine-threonine protein phosphatases*. J Lipid Res, 2004. **45**(3): p. 496-506.
79. Zhang, Y., B. Yao, S. Delikat, S. Bayoumy, X.H. Lin, S. Basu, M. McGinley, P.Y. Chan-Hui, H. Lichenstein, and R. Kolesnick, *Kinase suppressor of Ras is ceramide-activated protein kinase*. Cell, 1997. **89**(1): p. 63-72.
80. Obeid, L.M., C.M. Linardic, L.A. Karolak, and Y.A. Hannun, *Programmed cell death induced by ceramide*. Science, 1993. **259**(5102): p. 1769-71.
81. Eto, M., J. Bennouna, O.C. Hunter, M.T. Lotze, and A.A. Amoscato, *Importance of C16 ceramide accumulation during apoptosis in prostate cancer cells*. Int J Urol, 2006. **13**(2): p. 148-56.
82. Senkal, C.E., S. Ponnusamy, J. Bielawski, Y.A. Hannun, and B. Ogretmen, *Antiapoptotic roles of ceramide-synthase-6-generated C16-ceramide via selective regulation of the ATF6/CHOP arm of ER-stress-response pathways*. FASEB J, 2010. **24**(1): p. 296-308.
83. Senkal, C.E., S. Ponnusamy, Y. Manevich, M. Meyers-Needham, S.A. Saddoughi, A. Mukhopadhyay, P. Dent, J. Bielawski, and B. Ogretmen, *Alteration of ceramide synthase 6/C16-ceramide induces activating*

- transcription factor 6-mediated endoplasmic reticulum (ER) stress and apoptosis via perturbation of cellular Ca²⁺ and ER/Golgi membrane network.* J Biol Chem, 2011. **286**(49): p. 42446-58.
84. Schiffmann, S., J. Sandner, K. Birod, I. Wobst, C. Angioni, E. Ruckhäberle, M. Kaufmann, H. Ackermann, J. Lötsch, H. Schmidt, G. Geisslinger, and S. Grösch, *Ceramide synthases and ceramide levels are increased in breast cancer tissue.* Carcinogenesis, 2009. **30**(5): p. 745-752.
 85. Senkal, C.E., S. Ponnusamy, M.J. Rossi, J. Bialewski, D. Sinha, J.C. Jiang, S.M. Jazwinski, Y.A. Hannun, and B. Ogretmen, *Role of human longevity assurance gene 1 and C18-ceramide in chemotherapy-induced cell death in human head and neck squamous cell carcinomas.* Mol Cancer Ther, 2007. **6**(2): p. 712-22.
 86. Koybasi, S., C.E. Senkal, K. Sundararaj, S. Spassieva, J. Bielawski, W. Osta, T.A. Day, J.C. Jiang, S.M. Jazwinski, Y.A. Hannun, L.M. Obeid, and B. Ogretmen, *Defects in cell growth regulation by C18:0-ceramide and longevity assurance gene 1 in human head and neck squamous cell carcinomas.* J Biol Chem, 2004. **279**(43): p. 44311-9.
 87. Mizugishi, K., T. Yamashita, A. Olivera, G.F. Miller, S. Spiegel, and R.L. Proia, *Essential role for sphingosine kinases in neural and vascular development.* Mol Cell Biol, 2005. **25**(24): p. 11113-21.
 88. Kim, R.H., K. Takabe, S. Milstien, and S. Spiegel, *Export and functions of sphingosine-1-phosphate.* Biochim Biophys Acta, 2009. **1791**(7): p. 692-6.
 89. Lee, Y.M., K. Venkataraman, S.I. Hwang, D.K. Han, and T. Hla, *A novel method to quantify sphingosine 1-phosphate by immobilized metal affinity chromatography (IMAC).* Prostaglandins Other Lipid Mediat, 2007. **84**(3-4): p. 154-62.
 90. Van Meer, G. and Q. Lisman, *Sphingolipid transport: rafts and translocators.* J Biol Chem, 2002. **277**(29): p. 25855-8.
 91. Sato, K., E. Malchinkhuu, Y. Horiuchi, C. Mogi, H. Tomura, M. Tosaka, Y. Yoshimoto, A. Kuwabara, and F. Okajima, *Critical role of ABCA1 transporter in sphingosine 1-phosphate release from astrocytes.* J Neurochem, 2007. **103**(6): p. 2610-9.
 92. Takabe, K., R.H. Kim, J.C. Allegood, P. Mitra, S. Ramachandran, M. Nagahashi, K.B. Harikumar, N.C. Hait, S. Milstien, and S. Spiegel, *Estradiol induces export of sphingosine 1-phosphate from breast cancer cells via ABCA1 and ABCG2.* J Biol Chem, 2010. **285**(14): p. 10477-86.
 93. Kobayashi, N., T. Nishi, T. Hirata, A. Kihara, T. Sano, Y. Igarashi, and A. Yamaguchi, *Sphingosine 1-phosphate is released from the cytosol of rat platelets in a carrier-mediated manner.* J Lipid Res, 2006. **47**(3): p. 614-21.

94. Mitra, P., C.A. Oskeritzian, S.G. Payne, M.A. Beaven, S. Milstien, and S. Spiegel, *Role of ABCB1 in export of sphingosine-1-phosphate from mast cells*. Proc Natl Acad Sci U S A, 2006. **103**(44): p. 16394-9.
95. Schmidt, H., R. Schmidt, and G. Geisslinger, *LC-MS/MS-analysis of sphingosine-1-phosphate and related compounds in plasma samples*. Prostaglandins Other Lipid Mediat, 2006. **81**(3-4): p. 162-70.
96. Yatomi, Y., *Plasma sphingosine 1-phosphate metabolism and analysis*. Biochim Biophys Acta, 2008. **1780**(3): p. 606-11.
97. Kimura, T., K. Sato, A. Kuwabara, H. Tomura, M. Ishiwara, I. Kobayashi, M. Ui, and F. Okajima, *Sphingosine 1-phosphate may be a major component of plasma lipoproteins responsible for the cytoprotective actions in human umbilical vein endothelial cells*. J Biol Chem, 2001. **276**(34): p. 31780-5.
98. Kimura, T., K. Sato, E. Malchinkhuu, H. Tomura, K. Tamama, A. Kuwabara, M. Murakami, and F. Okajima, *High-density lipoprotein stimulates endothelial cell migration and survival through sphingosine 1-phosphate and its receptors*. Arterioscler Thromb Vasc Biol, 2003. **23**(7): p. 1283-8.
99. Kimura, T., H. Tomura, C. Mogi, A. Kuwabara, A. Damirin, T. Ishizuka, A. Sekiguchi, M. Ishiwara, D.S. Im, K. Sato, M. Murakami, and F. Okajima, *Role of scavenger receptor class B type I and sphingosine 1-phosphate receptors in high density lipoprotein-induced inhibition of adhesion molecule expression in endothelial cells*. J Biol Chem, 2006. **281**(49): p. 37457-67.
100. Tamama, K., H. Tomura, K. Sato, E. Malchinkhuu, A. Damirin, T. Kimura, A. Kuwabara, M. Murakami, and F. Okajima, *High-density lipoprotein inhibits migration of vascular smooth muscle cells through its sphingosine 1-phosphate component*. Atherosclerosis, 2005. **178**(1): p. 19-23.
101. Okajima, F., *Plasma lipoproteins behave as carriers of extracellular sphingosine 1-phosphate: is this an atherogenic mediator or an anti-atherogenic mediator?* Biochim Biophys Acta, 2002. **1582**(1-3): p. 132-137.
102. Maceyka, M., K.B. Harikumar, S. Milstien, and S. Spiegel, *Sphingosine-1-phosphate signaling and its role in disease*. Trends Cell Biol, 2012. **22**(1): p. 50-60.
103. Van Brocklyn, J.R., C.A. Letterle, P.J. Snyder, and T.W. Prior, *Sphingosine-1-phosphate stimulates human glioma cell proliferation through Gi-coupled receptors: role of ERK MAP kinase and phosphatidylinositol 3-kinase [beta]*. Cancer Letters, 2002. **181**(2): p. 195-204.
104. Malchinkhuu, E., K. Sato, T. Maehama, C. Mogi, H. Tomura, S. Ishiuchi, Y. Yoshimoto, H. Kurose, and F. Okajima, *SIP(2) receptors mediate inhibition of glioma cell migration through Rho signaling pathways independent of PTEN*. Biochem Biophys Res Commun, 2008. **366**(4): p. 963-8.

105. Young, N. and J.R. Van Brocklyn, *Roles of sphingosine-1-phosphate (S1P) receptors in malignant behavior of glioma cells. Differential effects of S1P2 on cell migration and invasiveness.* Exp Cell Res, 2007. **313**(8): p. 1615-27.
106. Arikawa, K., N. Takuwa, H. Yamaguchi, N. Sugimoto, J. Kitayama, H. Nagawa, K. Takehara, and Y. Takuwa, *Ligand-dependent inhibition of B16 melanoma cell migration and invasion via endogenous S1P2 G protein-coupled receptor. Requirement of inhibition of cellular RAC activity.* J Biol Chem, 2003. **278**(35): p. 32841-51.
107. Takuwa, N., W. Du, E. Kaneko, Y. Okamoto, K. Yoshioka, and Y. Takuwa, *Tumor-suppressive sphingosine-1-phosphate receptor-2 counteracting tumor-promoting sphingosine-1-phosphate receptor-1 and sphingosine kinase 1 - Jekyll Hidden behind Hyde.* Am J Cancer Res, 2011. **1**(4): p. 460-81.
108. Chae, S.S., J.H. Paik, H. Furneaux, and T. Hla, *Requirement for sphingosine 1-phosphate receptor-1 in tumor angiogenesis demonstrated by in vivo RNA interference.* J Clin Invest, 2004. **114**(8): p. 1082-9.
109. Hait, N.C., J. Allegood, M. Maceyka, G.M. Strub, K.B. Harikumar, S.K. Singh, C. Luo, R. Marmorstein, T. Kordula, S. Milstien, and S. Spiegel, *Regulation of histone acetylation in the nucleus by sphingosine-1-phosphate.* Science, 2009. **325**(5945): p. 1254-7.
110. Sauer, B., H. Gonska, M. Manggau, D.S. Kim, C. Schraut, M. Schafer-Korting, and B. Kleuser, *Sphingosine 1-phosphate is involved in cytoprotective actions of calcitriol in human fibroblasts and enhances the intracellular Bcl-2/Bax rheostat.* Pharmazie, 2005. **60**(4): p. 298-304.
111. Betito, S. and O. Cuvillier, *Regulation by sphingosine 1-phosphate of Bax and Bad activities during apoptosis in a MEK-dependent manner.* Biochem Biophys Res Commun, 2006. **340**(4): p. 1273-7.
112. Avery, K., S. Avery, J. Shepherd, P.R. Heath, and H. Moore, *Sphingosine-1-phosphate mediates transcriptional regulation of key targets associated with survival, proliferation, and pluripotency in human embryonic stem cells.* Stem Cells Dev, 2008. **17**(6): p. 1195-205.
113. Li, Q.F., C.T. Wu, Q. Guo, H. Wang, and L.S. Wang, *Sphingosine 1-phosphate induces Mcl-1 upregulation and protects multiple myeloma cells against apoptosis.* Biochem Biophys Res Commun, 2008. **371**(1): p. 159-62.
114. Strub, G.M., M. Paillard, J. Liang, L. Gomez, J.C. Allegood, N.C. Hait, M. Maceyka, M.M. Price, Q. Chen, D.C. Simpson, T. Kordula, S. Milstien, E.J. Lesnefsky, and S. Spiegel, *Sphingosine-1-phosphate produced by sphingosine kinase 2 in mitochondria interacts with prohibitin 2 to regulate complex IV assembly and respiration.* FASEB J, 2011. **25**(2): p. 600-12.

115. Xia, P., L. Wang, P.A. Moretti, N. Albanese, F. Chai, S.M. Pitson, R.J. D'Andrea, J.R. Gamble, and M.A. Vadas, *Sphingosine kinase interacts with TRAF2 and dissects tumor necrosis factor- α signaling*. J Biol Chem, 2002. **277**(10): p. 7996-8003.
116. Alvarez, S.E., K.B. Harikumar, N.C. Hait, J. Allegood, G.M. Strub, E.Y. Kim, M. Maceyka, H. Jiang, C. Luo, T. Kordula, S. Milstien, and S. Spiegel, *Sphingosine-1-phosphate is a missing cofactor for the E3 ubiquitin ligase TRAF2*. Nature, 2010. **465**(7301): p. 1084-8.
117. Hayden, M.S. and S. Ghosh, *Shared principles in NF- κ B signaling*. Cell, 2008. **132**(3): p. 344-62.
118. Morita, Y., G.I. Perez, F. Paris, S.R. Miranda, D. Ehleiter, A. Haimovitz-Friedman, Z. Fuks, Z. Xie, J.C. Reed, E.H. Schuchman, R.N. Kolesnick, and J.L. Tilly, *Oocyte apoptosis is suppressed by disruption of the acid sphingomyelinase gene or by sphingosine-1-phosphate therapy*. Nat Med, 2000. **6**(10): p. 1109-14.
119. Maceyka, M., H. Sankala, N.C. Hait, H. Le Stunff, H. Liu, R. Toman, C. Collier, M. Zhang, L.S. Satin, A.H. Merrill, Jr., S. Milstien, and S. Spiegel, *SphK1 and SphK2, sphingosine kinase isoenzymes with opposing functions in sphingolipid metabolism*. J Biol Chem, 2005. **280**(44): p. 37118-29.
120. Le Stunff, H., I. Galve-Roperh, C. Peterson, S. Milstien, and S. Spiegel, *Sphingosine-1-phosphate phosphohydrolase in regulation of sphingolipid metabolism and apoptosis*. J Cell Biol, 2002. **158**(6): p. 1039-49.
121. Laviad, E.L., L. Albee, I. Pankova-Kholmyansky, S. Epstein, H. Park, A.H. Merrill, Jr., and A.H. Futerman, *Characterization of ceramide synthase 2: tissue distribution, substrate specificity, and inhibition by sphingosine 1-phosphate*. J Biol Chem, 2008. **283**(9): p. 5677-84.
122. Johnson, K.R., K.P. Becker, M.M. Facchinetti, Y.A. Hannun, and L.M. Obeid, *PKC-dependent activation of sphingosine kinase 1 and translocation to the plasma membrane. Extracellular release of sphingosine-1-phosphate induced by phorbol 12-myristate 13-acetate (PMA)*. J Biol Chem, 2002. **277**(38): p. 35257-62.
123. Pitson, S.M., *Regulation of sphingosine kinase and sphingolipid signaling*. Trends Biochem Sci, 2011. **36**(2): p. 97-107.
124. Xia, P., J.R. Gamble, L. Wang, S.M. Pitson, P.A. Moretti, B.W. Wattenberg, R.J. D'Andrea, and M.A. Vadas, *An oncogenic role of sphingosine kinase*. Curr Biol, 2000. **10**(23): p. 1527-30.
125. French, K.J., R.S. Schrecengost, B.D. Lee, Y. Zhuang, S.N. Smith, J.L. Eberly, J.K. Yun, and C.D. Smith, *Discovery and evaluation of inhibitors of human sphingosine kinase*. Cancer Res, 2003. **63**(18): p. 5962-9.

126. Ruckhaberle, E., A. Rody, K. Engels, R. Gaetje, G. von Minckwitz, S. Schiffmann, S. Grosch, G. Geisslinger, U. Holtrich, T. Karn, and M. Kaufmann, *Microarray analysis of altered sphingolipid metabolism reveals prognostic significance of sphingosine kinase 1 in breast cancer*. *Breast Cancer Res Treat*, 2008. **112**(1): p. 41-52.
127. Johnson, K.R., K.Y. Johnson, H.G. Crellin, B. Ogretmen, A.M. Boylan, R.A. Harley, and L.M. Obeid, *Immunohistochemical distribution of sphingosine kinase 1 in normal and tumor lung tissue*. *J Histochem Cytochem*, 2005. **53**(9): p. 1159-66.
128. Song, L., H. Xiong, J. Li, W. Liao, L. Wang, J. Wu, and M. Li, *Sphingosine kinase-1 enhances resistance to apoptosis through activation of PI3K/Akt/NF-kappaB pathway in human non-small cell lung cancer*. *Clin Cancer Res*, 2011. **17**(7): p. 1839-49.
129. Kawamori, T., T. Kaneshiro, M. Okumura, S. Maalouf, A. Uflacker, J. Bielawski, Y.A. Hannun, and L.M. Obeid, *Role for sphingosine kinase 1 in colon carcinogenesis*. *FASEB J*, 2009. **23**(2): p. 405-14.
130. Kohno, M., M. Momoi, M.L. Oo, J.H. Paik, Y.M. Lee, K. Venkataraman, Y. Ai, A.P. Ristimaki, H. Fyrst, H. Sano, D. Rosenberg, J.D. Saba, R.L. Proia, and T. Hla, *Intracellular role for sphingosine kinase 1 in intestinal adenoma cell proliferation*. *Mol Cell Biol*, 2006. **26**(19): p. 7211-23.
131. Facchinetti, M.M., N.A. Gandini, M.E. Fermento, N.B. Sterin-Speziale, Y. Ji, V. Patel, J.S. Gutkind, M.G. Rivadulla, and A.C. Curino, *The expression of sphingosine kinase-1 in head and neck carcinoma*. *Cells Tissues Organs*, 2010. **192**(5): p. 314-24.
132. Sinha, U.K., V.J. Schorn, C. Hochstim, S.B. Chinn, S. Zhu, and R. Masood, *Increased radiation sensitivity of head and neck squamous cell carcinoma with sphingosine kinase 1 inhibition*. *Head Neck*, 2010. **33**(2): p. 178-88.
133. Li, J., H.Y. Guan, L.Y. Gong, L.B. Song, N. Zhang, J. Wu, J. Yuan, Y.J. Zheng, Z.S. Huang, and M. Li, *Clinical significance of sphingosine kinase-1 expression in human astrocytomas progression and overall patient survival*. *Clin Cancer Res*, 2008. **14**(21): p. 6996-7003.
134. Van Brocklyn, J.R., C.A. Jackson, D.K. Pearl, M.S. Kotur, P.J. Snyder, and T.W. Prior, *Sphingosine kinase-1 expression correlates with poor survival of patients with glioblastoma multiforme: roles of sphingosine kinase isoforms in growth of glioblastoma cell lines*. *J Neuropathol Exp Neurol*, 2005. **64**(8): p. 695-705.
135. Li, W., C.P. Yu, J.T. Xia, L. Zhang, G.X. Weng, H.Q. Zheng, Q.L. Kong, L.J. Hu, M.S. Zeng, Y.X. Zeng, M. Li, J. Li, and L.B. Song, *Sphingosine kinase 1 is associated with gastric cancer progression and poor survival of patients*. *Clin Cancer Res*, 2009. **15**(4): p. 1393-9.

136. Cuvillier, O. and T. Levade, *Sphingosine 1-phosphate antagonizes apoptosis of human leukemia cells by inhibiting release of cytochrome c and Smac/DIABLO from mitochondria*. *Blood*, 2001. **98**(9): p. 2828-36.
137. Limaye, V., X. Li, C. Hahn, P. Xia, M.C. Berndt, M.A. Vadas, and J.R. Gamble, *Sphingosine kinase-1 enhances endothelial cell survival through a PECAM-1-dependent activation of PI-3K/Akt and regulation of Bcl-2 family members*. *Blood*, 2005. **105**(8): p. 3169-77.
138. Vadas, M., P. Xia, G. McCaughan, and J. Gamble, *The role of sphingosine kinase 1 in cancer: oncogene or non-oncogene addiction?* *Biochim Biophys Acta*, 2008. **1781**(9): p. 442-7.
139. Bektas, M., S.P. Johnson, W.E. Poe, D.D. Bigner, and H.S. Friedman, *A sphingosine kinase inhibitor induces cell death in temozolomide resistant glioblastoma cells*. *Cancer Chemother Pharmacol*, 2009. **64**(5): p. 1053-8.
140. Leong, W.I. and J.D. Saba, *S1P metabolism in cancer and other pathological conditions*. *Biochimie*, 2010. **92**(6): p. 716-723.
141. Anelli, V., C.R. Gault, A.B. Cheng, and L.M. Obeid, *Sphingosine kinase 1 is up-regulated during hypoxia in U87MG glioma cells. Role of hypoxia-inducible factors 1 and 2*. *J Biol Chem*, 2008. **283**(6): p. 3365-75.
142. Anelli, V., C.R. Gault, A.J. Snider, and L.M. Obeid, *Role of sphingosine kinase-1 in paracrine/transcellular angiogenesis and lymphangiogenesis in vitro*. *FASEB J*, 2010. **24**(8): p. 2727-38.
143. Kapitonov, D., J.C. Allegood, C. Mitchell, N.C. Hait, J.A. Almenara, J.K. Adams, R.E. Zipkin, P. Dent, T. Kordula, S. Milstien, and S. Spiegel, *Targeting sphingosine kinase 1 inhibits Akt signaling, induces apoptosis, and suppresses growth of human glioblastoma cells and xenografts*. *Cancer Res*, 2009. **69**(17): p. 6915-23.
144. Guan, H., L. Song, J. Cai, Y. Huang, J. Wu, J. Yuan, J. Li, and M. Li, *Sphingosine kinase 1 regulates the Akt/FOXO3a/Bim pathway and contributes to apoptosis resistance in glioma cells*. *PLoS One*, 2011. **6**(5): p. e19946.
145. Zhang, H., W. Li, S. Sun, S. Yu, M. Zhang, and F. Zou, *Inhibition of sphingosine kinase 1 suppresses proliferation of glioma cells under hypoxia by attenuating activity of extracellular signal-regulated kinase*. *Cell Prolif*, 2012. **45**(2): p. 167-75.
146. Rosa, R., R. Marciano, U. Malapelle, L. Formisano, L. Nappi, C. D'Amato, V. D'Amato, V. Damiano, G. Marfe, S. Del Vecchio, A. Zannetti, A. Greco, A. De Stefano, C. Carlomagno, B.M. Veneziani, G. Troncone, S. De Placido, and R. Bianco, *Sphingosine kinase 1 overexpression contributes to cetuximab resistance in human colorectal cancer models*. *Clin Cancer Res*, 2013. **19**(1): p. 138-47.

147. Vessey, D.A., M. Kelley, J. Zhang, L. Li, R. Tao, and J.S. Karliner, *Dimethylsphingosine and FTY720 inhibit the SK1 form but activate the SK2 form of sphingosine kinase from rat heart*. *J Biochem Mol Toxicol*, 2007. **21**(5): p. 273-9.
148. Tonelli, F., K.G. Lim, C. Loveridge, J. Long, S.M. Pitson, G. Tigyi, R. Bittman, S. Pyne, and N.J. Pyne, *FTY720 and (S)-FTY720 vinylphosphonate inhibit sphingosine kinase 1 and promote its proteasomal degradation in human pulmonary artery smooth muscle, breast cancer and androgen-independent prostate cancer cells*. *Cell Signal*, 2010. **22**(10): p. 1536-42.
149. Estrada-Bernal, A., K. Palanichamy, A. Ray Chaudhury, and J.R. Van Brocklyn, *Induction of brain tumor stem cell apoptosis by FTY720: a potential therapeutic agent for glioblastoma*. *Neuro Oncol*, 2012. **14**(4): p. 405-15.
150. Saddoughi, S.A., S. Gencer, Y.K. Peterson, K.E. Ward, A. Mukhopadhyay, J. Oaks, J. Bielawski, Z.M. Szulc, R.J. Thomas, S.P. Selvam, C.E. Senkal, E. Garrett-Mayer, R.M. De Palma, D. Fedarovich, A. Liu, A.A. Habib, R.V. Stahelin, D. Perrotti, and B. Ogretmen, *Sphingosine analogue drug FTY720 targets I2PPP2A/SET and mediates lung tumour suppression via activation of PP2A-RIPK1-dependent necroptosis*. *EMBO Mol Med*, 2012. **5**(1): p. 105-21.
151. Ponnusamy, S., S.P. Selvam, S. Mehrotra, T. Kawamori, A.J. Snider, L.M. Obeid, Y. Shao, R. Sabbadini, and B. Ogretmen, *Communication between host organism and cancer cells is transduced by systemic sphingosine kinase 1/sphingosine 1-phosphate signalling to regulate tumour metastasis*. *EMBO Mol Med*, 2012. **4**(8): p. 761-75.
152. Visentin, B., J.A. Vekich, B.J. Sibbald, A.L. Cavalli, K.M. Moreno, R.G. Matteo, W.A. Garland, Y. Lu, S. Yu, H.S. Hall, V. Kundra, G.B. Mills, and R.A. Sabbadini, *Validation of an anti-sphingosine-1-phosphate antibody as a potential therapeutic in reducing growth, invasion, and angiogenesis in multiple tumor lineages*. *Cancer Cell*, 2006. **9**(3): p. 225-238.
153. Nagahashi, M., S. Ramachandran, E.Y. Kim, J.C. Allegood, O.M. Rashid, A. Yamada, R. Zhao, S. Milstien, H. Zhou, S. Spiegel, and K. Takabe, *Sphingosine-1-phosphate produced by sphingosine kinase 1 promotes breast cancer progression by stimulating angiogenesis and lymphangiogenesis*. *Cancer Res*, 2012. **72**(3): p. 726-35.
154. Hejazi, L., J.W. Wong, D. Cheng, N. Proschogo, D. Ebrahimi, B. Garner, and A.S. Don, *Mass and relative elution time profiling: two-dimensional analysis of sphingolipids in Alzheimer's disease brains*. *Biochem J*, 2011. **438**(1): p. 165-75.
155. Wong, J.W., H.J. Abuhusain, K.L. McDonald, and A.S. Don, *MMSAT: automated quantification of metabolites in selected reaction monitoring experiments*. *Anal Chem*, 2012. **84**(1): p. 470-4.

156. Day, B.W., B.W. Stringer, F. Al-Ejeh, M.J. Ting, J. Wilson, K.S. Ensbey, P.R. Jamieson, Z.C. Bruce, Y.C. Lim, C. Offenhauser, S. Charmsaz, L.T. Cooper, J.K. Ellacott, A. Harding, L. Leveque, P. Inglis, S. Allan, D.G. Walker, M. Lackmann, G. Osborne, K.K. Khanna, B.A. Reynolds, J.D. Lickliter, and A.W. Boyd, *EphA3 Maintains Tumorigenicity and Is a Therapeutic Target in Glioblastoma Multiforme*. *Cancer Cell*, 2013. **23**(2): p. 238-48.
157. Lee, J., S. Kotliarova, Y. Kotliarov, A. Li, Q. Su, N.M. Donin, S. Pastorino, B.W. Purow, N. Christopher, W. Zhang, J.K. Park, and H.A. Fine, *Tumor stem cells derived from glioblastomas cultured in bFGF and EGF more closely mirror the phenotype and genotype of primary tumors than do serum-cultured cell lines*. *Cancer Cell*, 2006. **9**(5): p. 391-403.
158. Chen, Z., A. Htay, W. Dos Santos, G.T. Gillies, H.L. Fillmore, M.M. Sholley, and W.C. Broaddus, *In vitro angiogenesis by human umbilical vein endothelial cells (HUVEC) induced by three-dimensional co-culture with glioblastoma cells*. *J Neurooncol*, 2009. **92**(2): p. 121-8.
159. Pardy, C., *Mutual information as an exploratory measure for genomic data with discrete and continuous variables*. 2013, University of New South Wales.
160. Mullen, T.D., Y.A. Hannun, and L.M. Obeid, *Ceramide synthases at the centre of sphingolipid metabolism and biology*. *Biochem J*, 2012. **441**(3): p. 789-802.
161. Hanahan, D. and R.A. Weinberg, *Hallmarks of cancer: the next generation*. *Cell*, 2011. **144**(5): p. 646-74.
162. Santos, C.R. and A. Schulze, *Lipid metabolism in cancer*. *FEBS J*, 2012. **279**(15): p. 2610-23.
163. Riboni, L., R. Campanella, R. Bassi, R. Villani, S.M. Gaini, F. Martinelli-Boneschi, P. Viani, and G. Tettamanti, *Ceramide levels are inversely associated with malignant progression of human glial tumors*. *Glia*, 2002. **39**(2): p. 105-13.
164. Torello, L.A., A.J. Yates, and L.A. Horrocks, *Effects of postmortem autolysis on the lipids of rat spinal cord*. *Virchows Arch B Cell Pathol Incl Mol Pathol*, 1981. **38**(2): p. 219-28.
165. Yao, J.K., S. Leonard, and R.D. Reddy, *Membrane phospholipid abnormalities in postmortem brains from schizophrenic patients*. *Schizophr Res*, 2000. **42**(1): p. 7-17.
166. Shaner, R.L., J.C. Allegood, H. Park, E. Wang, S. Kelly, C.A. Haynes, M.C. Sullards, and A.H. Merrill, Jr., *Quantitative analysis of sphingolipids for lipidomics using triple quadrupole and quadrupole linear ion trap mass spectrometers*. *J Lipid Res*, 2009. **50**(8): p. 1692-707.
167. Mu, H., X. Wang, H. Wang, P. Lin, Q. Yao, and C. Chen, *Lactosylceramide promotes cell migration and proliferation through activation of ERK1/2 in*

- human aortic smooth muscle cells*. Am J Physiol Heart Circ Physiol, 2009. **297**(1): p. H400-8.
168. Ishizuka, I., *Chemistry and functional distribution of sulfoglycolipids*. Prog Lipid Res, 1997. **36**(4): p. 245-319.
169. Berntson, Z., E. Hansson, L. Ronnback, and P. Fredman, *Intracellular sulfatide expression in a subpopulation of astrocytes in primary cultures*. J Neurosci Res, 1998. **52**(5): p. 559-68.
170. Pernber, Z., M. Molander-Melin, C.H. Berthold, E. Hansson, and P. Fredman, *Expression of the myelin and oligodendrocyte progenitor marker sulfatide in neurons and astrocytes of adult rat brain*. J Neurosci Res, 2002. **69**(1): p. 86-93.
171. Duchesneau, P., E. Gallagher, B. Walcheck, and T.K. Waddell, *Up-regulation of leukocyte CXCR4 expression by sulfatide: an L-selectin-dependent pathway on CD4+ T cells*. Eur J Immunol, 2007. **37**(10): p. 2949-60.
172. Takahashi, T. and T. Suzuki, *Role of sulfatide in normal and pathological cells and tissues*. J Lipid Res, 2012. **53**(8): p. 1437-50.
173. Krishnamurthy, K., G. Wang, J. Silva, B.G. Condie, and E. Bieberich, *Ceramide regulates atypical PKCzeta/lambda-mediated cell polarity in primitive ectoderm cells. A novel function of sphingolipids in morphogenesis*. J Biol Chem, 2007. **282**(5): p. 3379-90.
174. Bieberich, E., S. MacKinnon, J. Silva, S. Noggle, and B.G. Condie, *Regulation of cell death in mitotic neural progenitor cells by asymmetric distribution of prostate apoptosis response 4 (PAR-4) and simultaneous elevation of endogenous ceramide*. J Cell Biol, 2003. **162**(3): p. 469-79.
175. Bieberich, E., J. Silva, G. Wang, K. Krishnamurthy, and B.G. Condie, *Selective apoptosis of pluripotent mouse and human stem cells by novel ceramide analogues prevents teratoma formation and enriches for neural precursors in ES cell-derived neural transplants*. J Cell Biol, 2004. **167**(4): p. 723-34.
176. Hannun, Y.A. and L.M. Obeid, *Many ceramides*. J Biol Chem, 2011. **286**(32): p. 27855-62.
177. Saddoughi, S.A., E. Garrett-Mayer, U. Chaudhary, P.E. O'Brien, L.B. Afrin, T.A. Day, M.B. Gillespie, A.K. Sharma, C.S. Wilhoit, R. Bostick, C.E. Senkal, Y.A. Hannun, J. Bielawski, G.R. Simon, K. Shirai, and B. Ogretmen, *Results of a phase II trial of gemcitabine plus doxorubicin in patients with recurrent head and neck cancers: serum C(1)(8)-ceramide as a novel biomarker for monitoring response*. Clin Cancer Res, 2011. **17**(18): p. 6097-105.
178. Cuvillier, O., *Sphingosine in apoptosis signaling*. Biochim Biophys Acta, 2002. **1585**(2-3): p. 153-62.

179. Zhang, H., N.N. Desai, A. Olivera, T. Seki, G. Brooker, and S. Spiegel, *Sphingosine-1-phosphate, a novel lipid, involved in cellular proliferation*. J Cell Biol, 1991. **114**(1): p. 155-67.
180. Olivera, A. and S. Spiegel, *Sphingosine-1-phosphate as second messenger in cell proliferation induced by PDGF and FCS mitogens*. Nature, 1993. **365**(6446): p. 557-60.
181. Morii, T. and L. Weissbach, *Sphingosine 1-phosphate and cell migration: resistance to angiogenesis inhibitors*. Biochem Biophys Res Commun, 2003. **310**(3): p. 884-8.
182. Mullen, T.D., S. Spassieva, R.W. Jenkins, K. Kitatani, J. Bielawski, Y.A. Hannun, and L.M. Obeid, *Selective knockdown of ceramide synthases reveals complex interregulation of sphingolipid metabolism*. J Lipid Res, 2011. **52**(1): p. 68-77.
183. Sridevi, P., H. Alexander, E.L. Laviad, Y. Pewzner-Jung, M. Hannink, A.H. Futerman, and S. Alexander, *Ceramide synthase 1 is regulated by proteasomal mediated turnover*. Biochim Biophys Acta, 2009. **1793**(7): p. 1218-27.
184. Liang, J., M. Nagahashi, E.Y. Kim, K.B. Harikumar, A. Yamada, W.C. Huang, N.C. Hait, J.C. Allegood, M.M. Price, D. Avni, K. Takabe, T. Kordula, S. Milstien, and S. Spiegel, *Sphingosine-1-phosphate links persistent STAT3 activation, chronic intestinal inflammation, and development of colitis-associated cancer*. Cancer Cell, 2013. **23**(1): p. 107-20.
185. Bernardo, K., R. Hurwitz, T. Zenk, R.J. Desnick, K. Ferlinz, E.H. Schuchman, and K. Sandhoff, *Purification, characterization, and biosynthesis of human acid ceramidase*. J Biol Chem, 1995. **270**(19): p. 11098-102.
186. Park, J.H. and E.H. Schuchman, *Acid ceramidase and human disease*. Biochim Biophys Acta, 2006. **1758**(12): p. 2133-8.
187. Mao, C. and L.M. Obeid, *Ceramidases: regulators of cellular responses mediated by ceramide, sphingosine, and sphingosine-1-phosphate*. Biochim Biophys Acta, 2008. **1781**(9): p. 424-34.
188. Hara, S., S. Nakashima, T. Kiyono, M. Sawada, S. Yoshimura, T. Iwama, Y. Banno, J. Shinoda, and N. Sakai, *p53-Independent ceramide formation in human glioma cells during gamma-radiation-induced apoptosis*. Cell Death Differ, 2004. **11**(8): p. 853-61.
189. Seelan, R.S., C. Qian, A. Yokomizo, D.G. Bostwick, D.I. Smith, and W. Liu, *Human acid ceramidase is overexpressed but not mutated in prostate cancer*. Gene Chromosome Canc, 2000. **29**(2): p. 137-46.

190. Strelow, A., K. Bernardo, S. Adam-Klages, T. Linke, K. Sandhoff, M. Kronke, and D. Adam, *Overexpression of acid ceramidase protects from tumor necrosis factor-induced cell death*. J Exp Med, 2000. **192**(5): p. 601-12.
191. Saad, A.F., W.D. Meacham, A. Bai, V. Anelli, A.E.M. Mahdy, L.S. Turner, J. Cheng, A. Bielawska, J. Bielawski, T.E. Keane, L.M. Obeid, Y.A. Hannun, J.S. Norris, and X. Liu, *The functional effects of acid ceramidase over-expression in prostate cancer progression and resistance to chemotherapy*. Cancer Biol Ther, 2007. **6**(9): p. 1455-1460.
192. Ruckhäberle, E., U. Holtrich, K. Engels, L. Hanker, R. Gätje, D. Metzler, T. Karn, M. Kaufmann, and A. Rody, *Acid ceramidase 1 expression correlates with a better prognosis in ER-positive breast cancer*. Climacteric, 2009. **12**(6): p. 502-513.
193. Lucki, N.C. and M.B. Sewer, *Genistein stimulates MCF-7 breast cancer cell growth by inducing acid ceramidase (ASAHI) gene expression*. J Biol Chem, 2011. **286**(22): p. 19399-409.
194. Bedia, C., J. Casas, N. Andrieu-Abadie, G. Fabrias, and T. Levade, *Acid ceramidase expression modulates the sensitivity of A375 melanoma cells to dacarbazine*. J Biol Chem, 2011. **286**(32): p. 28200-9.
195. Kharel, Y., T.P. Mathews, A.M. Gellett, J.L. Tomsig, P.C. Kennedy, M.L. Moyer, T.L. Macdonald, and K.R. Lynch, *Sphingosine kinase type 1 inhibition reveals rapid turnover of circulating sphingosine 1-phosphate*. Biochem J, 2011. **440**(3): p. 345-53.
196. Gangoiti, P., M.H. Granado, A. Alonso, F.M. Goni, and A. Gomez-Munoz, *Implication of ceramide, ceramide 1-phosphate and sphingosine 1-phosphate in tumorigenesis*. Transl Oncogenomics, 2008. **3**: p. 81-98.
197. Paugh, B.S., L. Bryan, S.W. Paugh, K.M. Wilczynska, S.M. Alvarez, S.K. Singh, D. Kapitonov, H. Rokita, S. Wright, I. Griswold-Prenner, S. Milstien, S. Spiegel, and T. Kordula, *Interleukin-1 regulates the expression of sphingosine kinase 1 in glioblastoma cells*. J Biol Chem, 2009. **284**(6): p. 3408-17.
198. Estrada-Bernal, A., S.E. Lawler, M.O. Nowicki, A. Ray Chaudhury, and J.R. Van Brocklyn, *The role of sphingosine kinase-1 in EGFRvIII-regulated growth and survival of glioblastoma cells*. J Neurooncol, 2011. **102**(3): p. 353-66.
199. Heffernan-Stroud, L.A., K.L. Helke, R.W. Jenkins, A.M. De Costa, Y.A. Hannun, and L.M. Obeid, *Defining a role for sphingosine kinase 1 in p53-dependent tumors*. Oncogene, 2011.
200. Nava, V.E., J.P. Hobson, S. Murthy, S. Milstien, and S. Spiegel, *Sphingosine kinase type 1 promotes estrogen-dependent tumorigenesis of breast cancer MCF-7 cells*. Exp Cell Res, 2002. **281**(1): p. 115-27.

201. Radeff-Huang, J., T.M. Seasholtz, J.W. Chang, J.M. Smith, C.T. Walsh, and J.H. Brown, *Tumor necrosis factor-alpha-stimulated cell proliferation is mediated through sphingosine kinase-dependent Akt activation and cyclin D expression*. J Biol Chem, 2007. **282**(2): p. 863-70.
202. Pizzirani, D., C. Pagliuca, N. Realini, D. Branduardi, G. Bottegoni, M. Mor, F. Bertozzi, R. Scarpelli, D. Piomelli, and T. Bandiera, *Discovery of a New Class of Highly Potent Inhibitors of Acid Ceramidase: Synthesis and Structure-Activity Relationship (SAR)*. J Med Chem, 2013.
203. Bayless, K.J. and G.E. Davis, *Sphingosine-1-phosphate markedly induces matrix metalloproteinase and integrin-dependent human endothelial cell invasion and lumen formation in three-dimensional collagen and fibrin matrices*. Biochem Biophys Res Commun, 2003. **312**(4): p. 903-13.
204. Liu, Y., R. Wada, T. Yamashita, Y. Mi, C.X. Deng, J.P. Hobson, H.M. Rosenfeldt, V.E. Nava, S.S. Chae, M.J. Lee, C.H. Liu, T. Hla, S. Spiegel, and R.L. Proia, *Edg-1, the G protein-coupled receptor for sphingosine-1-phosphate, is essential for vascular maturation*. J Clin Invest, 2000. **106**(8): p. 951-61.
205. Kono, M., Y. Mi, Y. Liu, T. Sasaki, M.L. Allende, Y.P. Wu, T. Yamashita, and R.L. Proia, *The sphingosine-1-phosphate receptors SIP1, SIP2, and SIP3 function coordinately during embryonic angiogenesis*. J Biol Chem, 2004. **279**(28): p. 29367-73.
206. Schnute, M.E., M.D. McReynolds, T. Kasten, M. Yates, G. Jerome, J.W. Rains, T. Hall, J. Chrencik, M. Kraus, C.N. Cronin, M. Saabye, M.K. Highkin, R. Broadus, S. Ogawa, K. Cukyne, L.E. Zawadzke, V. Peterkin, K. Iyanar, J.A. Scholten, J. Wendling, H. Fujiwara, O. Nemirovskiy, A.J. Wittwer, and M.M. Nagiec, *Modulation of cellular SIP levels with a novel, potent and specific inhibitor of sphingosine kinase-1*. Biochem J, 2012. **444**(1): p. 79-88.
207. Peest, U., S.C. Sensken, P. Andreani, P. Hanel, P.P. Van Veldhoven, and M.H. Graler, *SIP-lyase independent clearance of extracellular sphingosine 1-phosphate after dephosphorylation and cellular uptake*. J Cell Biochem, 2008. **104**(3): p. 756-72.
208. Paugh, B.S., S.W. Paugh, L. Bryan, D. Kapitonov, K.M. Wilczynska, S.M. Gopalan, H. Rokita, S. Milstien, S. Spiegel, and T. Kordula, *EGF regulates plasminogen activator inhibitor-1 (PAI-1) by a pathway involving c-Src, PKCdelta, and sphingosine kinase 1 in glioblastoma cells*. FASEB J, 2008. **22**(2): p. 455-65.
209. Visentin, B., J.A. Vekich, B.J. Sibbald, A.L. Cavalli, K.M. Moreno, R.G. Matteo, W.A. Garland, Y. Lu, S. Yu, H.S. Hall, V. Kundra, G.B. Mills, and R.A. Sabbadini, *Validation of an anti-sphingosine-1-phosphate antibody as a potential therapeutic in reducing growth, invasion, and angiogenesis in multiple tumor lineages*. Cancer Cell, 2006. **9**(3): p. 225-38.

210. Adamski, J. and K. Suhre, *Metabolomics platforms for genome wide association studies--linking the genome to the metabolome*. *Curr Opin Biotechnol*, 2013. **24**(1): p. 39-47.
211. Sutphen, R., Y. Xu, G.D. Wilbanks, J. Fiorica, E.C. Grendys, Jr., J.P. LaPolla, H. Arango, M.S. Hoffman, M. Martino, K. Wakeley, D. Griffin, R.W. Blanco, A.B. Cantor, Y.J. Xiao, and J.P. Krischer, *Lysophospholipids are potential biomarkers of ovarian cancer*. *Cancer Epidemiol Biomarkers Prev*, 2004. **13**(7): p. 1185-91.
212. Hammad, S.M., J.S. Pierce, F. Soodavar, K.J. Smith, M.M. Al Gadban, B. Rembiesa, R.L. Klein, Y.A. Hannun, J. Bielawski, and A. Bielawska, *Blood sphingolipidomics in healthy humans: impact of sample collection methodology*. *J Lipid Res*, 2010. **51**(10): p. 3074-87.
213. Bui, H.H., J.K. Leohr, and M.S. Kuo, *Analysis of sphingolipids in extracted human plasma using liquid chromatography electrospray ionization tandem mass spectrometry*. *Anal Biochem*, 2012. **423**(2): p. 187-94.
214. Weckwerth, W., *Unpredictability of metabolism--the key role of metabolomics science in combination with next-generation genome sequencing*. *Anal Bioanal Chem*, 2011. **400**(7): p. 1967-78.
215. Adamski, J., *Genome-wide association studies with metabolomics*. *Genome Med*, 2012. **4**(4): p. 34.
216. Illig, T., C. Gieger, G. Zhai, W. Romisch-Margl, R. Wang-Sattler, C. Prehn, E. Altmaier, G. Kastenmuller, B.S. Kato, H.W. Mewes, T. Meitinger, M.H. de Angelis, F. Kronenberg, N. Soranzo, H.E. Wichmann, T.D. Spector, J. Adamski, and K. Suhre, *A genome-wide perspective of genetic variation in human metabolism*. *Nat Genet*, 2010. **42**(2): p. 137-41.
217. Mootha, V.K. and J.N. Hirschhorn, *Inborn variation in metabolism*. *Nat Genet*, 2010. **42**(2): p. 97-8.
218. Paz, M.F., R. Yaya-Tur, I. Rojas-Marcos, G. Reynes, M. Pollan, L. Aguirre-Cruz, J.L. Garcia-Lopez, J. Piquer, M.J. Safont, C. Balana, M. Sanchez-Céspedes, M. Garcia-Villanueva, L. Arribas, and M. Esteller, *CpG island hypermethylation of the DNA repair enzyme methyltransferase predicts response to temozolomide in primary gliomas*. *Clin Cancer Res*, 2004. **10**(15): p. 4933-8.
219. Vivanco, I., H.I. Robins, D. Rohle, C. Campos, C. Grommes, P.L. Nghiemphu, S. Kubek, B. Oldrini, M.G. Chheda, N. Yannuzzi, H. Tao, S. Zhu, A. Iwanami, D. Kuga, J. Dang, A. Pedraza, C.W. Brennan, A. Heguy, L.M. Liau, F. Lieberman, W.K. Yung, M.R. Gilbert, D.A. Reardon, J. Drappatz, P.Y. Wen, K.R. Lamborn, S.M. Chang, M.D. Prados, H.A. Fine, S. Horvath, N. Wu, A.B. Lassman, L.M. DeAngelis, W.H. Yong, J.G. Kuhn, P.S. Mischel, M.P. Mehta, T.F. Cloughesy, and I.K. Mellingshoff, *Differential sensitivity of glioma- versus*

- lung cancer-specific EGFR mutations to EGFR kinase inhibitors.* Cancer Discov, 2012. **2**(5): p. 458-71.
220. Guo, D., R.M. Prins, J. Dang, D. Kuga, A. Iwanami, H. Soto, K.Y. Lin, T.T. Huang, D. Akhavan, M.B. Hock, S. Zhu, A.A. Kofman, S.J. Bensinger, W.H. Yong, H.V. Vinters, S. Horvath, A.D. Watson, J.G. Kuhn, H.I. Robins, M.P. Mehta, P.Y. Wen, L.M. DeAngelis, M.D. Prados, I.K. Mellinghoff, T.F. Cloughesy, and P.S. Mischel, *EGFR signaling through an Akt-SREBP-1-dependent, rapamycin-resistant pathway sensitizes glioblastomas to antilipogenic therapy.* Sci Signal, 2009. **2**(101): p. ra82.
221. Guo, D., I.J. Hildebrandt, R.M. Prins, H. Soto, M.M. Mazzotta, J. Dang, J. Czernin, J.Y. Shyy, A.D. Watson, M. Phelps, C.G. Radu, T.F. Cloughesy, and P.S. Mischel, *The AMPK agonist AICAR inhibits the growth of EGFRvIII-expressing glioblastomas by inhibiting lipogenesis.* Proc Natl Acad Sci U S A, 2009. **106**(31): p. 12932-7.
222. Williams, K.J., J.P. Argus, Y. Zhu, M.Q. Wilks, B.N. Marbois, A.G. York, Y. Kidani, A.L. Pourzia, D. Akhavan, D.N. Lisiero, E. Komisopoulou, A.H. Henkin, H. Soto, B.T. Chamberlain, L. Vergnes, M.E. Jung, J.Z. Torres, L.M. Liao, H.R. Christofk, R.M. Prins, P.S. Mischel, K. Reue, T.G. Graeber, and S.J. Bensinger, *An essential requirement for the SCAP/SREBP signaling axis to protect cancer cells from lipotoxicity.* Cancer Res, 2013. **73**(9): p. 2850-62.
223. Gulati, S., Y. Liu, A.B. Munkacsı, L. Wilcox, and S.L. Sturley, *Sterols and sphingolipids: dynamic duo or partners in crime?* Prog Lipid Res, 2010. **49**(4): p. 353-65.
224. Worgall, T.S., *Sphingolipids: major regulators of lipid metabolism.* Curr Opin Clin Nutr Metab Care, 2007. **10**(2): p. 149-55.
225. Worgall, T.S., R.A. Juliano, T. Seo, and R.J. Deckelbaum, *Ceramide synthesis correlates with the posttranscriptional regulation of the sterol-regulatory element-binding protein.* Arterioscler Thromb Vasc Biol, 2004. **24**(5): p. 943-8.
226. Weigert, A., N. Weis, and B. Brüne, *Regulation of macrophage function by sphingosine-1-phosphate.* Immunobiology, 2009. **214**(9-10): p. 748-760.
227. Weigert, A., S. Schiffmann, D. Sekar, S. Ley, H. Menrad, C. Werno, S. Grosch, G. Geisslinger, and B. Brune, *Sphingosine kinase 2 deficient tumor xenografts show impaired growth and fail to polarize macrophages towards an anti-inflammatory phenotype.* Int J Cancer, 2009. **125**(9): p. 2114-21.
228. Buchen, L., *Cancer: Missing the mark.* Nature, 2011. **471**(7339): p. 428-32.
229. Poste, G., *Bring on the biomarkers.* Nature, 2011. **469**(7329): p. 156-7.
230. Endo, K., Y. Igarashi, M. Nisar, Q.H. Zhou, and S. Hakomori, *Cell membrane signaling as target in cancer therapy: inhibitory effect of N,N-dimethyl and*

- N,N,N-trimethyl sphingosine derivatives on in vitro and in vivo growth of human tumor cells in nude mice.* Cancer Res, 1991. **51**(6): p. 1613-8.
231. Lin, X., Z. Fuks, and R. Kolesnick, *Ceramide mediates radiation-induced death of endothelium.* Crit Care Med, 2000. **28**(4 Suppl): p. N87-93.
232. Henry, B., C. Moller, M.T. Dimanche-Boitrel, E. Gulbins, and K.A. Becker, *Targeting the ceramide system in cancer.* Cancer Lett, 2011.
233. Ji, C., Y.L. Yang, L. He, B. Gu, J.P. Xia, W.L. Sun, Z.L. Su, B. Chen, and Z.G. Bi, *Increasing ceramides sensitizes genistein-induced melanoma cell apoptosis and growth inhibition.* Biochem Biophys Res Commun, 2012. **421**(3): p. 462-7.
234. Radin, N.S., *Killing tumours by ceramide-induced apoptosis: a critique of available drugs.* Biochem J, 2003. **371**(Pt 2): p. 243-56.
235. Mizutani, Y., A. Kihara, and Y. Igarashi, *Mammalian Lass6 and its related family members regulate synthesis of specific ceramides.* Biochem J, 2005. **390**(Pt 1): p. 263-71.
236. Kharel, Y., M. Rajee, M. Gao, A.M. Gellett, J.L. Tomsig, K.R. Lynch, and W.L. Santos, *Sphingosine kinase type 2 inhibition elevates circulating sphingosine 1-phosphate.* Biochem J, 2012. **447**(1): p. 149-57.
237. Eberlin, L.S., I. Norton, A.L. Dill, A.J. Golby, K.L. Ligon, S. Santagata, R.G. Cooks, and N.Y. Agar, *Classifying human brain tumors by lipid imaging with mass spectrometry.* Cancer Res, 2012. **72**(3): p. 645-54.
238. Eberlin, L.S., I. Norton, D. Orringer, I.F. Dunn, X. Liu, J.L. Ide, A.K. Jarmusch, K.L. Ligon, F.A. Jolesz, A.J. Golby, S. Santagata, N.Y. Agar, and R.G. Cooks, *Ambient mass spectrometry for the intraoperative molecular diagnosis of human brain tumors.* Proc Natl Acad Sci U S A, 2013. **110**(5): p. 1611-6.
239. Spassieva, S.D., T.D. Mullen, D.M. Townsend, and L.M. Obeid, *Disruption of ceramide synthesis by CerS2 down-regulation leads to autophagy and the unfolded protein response.* Biochem J, 2009. **424**(2): p. 273-83.